STUDIES ON MONO-, BI-METALLIC AND NANO CATALYSTS OF NICKEL, PALLADIUM AND PLATINUM METALS AND THEIR APPLICATIONS IN SELECTIVE HYDROGENATION OF ACETYLENIC COMPOUNDS AND NITROAROMATICS OF INDUSTRIAL RELEVANCE

A THESIS SUBMITTED TO

UNIVERSITY OF PUNE

FOR THE DEGREE OF

DOCTOR OF PHILOSOPHY

(IN CHEMISTRY)

BY

Mr. Jayprakash M. Nadgeri

Research Guide

Dr. Chandrashekhar V. Rode

CHEMICAL ENGINEERING AND PROCESS DEVELOPMENT DIVISON

NATIONAL CHEMICAL LABORATORY

PUNE- 411 008, INDIA

September-2010

राष्ट्रीय रासायनिक प्रयोगशाला
(वैज्ञानिक तथा औद्योगिक अनुसंधान परिषद)
डॉ. होमी भाभा रोड, पुणे - 411 008. भारत
NATIONAL CHEMICAL LABORATORY
(Council of Scientific & Industrial Research)
Dr. Homi Bhabha Road, Pune - 411008. India

Certificate of the Guide

Certified that the work incorporated in the thesis entitled **" Studies on mono-, bi-metallic and nano catalysts of nickel, palladium and platinum metals and their applications in selective hydrogenation of acetylenic compounds and nitroaromatics of industrial relevance"** submitted by **Mr. Jayprakash M. Nadgeri** was carried out by the candidate under my supervision/guidance. Such material as has been obtained from other sources has been duly acknowledged in the thesis.

Dr. Chandrashekhar V. Rode

(Supervisor/Research Guide)

Communications Channels ☎ +91 20 25902000 +91 20 25893300 +91 20 25893400 Fax +91 20 25902601 (Director) +91 20 25902660 (Admin.) +91 20 25902639 (Business Development) URL : www.ncl-india.org

Declaration by the Candidate

I declare that the thesis entitled "**Studies on mono-, bi-metallic and nano catalysts of nickel, palladium and platinum metals and their applications in selective hydrogenation of acetylenic compounds and nitroaromatics of industrial relevance**" submitted by me for the degree of Doctor of Philosophy is the record of work carried out by me during the period from 11-10-2007 to 16-09-2010 under the guidance of Dr. C. V. Rode and has not formed the basis for the award of any degree, diploma, associateship, fellowship, titles in this or any other University or other institution of Higher learning.

I further declare that the material obtained from other sources has been duly acknowledged in the thesis.

Date: Jayprakash M. Nadgeri

Dedicated to my beloved

Father and

Late Mother

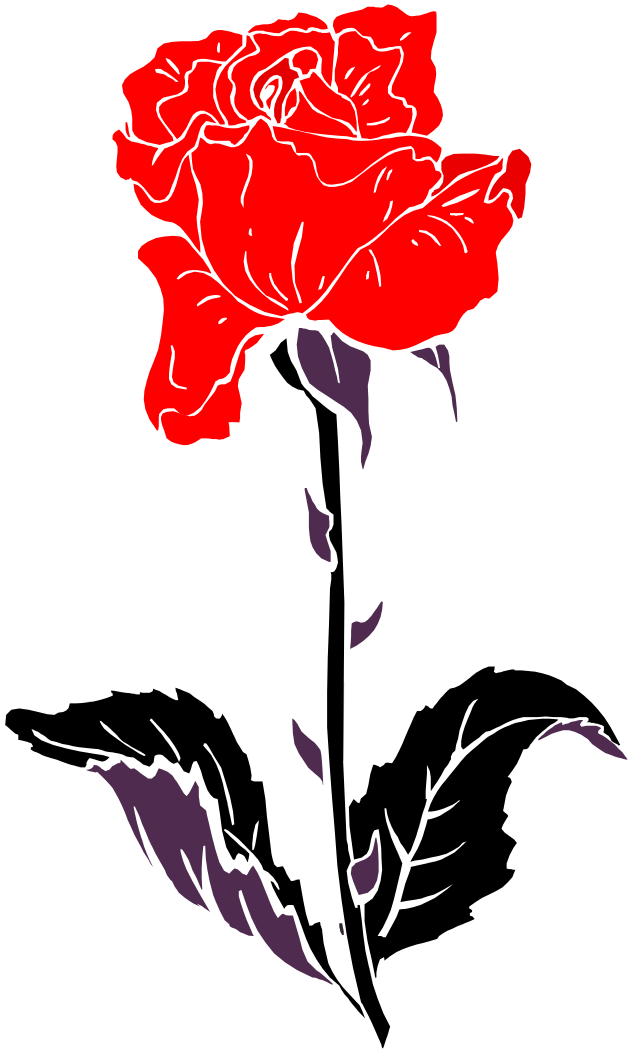

List of Contents:

List of Tables

List of Schemes

List of Figures

Abbreviations

B_1D	Butane-1,4-diol
B_2D	2-Butene-1,4-diol
B_3D	2-Butyne-1,4-diol
BE	Binding energy
BET	Brunauer-Emmett-Teller
C	Carbon
m-CNB	*m*-Chloronitrobenzene
DAB	3,3'-Dichloroazobenzene
DHAB	3,3'-Dichlorohydrazobenzene
EB	Ethylbenzene
FTIR	Fourier- transform infrared Spectroscopy
HRTEM	High resolution transmission electron microscopy
HPLC	High performance liquid chromatography
GC	Gas chromatography
NB	Nitrobenzene
PAP	*p*-Aminophenol
PH	phenylacetylene
PHA	phenylhydroxylamine
P_{H2}	Hydrogen pressure
PtF	1%Pt/C fresh catalyst
PtU	1% Pt/C used catalyst
PtUS	1% Pt/C used catalyst in presence of sodium carbonate
SEM	Scanning electron microscopy
STy	Styrene
TEM	Transmission Electron Microscopy
T	Temperature
TOF	Turnover frequency
TON	Turnover Number
XPS	X-Ray Photoelectron Spectroscopy
XRD	X-ray diffraction

Notation

a_1	concentration of hydrogen in liquid phase, $(= A_1/A^*)$, dimensionless
a_s	concentration of hydrogen on the catalyst surface, $(= A_s/A^*)$, dimensionless
a_p	external surface area of the pellet $[= 6(1 - \in_B)/d_p\ ]$,m^{-1}.
a_t	packing external surface area per unit volume of the reactor $[= S_{ex}(1 - \in_b)/V_B]$
a_w	catalyst area wetted, m^{-1}
A_1	concentration of hydrogen in liquid phase, kmol/m^3
A_s	concentration of hydrogen on the catalyst surface, kmol/m^3
A^*	concentration of hydrogen in equilibrium with liquid, kmol/m^3
b_1	concentration of B_3D in liquid phase $(= B_1/B_{li})$,dimensionless
B_1	concentration of B_3D in liquid phase, kmol/m^3
B_{li}	initial concentration of B_3D in liquid phase, kmol/m^3
c_1	concentration of B_2D in liquid phase, $(= C_1/B_{li})$,
C_1	concentration of B_2D in liquid phase, kmol/m^3
D_e	effective diffusivity, m^2/s
D_M	molecular diffusivity, m^2/s
d_p	particle diameter, m
f_d	fraction of catalyst wetted by dynamic liquid
f_s	fraction of catalyst wetted by the stagnant liquid
f_w	wetted fraction
F	liquid flow rate, kg/h
k_1, k_2	reaction rate constant, m^2/kg (m^3/kmol.s)
k_{21}	dimensionless rate constant $(= K_2/K_1)$
k_b, k_c	dimensionless equilibrium constant $(K_b = K_B B_{li}; K_c = K_c/B_{li})$
k_s	liquid-solid mass transfer coefficient, m s^{-1}
k_{gs}	gas-particle mass transfer coefficient, m s^{-1}
K_A, K_B, K_C	adsorption constants, m^3/kmol
$k_1 a_B$	gas-liquid mass transfer coefficient, s^{-1}

K_{ex}	exchange coefficient between dynamic and stagnant liquid, s^{-1}
L	reactor length, m
N_d	Nusslet number for the liquid phase in the dynamic zone
N_s	Nusslet number for the liquid phase in the stagnant zone
N_g	Nusslet number for the gas phase
q_B	stoichiometric ratio ($= B_{li}/A^*$)
r_1, r_2	reaction rate for the individual hydrogenation steps, $kmol/m^3/s$
R	radius of the pellet, m
R_A	overall rate of hydrogenation, $kmol/m^3/s$
R_{e1}	Reynolds number for the liquid phase
S_{ex}	external surface area of the catalyst pellet, m^2
U_g	gas velocity (superficial), m/s
U_1	liquid velocity (superficial), m/s
W	weight of catalyst, kg/m^3
Z	reactor length, *m*

Greek Letters

α_{gl}	dimensionless gas-liquid mass transfer coefficient
α_{1s}	dimensionless liquid-solid mass transfer coefficient
α_r	dimensionless reaction rate constant
$\in$	porosity of catalyst
$\in_b$	bed voidage

ABSTRACT OF THESIS

Studies on mono-, bi-metallic and nano catalysts of nickel, palladium and platinum metals and their applications in selective hydrogenation of acetylenic compounds and nitroaromatics of industrial relevance

Catalysis has been playing a major role for last few decades due to its wide range applications in various fields such as fuel cell as renewable source of energy, abatement of air pollution, waste water treatment, environmental protection by developing green processes. In particular, due to increasing awareness of environmental issues, chemical industries look for the cleaner, safer, environmentally acceptable alternative and sustainable processes. Chemical processes should have minimum waste generation, improved product quality and cost effectiveness. Traditionally, for manufacturing fine chemicals the synthetic organic chemists used the classical 'stoichiometric' routes, which generate large amount of organic or inorganic wastes in the range of 1-100 kg byproduct formed per kg of product, which gives serious impact on environment and hence on human life. Some of the well known examples of such processes are oxidations with permanganate and chromium compounds, reductions with metal acids and metal hydrides, halogenations, alkylation, nitration etc. These processes are now being replaced by catalytic routes and among these processes, catalytic hydrogenation reactions of various organic functional groups is one of the core technologies widely used in chemical industries. Although hydrogenation is supposed to be a well developed subjected area, there is a great deal that can be still done for fundamental understanding particularly, in designing new catalysts and routes for selective hydrogenation reactions of industrial relevance [1].

For this purpose, we undertook a detailed study on the preparation and characterization of mono-, bimetallic and nanocatalysts using nickel, palladium and platinum metals. These catalysts were evaluated for their activities for the selective hydrogenation of 2-butyne-1,4-diol to 2-butene-1,4-diol and butane-1,4-diols, phenylacetylene to styrene, nitrobenzene to *p*-aminophenol, *m*-chloronitrobenzene to *m*-chloroaniline.

Catalytic hydrogenation of acetylenic compounds e.g. 2-butyne-1,4diol and phenylacetylene is an industrially important reaction whose end products 2-butene-1,4 diol and styrene respectively are widely used in the manufacture of endosulfan (insecticide), tetrahydrofuran, vitamins A and B_6 and in polymer industries. Since, hydrogenation of 2-butyne-1,4diol and phenylacetylene involve consecutive as well as parallel reactions, controlling the selectivity to olefinic products is a challenging task. Several catalysts were reported for selective semi-hydrogenation of acetylenic compounds[2], however the major drawbacks associated with these catalysts are poor activity in subsequent reuses, and moreover, such processes require the complete removal of the additives for obtaining highest purity of the product for its end uses in the fine chemical or pharmaceutical sector. The noble metals such as palladium, ruthenium alone or in combination with other metals such as zinc, lead, cadmium, copper, and/or organic amines were also used as catalyst systems to improve selectivity to the intermediate, B_2D [3-9].

Hydrogenation of various nitroaromatic compounds is also a commercially important process and in the present thesis we have studied the following reactions (i) single step direct hydrogenation of nitrobenzene to *p*-aminophenol (PAP), with a particular emphasis on intermediate *p*-phenylhydroxylamine formed and its rearrangement to PAP and (ii) selective hydrogenation of *m*-chloronitrobenzene to *m*-chloroaniline, without/minimum dehalogenation [10]. Both these are multi step processes involving Fe/HCl reduction (Bechamp Process) which produced equivalent or higher amount of Fe-FeO sludge as a byproduct. The catalytic hydrogenation using supported metal catalysts is an excellent alternative to the conventional Bechamp process which gives better yield and selectivity to the desired products [11,12].

OBJECTIVES OF THE PRESENT INVESTIGATION

- Preparation of colloidal, bulk and nano structured supported mono, and bi-metallic catalysts involving various transition metals such as Ni, Pd, Pt.

- Physico-chemical characterization of the prepared catalysts by various techniques such as powder X-ray diffraction, SEM, EDAX, BET surface area, Raman, FTIR, Chemisorption, XPS.
- Standardization of analytical methods for the model reaction systems investigated using GC and HPLC.
- Activity testing of the prepared catalysts for selective hydrogenation of 2-butyne-1,4-diol, phenylacetylene, nitrobenzene and *m*-chloronitrobenzene, in high pressure batch and continuous reactors.
- To study the kinetics of formation and further rearrangement of an intermediate phenylhydroxylamine in hydrogenation of nitrobenzene to PAP.
- To study the role of additives on extent of dehalogenation in hydrogenation of *m*-chloronitrobenzene to *m*-chloroaniline
- Optimization of reaction parameters such as temperature, pressure, catalyst and substrate loading in order to achieve highest conversion and selectivity, for all the hydrogenation reaction studied in this work.
- To correlate the observed activity and selectivity patterns with the catalyst characterization data.

OUTLINE OF THE THESIS

The thesis contains total 7 chapters among which the first two chapters include general introduction including objectives and experimental techniques respectively. The scientific results are then divided in two parts viz. Part I dealing with selective hydrogenation of acetylenic compounds and Part II contains hydrogenation of nitroaromatic compounds. A brief summery of the thesis is outlined here.

Chapter 1 presents general introduction to catalysis, classification of heterogeneous catalysts, and reduction methods. At the end of this chapter, the scope and objectives of this thesis are given.

Chapter 2 includes preparation details for various types of mono and bimetallic catalysts such as Pt/C. Ni/C, Ni-Pt/C, colloidal Pd and supported nano catalysts, synthesis of carbon nanotubes, Pd functionalization of carbon nanotubes and experimental setup and procedure for hydrogenation reactions in batch and continuous reactors under high and atmospheric pressure conditions. Details of catalyst characterization techniques used such as FTIR, BET N_2 adsorption, Chemisorption, XRD, Raman, XPS, SEM, TEM and the analytical techniques such as GC and HPLC are also included.

Chapter 3 contains specific literature survey on hydrogenation of 2-butyne-1,4-diol to 2-butene-1,4-diol and butane-1,4diol and activity results of supported palladium nanoparticles, $Pt/CaCO_3$ and Pd-functionalized carbon nanotubes (CNTs) on this hydrogenation systems.

Continuous hydrogenation of 2-butyne-1,4-diol (B_3D) in presence of 1% $Pt/CaCO_3$ catalyst in a fixed-bed reactor gave 2-butene-1,4-diol (B_2D) and butane-1,4-diol (B_1D) without formation of any other side products. In case of continuous hydrogenation, higher selectivity (66%) to B_2D was obtained and the selectivity pattern was completely different from that found in case of batch slurry operation in which B_1D selectivity was very much higher (83%) than the B_2D selectivity (17%). The selectivity ratio of B_1D to B_2D could be altered by varying the H_2 pressure, temperature, liquid and gas flow rate conditions at the reactor inlet. A theoretical model was also developed incorporating the conditions of external and intraparticle mass transfer, partial wetting of the catalyst using reaction kinetics of 2-butyne-1,4-diol hydrogenation in a batch slurry reactor. The reactor model was validated by carrying out hydrogenation experiments under various reactor inlet conditions. The predictions obtained by the proposed reactor model was found to agree well with the experimental data over a wide range of operating conditions [13].

Another interesting study included in this chapter is activity and selectivity behavior of supported palladium nanoparticles. Pd nanoparticles supported on activated carbon and $CaCO_3$ showed the higher activity (9-21 times) and selectivity towards B_2D (> 99%) than the bulk Pd/C catalyst prepared by conventional method for 2-butyne-1,4-diol. The pulse titration study showed that metal dispersion for the nano catalyst was > 65% higher than that for the bulk catalyst [14]. Performance of Pd-functionalized carbon nanotubes

(CNTs) for the hydrogenation of 2-butyne 1, 4 diol was also studied. Pd-functionalized carbon nanotubes catalyst was prepared by supporting Pd on acid-treated carbon nanotubes. Pd-functionalized carbon nanotubes showed higher selectivity (93%) to 2-butene-1, 4-diol than Pd supported on commercial carbon (70% selectivity to 2-butene-1, 4-diol) with complete conversion of 2-butyne-1, 4-diol. Pd/CNTs catalyst was characterized by BET, FTIR, Raman, XRD, EDAX, ICP-OES, SEM and TEM analysis. The reusability of the catalyst was evaluated by the catalyst recycle experiments [15].

Chapter 4 deals with literature survey and activity results of colloidal Pd nanoparticles on hydrogenation of phenylacetylene. Colloidal Pd nanoparticles prepared by chemical reduction method using PVP as a capping agent showed 3.5 times higher reaction rate than the bulk catalyst for hydrogenation of phenylacetylene under milder reaction conditions. Effect of temperature and pressure was also studied to achieve the complete conversion and high selectivity to styrene. At 90% conversion of phenylacetylene, selectivity to styrene was found to be 90% which decreased to 68% for complete conversion of phenylacetylene. This is due to formation of ethylbenzene by further hydrogenation of styrene.

Chapter 5 contains literature survey and catalyst activity results of Pd/C catalysts on direct hydrogenation of nitrobenzene to *p*-aminophenol (PAP). The mechanistic pathway for hydrogenation of nitrobenzene to PAP involves two-steps (i) reduction of nitrobenzene to give phenylhydroxylamine (PHA) as an intermediate (ii) Bamberger rearrangement of PHA in presence of an aqueous acid to give PAP. Formation of aniline via further hydrogenation of PHA is a major competing reaction affecting the selectivity to PAP. Catalytic hydrogenation of nitrobenzene using 3% Pt/C catalyst at 303 K showed 95% selectivity to PHA at 36 % conversion of nitrobenzene which decreased to 75% for complete conversion of nitrobenzene due to the formation of aniline as a byproduct. Rearrangement of PHA in an inert atmosphere (Ar) gave a higher selectivity (77%) to PAP as compared to the rearrangement carried out under hydrogen atmosphere.

Another part of this chapter includes the study on optimization of reaction conditions and scale up of this important industrial hydrogenation system. The downstream process step

of neutralization of the reaction crude was also fine tuned in order to achieve the highest selectivity to *p*-aminophenol (75% isolated yield of PAP).

Chapter 6 contains literature survey and activity testing of the mono, bi-metallic catalysts containing Pd, Ni metals for selective hydrogenation of *m*-chloronitrobenzene to *m*-chloroaniline. In this work, we studied the role of an additive, sodium carbonate reducing the extent of dehalogenation to give 94% selectivity to *m*-chloroaniline. It was also found that the Ni-Pt based bimetallic catalysts showed high activity and almost complete selectivity (>99%) towards *m*-chloroaniline compared with Ni based monometallic catalysts.

Chapter 7 summarizes work presented in all the chapters and general conclusions arrived at from the discussed results.

Reference

1. H. U. Blaser, U. Siegrist H. Steiner, M. Studer in *Fine chemicals through heterogeneous catalysis*, Wiley-VCH, Weinheim (2001).
2. C. V. Rode *J. Jap. Petro. Inst.* 51 (2008) 119.
3. J. M. Winterbottom, H. Marwan, J. Viladevall, S. Sharma, S. Raymahasay *Stud. Surf. Sci. Catal.* 108 (1997) 59.
4. G. C. Bond, G. Webb, J. M. Winterbottom *J. Catal.* 1 (1962) 74.
5. T. Fukuda, T. Kusama *Bull Chem. Soc. Jpn.* 20 (1958) 28.
6. T. Fukuda, T. Kusama *Bull Chem. Soc. Jpn.* 31 (1958) 339.
7. M. M. Telkar, C. V. Rode, V. H. Rane, R. Jagannathan, R. V. Chaudhari *Appl. Catal. A.* 273 (2004) 11.
8. M. M. Telkar, C. V. Rode, V. H. Rane, R. Jaganathan, R. V. Chaudhari *Catal. Commun.* 6 (2005) 725.
9. M. M. Telkar, C. V. Rode, V. H. Rane, R. Jaganathan, R. V. Chaudhari *Appl. Catal. A* 216 (2001) 13.
10. C. V. Rode, R. V. Chaudhari *Ind. Eng. Chem. Res*. 33 (1994) 1645.

11. C. V. Rode, M. J. Vaidya, and R. V. Chaudhari *Org. Proc. Res. Dev.* 3 (1999) 465.
12. C. V. Rode, M. J. Vaidya, R. Jaganathan, R. V. Chaudhari *Chem. Eng. Sci.* 56 (2001) 1299
13. C. V. Rode, P. R. Tayade, J. M. Nadgeri, R. Jaganathan, R. V. Chaudhari *Org. Proc. Res. Dev.* 10 (2006) 27.
14. J. M. Nadgeri, M. M. Telkar, C. V. Rode *Catal. Commun.* 9 (2008) 441.
15. J. M. Nadgeri, A. C. Garade, R. A. Tambe, S. P. Gokhale C. V. Rode *Adv. Sci. Lett.* 3 (2010) 313.

Chapter I

Introduction

1.1. General Introduction:

Catalysis has played a major role in improving quality of human life by offering environmentally benign processes for the manufacture of various chemical products in day to day life. Catalysis is a multidisciplinary science that serves a broad range of applications covering specialty, fine, intermediate, and life science chemicals. About 85 to 90 % industrial processes are based on catalysis. Furthermore, about 80 % catalytic processes are carried out using heterogeneous catalysts [1]. The worldwide uses of catalysts in various sectors are shown in Figure 1.1 [2].

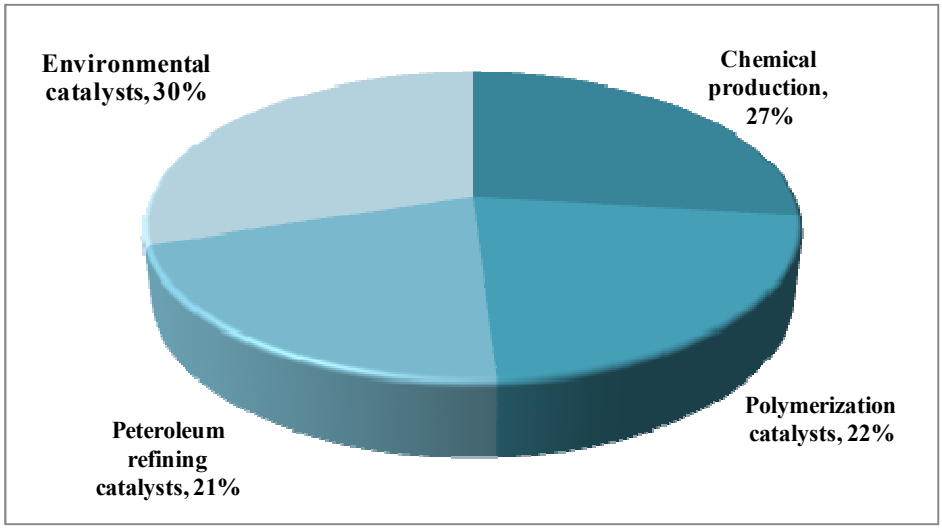

Figure 1.1. Catalytic process in various sectors

Environmental benigness of a chemical process is determined by the 'E-factor' that is evaluated by the ratio of $kg_{waste}/kg_{Product}$, where waste is everything formed in the reaction except the desired product formed. Formation of byproducts in various sectors of the chemical industries is shown in Table 1.1. As can be seen from this Table, E-factors for fine chemicals and pharmaceutical sectors are very high, due to the conventional multistep syntheses based on using stoichiometric reagents producing large amounts of organic or inorganic wastes, which pose serious impact on the environment and human life [3].

Table 1.1. *E*-factor for various sectors of the chemical industries [4, 5].

Industry segment	Product tonnage	kg byproduct/kg product
Petrochemicals	10^6-10^8	<0.1
Bulk chemicals	10^4-10^6	<1-5
Fine chemicals	10^2-10^4	5-50
Pharmaceuticals	10-10^3	25-100

In order to minimize such problems, chemical processes based on reagents need to be replaced by catalytic routes. The classical definition of 'catalysis' is given as 'a substance that increases the rate of approach to equilibrium of a chemical reaction without itself being substantially consumed in the reaction process' [6]. Depending upon the phases in which a catalyst exists, it is classified in two types,

1. Homogeneous catalyst, in which reactants, products and catalyst are in the same phase.
2. Heterogeneous catalyst, in which catalyst is in different phase than that of the reactants and products.

Heterogeneous catalysts have distinct advantages of easy recovery and recycling, over the homogenous catalysts. Some of distinct features of homogeneous and heterogeneous catalysis are summarized in Table.1.2.

Table 1.2. Distinction between homogeneous and heterogeneous catalysts [7]

	Homogeneous Catalyst	Heterogeneous catalyst
Advantages	• Mild reaction conditions • High activity and selectivity • Efficient heat transfer • No mass transfer limitation	• Facile separation of catalyst and products • Continuous processing • Elimination of corrosion problems
Disadvantages	• Toxic waste water after catalyst recycling • Contamination of product with catalyst • High costs due to catalyst losses (noble metal complexes) • Difficulties in separation and recycling • Not readily adapted to a continuous process • Corrosion problem	• Heat transfer problem • Lower selectivity • Diffusion to and within catalyst • Temperature control of highly exothermic reactions • Mass transfer limitations • Harsh reaction conditions • High mechanical stability required

Since, the present work involves studies on heterogeneous catalysts for hydrogenation reactions, further discussion is devoted to heterogeneous catalysts.

1.2. Types of heterogeneous catalysts:

Heterogeneous catalysts are classified in two categories, unsupported and supported [8]. Unsupported catalyst has several drawbacks such as difficulty in preparation, estimation of active metal component and thereby characterization is difficult. Sintering is a major issue in case of unsupported catalyst, which can be resolved by a simple way of affixing the small amount of metal particles to a thermally stable material usually known as a

'support'. It also gives better dispersion of active metal for efficient use of the catalyst. Supports used are porous materials such as activated charcoal, alumina powder, silica powder etc. having high surface area [9]. Metal loading on the support generally varies from 0.1 to 20% with degree of metal dispersion ranging from 10 to 80% and due to firm anchoring to the support, they do not readily coalesce or sinter easily under the reaction conditions. Both supported and unsupported catalysts are further divided into three categories metallic, oxide based, and nanosize as shown in Figure 1.2.

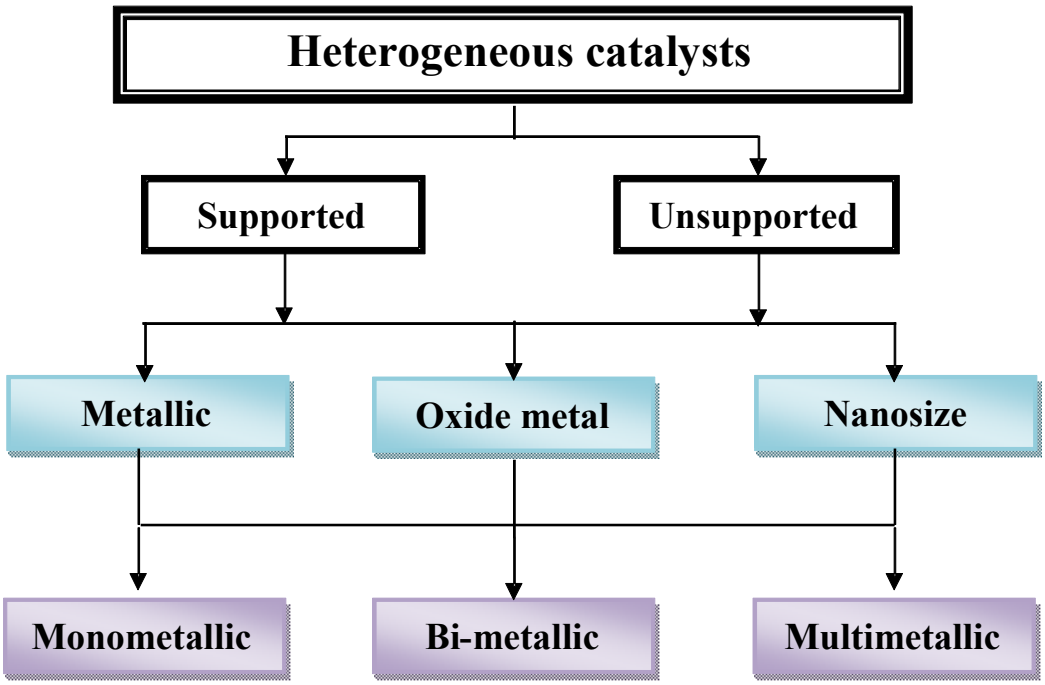

Figure 1.2. Types of heterogeneous catalysts

In case of supported or unsupported metallic catalysts depending on the number of metals involved, they are known as mono, bi- or multimetallic catalysts. Metals typically have high surface free energies, therefore they have a pronounced tendency to reduce their surface areas by particle growth [10]. In most of the cases a metal is dispersed on a suitable support. These supports may also alter the catalytic properties of the active phase which is known as metal-support interaction [11]. Metal oxides consisting of a

metal cation and the oxide anion are commonly used both as catalysts and as supports. The surface of these oxides is often partially occupied by hydroxyl groups, so it possesses some acidic character [12]. However, it is the variation in the oxidation states and the possibility of forming nonstoichiometric compounds that are responsible for their important redox catalytic properties [13].

1.2.1. Bimetallic catalysts:

In late eighties of last century, the use of bimetallics in catalysis significantly increased due to their surface modifications caused by the addition of a second metal leading to better activity and selectivity as compared to the monometallics [6,7]. Sinfelt has made pioneering contributions to the area of bimetallic catalysts and improved the performance of these catalysts and also has attempted to co-relate the catalyst activity with modified electronic structure and surface geometry [14-19**]**. Incorporation of the second metal enhances the catalyst performance by several ways

- Promotes the desired reaction leading to increase in selectivity to the desired product.
- Enhances the stability or prevents the deactivation of the catalyst, which leads to increase in catalyst reusability.
- Active even at mild conditions with respect to temperature, pressure and acidic or basic reaction conditions.

Sinfelt has classified bimetallic catalysts depending on miscibility of two metals as shown in Figure 1.3 [20].

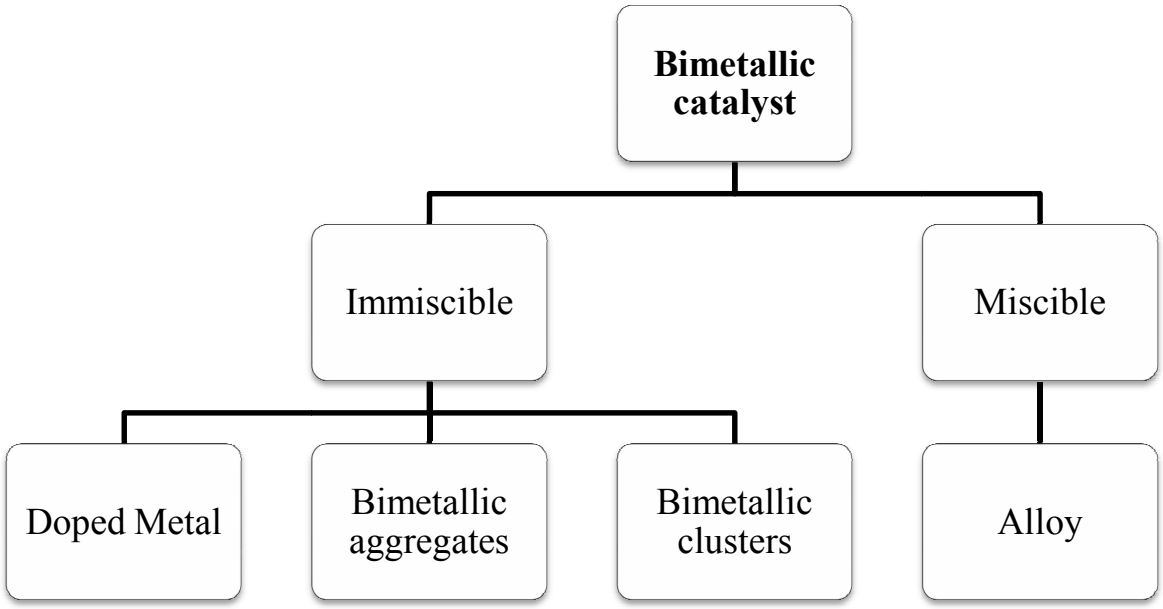

Figure 1.3. Classification of bimetallic catalyst

Immiscible catalysts are classified as (i) doped metal (ii) bimetallic aggregates and, (iii) bimetallic clusters. In doped metal catalyst, the second metal [usually alkali or alkaline earth metal e.g. 1%Pt-Cs /$CaCO_3$] may act as a promoter or a poison to the first metal, which may increase or decrease the rate of reaction [21, 22]. Depending on the content of a second metal and the size of metal group formed, it is further classified as aggregates or clusters. Bimetallic aggregates or clusters can be differentiated on the basis of total content of the second metal and the size of the aggregates [23, 24]. In a bimetallic cluster two metals are smaller than 100 Å and they are commonly in the size range of 10 to 50 Å. The clusters are generally dispersed on support having high surface area and total metal content of the system may be $\leq$ 1 %. In bimetallic aggregates, the concentration of both the metals have near about the equal proportion so that the properties of both metals can be seen.

In miscible bimetallic catalysts, alloys are the solid solutions of two metals, which are miscible with each other in such a way that a completely different species is formed e.g Ni-Cu [22]. It shows different properties from that of monometallic catalysts such as magnetic, electronic and surface properties [19, 21]**.** Generally, these alloys are prepared

by co-precipitating the two metal precursors to form a mixed metal oxide which is then reduced at high temperature.

1.2.2. Nano catalysts:

Metal nanoparticles have become the focus of many researchers over the past decade due to their potential in surface chemistry, catalysis and electronic microdevices [25]. These are near monodispersed particles generally < 10 nm (100 Å) in size having some unique characteristics such as (i) very high surface area, (ii) short range ordering, (iii) enhance interaction with environment, (iv) great variety of valence band electron structure, and (v) self structuring for optimum performance in chemisorption and catalysis [15]. Recently, they have been also exploited as novel catalysts for various reactions such as hydrogenation, hydroformylation, hydration, etc. The variation in adsorption and catalytic behavior of nano size catalysts is due to the change in their surface morphology, which in turn results from the method of preparation [26-29]. Metal nanoparticles can be prepared by physical and chemical methods. In case of physical method, the metal particles aggregates are subdivided mechanically to produce nanoparticles. It has a major drawback of reproducibility of synthesis, which leads to inconsistent catalytic activity [30]. Therefore, chemical methods like reduction of metal salt using reducing reagents like alcohol, hydrogen are well studied and most commonly used.

Stabilization of nanoparticles against aggregation:

Metal nanoparticles are only kinetically stable which needs to be stabilized against agglomeration in to bigger particles close to bulk. Stabilization of metal nanoparticles can be achieved by various methods [31, 32].

There are four types of stabilization

a. Electrostatic stabilization
b. Steric stabilization
c. Stabilization by ligands or a solvent

1.3. Performance criteria of a catalyst :

Three major criteria usually considered to assess the performance of a catalyst are given below [33].

1.3.1. Activity:

Catalyst efficiency can be evaluated by the turn over frequency (TOF).

Turn over frequency (time^{-1}):

It is the ratio of moles of reactant converted per mole of catalyst per unit time.

$$\text{TOF} = \frac{\text{Converted moles of substrate}}{\text{moles of catalyst used x time}} \qquad \text{…..1.1}$$

1.3.2. Selectivity:

Selectivity (S) is expressed by the ratio of the amount of desired product (P) formed to the amount of substrate consumed during the reaction. It also gives information about the possible reaction pathway. In addition to the desired reaction, parallel and sequential reactions can also take place (Figure 1.4). A high selectivity is essential for economical as well as ecological processes.

$$\text{Selectivity} = \frac{\text{moles of desired product}}{\text{converted moles of the reactant}} \qquad \text{…..1.2}$$

Sequential reactions **Parallel reactions**

$A \rightarrow P \rightarrow P_1$

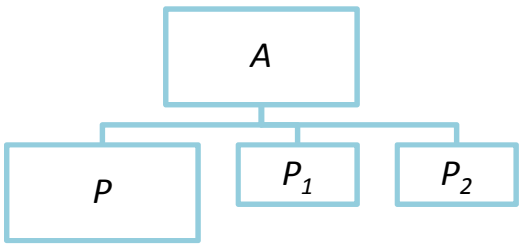

Figure 1.4. Sequential and parallel reactions

Where *A* is reaction starting material

P is desired product

P_1 & P_2 side products

Selectivity in catalysis is one of the most important factors that is influenced by structural, chemical, electronic, kinetic and energy factors [34].

1.3.3. Stability:

Stability of a catalyst is very important issue in any catalytic reaction. Chemical, thermal and mechanical stability of the catalyst determines the lifetime of catalyst. Number of factors including decomposition, coking and poisoning affect the stability of catalyst.

Turn over number:

Catalyst stability can be calculated in terms of turn over number and defined as the ratio of moles of reactant reacted per mol of catalyst.

$$\text{TON} = \frac{\text{Converted moles of substrate}}{\text{moles of catalysts used}} \qquad \text{…..1.3}$$

The TON term specifies the maximum use that can be made of a catalyst for a reaction under defined conditions by a number of molecular reactions or reaction cycles up to the decay of activity.

Suitability of a catalyst can be decided considering the following order of priority.

Selectivity > Stability > Activity

1.4. Major issues in heterogeneous catalysts:

1.4.1. Support:

In case of heterogeneous catalysts, choice of support depends on several factors including chemical nature, morphology, surface area, pore volume, pore size distribution, particle size, corrosion resistance, acidity, impurity levels and ability to give rise to metal-support interaction [9]. Major advantages of a suitable support are given below [35, 36].

- To reduce the amount of expensive active metal loading.

- To generate additional active sites leading to bifunctional catalysis.
- Increase the mechanical resistance of the catalyst composite.
- Stabilize the metal particle size.
- Increase the metal dispersion due to high surface area.

Different types of supports used in catalysis include metal oxides, silica, zeolites, activated carbons, pillered clays, red mud, polymers, carbon black, among which activated carbon, alumina and silica are most commonly used [37]. Metal particles anchored to the support material through bonding may give rise to metal-support effects due to geometric as well as electronic interactions [38, 39].

1.4.2. Metal dispersion:

The term dispersion refers to the ratio of the number of metal atoms on the surface to the total number of metal atoms present [40]. The metal dispersion of a supported catalyst may vary widely, depending on the physical form of the catalysts. The degree of dispersion of a supported metal can be determined by chemisorption technique which involves adsorption of a suitable gas on the active sites of a catalysts [41, 42].

1.4.3. Spillover:

This 'Spillover phenomenon' may occur due to the transport of active species (spillover species) adsorbed or formed on one phase (donar) onto second phase (acceptor), which does not from the active species under the same circumstances [43]. Major spillover phenomena are hydrogen spillover onto supports and metal to metal spillover. In hydrogen spillover, hydrogen atoms migrate from the metal surface to the interstitial volume of the support material known as hydrogen spillover. The catalyst activity is influenced due to the molecular hydrogen adsorbed its dissociation to form the active and transportation via surface diffusion to the catalyst surface to form the active sites for the reaction [44, 45]. A spillover source may be able to activate the adsorbing species. In metal to metal spillover phenomenon, not all metals are in the active form, active metal adsorbs molecular hydrogen on its surface and then spillover takes place onto the surface

that does not adsorb the molecular species directly. In a bimetallic catalyst e.g. Cu:Ru, hydrogen is adsorbed on Ru and then spill over takes place onto the Cu surface. This spillover hydrogen on the Cu then desorbs directly as the temperature is raised [46].

1.4.4. Transport phenomenon in multiphase catalytic system:

Liquid phase hydrogenations employing heterogeneous catalysts are multiple phase systems involving gas (H_2) + liquid (in case of immiscible liquids, liquid-liquid) + solid catalyst. Such a multiphase system usually has concentration and temperature gradients [47].

A general representation of a gas-liquid reaction in presence of a solid catalyst is shown below.

$$\mathbf{A_{(gas)}} + \mathbf{B_{(liquid)}} \xrightarrow{\mathbf{Catalyst\ (Solid)}} \mathbf{Product} \qquad \text{.....1.4}$$

For the reaction to take place in a multi phase catalytic system, the following steps must occur as shown in Figure 1.5. [47, 48].

- Dissolution of a gas (e.g. Hydrogen) into the liquid phase.
- Transport of dissolved gaseous reactant through the bulk liquid to the catalyst particle.
- Transport of the liquid reactants to the surface of catalyst particle
- Diffusion of the reactants into the pore structure of catalyst surface
- Adsorption of reactants on the catalyst, chemical reaction on the surface and desorption of products.
- Diffusion of products from the catalyst.

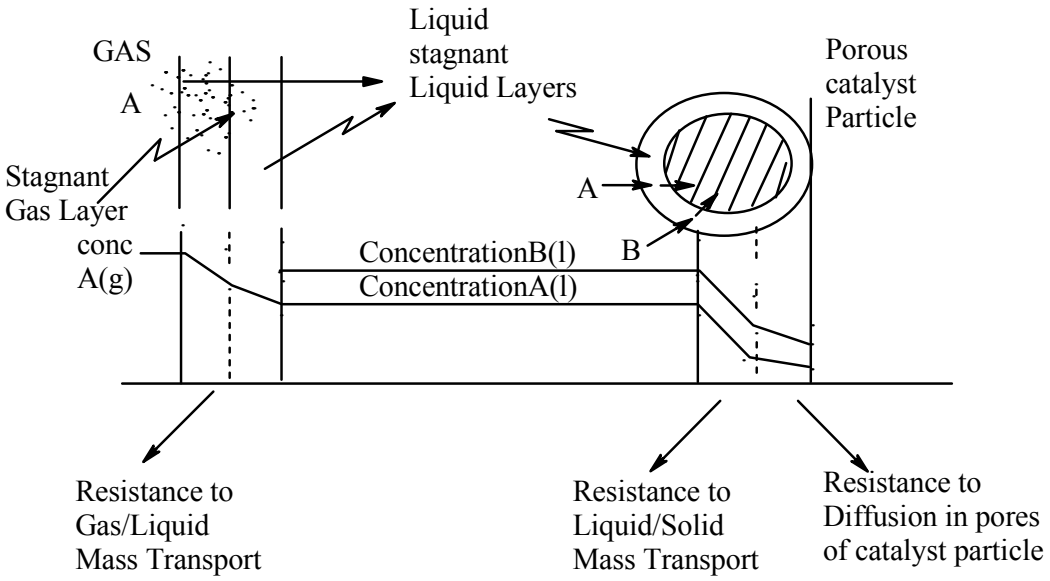

Figure 1.5. Transport mechanism in a multiphase system [49]

One of the above steps can be a rate determining step and it is important to study the above transport phenomenon critically while investigating the kinetics of a solid catalyzed reaction.

1.4.5. Promoter effect:

Promoter is a substance although not catalytically active but when added to a catalyst system improves the performance of the catalyst particularly leading to enhancement in the selectivity of the desired product [50]. The performance improvement could be due to (i) modification in the electronic characteristics of a catalysts (ii) structural changes (iii) inhibition of the growth of catalyst particles and, (iv) protection of the active phase against poisoning [51, 52]**.**

1.5. Catalyst preparation methods:

Solid catalyzed reactions involve the interactions between the substrate molecules on the surface of the active material hence, the most efficient catalysts should have a high population of active centers on the surface exposed to the reaction medium. Very fine

metal particles that have the high ratio of surface to bulk atoms needed for good catalyst activity however, these fine particles easily sinter under reaction conditions. Hence, the most common way of minimizing metal catalyst sintering is to disperse the active metal component over a porous and thermally stable, support [53, 54]. Essentially most of the preparation methods for supported metal catalysts involve two major steps namely, co-precipitation and deposition.

1.5.1. Co–precipitation:

It involves the addition of a precipitating agent to a solution containing both a support precursor and a catalyst precursor. The resulting precipitate contains species, either as single phase or multiple phases, from which the active component and the support material are eventually processed. The initial step in the preparation of a co- precipitated catalyst is the reaction between a solution of two or more metal salts and a base, generally a hydroxide, alkali carbonate or bicarbonate. The resulting precipitate may contain not only the insoluble hydroxides and/ or carbonates but also a mixed metal compound if the solubility equilibria are favorable. Even if the formation of a mixed metal compound is not favorable, some of the support material is usually trapped in the active metal precipitate. This causes formation of large crystals of the active metal compound. Smaller crystals are easier to reduce and generate more finely divided metal particles. One of the problems associated with the preparation of co- precipitated catalysts is formation of vapor liquid interface inside the pores of the solid during drying and calcinations of the precipitated catalyst precursor. Use of solvents with high surface tension e.g. water, resulting a partial collapse of the solid gives low surface area material. This problem can be overcome by using a solvent having surface tension lower than water. Hence, a well known ‘Sol-gel’ method is adapted in which the alcoholic solutions of the active metal and support precursors are used and the precipitation is initiated by addition of stoichiometric amount of water. For example, aq. alchoholic solution of tetraethoxysilane and palladium ammonium chloride with ammonia gives a gelatinous Pd-SiO_2 precipitate which is dried at 353-373 K and then heated to 723 K. This on reduction in H_2 gives a highly dispersed Pd/SiO_2 catalyst. Another commercially used

'Copper-cromite' or Adkins' catalyst is also prepared by co-precipitation method which involves the addition of copper nitrate solution to a solution of ammonium dichromate in ammonia giving a precipitate of copper ammonium dichromate. This precipitate is calcined and washed with acetic acid to give the copper-cromite catalyst.

Another problem associated with the co-precipitation method is relatively large amount of active metal is retained inside the particles of the support and therefore remains unavailable for the reaction. This problem can be overcome by a sequential precipitation procedure.

1.5.2. Deposition:

Deposition is a process in which the active component or precursor is added to a separately prepared carrier or support. This is preferred because (i) during co-precipitation, solid catalyst contains small metal particles trapped throughout the porous oxide support, reducing the effective use of the metal catalyst, (ii) it is difficult to form insitu support with a prescribed surface area and pore structure. Deposition can be accomplished in two ways:

1. Precipitation- deposition:

In this procedure, a precipitating agent is added slowly to a well stirred suspension of a support in a solution of the metal precursor [55]. For example slow addition of sodium hydroxide to a suspension of alumina in a nickel chloride solution gives Ni/ Al_2O_3 catalyst. Alternately, aqueous hydrolysis of urea liberates the base for homogeneous precipitation in an aqueous solution of metal precursor and the support. After isolation, the supported precipitate is washed, dried and calcined to produced supported oxide which is then reduced to give the active hydrogenation catalyst. Precipitation-deposition method is used to produce a variety of commercial catalysts e.g. Nickel on silica, alumina, magnesia, titania, thoria, ceria, and also precious metals like palladium, platinum on carbon etc. [56].

2. Reduction-deposition:

In this procedure, a solution of a metal salt containing the support is treated with reducing agent to give the supported reduced metal catalyst directly. For example, palladium on

carbon is obtained by treating a suspension of carbon in aq. palladium chloride in a reducing atmosphere. Similarly Pt/C catalysts are prepared, however with a small amount of palladium chloride is added to facilitate the complete reduction of chloroplatinic acid [57**].** In a photodeposition procedure the semiconductor support is suspended in a metal salt solution and irradiated with a mercury lamp, e.g. Pt/TiO_2 catalyst in which the small platinum crystallites obtained by photodeposition are uniformly distributed on the titania surface [58]. Other examples include Pt, Pd, Rh, Ag, Ir on supports such as ZnO, Nb_2O_5, ZrO_2, ThO_2 and WO_3 [58**].**

1.5.3. Impregnation:

Impregnation is defined as a means of catalyst preparation by the adsorption of a catalyst precursor salt from solution on to a support material. This is also known as wet-impregnation since, the pores of the support are filled with the solvent before coming in contact with the precursor salt [59]. In this method, an intense interaction between the surface of the support and the salt takes place leading to the adsorption of the salt on to the support due to stirring a suspension of the support in the salt solution for a long duration followed by the separation of the supported catalyst by filtration, centrifugation or evaporation. The supported salt is then calcined and then reduced to the metal. Several types of catalysts are prepared by this method particularly, highly loaded nickel on alumina, titania, silica, niobia and vanadium pentoxide as well as noble metals on various supports.

Major factors affecting the degree of impregnation and metal distribution are

- Solvent used: organic or aqueous
- pH of the solution
- Nature of the metal salt or complex used
- Presence of additives or modifiers

1.5.4. Incipient wetness:

Incipient wetness, also known as dry impregnation or capillary impregnation involves contacting a dry support with only enough solution of the impregnate to fill the pores of

the support [59]. The volume of liquid needed to reach this stage of incipient wetness is usually determined by slowly adding small quantities of the solvent to a well stirred weighed amount of support until the mixture turns slightly liquid. Some of the catalysts prepared commercially by this method include Pt/SiO_2, Pt/Al_2O_3, Ni/C, Ru/ C, Ni/Al_2O_3, Rh/Al_2O_3, Rh/SiO_3 etc. The experimental conditions influence dramatically the dispersion and location of the metal in resulting catalyst. For example, in case of Ni/Al_2O_3 catalysts pH and the weight loading of the metal affect the activity of resulting catalysts [60].

1.5.5. Ion exchange:

In this method, the pH of the impregnating solution must be either sufficiently high or low to provide the appropriate surface potential and the adsorbent must have proper charge. The pH at which the net charge on the support is zero is known as the isoelectric point (IEP) of the material. For a negatively charged surface, cationic species are attracted and get adsorbed. Similarly, negative species get adsorbed on a positive surface. The common cationic and anionic metal complexes used in catalyst preparation are given below in Table 1.3.

Table 1.3. Common cationic and anionic complexes for catalyst preparation [53]

Metal	Anion	Cation
Cobalt		$Co(NH_3)_4^{++}$
Nickel		$Ni(NH_3)_4^{++}$
Copper		$Cu(NH_3)_4^{++}$
Ruthenium		$Ru(NH_3)_5Cl^{++}$
Rhodium	$RhCl_6^{3-}$	$Rh(NH_3)_5Cl^{++}$
Palladium	$Pd\ Cl_4^{3-}$	$Pd(NH_3)_4^{++}$
Silver		$Ag(NH_3)_4^{++}$
Iridium	$IrCl_6^{3-}$	$Ir(NH_3)_5Cl^{++}$
Platinum	$PtCl_6^{2-}$	$Pt(NH_3)_4^{++}$
Gold	$AuCl_4^-$	

1.6. Catalytic hydrogenation:

Several organic transformations such as hydrogenation, oxidation, hydroformylation, hydration, alkylation, reductive amination, acylation, isomerization, carbonylation etc. (Figure 1.6), are being carried out using a variety of catalysts. Among these reactions, hydrogenation is the most studied reaction and is also a core technology used commercially [61, 62]. Therefore, this work is focused on hydrogenation of various functional groups and the following discussion summarizes some important aspects of the hydrogenation reaction.

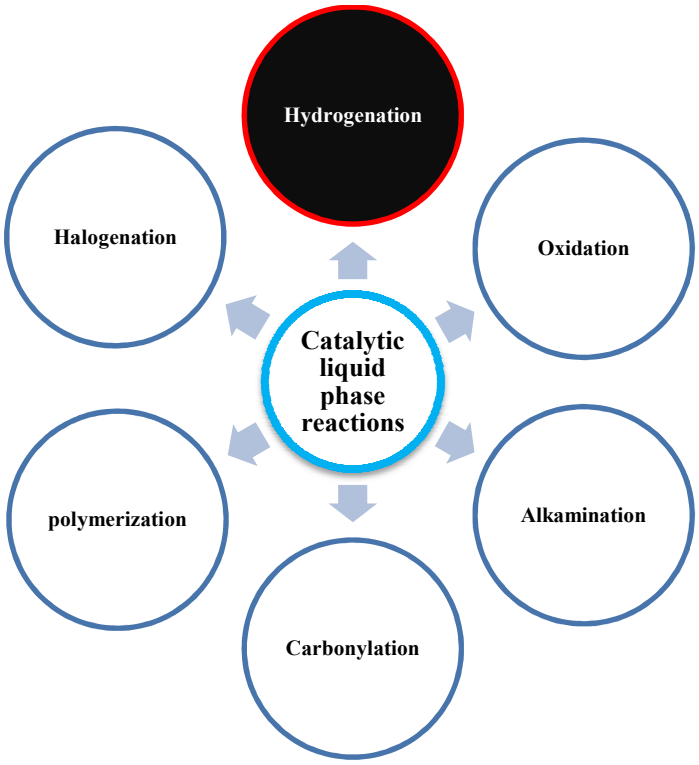

Figure 1.6. Types of catalytic liquid phase reactions

In early days, reduction of organic compounds were carried out by using reducing agents such as sodium borohydride, lithium aluminium hydride, zinc, iron, hydrogen sulfide etc. [62]. Major disadvantages of these methods are:

- Producing stoichiometric amount of organic or inorganic waste (kg of waste/kg of product), which causes serious environmental hazards.
- Reagents cannot be recycled.

- Separation of reagents from the product mixture is difficult.
- Being the multistep processes, rather time consuming and involve tedious work-up, which increase the manufacturing cost.
- Erosion of reactor takes place in case of iron acid reduction method.

These problems can be overcome by catalytic hydrogenation route. Hydrogenation is a process in which the reduction of organic compounds takes place by addition of molecular hydrogen in the presence of a catalyst. The hydrogen is commercially available in molecular form and its reactivity is very low even at high temperature and pressure conditions. Hence, a catalyst is necessary to facilitate the rate of a hydrogenation reaction.

1.6.1. Catalytically active metals for hydrogenation reactions:

Several metals are used for hydrogenation reactions that are summarized Figure 1.7. The choice of a metal depends on several factors but most commonly used hydrogenation catalysts are Raney nickel and noble metals catalysts as shown in dark shade in Figure 1.7. Use of these metals as catalysts in the industrial hydrogenation processes for the production of organic synthesis is shown in Table 1.4.

	VII b	VIII		I b
		Co COBALT	Ni NICKEL	Cu COPPER
	Ru RUTHENIUM	Rh RHODIUM	Pd PALLADIUM	Ag SILVER
Re RHENIUM	Os OSMIUM	Ir IRIDIUM	Pt PLATINUM	Au GOLD

Figure 1.7. Catalytically active metals [63]

Table 1.4. Heterogeneously catalyzed hydrogenation processes [64]

Process or product	Catalyst	Conditions
Methanol synthesis	ZnO-Cr_2O_3	523-673 K, 20-30 MPa
	CuO-ZnO-Cr_2O_3	503-553 K, 6 MPa
Fat hardening	Ni/Cu	423-473 K, 0.5-1.5 MPa
Benzene to cyclohexane	Raney Ni	Liquid phase 473-498 K, 5 MPa
	Noble metals	Gas phase 673 K, 2.5-3 MPa
Aldehydes and ketones to alcohols	Ni, Cu, Pt	373-423 K, 3 MPa
Esters to alcohols	$CuCr_2O_4$	523-573 K, 25-50 MPa
Nitriles to amines	Co or Ni on Al_2O_3	373-473 K, 20-40 MPa

Our work is mainly focused on nickel, platinum and palladium metals [65, 66] which will be discussed further.

1.6.1.1. Nickel:

The temperature at which nickel oxide is reduced by hydrogen greatly affects the activity of the resulting catalyst. There is a considerable temperature difference between the commencement and the completion of the reduction. Reduced nickel oxides are usually more active than completely reduced forms. Supported catalysts may require a higher temperature for activation with hydrogen than unsupported ones. Thus, reduced nickel is usually employed with a support such as Kieselguhr for practical uses. We carried out preparation of nickel catalyst by using impregnation method which involves several steps such as mixing, solvent evaporating, drying, calcination and activation (see Figure 1.8).

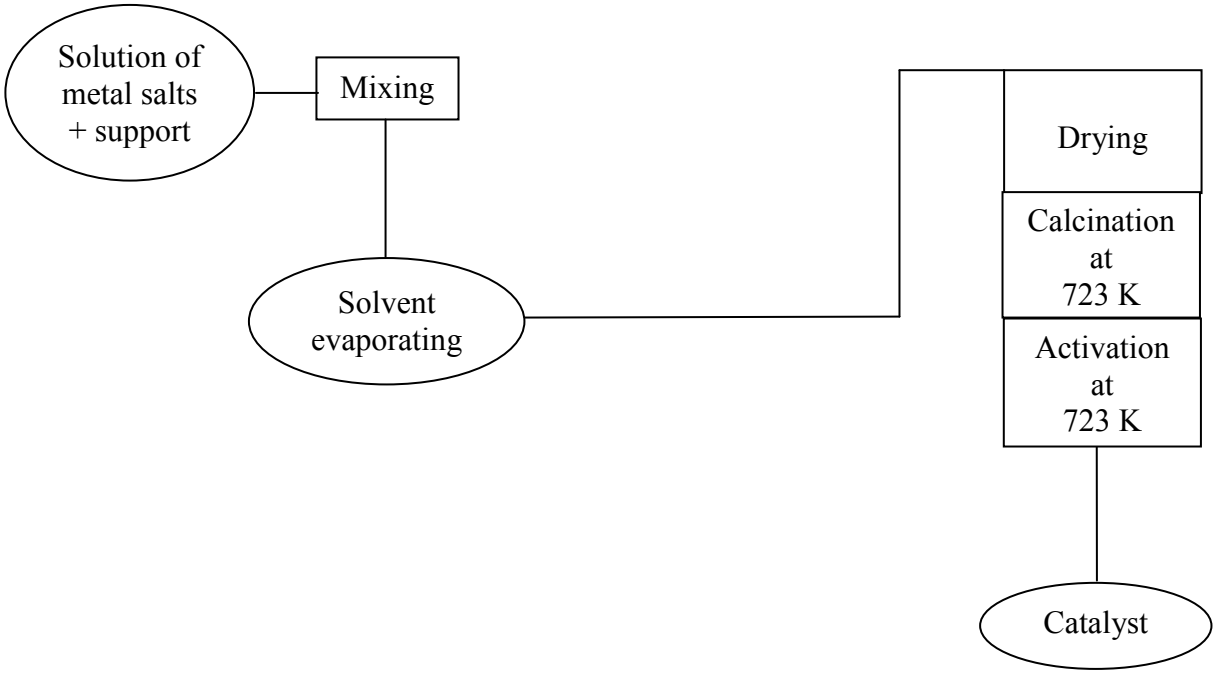

Figure 1.8. Preparation of Ni catalyst by precipitation method [67]

1.6.1.2. Platinum:

Platinum is one of the most capable metal for the hydrogenation of various functional groups under relatively mild conditions of low temperature and pressure. Platinum metal catalysts have been employed either in the form of unsupported fine particles of metal, usually referred to as blacks, or on the inert supports of porous nature. Unsupported catalyst may also be prepared in a colloidal form by liberating metal in the presence of suitable protective additives. The platinum catalyst is prepared by dissolving the chloroplatinic acid in water followed by its reduction usually using formaldehyde at an appropriate pH.

1.6.1.3. Palladium

Palladium is one of the best catalysts for the hydrogenation of acetylenic compound as well as for hydrogenolysis of C-C, C=O, C-X and C≡N bond. Palladium catalyst is prepared by dissolving palladium chloride in water and further treated with hydrochloric acid thus forming chloro palladic acid prior to reduction. Unsupported and supported

palladium catalysts [Pd^0] are also prepared by reduction of palladium salts using variety of reducing agents such as formaldehyde, sodium formate, hydrazine, hydrogen gas, and sodium borohydride etc. The various type of catalysts include palladium black, palladium oxide, Pd-$BaSO_4$, Pd-C, Pd $(OH)_2$- C; lead- poisoned Pd-$CaCO_3$ (Lindlar catalyst).

1.7. Effect of reaction conditions in hydrogenation reactions:

The optimum performance of any hydrogenation process with respect to the conversion and selectivity to the desired product not only depends on type of catalyst but also on the proper choice of process conditions such as catalyst loading, temperature, hydrogen gas pressure, choice of solvent [68] , agitation speed (in case of batch process), concentration of substrate, gas and liquid flow rates (for continuous processes).

1.7.1. Temperature:

According to the Arrhenius Law with increase in temperature the rate of hydrogenation reaction also increases however, it may also lead to the loss of selectivity due to formation of side products at higher temperature. Some other important effects are the catalyst deactivation at higher temperature particularly, in vapor phase hydrogenation and/or (ii) the reactants and products may be thermally sensitive, particularly in case of fine chemicals and pharmaceutical applications [69].

1.7.2. Hydrogen pressure:

In most of the hydrogenations, rate of reaction usually increases with the increase in pressure of the system and the reaction proceeds even with lower catalyst loading. Increase in rate of hydrogenation at higher the pressure is mainly due to the increase H_2 solubility, according to the Henry Law. It states that, at a constant temperature, the solubility of a gas in a liquid is directly proportional to the pressure of that gas above the surface of the solution [70].

$$S = k_H\, p \qquad \text{…..1.5}$$

Where,

S solubility of dissolved gas, Kmol/m^3. MPa

k_H proportionality constant

p partial pressure, MPa

1.7.3. Solvents:

Solvent is usually preferred for its ability to dissolve the reactants and/or reduction product, and it also acts as a heat sink since, most of the hydrogenations are highly exothermic reactions [71]. Most liquids that are stable under hydrogenation conditions and do not deactivate the catalyst can be used as solvents. Carboxylic acids, esters, ethers, amines, hydrocarbons, acetic acid, methanol, ethanol, water can be used as solvents. Solubility of H_2 in solvents commonly used for hydrogenation is shown in Table 1.5.

Table 1.5. Hydrogen solubility in various solvents [72]

Sr. No.	Solvent	H_e constant, (kmol/m^3.MPa)
1	Methanol	0.0423
2	1,4-dioxane	0.0352
3	Hexane	0.0201

1.8. Selectivity in catalytic hydrogenation:

Selectivity is the key issue in any hydrogenation [73] and it is defined as the ratio of amount of desired product formed to the sum of the amounts of all the products formed in a particular reaction [74]. The following types of selectivity patterns are usually observed in hydrogenation reactions: [7]

- Chemo-selectivity
- Regio-selectivity
- Stereo-selectivity

1.8.1. Chemo-selectivity:

Chemo-selectivity is defined as the selective hydrogenation of one functional group in the presence of other groups that can be hydrogenated [73].

e.g.

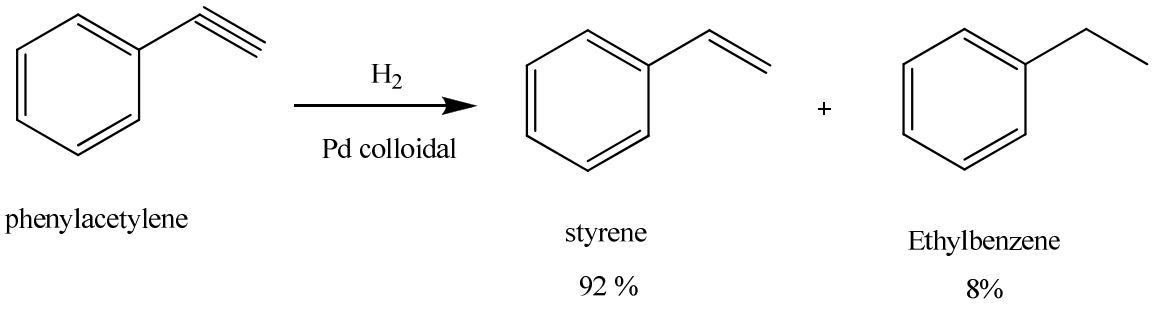

Hydrogenation of phenylacetylene to styrene (Scheme 1.1.)

1.8.2. Regio-selectivity:

The regioselectivity refers to the selective hydrogenation of one functional group in the presence of the same functional group at different positions of the substrate.

e.g.

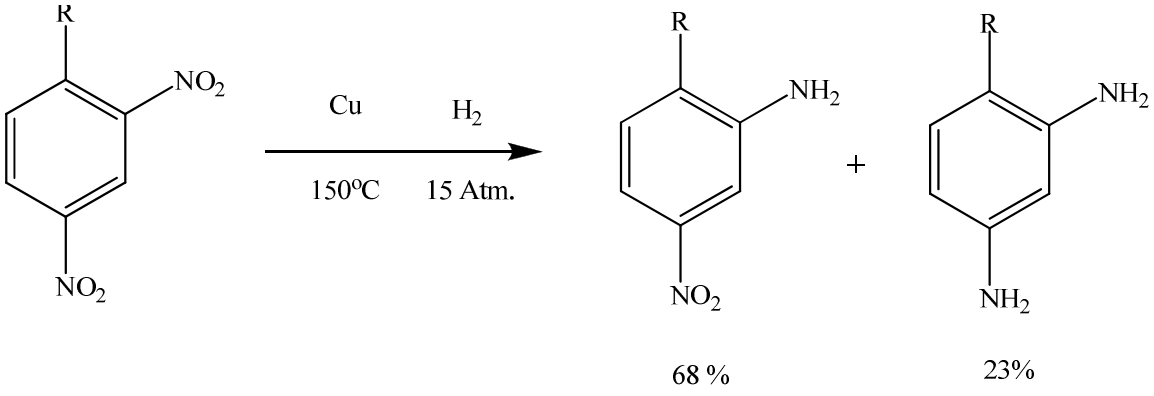

Hydrogenation of 1-substituted-2, 4-dinitrobenzene [75] (Scheme 1.2.).

1.8.3. Stereo-selectivity:

The stereo-selective hydrogenation is the preferential formation of one stereoisomer in presence of another isomer. When the steroisomers are enantiomers**,** the phenomenon is called enantioselectivity.

e.g.

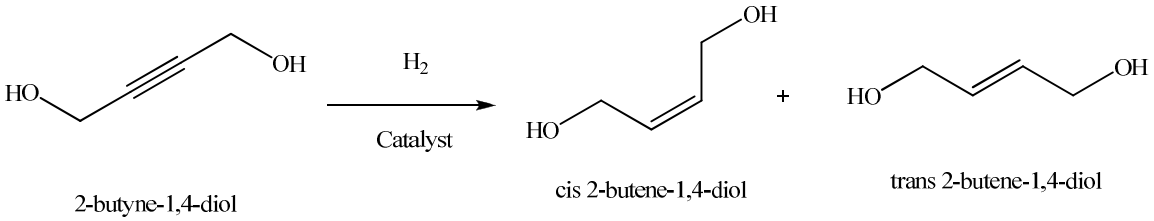

2-butyne-1,4-diol cis 2-butene-1,4-diol trans 2-butene-1,4-diol

Exclusive formation of *cis*- and *trans*-2-butene-1, 4-diol from hydrogenation of 2-butyne-1, 4-diol (Scheme 1.3).

1.9. Types of liquid phase catalytic hydrogenation reactions:

Catalytic hydrogenation of organic compounds possessing a variety of functional groups is the core technology practiced in the chemical industry, as shown Figure 1.9 [76]. In our study, we have focused on hydrogenation reactions of acetylenic compounds and nitroaromatics and the details of these reactions are discussed below.

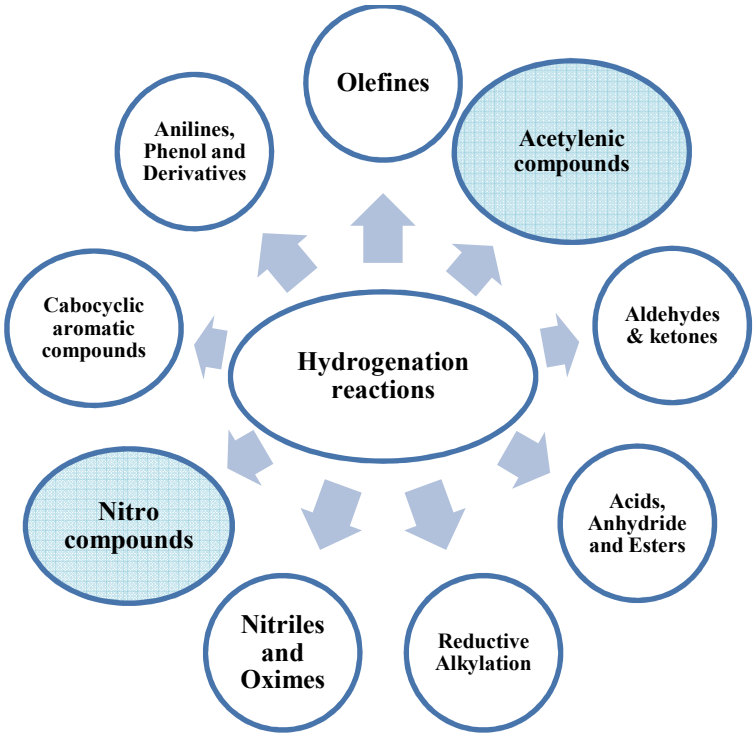

Figure 1.9. Liquid phase catalytic hydrogenation reactions

1.9.1. Hydrogenation of acetylenic compounds:

Selective hydrogenation of the carbon-carbon triple bonds, to the corresponding intermediate olefinic compounds is a challenging problem from both fundamental as well as application point of view [77]. In such processes, the intermediate olefin of the first hydrogenation step readily undergoes further hydrogenation to give a saturated alkane product [78]. However initially, the intermediate olefin has high selectivity until the starting acetylenic substrate is completely consumed. This is because the addition of second mole of hydrogen is often more rapid than of the first one. The acetylenic compounds are strongly adsorbed on the catalysts as compared to the olefins which may prevent their further hydrogenation to the saturated compounds. Nevertheless, complete selectivity to the olefinic compounds has been attempted by blocking the second stage hydrogenation even after starting acetylenic compound has been consumed completely. [79]. There are several catalysts reported for hydrogenation of acetylenic compounds, where Pd metal showed the higher activity as compared to other metals and the order of

reactivity of different metals is: Pd >>Rh ≥ Pt > Ru >> Ir > Os. In case of Pd, selectivity is independent of conversion while in case of Ir metal the selectivity gets decreased with increasing conversion [80]. The general mechanistic pathway for catalytic hydrogenation of acetylenic compounds is shown in Scheme 1.4. The hydrogenation of acetylenic compound involves the adsorption of acetylene and hydrogen on the catalyst surface and chemical reaction between the adsorbed species, and desorption of the products from the catalyst surface. Hydrogen atom chemisorbed on the metal surface reacts with simultaneously adsorbed π system of acetylene compound to give the intermediate olefin compound [81].

Step 1 Hydrogen molecule adsorbs to the surface of catalyst

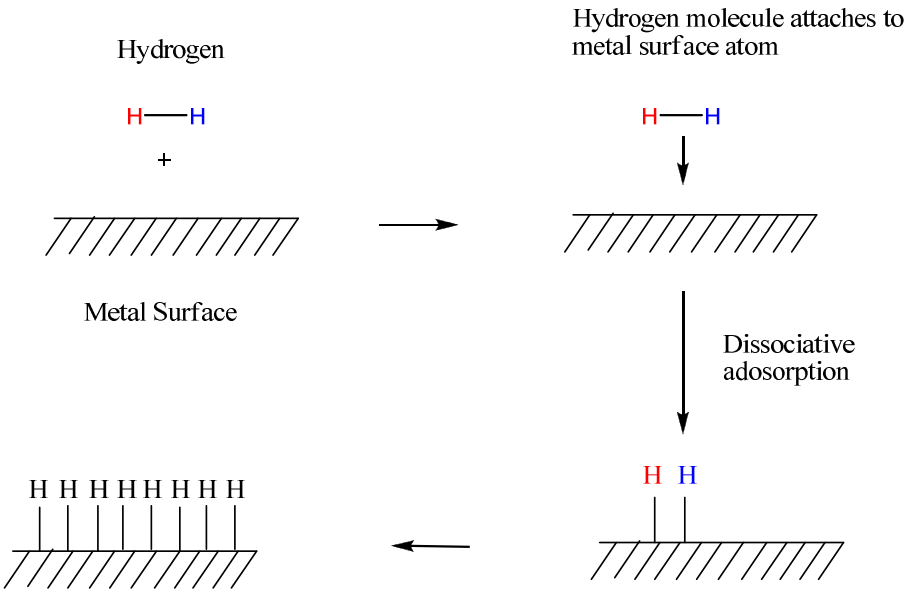

Step II

π system of acetylene compound adsorbs on to the surface of catalyst

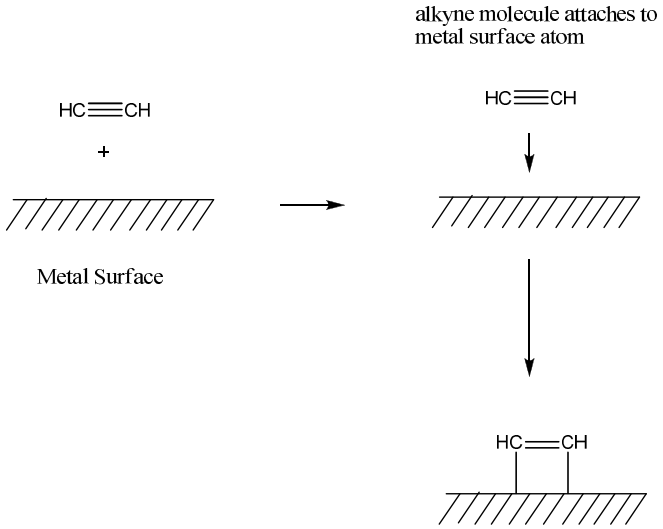

Step III

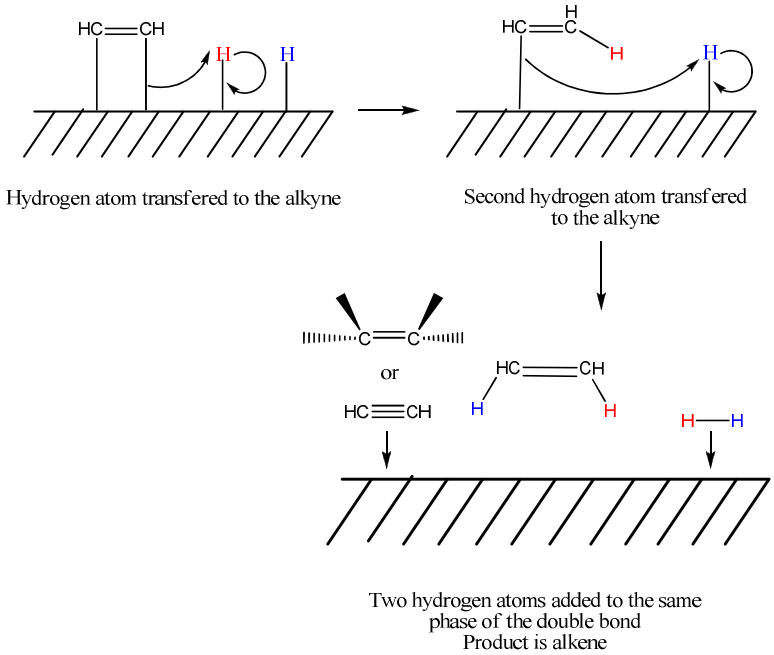

Scheme 1.4. Mechanistic pathway for catalytic hydrogenation of acetylenic compounds

In our work, we have studied catalytic hydrogenation of 2-butyne-1,4-diol and phenylacetylene to achieve the highest selectivity to intermediate olefinic compounds, 2-butene-1,4-diol and styrene respectively. We studied various catalyst systems such as $Pt/CaCO_3$, supported nano Pd catalyst and Pd/CNTs for the hydrogenation of butyene diol. Continuous hydrogenation of 2-butyne-1,4-diol was also investigated using 1% $Pt/CaCO_3$ catalyst in a fixed bed reactor. It was found that the selectivity pattern was completely different from that found in the case of batch slurry reactor and by varying the contact time, the selectivity to both butene- and butanediols could be varied over a wide range of conditions. Stable supported Pd nano catalysts showed several folds higher activity and selectivity and stability compared with the bulk Pd catalyst in a batch slurry reactor. Colloidal Pd nano catalyst developed for the hydrogenation of phenylacetylene, showed completely different selectivity pattern under atmospheric conditions.

1.9.2. Hydrogenation of nitroaromatics:

Catalytic hydrogenation of aromatic nitrocompounds is commonly practiced in industry for the production of the corresponding amino compounds [82, 83]. Aromatic amines are widely used as dye intermediates especially for azo dyes, pigments, and optical brighteners, as intermediates for photographic chemicals, pharmaceuticals and agricultural chemicals, antioxidents [84]. Since, these reactions are highly exothermic (493 KJ. mol^{-1} for nitrobenzene hydrogenation to aniline), care must be taken to prevent the reaction from becoming too violent. A general reaction pathway for hydrogenation of aromatic nitro compounds is shown in Scheme 1.5. [85]. This involves, initial hydrogenation of nitroaromatic compound which gives arylnitroso and arylhydroxylamine as an intermediate compound which undergoes further hydrogenation to get the corresponding aniline. Another route is the coupling reaction of these intermediate (arylnitroso, arylhydroxylamine) leading to the formation of the dimeric azo and azoxy compounds and its hydrogenation product, arylhydrazo compound. Finally, corresponding aniline is achieved by reduction of hydrazo compound [85].

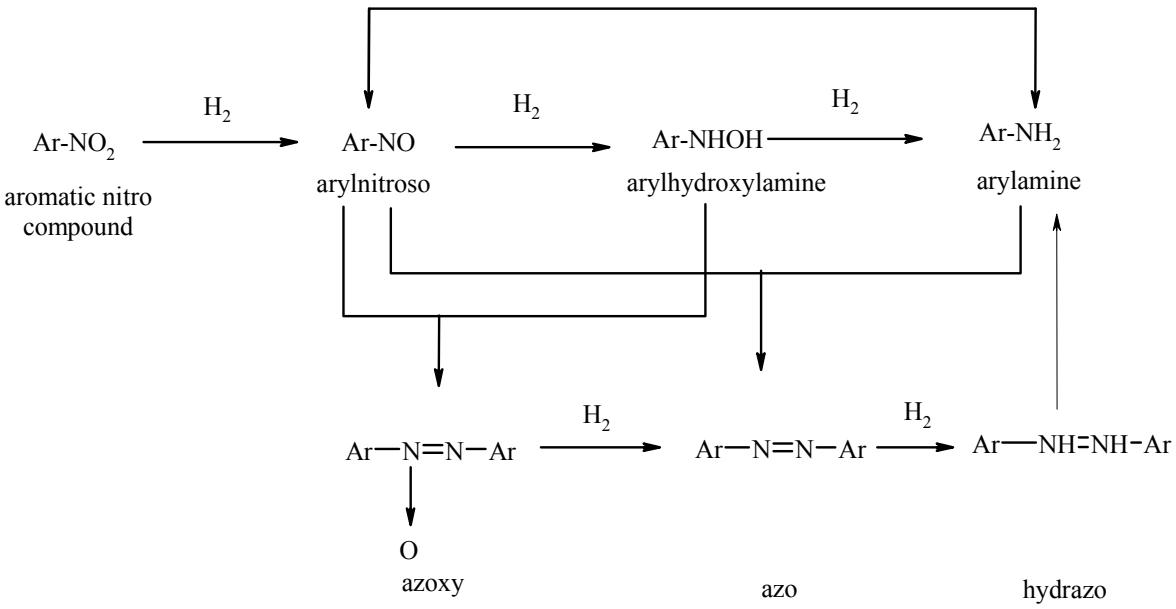

Scheme 1.5. Reaction pathway for hydrogenation of aromatic nitro compounds

In our work, we have studied the hydrogenation of nitrobenzene, *m*-chlronitrobenzene using supported Pt catalyst to achieve the highest selectivity to *p*-aminophenol and *m*-chlroaniline respectively. In case of hydrogenation of nitrobenzene to *p*-aminophenol, we studied two step separately viz. (i) partial hydrogenation of NB to PHA, and (ii) acid catalyzed rearrangement of PHA to PAP under mild reaction conditions. We found that rearrangement of PHA in an inert atmosphere gave a higher selectivity to PAP. The catalytic hydrogenation of nitrobenzene using 3% Pt/C catalyst at 303 K showed 95% selectivity to PHA at 36 % conversion of nitrobenzene which decreased to 75% for complete conversion of nitrobenzene due to the formation of aniline as a byproduct. It was found that process step of neutralization of the reaction crude at low temperature helps to achieve the highest selectivity to *p*-aminophenol (75% isolated yield of PAP) in a single step synthesis of *p*-aminophenol from nitrobenzene. In case of hydrogenation of *m*-chloronitrobenzene to *m*-chloroaniline, we found that sodium carbonate reduces the extent of dehalogenation. It was also found that the Ni-Pt bimetallic catalysts showed high activity and almost complete selectivity (> 99%) towards *m*-chloroaniline as compared with Ni monometallic catalysts.

1.10. Objectives of the thesis:

The thesis contains total 7 chapters among which the first two chapters include general introduction including objectives and experimental techniques respectively. The scientific results are then divided in two parts viz. Part I dealing with selective hydrogenation of acetylenic compounds and Part II contains hydrogenation of nitroaromatic compounds. The objectives of this thesis are given below.

- Preparation of colloidal, bulk and nano structured supported mono, and bi-metallic catalysts involving various transition metals such as Ni, Pd, Pt.
- Physico-chemical characterization of the prepared catalysts by various techniques such as powder X-ray diffraction, SEM, EDAX, BET surface area, Raman, FT-IR, Chemisorption, XPS.
- Standardization of analytical methods for the model reaction systems investigated using GC and HPLC.
- Activity testing of the prepared catalysts for selective hydrogenation of 2-butyne-1,4-diol, phenylacetylene, nitrobenzene and *m*-chloronitrobenzene, in high pressure batch and continuous reactors.
- To study the kinetics of formation and further rearrangement of an intermediate phenylhydroxylamine in hydrogenation of nitrobenzene to *p*-aminophenol.
- To study the role of additives on extent of dehalogenation in hydrogenation of *m*-chloronitrobenzene to *m*-chloroaniline
- Optimization of reaction parameters such as temperature, pressure, catalyst and substrate loading in order to achieve highest conversion and selectivity, for all the hydrogenation reaction studied in this work.
- To correlate the observed activity and selectivity patterns with the catalyst characterization data.

1.11. References:

1. (a) J. Weitkamp, R. Glaser In *Katalyse: Winnacker and Kuchler, Chemische Technik-Prozesse und Produkte.* Wiley-VCH, (2004); (b) M. Barteau, S. Benkovic, C. Brooks, T. Bruice, C. Campbell *Catal. Lett.* 76 (3-4) (2001) 111.
2. Frost, Sullivan in *Advacced catalysts-Global overview of Technological Developments*, D282 (2004).
3. R. A. Sheldon *J. Mol. Catal. A: Chem* 107 (1996) 75.
4. R.A. Sheldon *Chem. Ind*. (1997) 12.
5. R. A. Sheldon *Chem Ind.* (1992) 903.
6. M. Boudart in *Perspectives in catalysis*, J. M. Thomas, K. I. Zamaraev (Ed) Blackwell, Oxford, (1992) pp.183.
7. F. Cavani, F. Trifiro *Cat. Today* 34 (1997) 269.
8. R. L. Augustine in *Heterogeneous Catalysis for the Synthetic chemist, Supported Metals,* Marcel Dekker, New York (1996).
9. R. J. McNair in *Catalysis of organic reactions,* M. G. Scaros, M. L. Prunier (Ed), Marcel Dekker, New York, (1995) pp 2.
10. M. Bowker *Nature materials* 1 (2002) 205.
11. A. J. Tauster *Acc. Chem. Res.* 20 (1987) 389.
12. R. L. Augustine in *Heterogeneous Catalysis for the Synthetic chemist, Supported Metals,* Marcel Dekker, New York (1996) pp. 179.
13. H. K. Knozinger in *Ullmans encyclopedia of heterogeneous catalysis: Heterogeneous catalysis and solid catalyst,* VCH, Weinheim Vol. A 5.
14. J. H. Sinfelt, A. E. Barnett, G, W. Dembinski *US Pat. 3442973* (1969).
15. J. H. Sinfelt, A. E. Barnett, J. L. Carter *US Pat. 3769201* (1973).
16. J. H. Sinfelt, *Adv. Chem. Eng*. 5 (1964) 37.
17. J. H. Sinfelt, A. E. Barnett, J. L. Carter *US Pat. 3617518* (1971).
18. J. H. Sinfelt in *Catalytic reforming of hydrocarbons:Catalysis-Science and Technology,* J. R. Anderson, M. Boudart (Ed) Vol. 1 Berlin, Heidelberg, Springer-Verlag (1981) pp.257.
19. J. H. Sinfelt, J. H. Carter, D. J. C. Yates *J. Catal.* 24 (1972) 283.

20. J. H. Sinfelt in *Bimetallic catalysts : Discoveries, concepts and applications*, John Wiley & sons, New York (1983).
21. L. Guczi, Z. Schay *Stud. Surf. Sci. Catal.* 27 (1986) 313.
22. J. H. Sinfelt *Acc. Chem. Res.* 10 (1977) 15.
23. J. H. Sinfelt *Catal. Rev.* 9 (1) (1974) 147.
24. J. H. Sinfelt *J. Catal* 29 (1973) 308.
25. G. Schmid (Ed.) in *Clusters and colloids – from theory to applications,* Chapter 6, VCH, Weinheim, (1994).
26. T. S. Armadi, Z. L. Wang, T. C. Green, A. Henglein, M. A. El-Sayed *Science* 272 (1996) 1924.
27. S. Chen, K. Huang, J.A. Stearns *Chem. Mater.* 12 (2000) 540.
28. C. M. Shen, Y. K. Su, H. T. Yang, T. Z. Yang, H. G. Gao *Chem. Phys. Lett.* 373 (2003) 39.
29. M. M. Telkar, C. V. Rode, R. V. Chaudhari, S. S. Joshi, A. M. Nalawade *Appl. Catal A: General* 273 (2004) 11.
30. A. T. Bell *Science* 299 (2003) 1688.
31. A. Roucoux, J. Schulz, H. Patin *Chem. Rev.* 102 (2002) 3757.
32. J. D. Aiken III, R. G. Finke *J. Mol. Catal. A: Chem.* 145 (1999) 1.
33. J. Hagen in *Industrial catalysis: a practical approach,* Wiley-VCH, Weinheim, (1999) pp. 4.
34. M. E. Devis; S. L. Suib (Ed) *Selectivity in catalysis*, American chemical society, Washington, (1993) pp 1.
35. F. Cavani, F. Trifiro *Cat. Today* 34 (1997) 269.
36. G. C. Bond, R. Burch *Catalysis* 6 (1983) 27.
37. S. J. Tauster, S. C. Fung. R. T. K. Baker, J. A. Horsley *Science* 211 (1981) 1121.
38. R. L. Augustine in *Heterogeneous Catalysis for the Synthetic chemist catalyst supports,* Marcel Dekker, New York, (1995) pp.169.
39. J. H. Sinfelt *Science* 195 (1977) 641.
40. J. E. Benson, M. Boudart *J. Catal.* 4 (1965) 704.
41. J. H. Sinfelt, W. F. Taylor, D. J. C. Yates *J. Phys. Chem*. 69 (1965) 95.

42. L. Spenadel, M. Boudart *J. Phys. Chem.* 64 (1960) 204.
43. W. C. Conner, G. M. Pajonk, S. J. Teichner *Adv. Catal.* 34 (1986) 55.
44. W. C. Conner, J. L. Falconer *Chem. Rev.* 95 (1995) 759.
45. G. A. Somorjai *J. Phys. Chem.* 94 (1990) 1013.
46. (a) J. T. Yates Jr., C. H. F. Penden, D. W. Goodman, *J. Catal*. 94 (1985) 576; (b) D. W. Goodman, C. H. F. Penden *J. Catal.* 95 (1985) 321.
47. R. J. McNair in *Catalysis of organic reactions*, M. G. Scaros, M. L. Prunier (Ed), Marcel Dekker, New York, 1995 pp 4.
48. J. Hagen in *Industrial Catalysis: A practical approach,* Wiley-VCH, Weinheim, 1999 pp. 83.
49. E. Santcesaria *Catal. Today* 34 (1997) 411
50. M. Freifelder in *Practical catalytic hydrogenation techniques and applications*, Wiley-Interscience, New York, (1971) pp. 57.
51. J. Hagen in *Industrial catalysis: a practical approach*, Wiley-VCH, Weinheim, (1999) pp. 174.
52. I. Chorkendorff, J. M. Niemantsverdriet in *Concepts of modern catalysis and kinetics,* Wiley-VCH, Weinheim (2003) pp 335.
53. R. L. Augustine in *Heterogeneous Catalysis for the Synthetic chemist, Supported Metals,* Marcel Dekker, New York (1996) pp. 267.
54. C. Perego, P. Villa *Catal. Today* 34 (1997) 281.
55. L. A. M. Harmans, J. W. Geus. *Stud. Sur. Sci. Catal* 3 (1979) 113.
56. P. Turlier, H. Praliaud, P. Moral, G. A. Martin, J. A. Dalmon *Appl. Catal.* 19 (1985) 286.
57. R. Baltzly *J. Am. Chem. Soc.* 74 (1952) 4586.
58. B. Kraeutler, A. J. Bard *J. Am. Chem. Soc* 100 (1978) 4317.
59. S. -Y. Lee, R. Aris *Catal. Rev.* 27 (1985) 207.
60. M. Domingo-Gracia, L. Vincente-Gutierrez, C. Moreno-Castilla *React. Kinet. Catal. Lett.* 43 (1991) 93.
61. M. Freifelder in *Practical catalytic hydrogenation techniques and applications*, Wiley-Interscience, New York, (1971).

62. M. Hudlicky in *Reductions in organic chemistry*, Publisher- John Wiley & Sons., New York (1984).
63. R. L. Augustine in *Heterogeneous Catalysis for the Synthetic chemist,* Marcel Dekker, New York (1996) pp. 213.
64. *Ullmans encyclopedia of industrial chemistry* VCH, Weinheim Vol A 5 pp 340.
65. M. Freifelder in *Practical catalytic hydrogenation techniques and applications*, Wiley-Interscience, New York, (1971) pp. 5.
66. R. L. Augustine in *Heterogeneous Catalysis for the Synthetic chemist,* Marcel Dekker, New York (1996) pp. 153.
67. D. R. Goodman in *Catalyst handbook*, 2nd edition, M. V. Twigg (Ed) Manson, England (1996) pp. 162.
68. J. Hagen in *Industrial Catalysis: a practical approach,* Wiley-VCH, Weinheim, (1999) pp. 208.
69. R. L. Augustine in *Catalytic hydrogenation: Techniques and application in organic synthesis,* Marcel Dekker Inc, New York (1965) pp 67.
70. P. V. Danckwerts in *Gas-liquid reaction,* McGraw-Hill, New York pp 17.
71. M. Freifelder in *Practical catalytic hydrogenation techniques and applications*, Wiley-Interscience, New York, (1971) pp. 78.
72. B. Erwin *J. Chem. Eng. Data*. 30 (1985) 269.
73. R. L. Augustine in *Heterogeneous Catalysis for the Synthetic chemist,* Marcel Dekker, New York (1996) pp. 315.
74. C. N. Satterfiled in *Heterogeneous catalysis in practice* McGraw-Hill, New York (1980) pp. 9
75. W. H. Jones, W. F. Benning, P. Davis, D. M. Mulvey. P. I. Pollok, J. C. Schaeffer, R. Tull, L. M. Weinstock *Ann. N. Y. Acad. Sci.* 158 (1969) 471.
76. R. L. Augustine in *Catalytic hydrogenation: Techniques and application in organic synthesis,* Marcel Dekker, Inc New York (1965).
77. C. V. *Rode J. Jap. Petro. Inst*. 51 (2008) 119.
78. P. N Rylander in *Catalytic hydrogenation over platinum metals,* Academic press: New York, (1967) pp. 59.

79. S. Nishimura in *Handbook of heterogeneous catalysis of organic reactions: Hydrogenation of alkynes,* Wiley-Interscience, New York (2001) pp. 148.
80. G. C. Bond. P. B. Wells. *Adv. Catal.* 15 (1965) 91.
81. G. F. Hennion, W. A. Schroeder, R. P. Lu, W. B. Scanlon, *J. Org. Chem*. 21 (1956) 1142.
82. A. M. Stratz in *Catalysis in organic reactions: Chemical Industries series,* CRC Press 18 (1984) 335.
83. R. S. Downing, P. J. Kunkeler, H. van Bekkum *Catal. Today*. 37 (1997) 121.
84. G. Booth in *Ullman's encyclopedia of chemical technology: nitro compounds, aromatics,* Vol. A 17, Wiley-VCH, (2000) pp 411.
85. A. M. Stratz in *Catalysis of Organic Reactions*; Kosak, J. R. (Ed). Marcel Dekker; New York (1984) pp. 335.

Chapter II

Experimental and characterization techniques

2.1. Materials:

Nitrobenzene, aniline, polyvinylpyrollidone, formaldehyde, sodium hydroxide, ethanol, HCl, dimethyl sulfoxide were purchased from S.d. fine chemicals, India. Methanol (HPLC), methanol (LR), 2-butyne-1,4-diol, and charcoal were obtained from Merck, India. *p*-Aminophenol, $Ni(NO_3)_2$, $PtCl_4$, $PdCl_2$, 4-chloronitrobenzene, 2-chloronitrobenzene, 3-chloronitrobenezene, 2-chloroaniline, 3-chloroaniline, 4-chloroaniline, phenylacetylene, ethylbenzene, styrene, 2-butene-1,4-diol and butane-1,4-diol were purchased from Sigma-Aldrich, Banglore, India. Distilled water was deionized by using Millipore (Mili-Q) water system. High purity grade nitrogen and hydrogen cylinders used for the hydrogenation reactions were procured from M/s. Inox Ltd. Mumbai.

2.2. Catalyst preparation:

Various catalysts were used for hydrogenation reactions and the details of catalyst preparation are given below. A schematic of the experimental setup used for the catalyst preparation is shown in Figure 2.1.

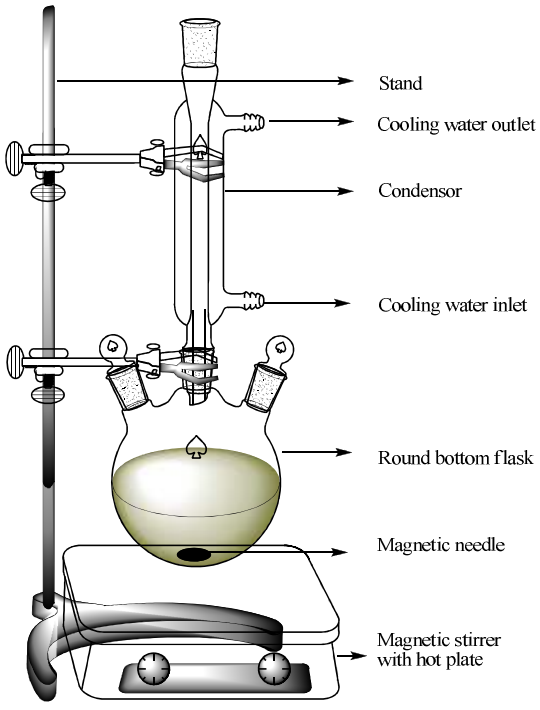

Figure 2.1. General setup for catalyst preparation

2.2.1. 1% Pt/$CaCO_3$ catalyst:

For the preparation of 1%Pt/$CaCO_3$ catalyst, 0.166 g of $PtCl_4$ was completely dissolved in minimum amount of water by adding a small quantity of HCl. Under stirring, already prepared slurry of 10 g $CaCO_3$ was added to the above solution and temperature was maintained at 353 K. After 1h, formaldehyde was also added under stirring. Then the reaction mixture was cooled, filtered to obtain the catalyst, which was then dried at room temperature under vacuum. The powdered catalyst was then pelletized in the form of pellets of 4-mm diameter to be used in the fixed bed reactor for the hydrogenation of 2-butyne-1,4-diol.

2.2.2. 1% Pt/C catalyst:

For the purpose of preparing Pt/C catalyst first, the charcoal support was activated by an acid treatment. In a typical procedure, 10 g of charcoal was refluxed with 100 mL 10% HNO_3 for 6 h, under magnetic stirring. After filtration through Whatman filter paper, it was then washed several times with distilled water till the pH of the filtrate became ~7. This activated charcoal was then dried in an oven for 12 h, at 373 K.

For the preparation of 1% Pt/C catalyst, 0.053 g of $H_2PtCl_4.6H_2O$ was completely dissolved in minimum amount of water. Under stirring, already prepared slurry of 2 g activated carbon was added to the above solution, and the temperature was maintained at 353 K. After stirring for 1 h, formaldehyde was added. Then the reaction mixture was cooled to room temperature and then filtered to obtain 1% Pt/C catalyst which was dried at room temperature under vacuum. Similarly 2, 3 and 5% Pt supported on carbon catalysts were prepared using the procedure described above.

2.2.3. Supported bulk Pd catalyst:

For the preparation of 0.25 % Pd/C catalyst, 0.0083 g of $PdCl_2$ was completely dissolved in minimum amount of water. Under stirring, already prepared slurry of 2 g carbon was added to the above solution and the temperature was maintained to 353 K. After stirring for 1 h, formaldehyde was added. Then the reaction mixture was cooled to room temperature and then filtered to obtain the reduced catalyst. After the filtration, catalyst

was dried at room temperature under vacuum. Similarly, Pd catalyst supported on alumina, silica and calcium carbonate were prepared.

2.2.4. Colloidal Pd catalyst:

0.343 g of polymer polyvinylpyrrolidone (PVP) was added to 15 ml of H_2PdCl_4 solution (prepared by addition of 0.0083 g of $PdCl_2$ to a mixture of 13 ml of water and 2 mL of 0.2M HCl). To this solution, 30 mL of mixture of ethanol:water (30:70) was added. The initial pH of the solution was found to be 3 which was adjusted to pH 7 by adding slowly 10% (w/w) NaOH. This solution was diluted to 100 mL by adding a mixture of ethanol:water and refluxed in a 250 mL flask at 353 K for 3 h. After 3 h, the color changed to dark brown to form polymer protected Pd nanoparticles.

2.2.5. Supported nano Pd catalyst:

First the colloidal Pd catalyst was prepared as per the procedure given in section 2.2.4. For depositing the colloidal Pd on to the support, activated carbon (2 g) was added to the above solution under stirring for 16 h, after which the solid catalyst was separated by filtration. In a similar way, Pd nanoparticles supported on alumina, silica and calcium carbonate were prepared.

2.2.6. Pd supported on CNT catalyst:

In order to prepare Pd/CNT catalyst, first the multiwalled CNTs were grown on MgO-supported, Fe-Mo powder catalyst by thermal decomposition of methane in a quartz tubular furnace (Firstnano-ET2000, USA). Typically, 100 mg of the catalyst on a quartz plate was placed into the center of the quartz tube and furnace was heated to 1223 K in an argon flow of 1000 sccm. The reaction began as Ar was replaced by a mixture of CH_4 (1000 sccm) and H_2 (200 sccm). After 30 minutes, the flow was switched to Ar again to cool the furnace to ambient temperature. The synthesized CNTs were purified by acid treatment with 3-4 N aqueous solution of HNO_3. Further the CNTs were magnetically stirred at room temperature for 6 h, filtered through Whatman 200 nm, 47 mm diameter PTFE membrane and then washed several times with de-ionized water till the pH reached close to 7. The purified sample of CNTs was then dried in air at room temperature. The

sample was then heated at 773 K in H_2 atmosphere to remove the amorphous carbon and graphitic nanoparticles. The purified CNTs were treated with a mixture of HNO_3 and H_2SO_4 at 353 K for a period of 24 h. The acid treated CNTs were again filtered through the Whatman PTFE membrane and washed with de-ionized water till the pH reached close to 7 and then vacuum dried at room temperature.

The stock solution of $PdCl_2$ was prepared by first dissolving 0.0167 g of $PdCl_2$ in aqueous hydrochloric acid (26% v/v) under stirring at 353 K. After complete dissolution of $PdCl_2$, the solution was cooled to room temperature and then diluted to 100 mL by adding distilled water. 7.5 mL stock solution of $PdCl_2$ was then sonicated with 15 mg of CNT sample for 1 h. After 1 h, $NaBH_4$ (reducing agent) was added slowly until the solution became colourless and the catalyst was filtered and dried at 353 K for 3 h.

2.2.7. Supported Ni catalysts:

The monometallic nickel catalyst was prepared by an impregnation method. Slurry of 10 g of activated carbon was made in distilled water. To this hot slurry, a solution of $Ni(NO_3)_2.6H_2O$ (4.95 g dissolved in 10 mL of water) was added. After stirring for 6 h, water was removed under vacuum using a rotary evaporator to obtain a solid cake. This solid was dried overnight at 383 K and calcined in a static air furnace at 723 K for 10 h. The reduction of the catalyst was carried out in an electric furnace using silica quartz tube at 723 K and at H_2 flow rate of 5×10^{-5} m^3/min for 5 h. The catalyst was cooled under nitrogen flow of 3×10^{-5} m^3/min. In a similar way, Ni catalyst supported on alumina was prepared.

2.2.8. Ni-Pt bimetallic catalyst:

A bimetallic Ni-Pt/C catalyst was prepared by addition of chloroplanic acid ($H_2PtCl_4.6H_2O$) to the already prepared Ni/C catalyst (see section 2.2.7). This suspension was refluxed for 4 h and then formaldehyde was added as a reducing agent. This solution was stirred further for 2 h and then filtered to give bimetallic Ni-Pt/C catalyst.

2.3. Physiochemical characterization of catalysts:

The prepared catalyst samples were characterized by various physico-chemical methods such as BET surface area analyzer, X-ray diffraction analysis, Raman spectroscopy, infrared spectroscopy, SEM, TEM, XPS and H_2 pulse titration. This section of chapter 2 gives a brief account of the theory and principles of various characterization techniques used for the current study. The procedure for each experimental technique is described. Characterization results are discussed in the relevant chapters.

2.3.1. Surface area measurement:

The Brunauer-Emmett-Teller (BET) is the most widely acceptable method for analyzing multilayer physisorption isotherms of inert gases to determine the surface area of solids and the distribution of mesopore size in these solids [1].

Surface area is calculated by comparing the integrator count due to desorption with that form the calibration signal the mass, W, adsorbed is given by equation (2.1)

$$W = \frac{A}{A_{cal}} V_{cal} \frac{P_a M}{RT} \qquad \text{…..2.1}$$

Where,

W	mass of adsorbate adsorbed on the sample
V_{cal}	calibration volume (cm^3)
A	sample integrator counts
A_{cal}	calibration integrator counts
P_a	ambient pressure
M	adsorbate molecular weight (28 for N_2)
T	temperature in K
R	gas constant (82.06 $cm^3.atm.K^{-1}.mol^{-1}$)

The BET equation (2.2) yields a straight line when $1/W(P_0/P - 1))$ is plotted versus P/P_0. The slope, $(C - 1)/W_m C$, and the intercept, $1/W_m C$, are used to determine the weight adsorbed at the monolayer.

$$\frac{1}{W(P_0/P-1)} = \frac{C-1}{W_m C}\frac{P}{P_0} + \frac{1}{W_m C} \quad \text{…..2.2}$$

Where,

- W weight of adsorbate adsorbed at relative pressure P/Po
- P Partial pressure of adsorbate
- P_0 saturated vapor pressure of adsorbate
- Wm weight of adsorbate adsorbed at a coverage of one monolayer
- C a constant which is a function of the adsorbate heats of condensation and adsorption

The value of the slope *S* and the y-intercept *i* of the line are used to calculate the monolayer adsorbed gas quantity W*m* and the BET constant *C*, using the following equation.

$$W_m = \frac{1}{s+i} \quad \text{…..2.3}$$

The total surface area of the sample, S_t, is determined from equation (2.4),

$$S_t = \frac{W_m N A_{cs}}{M_a} \quad \text{…..2.4}$$

Where,

- M_a adsorbate molecular weight
- W_m weight of adsorbate adsorbed at a coverage of one monolayer
- N Avogadro's number = 6.023×10^{23}
- A_{cs} cross sectional area of adsorbate molecule for N_2 gas 16.2×10^{-20} m^2

Specific surface (m^2/g) is given by equation (2.5),

$$S_{BET} = \frac{S_t}{\text{weight of sample}} \quad \text{…..2.5}$$

BET surface areas of the specimen have been measured by using of N_2 adsorption at 77 K preformed on a Quantachrome CHEMBET 3000 instrument.

2.3.2. Temperature programmed reduction (TPR) method:

Temperature programmed reduction method is a technique in which a chemical reaction is monitored between metal particles and hydrogen gas while the temperature increases linearly with time. This method is used to find the most efficient reduction conditions for the catalyst. Catalyst precursor is subjected to a programmed temperature technique method while a reducing gas mixture (H_2:N_2) is flown over it.

In typical procedure, a U-tube (Quartz) was filled with the solid catalyst. This sample holder is positioned in a furnace which is equipped with a temperature controller. A thermocouple is placed in the U-tube for temperature measurements. Equal quantities of fresh vacuum dried catalyst were taken in the U-tube. Initially, U-tube was purged with inert gas (nitrogen) to remove the air present in the lines, and then heated to 250^{o}C for 30 min in N_2 atmosphere with a flow rate of 60 ml/min in order to remove the moisture and surface impurities present on the sample, and then it was cooled to room temperature. The nitrogen was replaced by (5% H_2 in N_2) for the TPR experiments. Mass flow controller was used to maintain the mixture of 5 % hydrogen in nitrogen gas. Finally, the sample in the U-tube heated from 30^{o}C to 500^{o}C using a temperature controller, with the ramp rate of 15^{o}C/min. The hydrogen consumed for complete reduction of the sample at certain temperatures, was detected by TCD, and was recorded.

2.3.3. H_2 pulse titration (chemisorption):

In our work, chemisorption of catalyst samples was carried out using Quantachrome make Chembet-3000 instrument, equipped with a thermal conductivity detector.

General experimental procedure for the pulse titration is given below

1. Accurately weighed (~ 0.050 g) sample was placed in a sample cell holder (Figure 2.2) and then the sample was heated under the flow of nitrogen gas at 200^{o}C for 1 hour, by this treatment, the sample surface was cleaned and the moisture was completely removed.

2. After the sample was cooled to room temperature, the sample cell holder was connected to the spectrometer connection for pulse titration (see Figure 2.2).
3. Then the temperature was increased to 300^{o}C by using temperature controller with a heating rate of 10^{o}C/min in an inert atmosphere.
4. After attaining the temperature, nitrogen gas was replaced by a mixture of 5% hydrogen in nitrogen and kept it for half an hour.
5. Mixture of 5% hydrogen in nitrogen was replaced by nitrogen gas, kept it for 1 hour, and then cooled to room temperature. By this treatment, metal surface was cleaned and ready for the H_2 chemisorption analysis.
6. Using the calibrating syringe, 100 µL of the hydrogen gas was injected to the sample. This was repeated until three consecutive peaks with the same integrated area were obtained.
7. The volume of adsorbed hydrogen and metal dispersion at STP was calculated using TPR win software provided by Quantachrome.

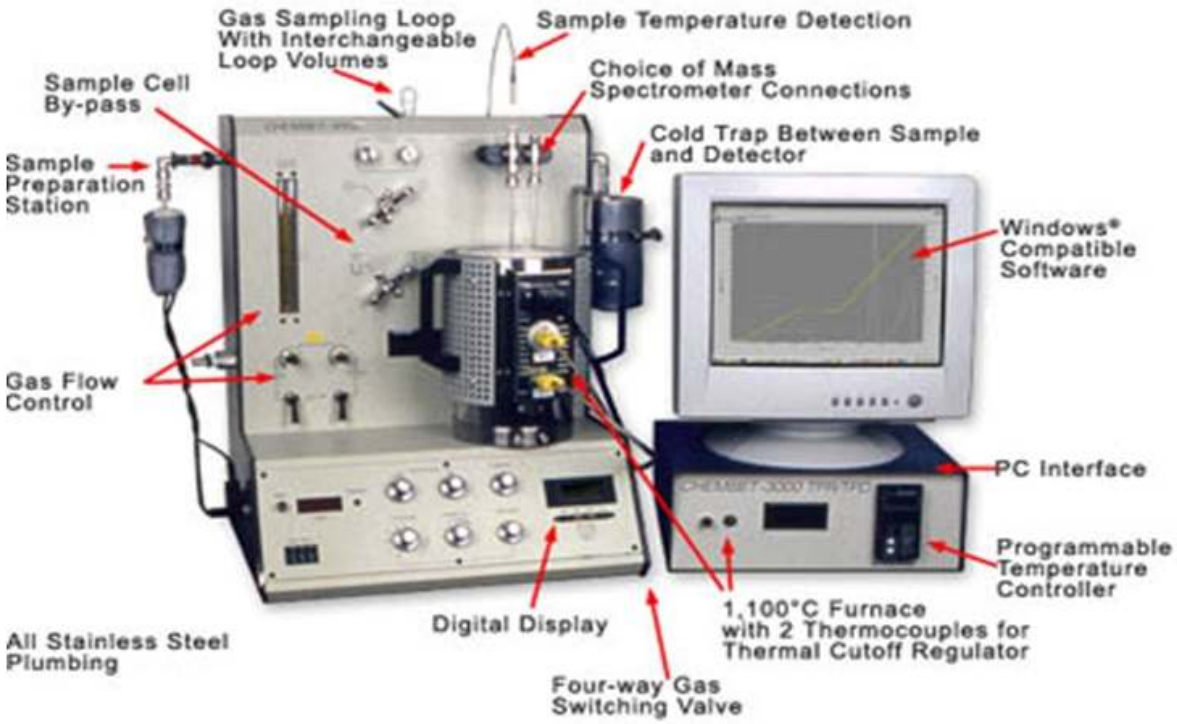

Figure 2.2. Quantachrome Chembet-3000 instrument

2.3.4. X-ray diffraction:

Powder X-ray diffraction method is widely used for material characterization especially qualitative identification of crystalline phases. It provides the information about the identification of crystalline phases, lattice parameters, crystallite size measurement. It can detect crystalline materials having crystallites of greater than 3-5 nm and up to 100 nm.

The X-ray diffraction patterns are obtained by measurement of the angles by which an X-ray beam is diffracted by the sample. Bragg's equation relates the distance between two hkl planes (d) and the angle of diffraction (2θ) as given in equation 2.6 [2].

$$n\lambda = 2d\sin\theta \quad \text{…..2.6}$$

Where,

λ	wavelength of the X-ray, nm
n	integer called order of the reflection
d	distance between two lattice plane
θ	angle of incidence plane, degree

The average crystalline size of the metal particle can be estimated by Debey-Scherrer equation 2.7 [3].

$$< L >= \frac{K\lambda}{\beta\cos\theta} \quad \text{…..2.7}$$

In which,

<L>	is a measure for the dimension of the particle in the direction perpendicular to the reflecting plane
λ	is the X-ray wavelength, nm
β	is the peak width
θ	is the angle between the beam and the normal on the reflecting plane, degree
K	is a constant i.e. (0.9)

For calculation for peak width

$$\beta = \sqrt{B_1^2 - B_2^2} \quad \text{…..2.8}$$

Where,

B_1 is the FWHM (full width half maxima)

B_2 is the instrument broadening (0.15)

X-ray powder diffraction patterns have been recorded on a PAnalytical PXRD Model X-Pert PRO-1712, using Ni filtered Cu Kα radiation (λ=0.154 nm) as a source (current intensity, 30 mA; voltage, 40 kV) and a X-celerator detector. The samples were scanned in the 2θ range of 5-80°. The species present on the surface were identified by their characteristic 2θ values of the relevant crystalline phase.

2.3.5. X-ray photoelectron spectroscopy:

The X-ray photo electron spectroscopy [4-7] is based on the photoelectric effect, which involves the bombardment of a sample surface with X-ray and measurement of the concomitant photoemitted electrons. The photoemitted electrons have discrete kinetic energies that are characteristic of the emitting atoms and their bonding states. The shifts in core-level energies give information on the surface elemental composition, the oxidation state of the elements and chemical analysis [8].

The kinetic energy, E_k, of these photoelectrons is determined by the energy of the X-ray radiation, $h\nu$, and the electron binding energy E_b as given by,

$$E_k = h\nu - E_b \quad \text{…..2.9}$$

The experimentally measured energies of the photoelectrons are given by

$$E_k = h\nu - E_b - \psi \quad \text{…..2.10}$$

Where,

E_k is the kinetic energy of the photoelectron

h is Plank's constant

ν is the frequency of the exciting radiation

E_b is the binding energy of the photoelectron with respect to the Fermi level of the sample

ψ is the work function of the spectrometer

The shape of each peak and the binding energy can be slightly altered by the chemical state of the emitting atom. Hence, XPS can provide information on chemical bonding. The number of catalytic properties such as oxidation state of active species, interaction of a metal with a support, change in oxidation state upon activation of the catalyst, nature surface impurities, can be studied by using this characterization technique. XPS measures the intensity of photoelectrons as a function of their kinetic energy.

X-ray photoelectron spectra were acquired on a VG Microtech Multilab ESCA 3000 spectrometer using a non-monochromatized MgKα X-ray source (hν= 1253.6 eV). Base pressure in the analysis chamber was 4×10^{-10} Torr. The errors in all the B.E. values were within ± 0.1 eV. The binding energy correction was performed using the C_{1S} peak of carbon at 284.6 eV as the reference.

2.3.6. Fourier-transform infrared spectroscopy (FTIR):

In FTIR spectroscopy, the incident electromagnetic wave is absorbed by a molecule upon excitation of molecular vibration modes. Application of FTIR spectroscopy in catalysis is to identity adsorbed species and the way in which these species are chemisorbed on the surface of the catalyst [9]**.** The frequency of these vibrations depends upon the nature and binding of the molecules.

FTIR spectroscopy in the frame work region (400-4000cm^{-1}) provides additional information to identify the adsorbed species and adsorbed reaction intermediates and their structures on catalyst surfaces [10].

FTIR spectra was recorded on a Perkin-Elmer instrument. The pellets for analysis were prepared by mixing 3 mg of the catalyst with 50 mg of KBr. FTIR spectra were recorded between 450 to 4000 cm^{-1} with accumulation of 20 scan and 4 cm^{-1} resolution

2.3.7. Transmission electron microscopy:

Transmission electron microscopy technique involves a primary electron beam of high energy and high intensity passing through a condenser to produce parallel rays, which impinge on the sample. As the attenuation of the beam depends on the density and the thickness, the transmitted electrons form a two-dimensional projection of the sample mass, which is subsequently magnified by the electron optics to produce a so-called bright field image. The dark field image is obtained from the diffracted electron beams, which are slightly off angle from the transmitted beam [11-14].

This technique allows the size distribution, external morphology, chemical composition and shape of metal particles in supported and unsupported catalyst to be characterized down to the level of atomic resolution better than 0.5 nm [10].

Operating conditions of a TEM instrument is 100-200 keV electrons, 10^{-6} mbar vacuum, 0.5 nm resolution and a magnification of 3 x 10^5 to 10^6. TEM analysis was performed on a Jeol Moeld JEM 1200 electron microscope operated at an accelerating voltage of 120 kV. A small amount of the solid sample was sonicated in methanol for 1 min. A drop of prepared suspension was deposited on a Cu grid coated with carbon layer and grid was dried at room temperature before analysis.

2.3.8. Scanning electron microscopy:

Scanning electron microscopy is a technique to probe the morphological features of catalyst materials. SEM scans over a sample surface with a probe of electrons (5-50 eV) and detects the yield of either secondary or backscattered electrons as a function of the position of the primary beam. Contrast is generally caused by the orientation such that the part of the surface facing the detector appears brighter than the part of the surface with its surface normal pointing away from the detector. The interaction between the electron beam and the sample produces different types of signals providing detailed information about the surface structure and morphology of the sample [15]. When an electron from

the beam encounters a nucleus in the sample, the resultant Coulombic attraction leads to a deflection in the electron's path, known as Rutherford elastic scattering. A fraction of these electrons will be completely backscattered, re-emerging from the incident surface of the sample. Since the scattering angle depends on the atomic number of the nucleus, the primary electrons arriving at a given detector position can be used to produce images containing topological and compositional information [16]. A major advantage of SEM is that bulk samples can also be directly studied by this technique

The chemical composition of the sample was determined by energy dispersion X-ray (EDX) attached to a scanning electron microscopy (SEM: JEOL JSM 500)

2.3.9. Raman spectroscopy:

Raman spectroscopy is based on the inelastic scattering of photons, which loses energy by exciting vibrations in the sample [17]. Raman spectroscopy is generally used for characterizing the materials to find the crystallographic orientation of a sample, chemical structure of molecules. It allows studying surface metal oxide species on typical oxide support materials. It offers to study the molecular vibrations below 1100 cm^{-1} [17]. The radial breathing mode is commonly used technique to evaluate the diameter of sample and used to understand the structure of the composition.

The Raman spectra of sample were recorded on a Horiba JY LabRAM HR800 micro-Raman spectrometer with 17 mW 632.8 nm laser excitation.

2.4. Catalyst activity measurement:

2.4.1. Continuous high pressure reactor setup:

Bench scale continuous hydrogenation experiments were carried out in a high-pressure, fixed-bed reactor supplied by M/s. Geomechanique, France. A schematic of the reactor setup is shown in Figure 2.3. It consisted of stainless steel tube of 0.35 m length and 1.5 x 10^{-2} m inner diameter that was heated by two tubular furnaces whose zones (TIC1 and TIC2) were independently controlled at the desired bed temperature. The reactor was provided with two thermocouples [Chromel-Alume thermocouples (type K)] to measure the temperature at two different points. The reactor was equipped with mass flow controllers, pressure indicator, and controller (PIC) devices. A storage tank was

connected to the metering pump through a volumetric burette to measure the liquid flow rate. The pump had a maximum capacity of 3 x 10^{-4} m^3/h under a pressure of 10 MPa. The gas outlet line was equipped with a backpressure controller, which maintained a constant pressure in the unit by continuous pressure release. The other end of the reactor was connected to a gas-liquid separator through a condenser. The experiments were carried out over 10 and 20 g of catalyst in the form of pellets having 4 mm diameter. The section 5 cm and 5 cm below the catalyst bed was packed with inert packing (carborundum), thus providing the catalyst bed depth of ~25 m . The reactor was flushed thoroughly with H_2 at room temperature before the start of the actual experiment. After attaining the desired temperature, the reactor was pressurized with H_2. The liquid feed was "switched on" after the reactor has reached the operating pressure and kept there for 1 h to obtain the constant liquid flow rate. Liquid samples were withdrawn at regular intervals of time and were analyzed by gas chromatography.

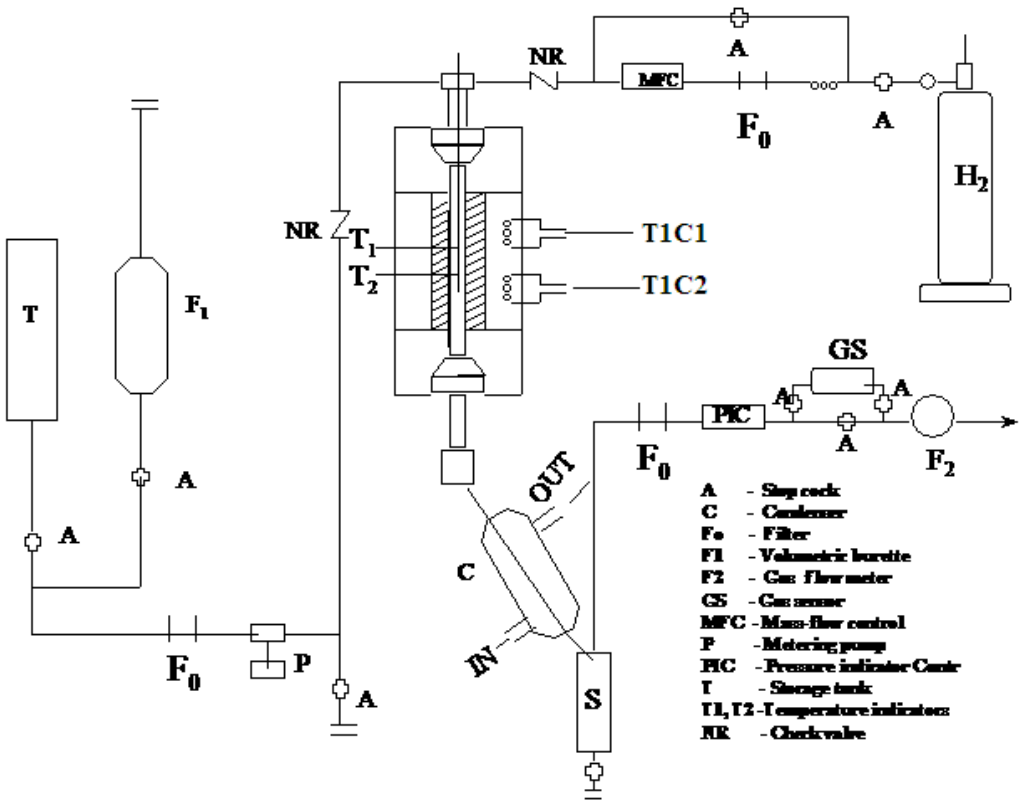

Figure 2.3. Continuous reactor setup

2.4.2. Batch reactor set up:

All the batch hydrogenation experiments were carried out in a 300 mL capacity stirred autoclave supplied by Parr Instruments Co. USA, which was equipped with heating arrangement, overhead stirrer, thermo well, internal cooling coil, gas inlet and outlet, liquid sampling valve, safety rupture disc, pressure gauge as well as transducer for digital pressure display, separate automatic controller to control the temperature, agitation speed, solenoid valve and high temperature cutoff module. Water circulation through the internal cooling loop equipped with automatic cut-off arrangement controlled the temperature inside the reactor with an accuracy of ±1° C. A schematic of the batch slurry reactor set-up is shown in Figure 2.4.

In a typical hydrogenation experiment, required amount of substrate was charged into the reactor. Total volume of the liquid phase was always kept to 100 mL by adding

appropriate solvent and the required amount of slurry of catalyst was charged in an autoclave carefully and reactor vessel was closed. The contents were first flushed 2-3 times with N_2 gas for the removal of trapped air and then flushed with H_2. Then the temperature was ramped to the required temperature. After attaining the desired temperature, the system was pressurized with H_2 gas to the desired pressure. Initial liquid sample was withdrawn before starting the reaction, by switching the stirrer on and the progress of the reaction was monitored by observing the pressure drop in the reservoir as a function of time. When the reaction was over, as indicated by a constant H_2 pressure on the pressure display, the reactor was cooled to room temperature and excess H_2 gas was vented out safely and the reactor contents were discharged. Samples were withdrawn at regular time intervals for the analysis using gas and liquid chromatography.

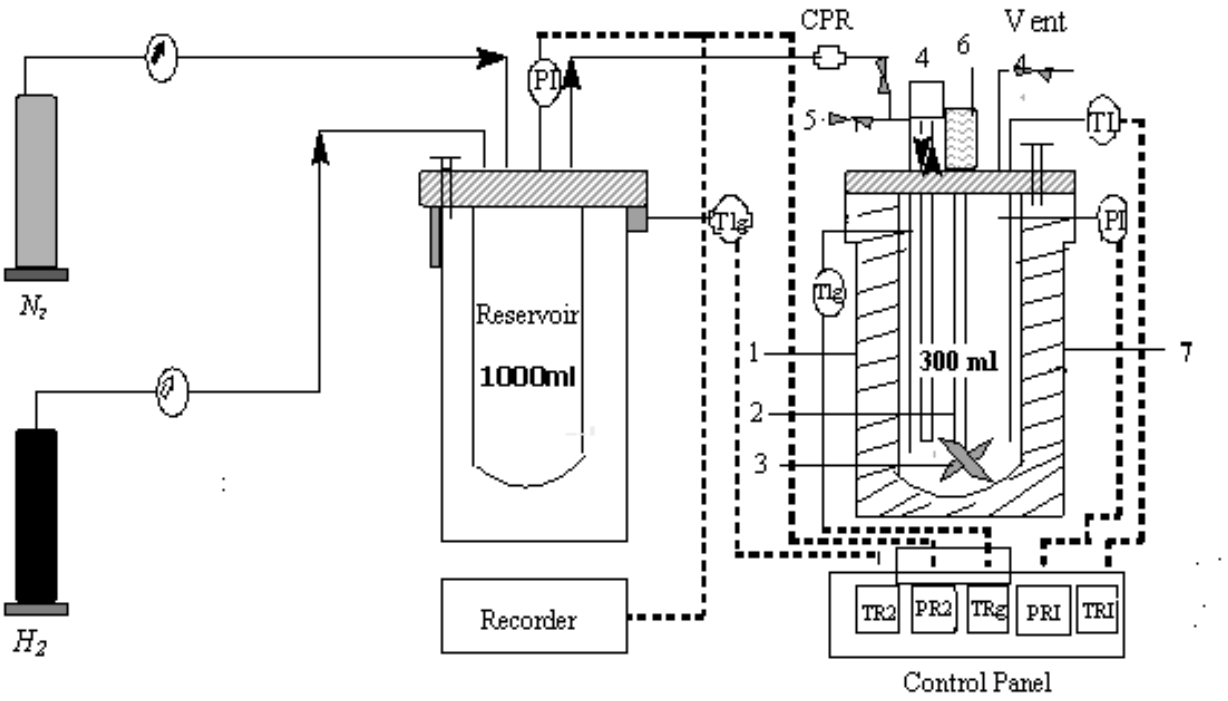

Figure 2.4. Parr reactor setup

(1) Reactor (2) stirrer shaft (3) impeller (4) cooling water (5) sampling valve (6) magnetic stirrer (7) electric furnace

TI: Thermocouple **PI**: Pressure transducer **TIg**: Thermocouple for gas **N**: Nitrogen cylinder **H_2**:Hydrogen gas cylinder **PR**: Pressure regulator **CPR**: Content pressure regulator **TR1**: Reactor temperature indicator **PR1**: Reactor pressure indicator **TR2**: Reservoir temperature Indicator **TRg**: Gas temperature indicator **PR2**: Reservoir pressure indicator

2.4.3. Atmospheric reaction set up:

Hydrogenation of phenylacetylene was conducted at atmospheric pressure, in a 250 mL capacity three-necked glass reactor fitted with a cooling condenser (Figure 2.5). In a typical experiment, phenylacetylene (49 mmol), and methanol (90 mL) were charged to the reactor and the system was purged with N_2 for 10 min. To this, 5 ml of colloidal Pd

catalyst was added and the hydrogenation was started by bubbling H_2 gas at a desired flow rate through the reaction mixture and the H_2 flow was regulated by a needle valve (30 mL/min). This time was considered as the start of the catalytic reaction. All the reactions were performed up to 100% conversion, and this was taken as the end of the reaction. Agitation was carried out with a magnetic stirring bar. Timely samples were taken and analyzed on GC.

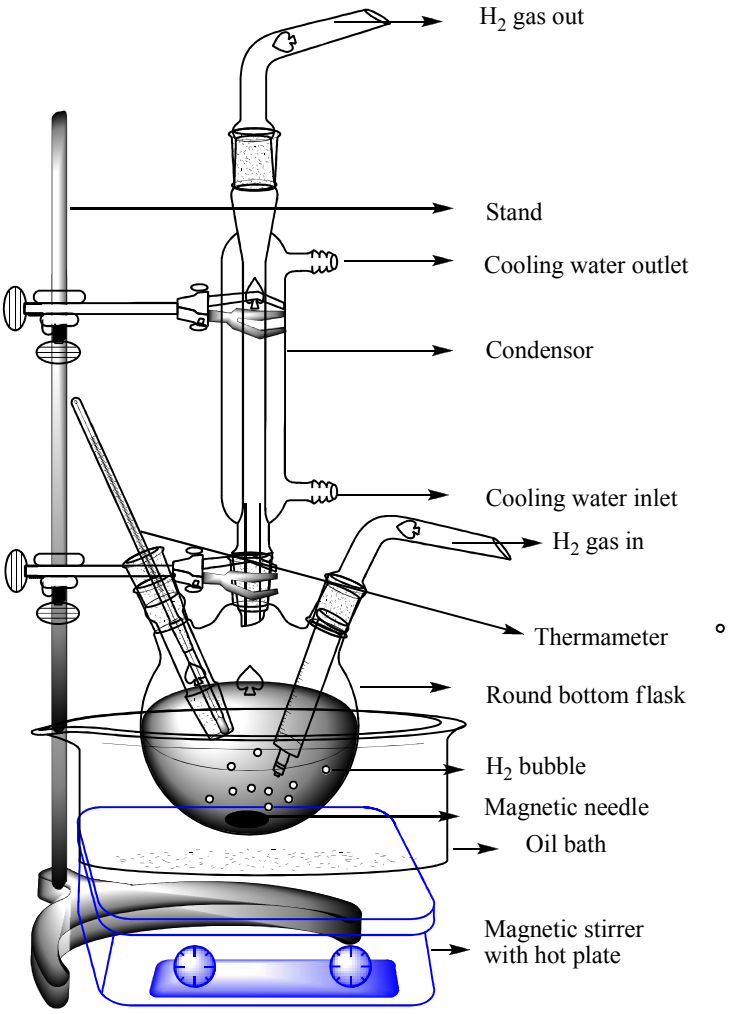

Figure 2.5. Atmospheric reactor setup

2.5. Analytical methods:

Chromatography:

Chromatography is a separation process that is achieved by distributing the components of a mixture between two mutually immiscible phases, one phase is stationary and other is mobile. A sample component introduced in a mobile phase carried along with a column containing a distributed stationary phase. The species of sample undergo repeated interactions between the mobile phase and stationary phase. Those components held preferentially in the stationary phase are retained longer in the system than those that are distributed selectively in the mobile phase. Separation can be achieved by selection of both phases, and the sample component gradually separated in bands in the mobile phase. As a consequence, solutes are eluted from the system as local concentrations in the mobile phase in the order of their increasing distribution coefficients with respect to the stationary phase: the least retained component emerges first; the most strongly retained component elutes last [18, 20]**.**

Applications:

Depending on mobile phase the chromatographic techniques are divided in to two parts

- Gas chromatography
- Liquid chromatography

1. Gas Chromatography:

In gas chromatography, inert gas used as a mobile phase e.g. He, H_2, N_2 and analysis sample must be thermally stable and volatile that of organic/inorganic compounds. Colum is heart of chromatography where actual separation is take place. The details of stationary phases used for the quantitative and qualitative analysis are shown in Table. 2.1

Table 2.1. Selected stationary phases used for gas-liquid chromatography analysis.

Column trade name & Column details	Stationary phase	Operating range /limit	Compounds analyzed in this work
HP-FFAP, **(Free Fatty acid phase column) 30 m x 0.53 mm x 1.0 µm***	5% methylpolysiloxane + polyethylene glycol (Nitroterephthalic acid modified polyethylene glycol) High polarity	60 - 250^{o}C	Used for the analysis of 2-butyne-1,4-diol, 2-butene-1,4-diol, butanediol
HP-1 **30 m x 0.32 mm x 1 µm***	100% Dimethylpolysiloxane, Non polar	325/350^{o}C	Nitrobenzene, aniline, *m*- , *p*-, *o*-chlronitrobenzene, *m*-, *p*-, *o*-chlroaniline,
HP-5 **30 m x 0.32 mm x 1 µm***	(5%-Phenyl)-methylpolysiloxane, Non-polar	-60 - 325^{o}C	Phenylacetylene, styrene, ethylbenzene

* Column length x column ID x film thickness

Hewlett- Packard model equipped with flame ionization detector (FID) was employed for the analysis of samples. Major advantages of FID include a detection limit that is approximately two to three order of magnitude smaller than that for a thermal conductivity and helium gas used as a carrier. On basis of plot of response Vs time, the qualitative and quantitative analysis were determined by using gas chromatography.

2. High performance liquid chromatography:

Hewlett-Packard model 1050 liquid chromatograph equipped with an ultraviolet detector and HP 1100 series auto sampler was employed for the analysis of liquid samples. HPLC

analysis was performed on a 25 cm RP-18e* column supplied by Hewlett-Packard. The products and reactants were detected using a UV detector at λmax, 254 nm using 30% acetonitrile:5% Buffer:water as the mobile phase at a column temperature of 313 K and flow rate of 1 mL/min. Samples of 10 µL were injected into the column using an auto sampler.

HPLC analysis Conditions	
Column Details	
Dimensions (Length, ID)	Lichrocart RP 18e* (250 X 4 mm)
Particle size	5µm
Stationary Phase	RP 18
Mobile Phase analysis details	
Mobile Phase	Acetonitrile:Buffer(pH:7):water (30:5:65)
Flow rate	1 ml/min
Temperature	25^0C
Sample volume	10 µL diluted to 10 ml
Washing Phase	Methanol:water (50:50)
HPLC column washing mobile phase Flow rate	0.3 ml/min (overnight)
Detector	UV-Vis
λmax	254 nm

Calculation for response factor, % conversion and % selectivity:

$$\text{Rf} = \frac{\text{Concentration in moles}}{\text{area under the respective peak}} \qquad \text{…..2.11}$$

$$\%, \text{Conversion} = \frac{\text{Intial moles of substrate} - \text{Final moles of substrate}}{\text{Initial moles of substrate}} \text{ x } 100 \qquad \text{…..2.12}$$

$$\%, \text{Selectivity} = \frac{\text{moles of product formed}}{\text{moles of substrate consumed}} \text{ x } 100 \qquad \text{…..2.13}$$

2.6. References:

1. S. Brunauer, P. H. Emmett, E. Teller *J. Am. Chem. Soc.* 60 (1938) 309
2. I. Chorkendorff, J. W. Niemantsverdriet in *Concepts of modern catalysis and kinetics*, Wiley-VCH, Weinheim, (2003) pp 131.
3. A. L. Petterson *Phy. Rev.* 56 (1939) 978.
4. P. K. Ghosh in *Introduction to photoelectron spectroscopy*, Wiley, New York, (1983).
5. J. F. Watts in *Introduction to surface analysis by XPS and AES*, Wiley, New York, (2003).
6. D. Briggs, M. P. Seah (Eds.) in *Practical surface analysis*; *Auger and X-ray photo electron spectroscopy,* Vol. 1, 2nd edition, Wiley, New York (1990).
7. S. Hüfner in *Photoelectron spectroscopy*, Springer-Verlag, Berlin, (1995).
8. W. M. Deglass, G. L. Haller, R. Kellerman, J. H. Lunsford in *Spectroscopy in heterogeneous catalysis,* Acadamic press, New York, (1979)
9. I. Chorkendorff, J. M. Niemantsverdriet in *Concepts of modern catalysis and kinetics,* Wiely-VCH, Weinheim (2003) pp. 155.
10. J. Hagen in *Industrial catalysis*, 2nd edition, Wiley-VCH, Germany, (2006) pp 215.
11. G. Lawes in *Scanning Electron microscopy and X-ray microanalysis*, John Wileyand Sons Ltd., Chichester (1987).
12. J. R. Fryer in *Chemical applications of transmission electron microscopy*, Acadamic press, San Diego, (1979).
13. J. M. Thomas, O. Terasaki, P. L. Gai, W, Zhou, J. Gonzalez-Callbet *Acc. Chem. Res.* 34 (2001) 583.
14. A. Alfredsson, M. Keung, A. Monnier, G. D. Stucky, K. K. Unger, F. Schuth *J. Chem. Soc. Chem. Comm.* (1994) 921.
15. J. I. Goldstein, H. Yakowitz (Eds.) in *Practical scanning electron microscopy*, Plenum press, New York, (1975).
16. G. Lawes in *Scanning electron microscopy and X-ray microanalysis*, John Wiley and Sons Ltd., Chichester, (1987).
17. J. M. Niemantsverdriet in *Spectroscopy in catalysis,* 3rd edition, Wiley-VCH, Weinheim, 2007, pp 238.

18. P. W. Raymond in *Principles and practice of chromatography,* Book I, Chrom-Ed Book Series, (2003) pp.2.
19. H. H. Willard, L. L. Merritt, J. A. Dean, F. A. Settle in *Instrumental methods of analysis*, 7^{th} edition, CBS Publishers, New Delhi (2007) pp 247.

Part I

Hydrogenation of acetylenic compounds

Chapter III

Hydrogenation of 2-butyne-1,4-diol to 2-butene-1,4-diol and butane-1,4-diol

3.1. Introduction:

Hydrogenation of carbon-carbon triple bond to partial/complete hydrogenation products has been the topic of great importance from both fundamental as well as industrial point of view [1, 2]. It is challenging to achieve complete selectivity to olefinic compounds in such processes since the intermediate olefin of the first hydrogenation step readily undergoes further hydrogenation to give a saturated alkane product [3]. One Such industrial example is the catalytic hydrogenation of 2-butyne-1,4-diol (B_3D) for the manufacture of *cis*-2-butene-1,4-diol (B_2D) and butane-1,4-diol(B_1D) [3,4]. The geometric *cis* isomer is predominantly obtained (> 99%) due to the *cis* addition of hydrogen over heterogeneous catalysts under mild conditions [1]. The *trans*-isomer is regarded to be formed due to isomerization of *cis*-isomer however, under hydrogenation conditions isomerization is greatly suppressed due to fast desorption of the intermediate olefinic diol. 2-Butene-1,4-diol (B_2D) and butane-1,4-diol (B_1D) have wide ranging applications in the manufacture of various sectors details are given below.

3.1.1. Importance of 2-butene-1,4-diol:

2-Butene-1,4-diol has large number of applications as shown in Figure 3.1 especially in a variety of chemical and pharmaceutical industries. As B_2D possesses two replaceable hydroxyl groups and one double bond a large number of chemicals and intermediates are possible from its downstream processing.

- Butenediol is a starting material for the production of endosulfan, a commonly used insecticide. It is produced by Diels-Alder reaction of butenediol with hexachlorocyclopentadiene [5].
- Hydroformylation of B_2D is an important step in the production of vitamin A (Schemes 3.1 and 3.2) [6-10].
- B_2D is also used for the production of pyridoxine (Vitamin B_6) and as bactericide [11-13].
- It is used as an additive in paper industry and as a stabilizer in resin manufacture.
- Lubricant for bearing system and in the synthesis of allyl phosphates.
- Used in the synthesis of diarylate monomer.

- Used in the preparation of biologically active haloacetates such as *cis*- and *trans*-1-iodoacetoxy-2-butene-1,4-ol, *cis*-1-bromacetoxy-2-butene-4-bromide, 1-bromacetoxy -2-butene-4-chlroide etc. [14].

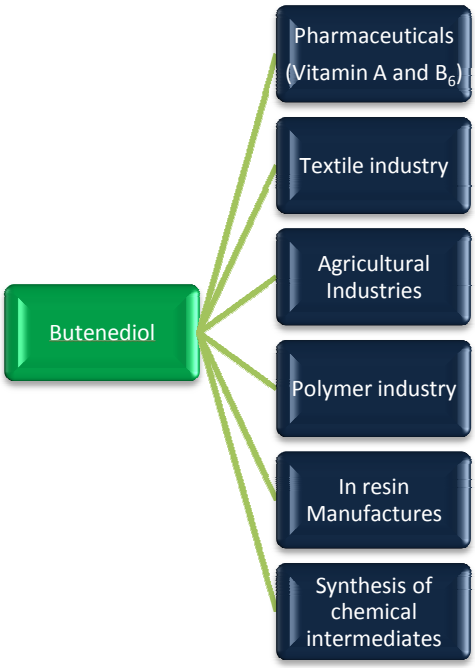

Figure 3.1. Importance of 2-butene-1,4-diol

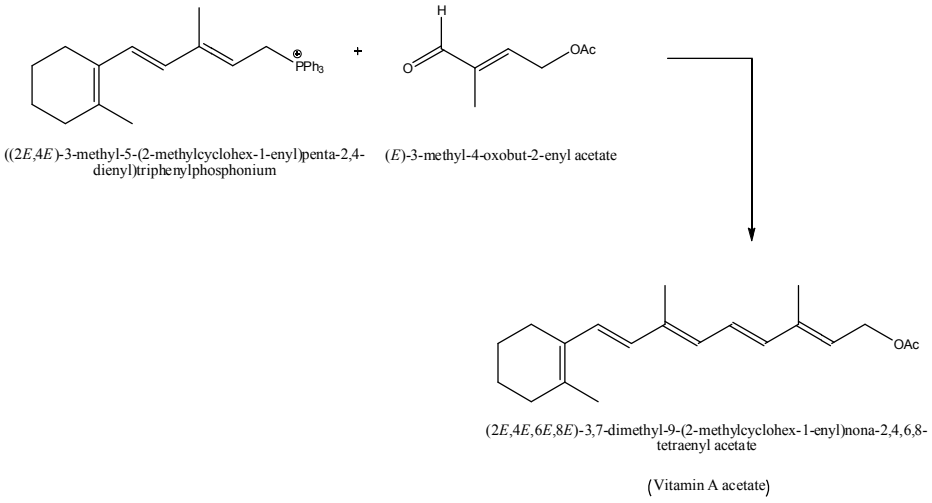

Scheme 3.1. Vitamin A synthesis

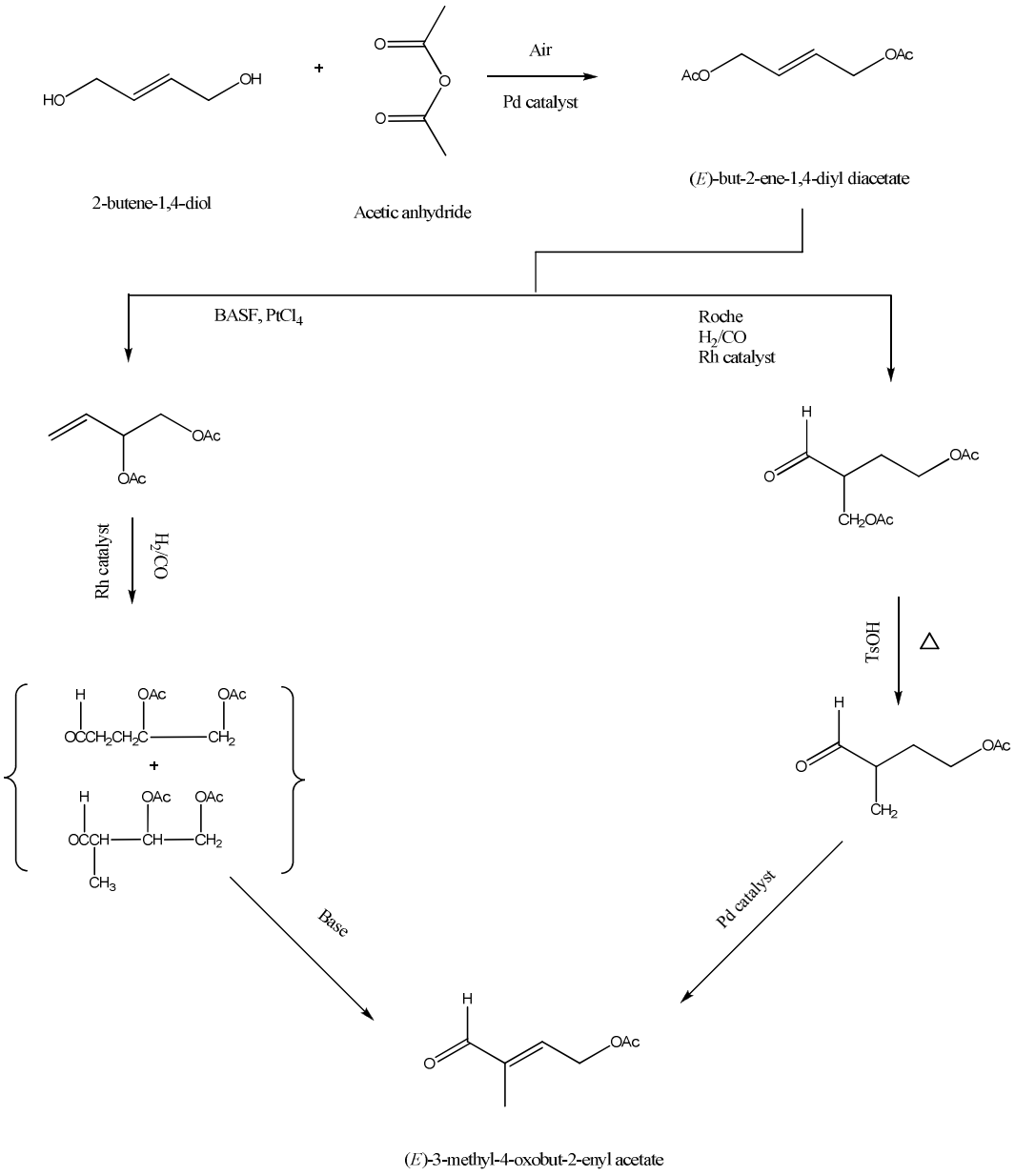

Scheme 3.2. Steps involved in preparation of 3-methyl-4-oxobut-2-enyl acetate from butenediol

3.1.2. Importance of butane-1,4-diol:

As shown in Figure 3.2 the saturated product butanediol of the hydrogenation of butynediol process is mainly consumed for the production of polyurethanes, polybutylene terephthalate (PBT), γ-butyrolactone and tetrahydrofuran [15-16]. Among these THF is not only used as a solvent in polyvinyl chloride (PVC), coating, high precision magnetic tape but also in making of the highest volume derivative, polytetramethylene ether glycol (PTMEG), which is mainly used for production of spandex fibers as well as thermoplastic, polyurethanes (TPU) and copolyester (COPE), polymers, solvents and fine chemicals. γ-butyrolactone (GBL) produced from butane-1,4-diol, provides the feedstock for the N-methyl-2-pyrrolidone (NMP) and 2-pyrrolidone, and also used in agrochemicals and as an intermediate for several other products. NMP is used in various sectors such as electronic industry, lube oil extraction, paint strippers, magnetic wire coating and engineering resins. 2-pyrrolidone is an intermediate used in pharmaceutical sectors, cosmetics, and hair spray, germicide and tablet binders and in high value polyvinyl pyrrolidone polymers. One of the important applications of butane-1, 4-diol is in the production of fire resistant polymers.

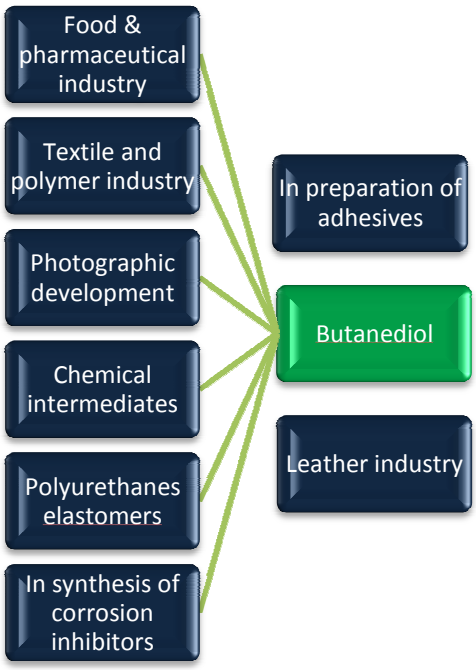

Figure 3.2. Importance of butane-1,4-diol

The world wide capacity for butane-1,4-diol is 3,92,000 tonnes in year 2008 and expected demand for year 2012 is 4,24,000 tonnes with expected annual growth rate of 4.5%.

3.2. Conventional manufacturing processes for butane-1,4-diol:

3.2.1. Reppe process:

The first commercial process for the synthesis of 2-butyen-1,4-diol is based on Reppe process (Scheme 3.3) which involves condensation reaction of formaldehyde with acetylene in presence of copper acetylide which gives B_3D and further hydrogenation of B_3D gives B_2D and B_1D (Scheme 3.3) [17]**.** First synthesis of butanediol was carried out by hydrolysis of N, N'-Dinitro-1,4-butamine, in year 1890 [18]**.**

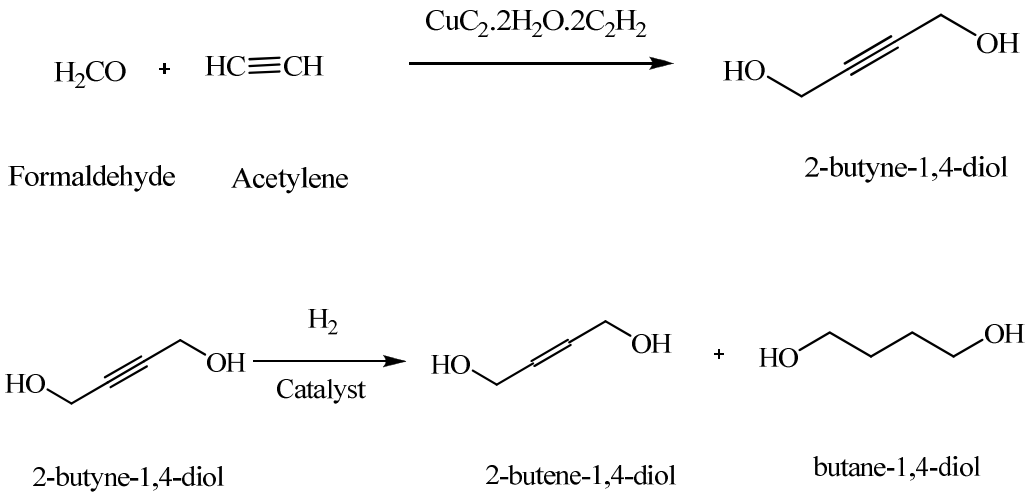

Scheme 3.3. Reppe process

3.2.2. Mitsubishi process:

The first non-acetylene process was developed and commercialized by Mitsubishi (Scheme 3.4), which proceeds via acetoxylation of butadiene followed by hydrogenation and hydrolysis. This process can be designed to make butanediol and THF (Scheme 3.4) [19, 20].

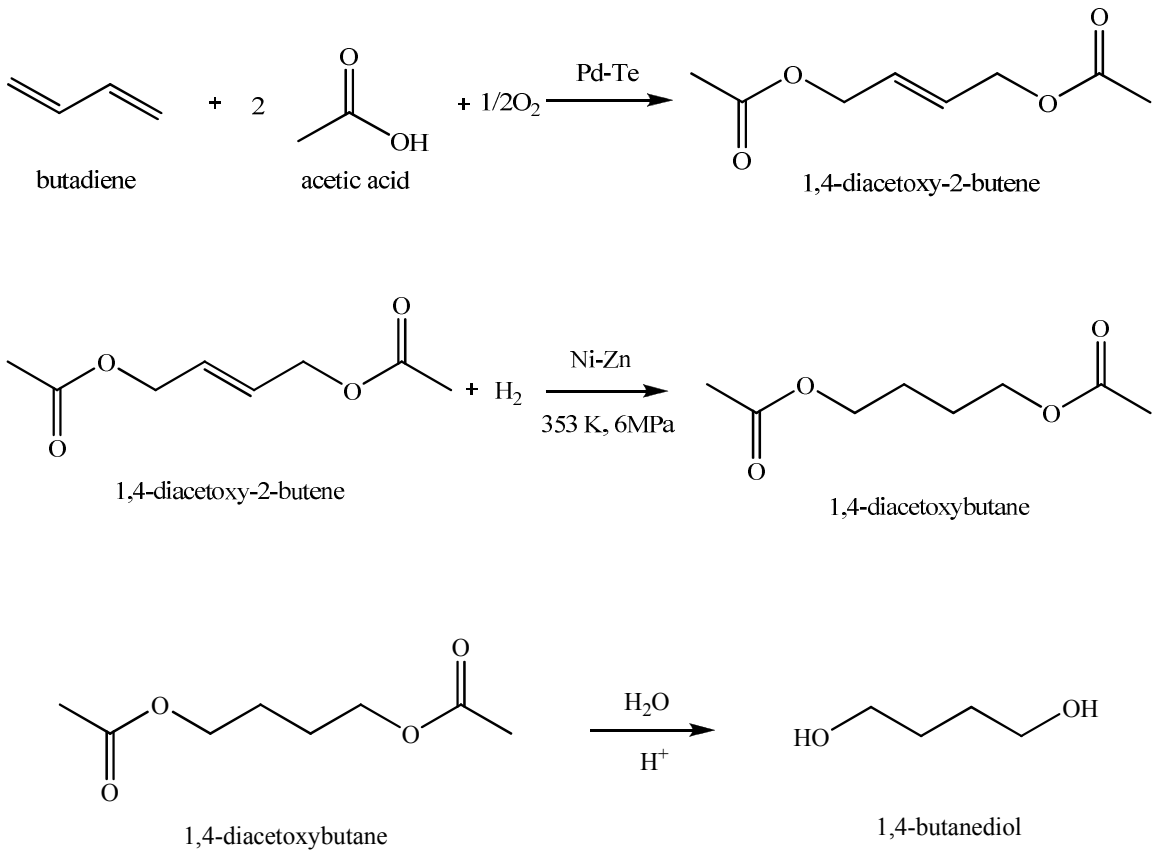

Scheme 3.4. Mitsubishi process

3.2.3. Lyondell process:

Lyondell (formerly Arco chemical) established the process using propylene oxide as a feedstock**.** In this multistep process (Scheme 3.5) initially, isomerization of propylene oxide to allyl alcohol takes place. Further, hydroformylation of allyl alcohol gives 4-hydroxy-butyraldehyde. Finally, the hydrogenation of 4-hydroxy-butyraldehyde gives B_1D**.**

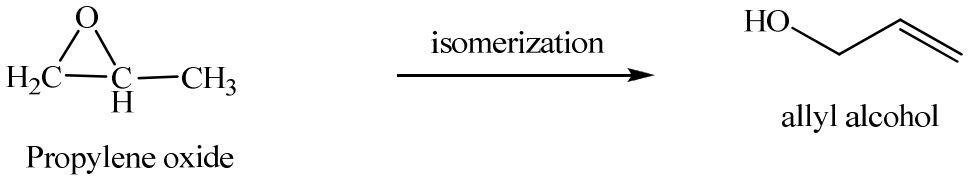

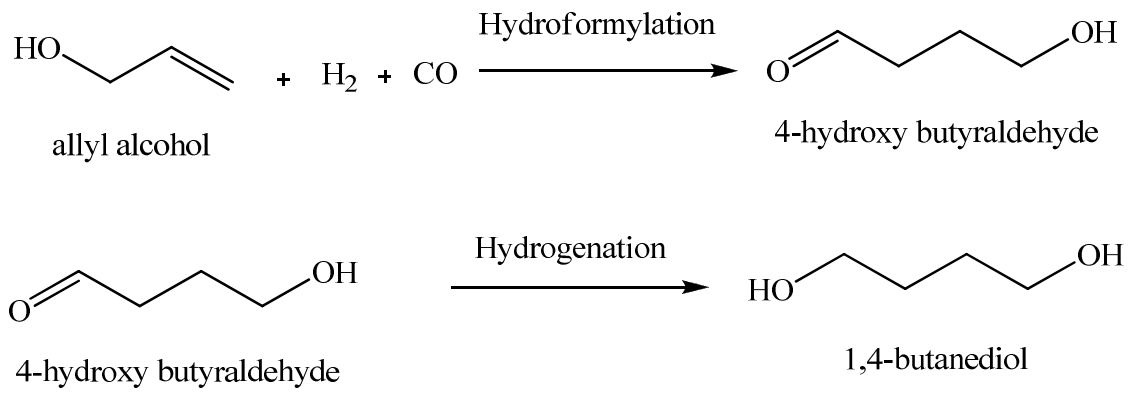

Scheme 3.5. Lyondell process

3.2.4. Davy process:

In Davy process (Scheme 3.6), maleic anhydride is used as a starting material. In this multistep process, initial two steps give monoester and diester, which undergoes hydrogenation using copper chromite catalyst at very high temperature (463-523 K) and pressure (6 MPa), to give B_1D along with formation of THF and γ-butyrolactones.

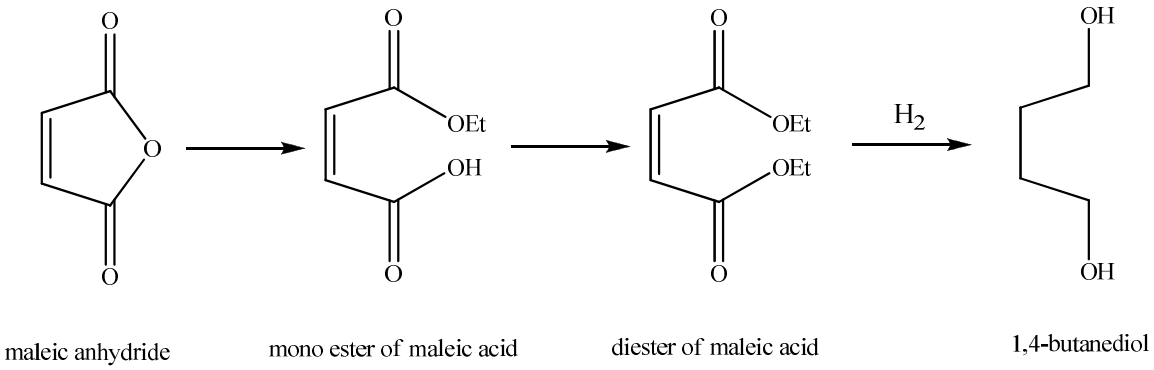

Scheme 3.6. Davy process

3.2.5. From acrolein:

Initially acrolein acetal is obtained by the reaction of acrolein and 2-methylpropane-1,3-diol and the aldehydes are synthesized by hydroformylation of acrolein acetal, using Rh catalyst and finally butane-1,4-diol is obtained by hydrolysis/hydrogenation of aldehydes along with formation of the side products such as THF, *n*-propanol, *n*-butanol (Scheme 3.7) [21].

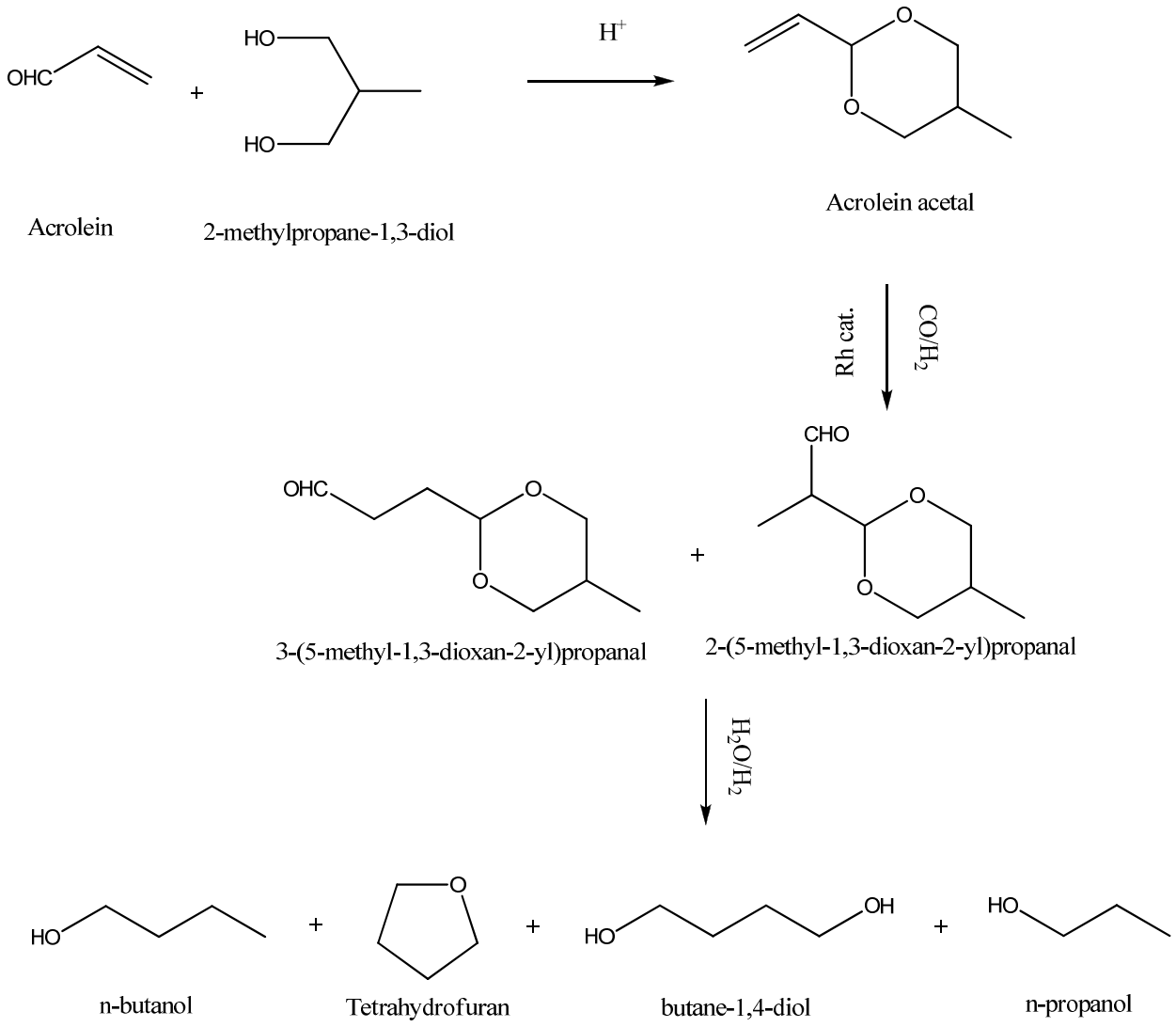

Scheme 3.7. Process from acrolein to butane-1,4-diol [21]

3.2.6. From furan:

Butane-1,4-diol can be obtained from furan in presence of water at 433 K and 3 MPa hydrogen pressure along with formation of THF, butyrolactone and *n*-butanol (Scheme 3.8) [22].

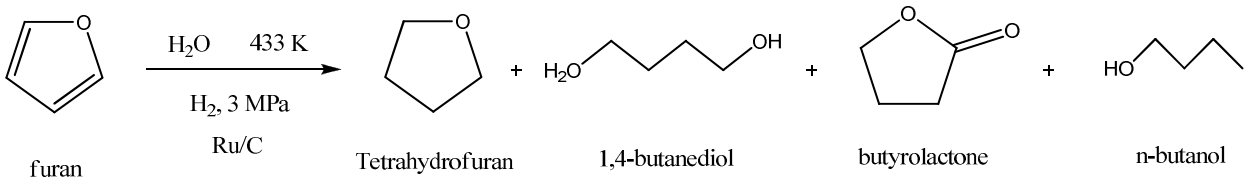

Scheme 3.8. Process from furan to butane-1,4-diol

3.2.7. From succinic acid :

Another route to get butane-1,4-diol is hydrogenation of succinic acid with formation of tetrahydrofuran and butyrlactone (Scheme 3.9) [23].

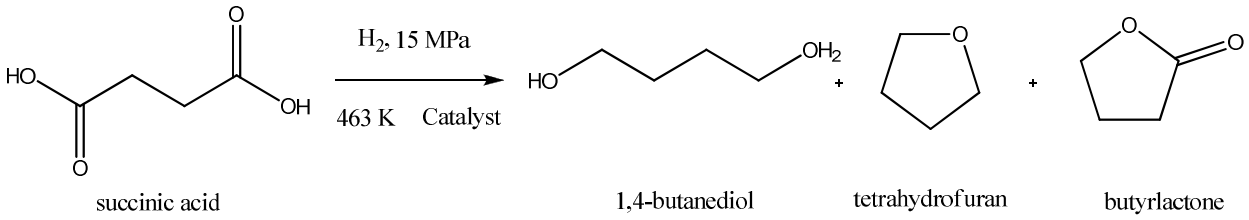

Scheme 3.9. Process from succinic acid to butane-1,4-diol

3.3. Literature survey on hydrogenation of 2-butyne-1,4-diol to 2-butene-1,4-diol and butane-1,4-diol:

Hydrogenation of B_3D to B_2D and B_1D initially used to be carried out by Raney Ni catalyst under severe reaction conditions e.g. temperature of 400-500 K and hydrogen pressure of 5-30 MPa which gave low conversion and selectivity to B_2D and B_1D products [24, 25]. 40 % Ni/SiO_2 catalyst showed 34 % selectivity towards B_1D along with formation of several side products such as butyraldehyde and butanol with complete conversion of B_3D [26]. The catalyst activity increased with increase in Ni metal loading from 10 to 40%, while the selectivity to B_1D dropped down from 93 to 84 % [27]. Highest selectivity of 98 % to B_1D was obtained using Ni supported on pumice stone under severe reaction conditions i.e. temperature of 423 K and pressure of 8 MPa [28]. Enhancement in catalytic activity and selectivity was found by the addition of a co-metal with Ni based catalyst. Bimetallic Ni-Cu/$AlPO_4$ catalyst showed 150 times higher activity and 98 % selectivity towards the B_1D [27]. Major drawback in nickel catalyst

system was the loss of catalytic activity due to formation carbonaceous polymers on to the catalyst surface during the hydrogenation of B_3D, which was observed by Hort et al. [29, 30].

The well known Lindlar catalyst consisting of 5%Pd/$CaCO_3$ poisoned with lead acetate has been in commercial use for the semi-hydrogenation of B_3D to B_2D, however maximum selectivity to B_2D achieved was 85 to 87% [31-33]. Using Lindlar catalyst, more detailed study of different poisons (e.g. quinoline, piperidine, lead acetate) and supports such as $CaCO_3$, $BaCO_3$, $BaSO_4$, alumina on the hydrogenation of butynediol was carried out by Fukuda et al. [34, 35]. He found that the activity decreased with increasing amount of poison (lead acetate) for both hydrogenation steps i. e. hydrogenation of B_3D to B_2D and that of B_2D to B_1D. Nevertheless, several other catalyst systems have also been reported in the literature and a summary is presented in Table 3.1**.** The noble metals such as palladium, ruthenium alone or in combination with other metals such as zinc, lead, cadmium, copper, and/or organic amines also were used as catalyst systems to improve the selectivity to the intermediate, B_2D [36-42]**.** A monometallic Pd/C catalyst was reported to give 60-70% selectivity to B_2D while, remaining was a mixture of saturated diol (B_1D) along with other side products due to the double bond migration [6,7, 42]**.** Although, Pd has been known as a very good catalyst for the alkyne hydrogenations, it has also strong affinity towards double-bond, due to which several side products are normally formed in the hydrogenation of B_3D [43]. The Pd metal on different oxide supports like MgO, NiO, CuO, ZrO_2 MoO_3 showed almost complete (~ 99 %) selectivity towards the B_1D [31, 44-46].

By changing the acidic properties of the support, $AlPO_4$ for the Ni and Ni-Cu metals, the activity and selectivity behavior were studied by Bautista et al. [27]. He found that increasing acidity of catalyst increases the catalyst activity by almost 175 times. Musolino et al. have investigated in detail the role of supports and solvents on product distribution in the hydrogenation of B_3D over 0.5 Pd/C catalyst [47]. They found that Pd supported on acid modified carbon showed high activity and selectivity to isomerization products such as *cis*- and *trans*-2-butene-1,4-diol, 2-hydroxytetrahydrofuran, *cis*- and

trans- crotyl alcohol, *n*-butanol [47]. On this basis, he proposed a reaction pathway for the hydrogenation of 2-butyen-1,4-diol as shown in Scheme 3.10. Among various solvents such as ethanol, tetrahydrofuran, ethyl acetate and water used for this reaction system, water showed the highest activity and selectivity to B_1D [47]. Homogeneous catalyst system involving Pd with bidentate ligands using various polyethers (e.g. diglyme) as solvents showed complete conversion of B_3D with the selectivities of 6 % and 94 % to B_2D and B_1D respectively, in a temperature range of 278-328 K and 3-6 MPa hydrogen pressure [48, 49].

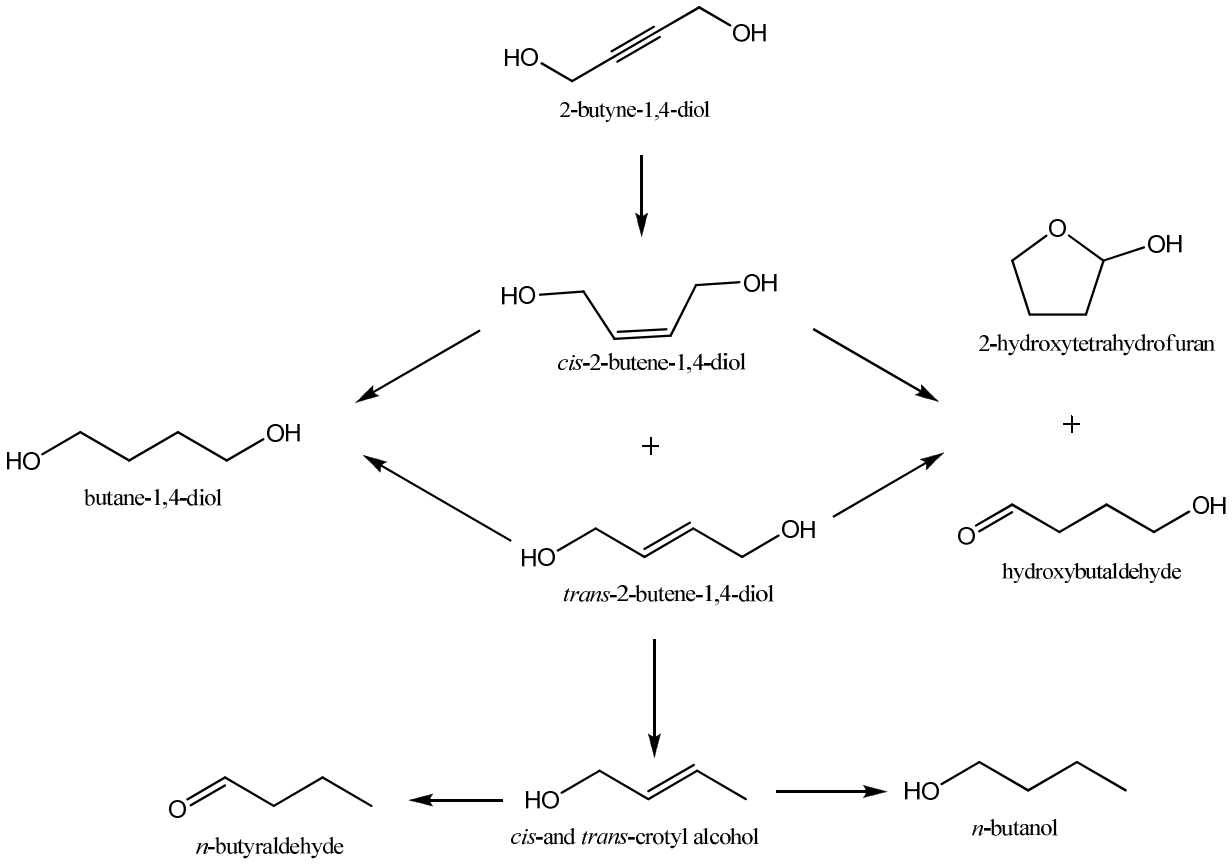

Scheme 3.10. Hydrogenation of B_3D and its product distribution [54]

Telkar et al. studied the role of ammonia, catalyst loading and catalyst pre-treatment on the activity and selectivity behavior in a batch and continuous hydrogenation of B_3D using 1% $Pt/CaCO_3$ catalyst [50]. Formation of B_1D is possible either directly from carbyne type intermediate or via B_2D hydrogenation through carbene species. A plausible

mechanistic pathway has been also proposed based on carbyne and carbene type of intermediates [50, 51]**.**

Hydrogenation of B_3D has been also reported in supercritical CO_2 medium, in which the reactor wall (ss) was supposed to catalyze the reaction to give a complete selectivity to B_1D with 100 % conversion of B_3D [52, 53]. Kiwi-Minsker and Joannet studied the solvent free selective hydrogenation reaction using nano Pd supported on the activated carbon fibers made from poly(acrylonitrile) in the form of plain woolen fabrics. They observed ≥ 98 % selectivity toward the B_2D with 90 % conversion [54, 55].

Table 3.1. Summary of literature on hydrogenation of 2-butyene-1,4-diol to 2-butene-1,4-diol and butane-1,4-diol.

Sr. No.	Catalyst used	Conversion, %	Reaction conditions	Selectivity, %			Ref.
				B_2D	B_1D	Other	
1.	Nano Pd/Al_2O_3 and Pd	94	T=323 K; P_{H_2}=0.6 MPa	100			56
2.	Nano Pd/activated carbon fibers (polyacrylonitrile fibers in the form of plain woolen fabric)	≤ 90	T=352-392 K; P_{H_2}=1-2MPa; Solvent free	98			54
3.	Nano Pd/Al_2O_3	94		100			57
4.	Nano Pd, bulk Pd	100	T=323 K ; P_{H_2}=2.4 MPa	99.9			36
5.	Pd	95	T=293-333K; P_{H_2}=0.1-0.3 MPa	97			58
6.	Pd/ACF	80	T=293-341 K;	97			59

			P_{H_2}=2.0MPa				
7.	Pd/ $CaCO_3$		T=358-368 K				60
8.	1%Pd /C, Al_2O_3, $CaCO_3$, $BaCO_3$, $MgCO_3$, ZSM-5	100	T=323-353 K; P_{H_2}=2.4-6.9 MPa	100			61
9.	Pd/C & Pd/TiO_2	100	T=303-333 K; T=298 K	60-75 99		20-30 -	62
10.	5% Pd/C	100	T= 333 K	99.2			63
11.	$Pd/CaCO_3$ in presence of quanoline and lead acetate	52	T=285-289 K; P_{H_2}=0.2-0.3 MPa	73			35
12.	Pd/FCN	90	T=353K; P_{H_2}=10 MPa	-	91-92		64
13.	Pd/C	100	T=333-353 K; P_{H_2}=4.0 MPa	97			65
14.	Pd	100	Basic	5	95		48
15.	Pd supported on bacterial biomass	62		100			66
16.	Pd-Ag/Al_2O_3	100	T=353 K; P_{H_2}=0.103 MPa	85			67
17.	Pd-Zn-$CaCO_3$	100	T=303-353 K; P_{H_2}=0.8-3.5 MPa	99			68
18.	Pd-Zn/$CaCO_3$	90	T=273-423 K;	80-97			69

			P_{H_2}=0.1-3 MPa			
19.	PdO-ZnO/Al_2O_3	80	T=345 K; P_{H_2}=0.2-0.5 MPa	90		70
20.	Pd/Al_2O_3 and Zinc acetate	100	T=288-523 K; P_{H_2}=0.1-2 MPa		87	71
21.	2:1 Ru/C-Pd/C Pd/C	100	T=483 K;		89 71	72
22.	Pd-Pb-Cd	89	T=423 K; P_{H_2}=1.5 MPa	85		34
23.	Pd-Cu/$BaSO_4$	80	T=303-353 K; P_{H_2}=0.2-0.5 MPa	98		73
24.	Pd-Cu, Ni-Cu	100 45	T=313-393 K; P_{H_2}=0.3-1 MPa	84-87 48		41
25.	Pd-Cu		T=313-373 K; P_{H_2}=0.1-2 MPa	85-87		74
26.	Pd-Zn-Cd/Al_2O_3 Pd-Zn-Bi/Al_2O_3	90	T=303-353 K; P_{H_2}=1-1.6 MPa	89-92		39
27.	1% Pt/$CaCO_3$	100	T=323-353 K; P_{H_2}=2.5-6.9 MPa	>99		75

28.	Suspended Pd & Raney Ni		T=303-343 K; atm pressure	90			76
29.	Raney Ni	100	T=343-353K; P_{H_2}=2.0 MPa		95		77
30.	Ni/Al_2O_3		pH 5-11; T=293-428 K; P_{H_2}=0.2-7 MPa	95 yield			78
31.	Supported Ni & Ni-Cu		T=313 K; P_{H_2}=0.3-0.7 MPa	5	95	-	27
32.	$Ni(OAc)_2$		T=503-523 K; P_{H_2}=25 MPa	97.9			79, 80
33.	Unsupported Ni Containing Cu 30-40 % ; Mn 1-10% in presence of Mo oxide	100	T=353-393 K; P_{H_2}=3 MPa		47-82		81
34.	Metal oxide catalyst NiO : 38.6, CuO:12.9, Al_2O_3:36.9, Mn_3O_4:3.9, MoO_3:1.9, Na_2O_3 :0.8 of wt %	100	T=413 K; P_{H_2}=26 MPa		98.5		82
35.	Ni/Pumice stone	100	T=288-423 K;		97-98	3-2	83

			P_{H_2}=5-8 MPa		Butanol	
36.	Raney Ni + Cu	100	T=333-373 K; P_{H_2}=0-4 MPa		78-89	84
37.	Raney Ni, Supported Ni	80	413-433 K; P_{H_2}=15-30 MPa	80		22
38.	Ni:Cu:Mn/Al_2O_3	100	T=423 K; P_{H_2}=7 MPa		100	85
39.	Pd/C Supercritical CO_2		P_{H_2}=0.2-0.8 MPa			86
40.	Supercritical CO_2 promoted SS wall reactor	100	T=323 K; P_{H_2}=4.0 MPa		83	87
41.	Supercritical CO_2	100	T=323 K; P_{H_2}=2-6MPa		84	88

Although achieving the complete selectivity either to B_1D or B_2D has been attempted by several researchers, still the major challenges of this industrially important process are as follows:

- Monometallic Ni, Co based catalysts give low selectivity (< 60%) towards B_2D under severe reaction conditions i.e. temperature (423 K) and pressure (20 MPa) along with formation of various side products.
- Pd catalyst is widely studied for hydrogenation of B_3D, which shows only 60-70 % selectivity towards the B_2D.
- A systematic comparison of performance in batch and continuous reactors is lacking for the hydrogenation of B_3D.

- Due to the formation of various side products such as butanol, *n*-butyraldehyde, γ-butyrolactone γ-hydroxybutyraldehyde, and acetals, pure product separation is difficult and time consuming.
- Bimetallic catalysts show higher activity and selectivity towards butanediol than that for monometallic catalyst but deactivation of catalysts was observed.

Therefore the major objectives of our work were:

1. To investigate the activity and selectivity of 1% $Pt/CaCO_3$ catalyst for continuous hydrogenation of B_3D in a fixed-bed reactor. To study the effect of various reaction parameters on the conversion and selectivity behavior for the continuous hydrogenation of B_3D. To develop a reactor model that provides reasonably accurate conversion and selectivity predictions for various reactor inlet conditions.
2. To prepare palladium nano particles, their performance evaluation in selective hydrogenation reaction of B_3D in a batch slurry reactor.
3. To explore the suitability of Pd functionalized CNTs as a catalyst, characterization and activity evaluation for hydrogenation of B_3D.

3.4. Experimental:

3.4.1. Catalyst preparation:

Details of catalysts preparation for 1% $Pt/CaCO_3$, supported nano Pd, Pd supported on CNTs and Pd/C catalyst have been described in chapter II, section 2.2.

3.4.2. Catalyst activity testing:

3.4.2.1. Continuous hydrogenation reaction setup:

The details for continuous hydrogenation reaction setup and experimental procedure is described in chapter II, section 2.4.1.

3.4.2.2. Batch hydrogenation reaction setup:

The experimental batch setup used for high pressure reaction and experimental procedure is described in chapter II, section 2.4.2.

3.4.3. Catalyst characterization:

The details of catalyst characterization have been described in chapter II, section 2.3.

3.4.4. Analytical techniques:

The quantitative analysis of liquid samples were analyzed by gas chromatography method having FID detector, HP-FFAP capillary column and helium gas used as carrier by using temperature programming method (80-190^{o}C), details of which are described in chapter II, section 2.5.

3.5. Results and discussion:

Initial hydrogenation of 2-butyne-1,4-diol gives olefinic compound, 2-butene-1,4-diol which on further hydrogenation gives butane-1, 4-diol. The reaction pathway for hydrogenation of 2-butyne-1,4-diol as shown in Scheme 3.10, involves parallel and consecutive reactions forming other side products such as γ-hydroxybutyraldehyde, *n*-butyraldehyde, *n*-butanol, *n*-butanal due to the possibility of double bond migration and condensation reactions of γ-butyraldehyde and butane-1, 4-diol in presence of a catalyst [4, 6, 10].

We have carried out our studies on the following aspects of hydrogenation of 2-butyne-1,4-diol and the results are discussed separately under three sub sections:

- Continuous hydrogenation of 2-butyne-1,4-diol using 1% $Pt/CaCO_3$ catalyst
- Hydrogenation of 2-butyne-1,4-diol using supported Pd nano catalyst
- Pd-funtionalized carbon nanotubes for selective hydrogenation of 2-butyne-1,4-diol

3.6. Continuous hydrogenation of 2-butyne-1,4-diol and 2-butene-1,4-diol using 1% $Pt/CaCO_3$ catalyst:

Continuous catalytic hydrogenation of 2-butyne-1,4-diol was carried out in a fixed bed reactor (30 g capacity) over 1% $Pt/CaCO_3$ catalyst to give 2-butene-1,4-diol. We found that selectivity pattern obtained in a fixed-bed reactor was different from that obtained in the slurry reactor at similar conversion levels and that the selectivity ratio of B_1D and

B_2D could be altered by varying the H_2 pressure, temperature, liquid and gas flow rate conditions at the reactor inlet. The predictions obtained by the proposed reactor model were compared with the experimental data and were found to agree well over a wide range of operating conditions. The main objectives of this work were (i) to investigate the activity and selectivity behavior of 1%Pt/$CaCO_3$ catalyst for continues hydrogenation of B_3D in a fixed-bed reactor, (ii) to study the effect of various reaction parameters on the conversion and selectivity behavior for the continuous hydrogenation of B_3D and (iii) to develop a reactor model for predicting the conversion and selectivity under various inlet conditions. For this purpose, the effects of temperature, H_2 pressure, liquid and gas flow rates, catalyst loading on the conversion of B_3D and the product selectivities were investigated. The range of reaction conditions is given in Table 3.2

Table 3.2. Range of operating conditions

1.	Catalyst	1%Pt/$CaCO_3$
2.	Initial concentration of B_3D	1.16 kmol/m^3
3.	Solvent	Water
4.	Hydrogen pressure	1-7 MPa
5.	Liquid velocity, U_l	10-60 mL/h
6.	Gas velocity, U_g	20-80 NL/h
7.	Reactor diameter (i.d.)	0.015 m
8.	Total reactor length	0.35m
9.	Catalyst packing length	0.25 m
10.	Bed voidage	0.7
11.	Particle diameter, d_p	0.004 m
12.	Density of catalyst, ρ	1685 kg/m^3
13.	Porosity of the catalyst, ϵ	0.1050
14.	Tortosity of the catalyst, τ	6.2

In all experiments, the concentrations of the reactants and products in the reactor effluent were determined from which the conversion and selectivity were calculated. The material balance as per the reaction Scheme 3.11, was found to be in the range of 98-100% in all the experiments. Reproducibility of the rate, conversion, and selectivity measurements was found to be within 3-4% error as indicated by a few repeated experiments. The results are discussed below.

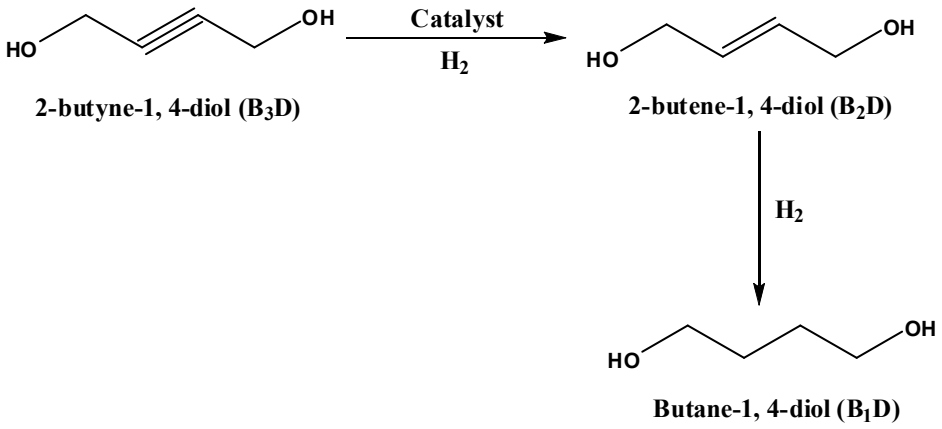

Scheme 3.11. Hydrogenation of B_3D

3.6.1. Catalyst activity and product distribution:

For 1% $Pt/CaCO_3$ catalyst, the products of B_3D hydrogenation were B_2D and B_1D as per the reaction Scheme 3.11 and Table 3.3 shows the variation of conversion and selectivity as a function of contact time defined as a ratio of catalyst loading to the liquid flow rate (W/F, h). Obviously, the conversion of B_3D increased with increase in contact time. The selectivity pattern was completely different from that found in case of batch slurry operation in which B_1D selectivity was very much higher (83%) than the B_2D selectivity (17%) [75]. As can be seen from Table 3.3, varying the contact time at different conversion levels could vary the selectivity to both B_2D as well as B_1D over a wide range. This is an attractive option for a commercial operation where the desired products

mixture of B_1D and B_2D can be achieved, depending on the fluctuation in the market demand.

Table 3.3. Activity and selectivity pattern for 2-butyne-1,4-diol hydrogenation in a fixed-bed reactor

Sr. No.	W/F (h)	Conversion (%)	Selectivity (%)	
			B_2D	B_1D
1.	0.33	14	34	66
2.	0.50	30	42	58
3.	0.66	40	49	51
4.	1.11	55	59	41
5.	2	78	73	27

Some preliminary experiments showed that the activity of 1%Pt/$CaCO_3$ for the hydrogenation of B_3D was constant for >100 h in the temperature range of 333-373 K (Figure 3.3), confirming the uniform activity for the duration of all experiments carried out in this work. Therefore, all the data collected for the purpose of reactor modeling and reactor performance studies were under steady-state conditions.

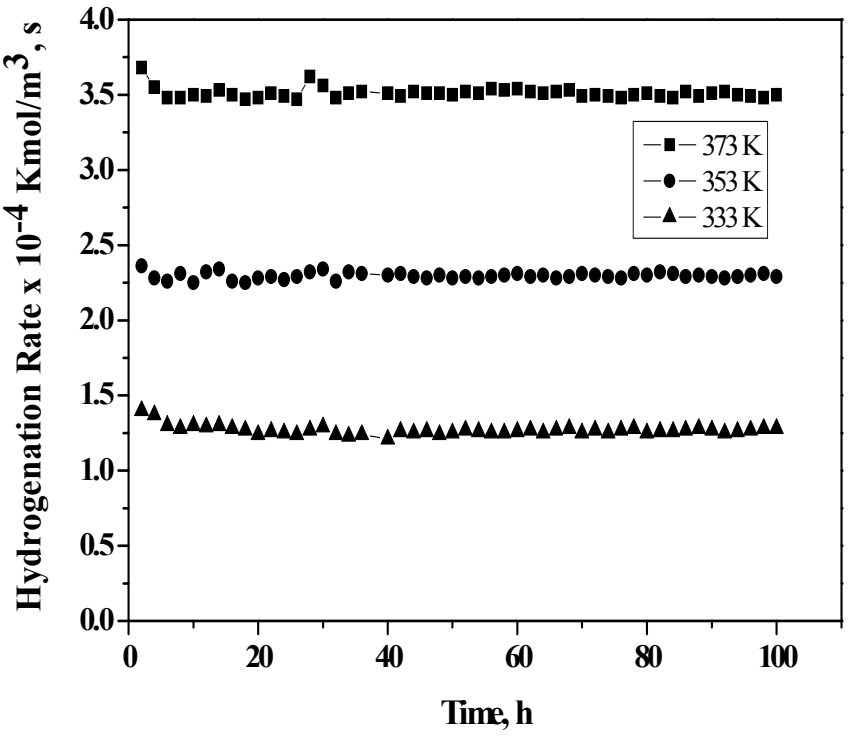

Figure 3.3. Time on stream catalyst activity profile.

Reaction conditions: hydrogen pressure, 2 MPa; hydrogen flow rate, 20 L/h; liquid flow rate, 20 mL/h; catalyst weight, 20 g.

3.6.2. Effect of reaction parameters:

3.6.2.1. Effect of liquid flow rate:

The effect of liquid flow rate on conversion of B_3D was studied in the range of 10-60 mL/h, under constant temperature, H_2 pressure, and gas flow rate conditions, and the result are shown in Figures 3.4 and 3.5. The conversion of B_3D decreased almost proportionately (from 70 to 12%) with increase in liquid flow rate from 10 to 60 mL/h (see Figure 3.4). One of the main reasons for decrease in the conversion is that, as the liquid flow rate was increased, the residence time of B_3D in the reactor was reduced and less time was available for the intimate contact of H_2 with liquid B_3D and with the

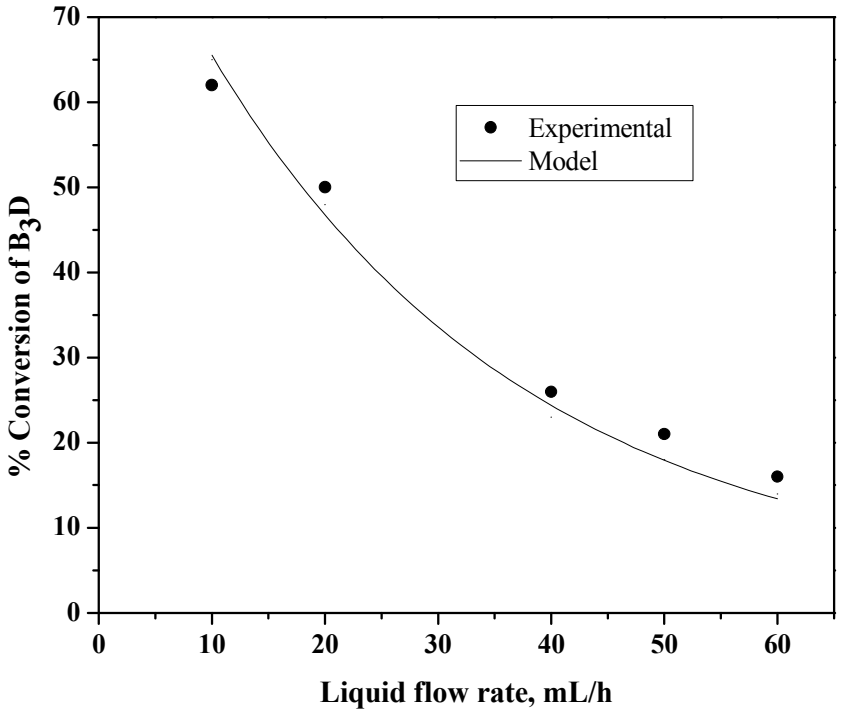

Figure 3.4. Effect of liquid flow rate on conversion.

Reaction conditions: hydrogen pressure, 2 MPa; hydrogen flow rate, 20 L/h; temperature, 373 K; catalyst weight, 10 g.

catalyst pellets; thus proper diffusion was not possible. Another reason is that, although the increase in the liquid flow rate could wet more surface area of catalyst pellets and there was an increase in the gas-liquid and liquid-solid mass transfer coefficient, at lower liquid velocity, catalyst particles were partially wetted; under these conditions, the rate of would increase due to direct transfer of the gas-phase reactant to the catalyst surface (already wetted internally due to capillary forces). Hence with an increase in gas-liquid flow rate, an increase in the wetted fraction was expected to retard the rate of reaction [89, 90]. The overall rate of hydrogenation (Figure 3.6) decreased with increase in the liquid flow rate. In the range of 10-25 mL/h liquid flow rate, the fall in the rate is fast, and eventually it becomes slower. The model predictions for the effect of liquid flow rate on the conversion and overall rate of hydrogenation are in well agreement with the experimental results (See Figures 3.4 and 3.6).

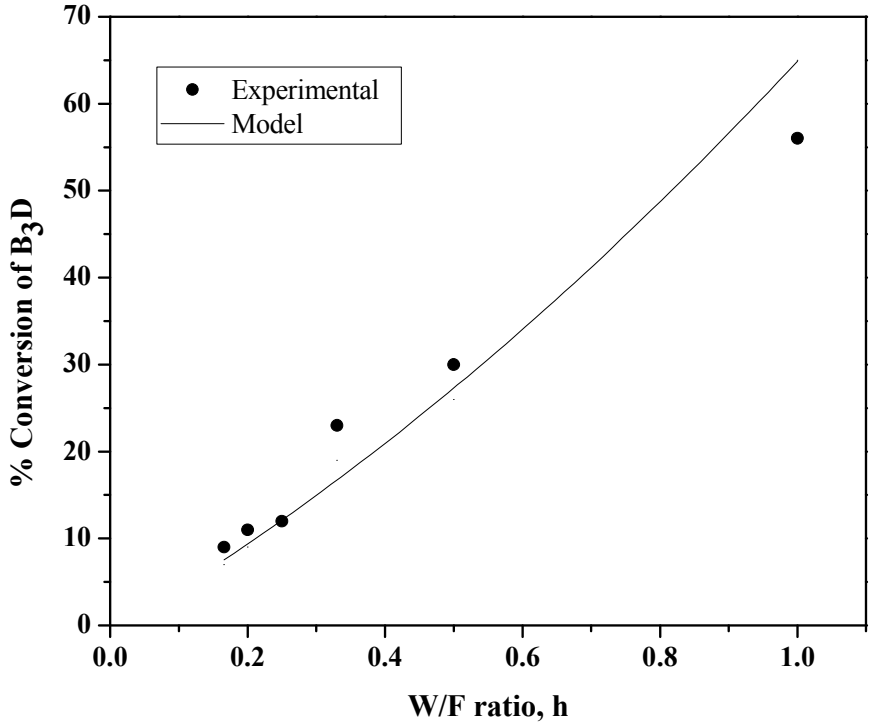

Figure 3.5. Effect of liquid flow rate on conversion.

Reaction conditions: hydrogen pressure, 2 MPa; hydrogen flow rate, 20 L/h; temperature, 373 K; catalyst weight, 20 g.

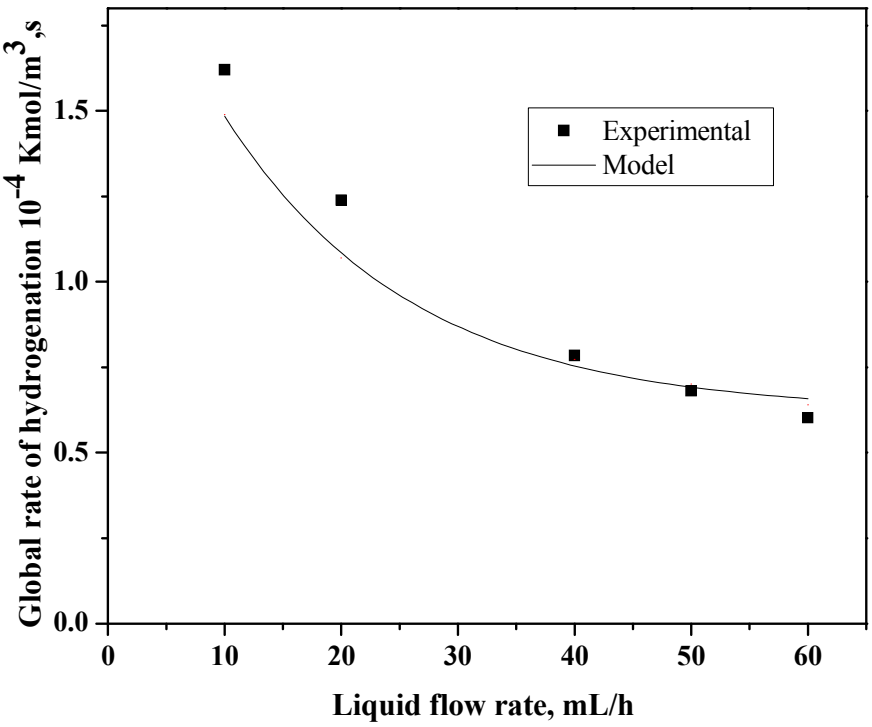

Figure 3.6. Effect of liquid flow rate on rate of hydrogenation.

Reaction conditions: hydrogen pressure, 2 MPa; hydrogen flow rate, 20 L/h; temperature, 373 K; catalyst weight, 20 g.

3.6.2.2. Effect of hydrogen pressure:

The effect of hydrogen pressure on the conversion of B_3D was studied in the range of 1-7 MPa H_2 pressure for 10 and 20 g of catalyst loadings and at 373 K, and the results are shown in Figure 3.7 Initially, B_3D conversion increased almost linearly with increase in pressure upto 4 MPa H_2 pressure. The overall rate of hydrogenation was also found to increase in H_2 pressure (Figure 3.8) for both the catalyst loadings. The increase in H_2 pressure increases the gas-liquid and liquid-solid transfer coefficient, leading to higher conversion and hydrogenation rates. It was interesting to note that with increase in H_2 pressure, the selectivity patterns of B_2D and B_1D were exactly opposite to each other (see Figure 3.9). In the lower range of H_2 pressure (1-4 MPa), the difference between the selectivities of B_2D and B_1D was larger; enventually, 50:50 formation of B_2D and B_1D

could be obtained at 7 MPa H_2 pressure. The predictions of the model equations for the effect of pressure on the conversion of B_3D, selectivity of B_2D and B_1D, and overall rate of hydrogenation is in good agreement with the experimental results.

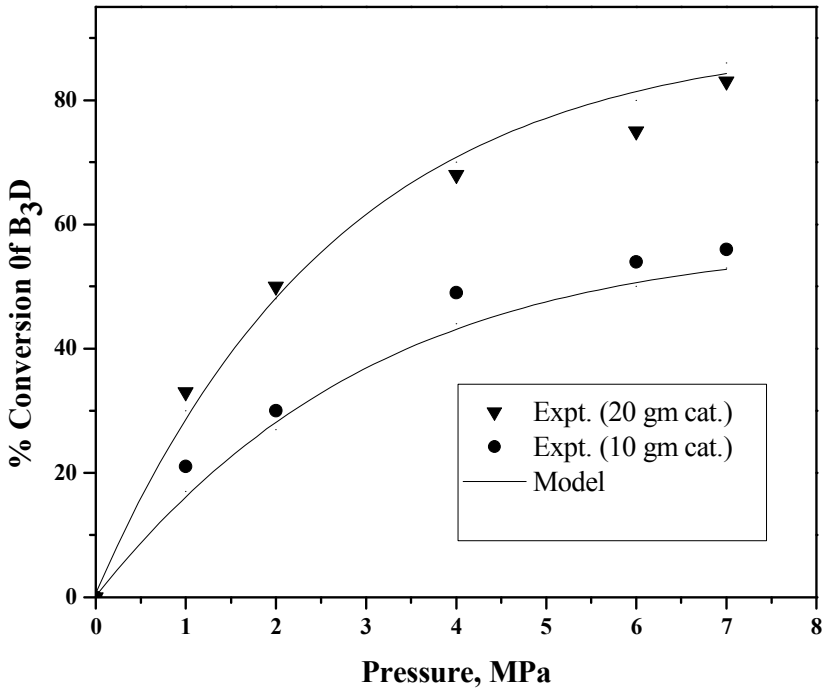

Figure 3.7. Effect of hydrogen pressure on conversion.

Reaction conditions: liquid flow rate, 20 mL/h; hydrogen flow rate, 20 L/h; temperature, 373 K.

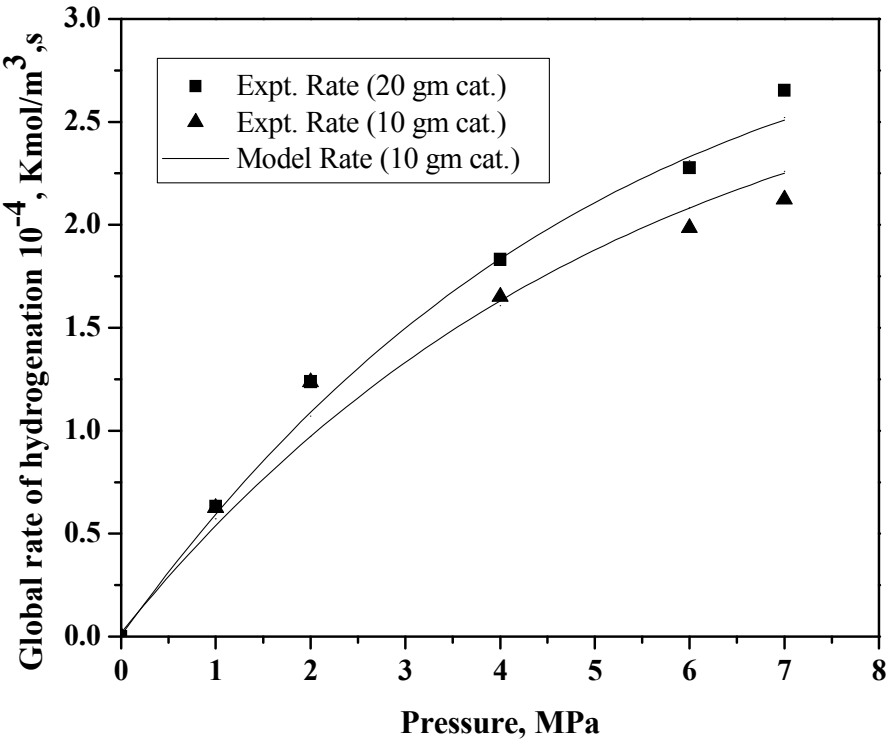

Figure 3.8. Effect of hydrogen pressure on rate of hydrogenation.

Reaction conditions: liquid flow rate, 20 mL/h; hydrogen flow rate, 20 L/h; temperature, 373 K.

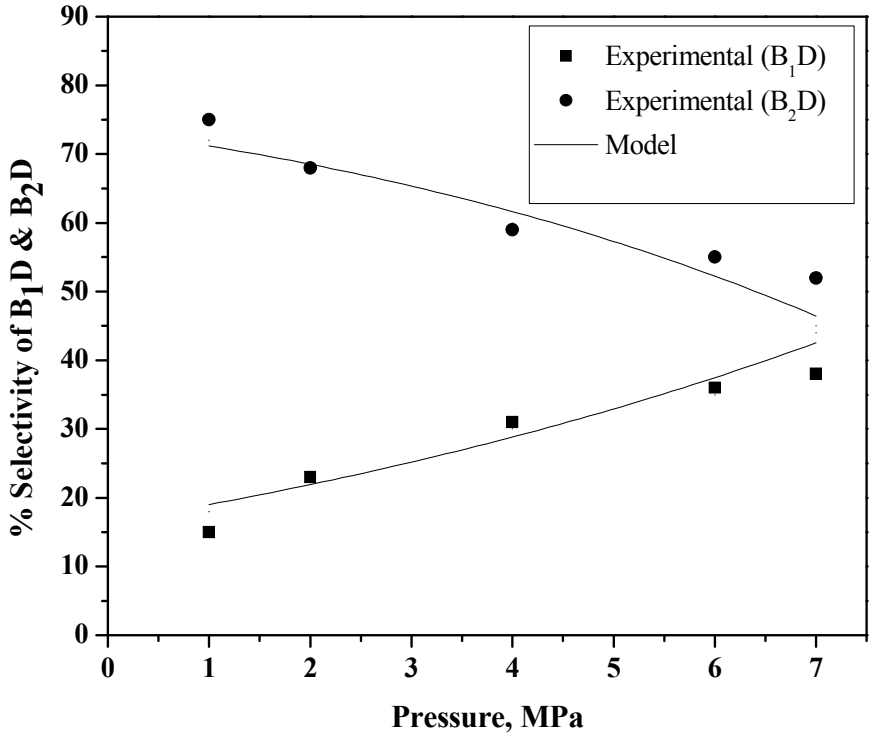

Figure 3.9. Effect of hydrogen pressure on selectivity of B_2D and B_1D.

Reaction conditions: liquid flow rate, 20 mL/h; hydrogen flow rate, 20 L/h; temperature, 373 K; catalyst weight, 20 g.

3.6.2.3. Effect of hydrogen flow rate:

The effect of hydrogen gas flow rate on conversion of B_3D and selectivities of B_2D and B_1D were studied in the range of 20-80 L/h at constant pressure, temperature, and liquid flow rate conditions. The conversion of B_3D was slightly lower at the lower and higher gas flow rates as compared with that in the middle range (Figure 3.10). The reason for this situation is that at lower gas flow rate the gas cannot overcome the gas-liquid mass transfer resistance, while at higher gas flow rates, although the gas reduces the liquid film thickness around the catalyst pellets, the gas phase becomes continuous, and the liquid phase becomes dispersed. With further increase in gas flow rate, the flow regime changes to spray flow regime, and this causes greater velocities in the liquid phase by

increasing the drag forces on the liquid phase. The selectivities to both B_2D and B_1D were nearly constant since the change in gas flow rate did not affect the intrinsic reaction kinetics to a considerable extent.

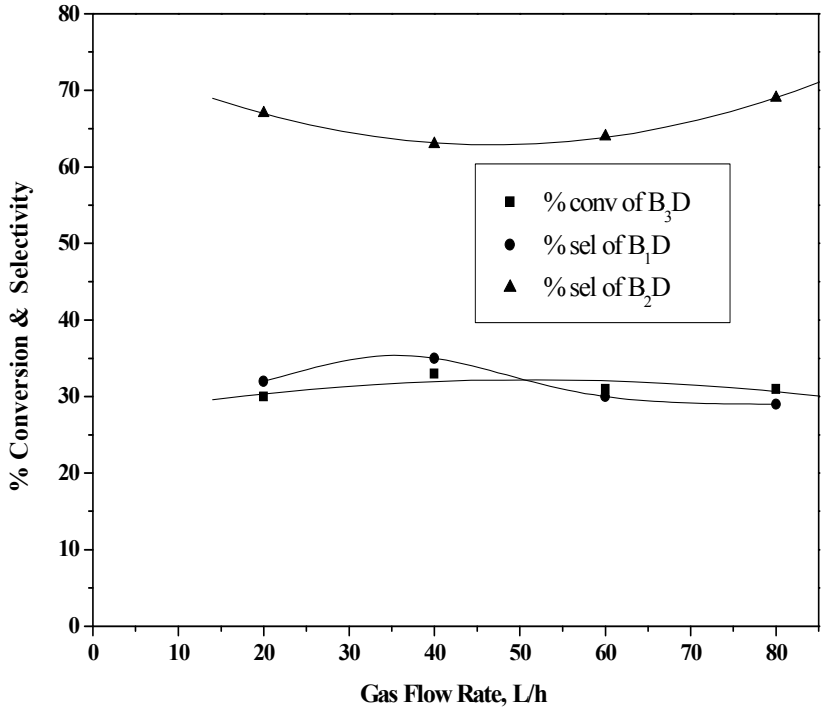

Figure 3.10. Effect of gas flow rate on conversion of B_3D.

Reaction conditions: liquid flow rate, 20 mL/h; hydrogen pressure , 2 MPa; hydrogen flow rate, 20 L/h; temperature , 373 K; catalyst weight, 10g.

3.6.2.4. Effect of temperature:

The effect of temperature on conversion of B_3D and selectivity patterns of B_2D and B_1D were studied by varying the temperature from 333 K to 373 K (Figure 3.11). The conversion increased from 5 to 30% with increase in temperature from 333 K to 373 K since, the temperature has a greater impact on the reaction kinetics. The selectivity patterns of B_1D and B_2D showed opposite trends with an increase in temperature, obviously because at higher temperature B_2D gets converted to the saturated diol B_1D.

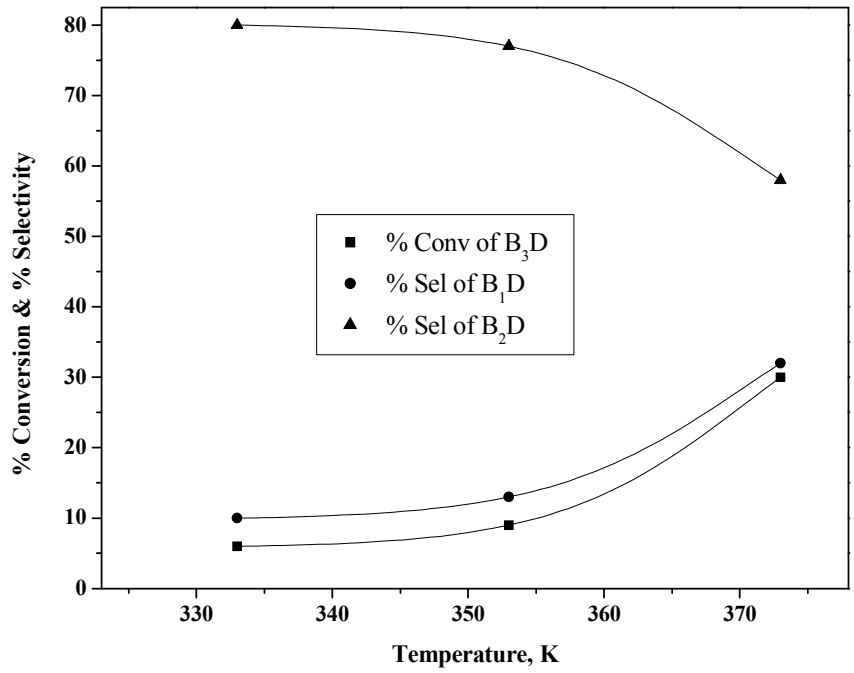

Figure 3.11. Effect of temperature on conversion of B_3D and selectivity of B_1D and B_2D.

Reaction conditions: liquid flow rate, 20 mL/h; hydrogen pressure, 2 MPa; H_2 flow rate, 20 L/h; catalyst weight, 10 g.

3.6.3. Reactor modeling:

A trickle-bed reactor model for the hydrogenation of B_3D was developed using rate data equations proposed by Telkar et al. based on the kinetic data in a slurry reactor to represent the intrinsic kinetics for different reaction steps as shown in Scheme 3.11 [75].

$$r_1 = \frac{wk_1 A^* B_1}{(1+K_B B_1+K_c C)^2} \quad \text{....3.1}$$

$$r_2 = \frac{wK_2A^*C_1}{(1+K_1B_1+K_c\,C_1)^2} \quad \text{....3.2}$$

The overall rate of hydrogenation can be given as

$$R_A = \frac{wk_1A^*(B_1+k_2C_1)}{(1+K_BB_1+K_cC_1)^2} \quad \text{....3.3}$$

Where *A, B_1* and *C_1* represents the concentration of H_2, B_2D and B_1D. A nonlinear least-squares regression analysis was used to obtain the values of the kinetic parameters in the above rate equation. For this purpose an optimization program based on the Marquardt's method [91] was used. The different kinetic parameter values evaluated for the above rate equation are given in Table 3.4

Table 3.4. Kinetic parameters for the hydrogenation of B_3D

Temperature (K)	rate constants ($(m^3)^2$/kmol.kg.s)		adsorption constants (kmol/m^3)	
	k_1	k_2	K_B	K_c
333	1.940	1.210	8.101	2.11
343	3.178	2.790	9.80	2.60
353	5.037	6.140	11.728	3.183
363	7.802	12.934	13.898	3.843
373	11.804	26.178	16.32	4.594

To develop a trickle-bed reactor model applicable to hydrogenation of B_3D, the approximate solution of the catalytic effectiveness factor was performed for partial wetting of catalyst particles [92]. The overall catalyst effectiveness factor could be expressed as a sum of weighted average of the effectiveness factor in the dynamic liquid-covered, stagnant liquid-covered and complete gas-covered zones and with the assumptions that (a) gas and liquid phases are in plug flow; (b) the liquid-phase reactant

is nonvolatile and was in excess as compared to the gaseous reactant; (c) the gas-liquid, liquid-solid, and intraparticle mass transfer resistances for H_2 are considered, whereas the liquid-solid and intraparticle mass transfer resistances for the liquid phase were negligible; (d) the interphase and intraparticle heat transfer resistances were negligible. The catalyst effectiveness factor equation for the hydrogenation of B_3D could be developed on the basis of the approaches already reported in the literature [93, 94]. Under the conditions of significant intraparticle gradient for the gas-phase reactant (H_2) and when the liquid-phase reactant was in excess, the overall rate of hydrogenation of B_3D was given as

$$R_A = \frac{\eta_c w k_1 A^* (B_1 + k_{21} C_1)}{(1 + K_B B_1 + K_C c)^2} \quad \text{....3.4}$$

Where η_c , the overall effectiveness factor for the spherical catalyst particle was given as

$$\eta_c = \frac{1}{\emptyset}\left(\coth 3\emptyset - \frac{1}{3\emptyset}\right) \quad \text{....3.5}$$

$\emptyset$ is the Thiele parameter, and final dimensionless parameters are given in Appendix 1. For calculating $\emptyset$, the values of effective diffusivity were estimated using the standard correlation [95, 96]. Various correlation used to calculate the different coefficients in this work are given in Appendix 1. The saturation solubility of hydrogen was calculated as

$$(A^*)_T = [P - (P_V)_T](H_e)_T \quad \text{....3.6}$$

Where, P_v is the vapor pressure of solvent.

At steady-state conditions, the sum of the convection term and gas-liquid mass transfer term were in equilibrium with the liquid-solid mass transfer term in the dynamic zone and the volumetric mass exchange between the dynamic and stagnant zone. The final mass balance equations in dimensionless form for species A (H_2) are given as

$$\frac{da_{1d}}{dz} = \propto_{g1} (1 - \propto_{1d}) - \frac{\eta_c \propto_r (b_1 + k_{21}c_1}{(1 + b_1k_b + c_1k_c)^2} x \left\{\frac{f_d a_{1d}}{(1 + \eta_c \emptyset^2/N_d)} + \frac{f_s a_{1d}}{(1 + \eta_c \emptyset^2/N_s + \eta_c \emptyset^2/\propto_s N_s)}\right\} \quad \text{....3.7}$$

Similarly, the mass balance of liquid-phase reactant/products in dimensionless form can be given as

$$\frac{db_{1d}}{dz} = -\frac{\eta_c \propto_r b_1 \chi}{q_B(1+b_1k_b+c_1k_c)^2} \quad \text{....3.8}$$

This equation represents the change in the concentration of B_3D in liquid phase in terms of dimensionless parameters.

$$\frac{dc_{1d}}{dz} = -\frac{\eta_c \propto_r (b_1 - k_{21}\, c_1)\chi}{q_B(1+b_1k_b+c_1k_c)^2} \quad \text{....3.9}$$

B_2D in liquid phase in terms of dimensionless parameters.

$$\frac{dp_{1d}}{dz} = -\frac{\eta_c \propto_r k_{21}\, c_1 \chi}{q_B(1+b_1k_b+c_1k_c)^2} \quad \text{....3.10}$$

This equation represents the change in the concentration of B_1D in liquid phase in terms of dimensionless parameters, where

$$\chi = \left\{\frac{f_d a_{1d}}{(1+\eta_c \emptyset^2/N_d)} + \frac{f_s a_{1d}}{(1+\eta_c \emptyset^2/N_s + \eta_c \emptyset^2/\propto_s N)} + \frac{(1-f_d-f_s)a_{1d}}{(1+\eta_c \emptyset^2/N_g}\right\} \quad \text{....3.11}$$

A programme code in Q-Basic was developed to get the output of eqs. 3.7-3.10. These equations were solved using a fourth-order Runge-Kutta method with the following initial conditions:

At $z = 0$; ….3.12

$a_1 = b_1 = 1$;

$c_1 - P_1 = 0$

The model equations developed above, allowed the prediction of concentrations of products/reactants along the length of the reactor. At any given length of the reactor the fractional conversion of B_3D (X_B) could be given as

$$X_B = 1 - b_1 \quad \text{….3.13}$$

The overall rate of hydrogenation was calculated as

$$R_A = \frac{U_1}{L}(C_1 + 2P_1) \quad \text{….3.14}$$

Here U_1, is the liquid velocity in m/s, L is the length of the catalyst bed in m, C_1, P_1 are the concentrations of B_2D and B_1D respectively. The selectivities of B_2D and B_1D were calculated as

$$S_{B_2D} = \frac{c_1}{(1-b_1)} \text{ X } 100 \quad \text{….3.15}$$

$$S_{B_1D} = \frac{P_1}{(1-b_1)} \text{ X } 100 \quad \text{….3.16}$$

The applicability of the model was verified by comparing the predicted concentration vs time profiles as well as conversion of B_3D and selectivities to B_2D and B_1D with the experimental results under various conditions. These results have already been discussed above and are shown in Figures 3.6-3.9, which showed an excellent agreement between the predicted values and the experimental data.

3.7. Hydrogenation of 2-butyne-1,4-diol using supported Pd nano catalyst:

Due to the growing importance of metal nanoparticles as catalysts, our aim of this work was to study the selective hydrogenation of 2-butyne-1,4-diol to 2-butene-1,4-diol using supported palladium nano particles. This is the continuation of the work reported by our group previously on the same system however, here we are reporting the new results which explicitly show the better performance of the Pd nanocatalysts than that of the bulk Pd catalyst [97].

Pd/C catalyst prepared in the presence of PVP as a stabilizer gave Pd particle size in a narrow range of 3-5 nm. PVP has a polycationic nature due to the presence of quaternary nitrogen, which helps in stabilizing the Pd nuclei formed during the reduction. The interaction between the negative charge of oxygen containing groups on an activated carbon surface and the cationic PVP causes the polymer to occupy the adsorption sites on the carbon [98, 99]**.**

Catalytic activity of supported palladium nanoparticles was tested for liquid phase hydrogenation of B_3D and the results are presented in Figure 3.12. As can be seen from Figure 3.12 , catalytic performance (% conversion) for these supported Pd nanoparticles catalyst showed much higher (9-21 times) activity than the bulk Pd/C catalyst prepared by conventional method. Activity for nanoparticle catalyst is higher due to the enhancement in rate of hydrogenation as evident from the hydrogen absorption vs. time plot for butyne diol hydrogenation shown in Figure 3.13. The dramatic enhancement of activity of supported Pd nanocluster catalyst is mainly due to the narrow particle size distribution giving an average size of 4 nm, and very high dispersion of Pd^o nuclei.

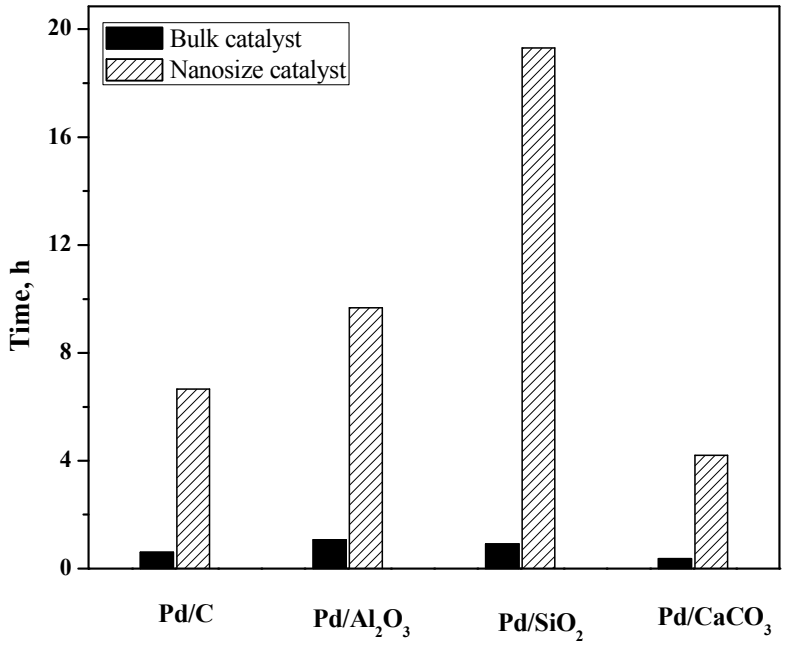

Figure 3.12. Conversion of B_3D

Reaction conditions: B_3D, 0.34 mol; temperature, 323 K; hydrogen pressure, 2.068 MPa; catalyst weight, 0.075 g. agitation speed, 1000 rpm

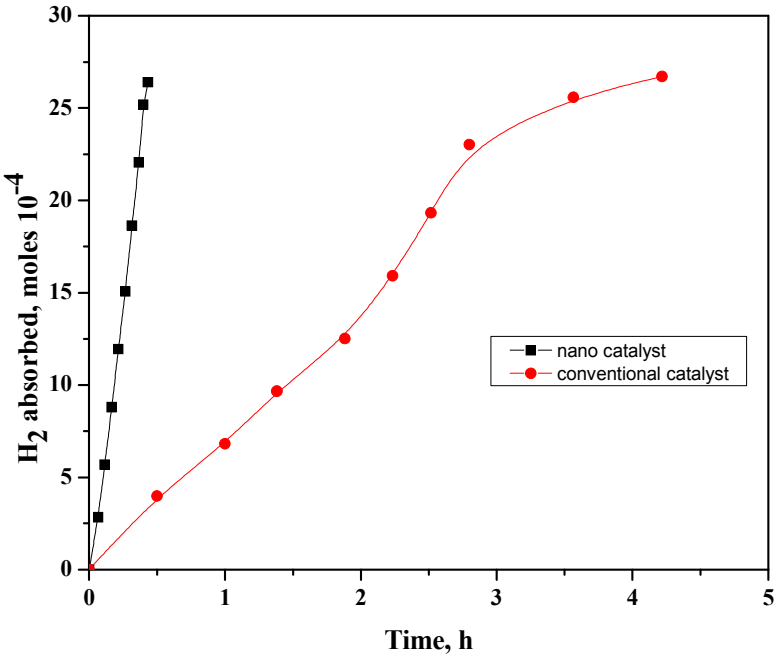

Figure 3.13. Hydrogen consumption vs. time plot

Reaction conditions: B_3D, 0.34 mol; temperature, 323 K; hydrogen pressure, 2.068 MPa; catalyst (0.25 % Pd/$CaCO_3$) 0.075 g; agitation speed, 1000 rpm

The pulse titration of (hydrogen) studies (Table 3.5) showed that the metal dispersion found for the nano catalyst was >65% higher that for the bulk Pd/C catalyst. The low Pd loading (0.25%) as well as the decreased average crystallite size (H/Pd ratio = 1) from 12.7 nm (bulk Pd) to 7.6 nm for the nano catalyst contribute to a very high metal dispersion leading to the enhancement in the catalytic activity.

Table 3.5: Catalyst characterization by pulse titration

Catalyst	Dispersion (%)	Metal Surface area (m^2/g)	H_2 Adsorbed (μmole/g)	Crystallite size (nm)
Pd/C bulk	8.8	0.10	1.03	12.7
Pd/C nano	14.7	0.16	1.73	7.6

The nanosize Pd^o particles are protected by the bulky polymer groups of the stabilizer PVP on the surface, which cannot penetrate through the micropores of the carbon support, whereas in case of conventional Pd/C catalyst, Pd^0 is adsorbed in several ways including the micropores of the support and such sites would be inaccessible for hydrogenation [100]**.** It was also observed that the size of Pd particles did not change after deposition on the support (average dTEM = 2.8 and 3 nm before and after deposition, respectively). The observed catalyst activity was also several times (x4) higher than reported recently for a heterogeneous Pd nanocluster catalyst (TOF 10,100 h^{-1}), which was prepared from Pd mixed monolayer protected clusters (Pd MMPC) and carboxylic acid-silica colloid and then activating the catalyst by calcination at 773 K [101]. The apparent activation energy of hydrogenation of butyne diol to butane diol over Pd nanoparticle catalyst evaluated in our work (Figure 3.14) was 13.6 kJ/mol which is about one third than that observed is case of bulk Pd catalyst (39.42 kJ/mol) [102].

Detailed calculations for the activation energy is given below

Rate of reaction at various temperatures were calculated using the equation 3.17 & the results are presented in Table 3.6.

$$\text{Rate of reaction} = \frac{\text{moles of hydrogen consumed}}{\text{time in sec}} \qquad \text{…..3.17}$$

Table 3.6. Rate of reaction at various temperatures

Temperature	K^{-1}, (1/T)	Rate of reaction, mol/sec.cm^3	lnR
323	0.00310	8.41×10^{-7}	-13.98
338	0.00296	1.114×10^{-6}	-13.76
353	0.00283	1.3435×10^{-6}	-13.52

The activation energy of the reaction was calculated according to Arrhenius equation 3.18,

$$k = Ae^{-Ea/RT} \quad \text{.....3.18}$$

Where,

k rate constant

A pre-exponential factor

R gas constant, 8.31 J/molK

T Temperature

Ea activation energy

By rearranging this equation 3.18

$$\ln R = \ln k_0 - \frac{E_a}{RT} \quad \text{……3.19}$$

which is in the form of *y*= mx + c

Where,

Slope= m = - Ea/R

Intercept = c = $\ln k_o$

The lnR (rate constant) was plotted vs. the inverse of the temperature.

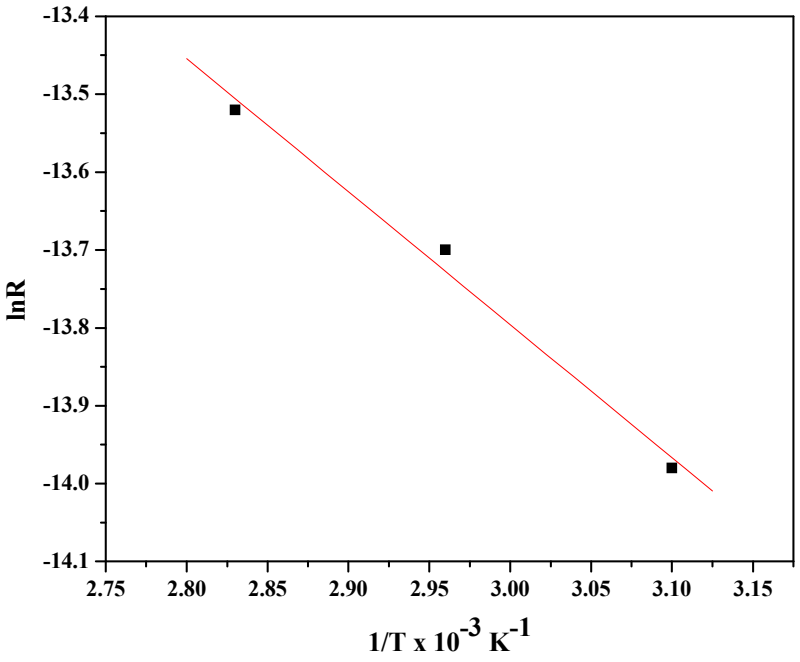

Figure 3.14: Arrhenius plot

Reaction conditions: B_3D, 0.34 mol; hydrogen pressure, 2.068 MPa, catalyst (0.25 % $Pd/CaCO_3$), 0.075 g; agitation speed 1000 rpm.

Slope of plot (m) was found to be -1641.37

Activation energy $E_a = -mR$

= slope x 8.31

=13.639 KJ/mol

Such dramatic decrease in apparent activation energy for nanoparticle Pd catalyst suggests either: (i) being a gas-liquid- solid reaction, the reaction could be operating under conditions such that the mass transfer resistances are significant or (ii) the different adsorption characteristic of butyne diol from those for the bulk palladium catalyst. The initial rate data of the present work was independent of agitation speed and also the factor α_1 (defined as the ratio of the observed rate of reaction to the maximum rate of gas-liquid mass transfer rate) estimated was < 0.03. These two criteria clearly confirmed that the results on catalyst activity of the Pd nanoparticles obtained in the present work were independent of mass transfer resistance [37]. Due to very small catalyst particle size, the

intraparticle and liquid-solid mass transfer resistance also do not have any influence on the activity [37, 102]. Hence, the lower activation energy for the nanoparticle Pd/C catalyst is purely due to its specific adsorption characteristics which needs to be investigated further to reveal the nature adsorption.

Another interesting feature of our catalyst was a change in selectivity pattern in case of 2-butyne-1,4-diol hydrogenation (Figure 3.15). The commercially used 1% Pd/C catalyst gave saturated butane diol as the major product while, the supported Pd nanocluster catalyst gave almost complete selectivity to the intermediate olefinic diol (B_2D) [75]. It is believed that α- and β-Pd-hydride species are formed during hydrogenation and that β sites promote alkane selectivity due to mainly higher amount of hydrogen dissolved within the particles [103] **.** However, it has been shown that for very small particles, β-Pd-hydride phase is rarely formed [104, 105] hence a dramatic size reduction in case of nanocluster Pd/C catalyst could lead to the enhanced selectivity to the olefinic diol. The increased effect of steric hindrance (geometric effect) due to the stabilizer in case of the protected Pd nano particles also contributes to the higher selectivity to the olefinic diol [36].

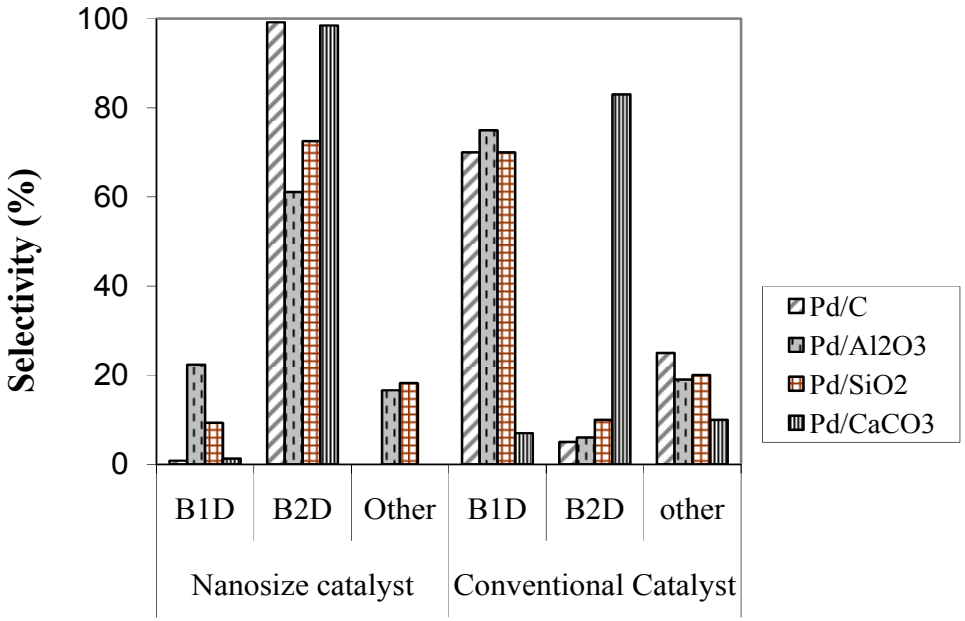

Figure 3.15. Catalytic performance of nanosize and bulk Pd on different supports

Reaction conditions: B_3D, 0.34 mol; temperature, 323 K; hydrogen pressure, 2.068 MPa; catalyst weight, 0.075 g; agitation speed, 1000 rpm.

After the hydrogenation run, the catalyst was separated by filtration and the reaction mixture was analyzed for Pd content by AAS, which showed Pd in the range of less than 5 ppm. The clear filtrate was tested for the hydrogenation of fresh butynediol, and which showed no hydrogenation activity. Both these results rule out the possibility of leaching of Pd metal from the supported Pd nanocluster catalyst.

Several Pd nano particle catalysts using PVP as a stabilizer and supported on alumina, silica, and calcium carbonate were prepared similar to Pd nanoparticles supported on carbon. These results obtained were compared with the corresponding conventional Pd catalyst is very low (5-10%) except for Pd supported on $CaCO_3$ where the selectivity obtained is 83%. The other side products obtained were butyraldehyde, butanol and

acetals [37]. The formation of other side products were minimized or completely eliminated (Pd/C and Pd/$CaCO_3$) using nanosize Pd catalyst.

In the present work, PVP was used as a stabilizer because it has two hetero atoms (oxygen, nitrogen) which make the capping of metal particles more efficient leading to size reduction of Pd [36]. PVP also prevents the Pd particle aggregation and grain growth effectively due to its steric effect [106].

3.8. Pd-funtionalized carbon nanotubes for selective hydrogenation of 2-butyne-1,4-diol:

Carbon is one of the best supports for several active metal functions in heterogeneous catalysis, mainly due to its high resistance to acidic/basic media and easy separation from the reaction crude for subsequent reuse [107, 108]. Although the carbon nano tubes were being prepared by thermal decomposition of hydrocarbons over solid catalyst since long, it has become the focus of research from both technological as well as fundamental point of view recently [109, 110]. In the area of heterogeneous catalysis, CNTs have been used as catalysts as well as support material due to their specific structural and electronic properties [111, 112]. The activity of CNTs for particular reaction can be enhanced by functionalizing it with suitable surface modifying agent followed by the loading of metallic salt [113]. Metal functionalized CNTs are robust and more promising as catalysts than the normal carbon supported catalysts for industrially important reactions such as hydrogenation due to their uniform pore dimensions, higher H_2 uptake capacity, large specific surface area, and the hydrophobic character of surface and good chemical stability [114]. Hence, one of the objectives of this work was to explore the suitability of functionalized CNTs as a catalyst for hydrogenation of B_3D. For this purpose, we prepared Pd functionalized CNTs by thermal decomposition method followed by the deposition of Pd on acid treated CNTs via covalent attachment with –COOH and –OH groups present on the nanotube surface. The prepared material was characterized by various techniques like BET surface area measurement, TEM, SEM, EDX, ICP-OES, FT-IR, Raman and XRD and its catalytic performance was evaluated for the hydrogenation of 2-butyne-1,4-diol. We found that the Pd functionalized CNTs showed complete

conversion of B_3D with 93% selectivity to the olefinic diol (B_2D). This catalyst could be recycled successfully for three times maintaining its original activity and selectivity.

3.8.1. Catalyst characterization:

3.8.1.1. BET surface area measurements:

The specific BET surface area of CNTs, Pd/CNTs and Pd/C catalysts are presented in Table 3.7. The specific BET surface area of the catalysts decreased in the following order: Pd/C > CNTs > Pd/CNTs. Among the three catalysts, Pd/C showed the highest surface area of 825 m^2/g. Interestingly, BET surface area of CNTs decreased marginally from 162 to 151 m^2/g after impregnation of Pd on CNTs. This marginal decrease in surface area was due to a well dispersion of Pd on CNTs and also indicates that no structural damage (e.g. pore blockage) was observed during post synthesis impregnation process.

Table 3.7. Catalyst activity test

Entry	Catalysts	BET surface area, m^2/g	Conversion, %	Selectivity, %		
				B_2D	B_1D	Other
1	CNTs	162	-	-	-	-
2	Pd/CNTs	151	100	93	7	-
3	Pd/C	816	100	70	6	24

Reaction conditions: B_3D, 0.034 mol; temperature, 333 K; hydrogen pressure, 0.69 MPa; water, 87 mL; catalyst weight, 0.005 g; agitation speed, 1000 rpm.

3.8.1.2. Fourier transform infra-red (FTIR) studies:

The presence of –COOH and –OH groups on CNTs due to acid treatment were confirmed by FTIR analysis. The FTIR spectra of CNTs and Pd/CNTs are presented in Figure 3.16. CNTs sample showed bands at 1630 and 3445 cm^{-1} (Figure 3.16 (a) and (b)) due to the C=O and O-H stretching respectively indicating the presence of –COOH and –OH group

[115-116] Two weak bands were also observed at 2850 and 2925 cm^{-1} in CNTs which could be assigned to C-H symmetric and asymmetric stretching respectively [117-118]. Similar to CNTs, Pd/CNTs sample also showed bands at 1630, 2925 and 3445 cm^{-1} due to C=O, C-H (asymmetric) and O-H stretching respectively.

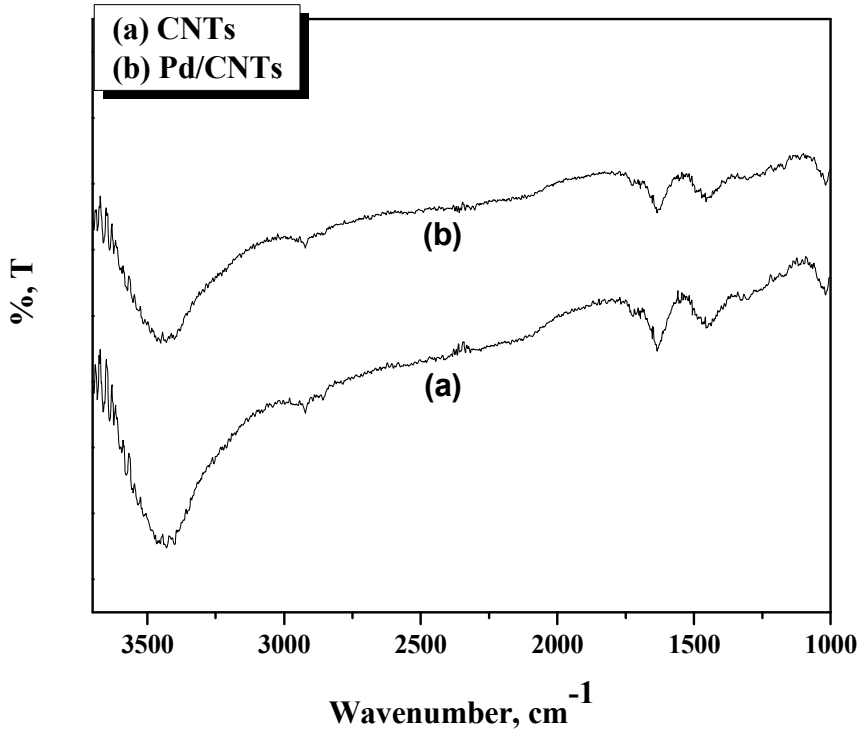

Figure 3.16. FTIR spectra of (a) acid treated CNTs (b) Pd/CNTs.

3.8.1.3. Raman spectroscopy:

Figure 3.17 shows the Raman spectra of purified as well as acid-treated CNTs. Raman spectroscopy offers to assess the defects in the structure and crystallanity of CNTs [119]. The Raman spectra of CNTs showed two first-order characteristic peaks viz. G-band peak due to the in-plane oscillations of sp^2 carbon atoms in CNTs [120] and D-band peak due to the presence of defects in CNTs [121]. The G- and D-band peaks for purified CNTs were observed at 1569 and 1321 cm^{-1} respectively. After the acid treatment, these peaks appear slightly shifted to 1572 and 1322 cm^{-1}. The intensity ratio of D- to G-band

(I_D/I_G) indicates the extent of defects within CNTs [122]. The smaller the value of I_D/I_G is, the lesser the structural defects in CNTs would be. In our case, the values of I_D/I_G for purified CNTs and COOH-functionalized CNTs were estimated to be 0.7536 and 1.0436 respectively. This confirms that the acid treatment has created defects on the nanotube surface and favored the formation of –COOH functionalized nanotubes.

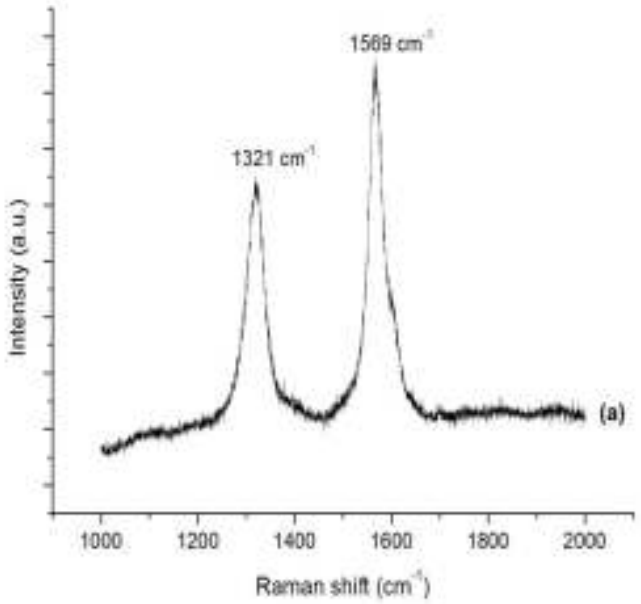

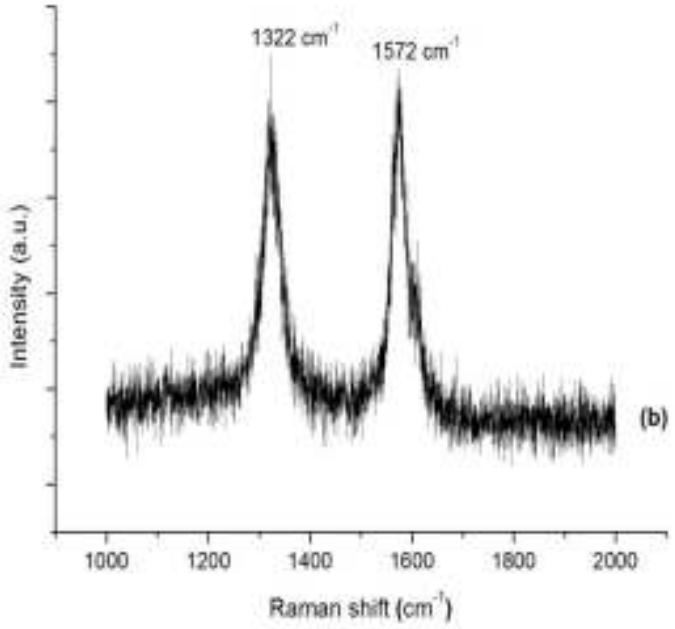

Figure 3.17. Raman spectra of (a) purified and (b) acid-treated CNTs

3.8.1.4. XRD analysis:

XRD patterns of CNTs and Pd/CNTs catalysts are shown in Figure 3.18. CNTs showed typical peaks at 2θ =25.8^{o} and 44.2^{o} corresponding to diffraction of (0 0 2) and (1 0 0) planes.[123, 124] Interestingly, the intensity of peaks at 2θ = 25.8^{o} and 44.2^{o} was significantly reduced and new peaks at 2θ = 40.2^{o}, 46.7^{o} and 68.1^{o} appeared after 5% Pd loading on CNTs. The peaks at 2θ = 40.2^{o}, 46.7^{o} and 68.1^{o} can be assigned to (1 1 1), (1 1 0) and (1 0 0) crystalline plane respectively for loaded Pd metal [125]. It can be also observed from XRD pattern of the prepared catalyst (Figure 3.18) that Pd was reduced to Pd^{o} state in Pd/CNTs catalyst [126]. The average particles size of Pd in prepared Pd/CNTs catalyst calculated by the Scherrer equation was found to be of 12 nm.

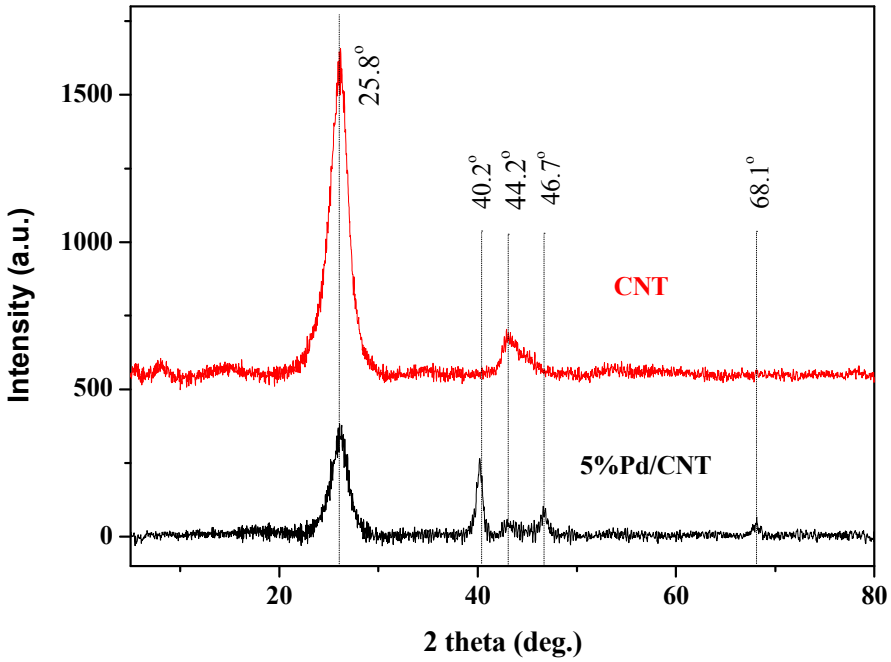

Figure 3.18. XRD pattern for (a) CNTs (b) Pd/CNTs.

3.8.1.5. EDX and ICP-OES analysis:

EDX analysis of Pd/CNTs sample is presented in Figure 3.19. The presence of signal corresponding to Pd metal indicates deposition of Pd on CNTs. The presence of Pd on CNTs was also confirmed and estimated quantitatively by ICP-OES analysis, which showed the impregnation of 4.1% of Pd on CNTs.

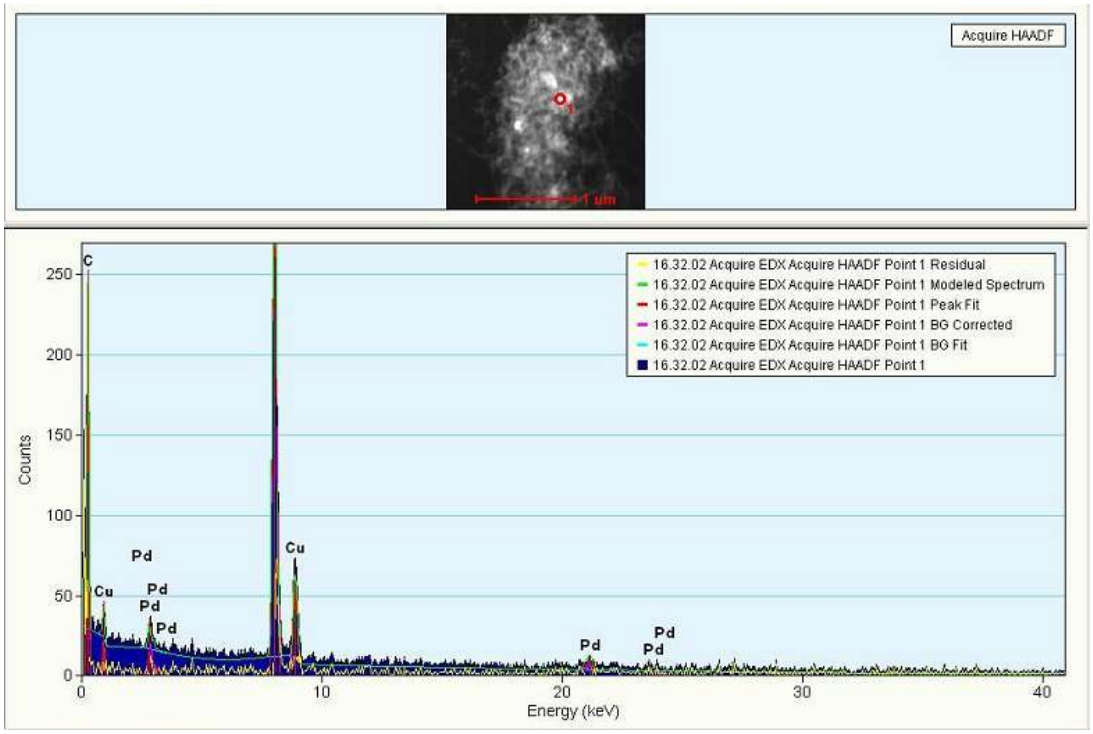

Figure 3.19. EDX of Pd supported on CNTs.

3.8.1.6. SEM and TEM analysis:

SEM image of the prepared CNTs is shown in Figure 3.20. The CNTs showed tubes or rod like morphology which was also confirmed from TEM analysis. TEM images of prepared CNTs and Pd/CNTs samples are shown in Figure 3.21. As can be seen from Figure 3.21a that CNTs were double walled having average external diameter ranging from 22 to 25 nm. Low magnification TEM images (Figure 3.21b-c) clearly showed that Pd particles were well dispersed on CNTs.

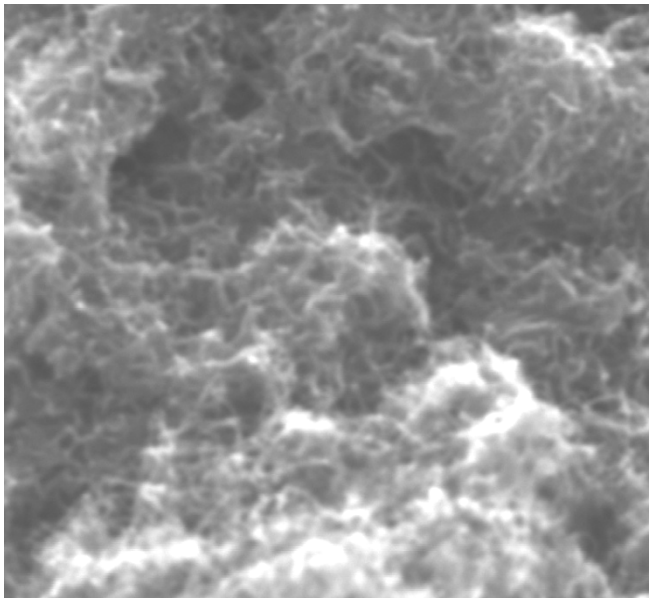

Figure 3.20. SEM photograph of as synthesized CNTs.

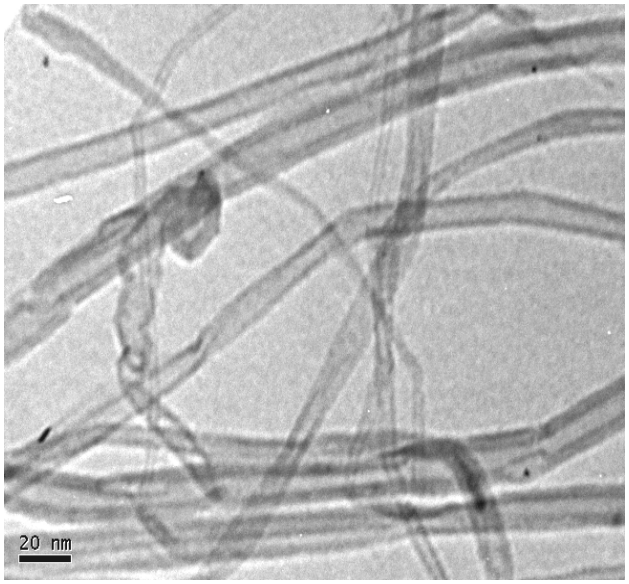

(a)

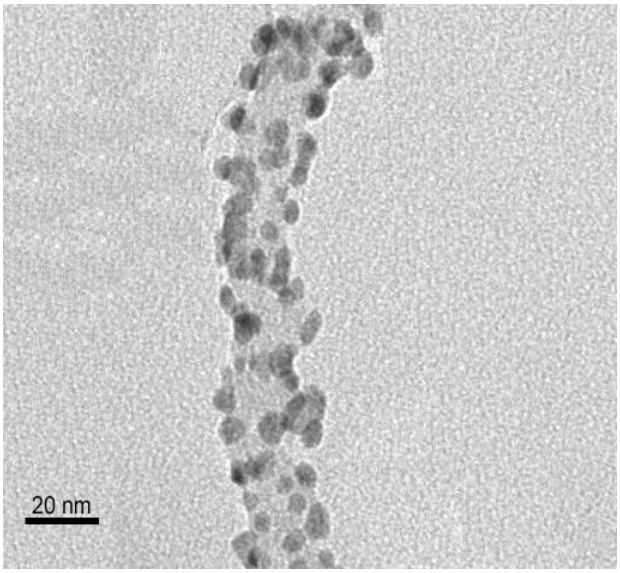

(b)

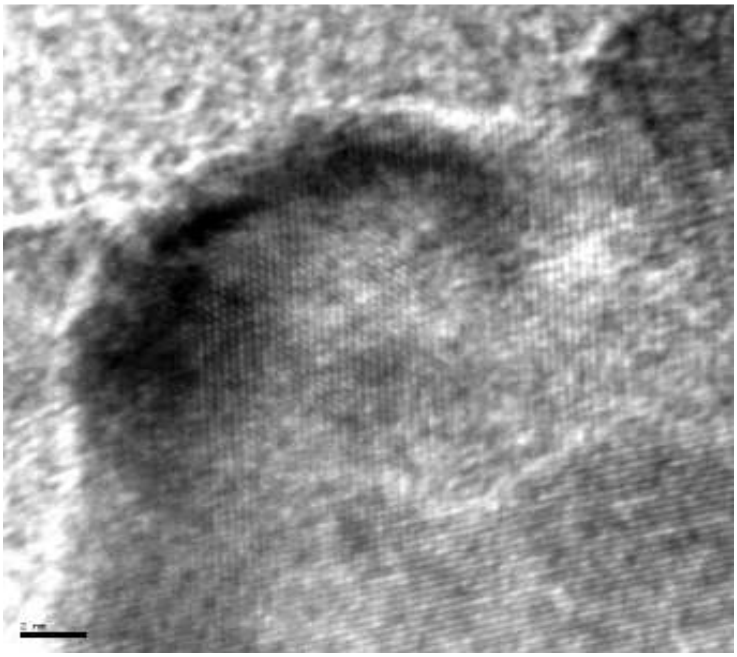

(c)

Figure 3.21. TEM images of (a) CNTs, (b) and (c) Pd/CNTs.

3.8.2. Catalyst performance study:

3.8.2.1. Catalyst activity:

The catalytic performance of the prepared Pd/CNTs catalyst was evaluated and compared with commercial Pd/C catalyst for liquid phase hydrogenation of B_3D to B_2D and B_1D (Table 3.7 and Scheme 3.11). CNTs itself showed no catalyst activity for the hydrogenation of B_3D. However, significant activity of CNTs was observed after dispersion of Pd on it. As can be seen from Table 3.7 both commercial Pd/C and Pd/CNTs catalysts showed complete conversion of B_3D after 5 h inspite of very low surface area of Pd/CNTs (151 m^2/g) as compared to that of Pd/C (816 m^2/g) indicating that the metal dispersion is much better on CNTs than that on the bulk carbon support. Another interesting observation was that Pd/CNTs catalyst showed very high selectivity (> 92%) to B_2D as compared to that obtained for commercial Pd/C catalyst (70%) to B_2D. The lower selectivity to B_2D (70%) with Pd/C catalyst was due to the formation of B_1D and other side products like γ-hydroxybutyraldehyde, n-butryaldehyde, n-butanol

etc. It has been reported that in case of CNTs, electrons are mainly residing along the tube axis giving rise to formation of pure quantum wires (1D-system) [127]. This will lead to the change in electronic environment causing the modified adsorption characteristics of the Pd dispersed on CNTs eventually giving rise to higher selectivity to B_2D.

3.8.2.2. Effect of reaction time:

Since, hydrogenation of B_3D involves consecutive/parallel reactions, the effect of reaction time on the B_3D conversion and products selectivity was also studied at 333 K and 0.69 MPa hydrogen pressure and the results obtained are presented in Figure 3.22. The conversion of B_3D increased from 5 to 96% with increase in reaction time from 0.5 to 4 h, thereafter it increased marginally from 96 to 100% with further increase in reaction time from 4 to 5.5 h. Initially, complete selectivity (100%) to B_2D was obtained after 1h which marginally decreased to 92% with increase in reaction time from 1 to 5.5 h. The decrease in B_2D selectivity was mainly due to its further hydrogenation to B_1D. The selectivity to B_1D increased from 0 to 8% with increase in reaction time from 0.5 to 5.5 h.

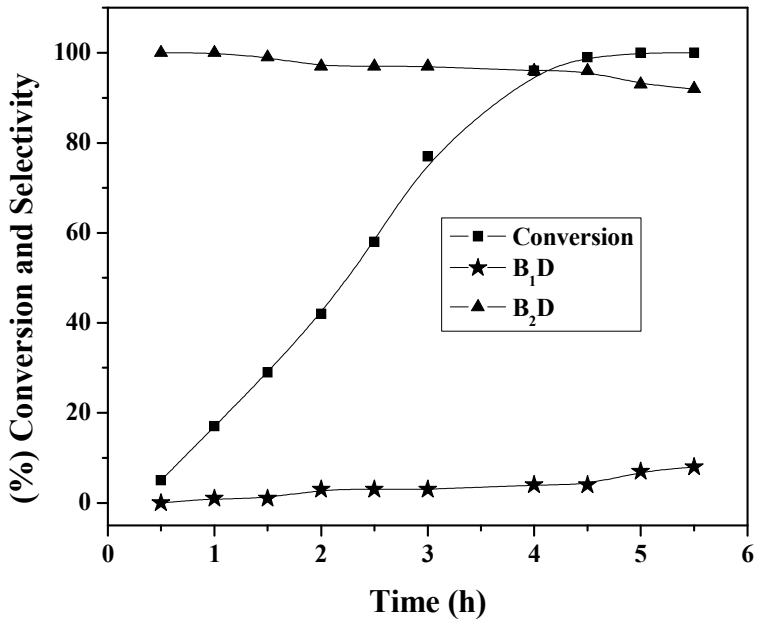

Figure 3.22. Effect of reaction time on conversion and product selectivity

Reaction conditions: B_3D, 0.034 mol; water, 87 mL; catalyst weight, 0.005 g; hydrogen pressure, 0.69 MPa; temperature, 333 K; agitation speed, 1000 rpm.

3.8.2.3. Catalyst recycle study:

The reusability of the catalyst for the hydrogenation of B_3D was assessed by the catalyst recycle experiment which is described below. After the first hydrogenation run, the catalyst was filtered and washed it with distilled water for several times, then dried at room temperature and then in an oven at 383 K for 2 h and reused it for subsequent runs. This procedure was followed for three subsequent hydrogenation experiments and the results are shown in Figure 3.23. The catalyst was found to retain its activity even after the third recycle experiment giving 100% conversion of B_3D with 93% selectivity to B_2D.

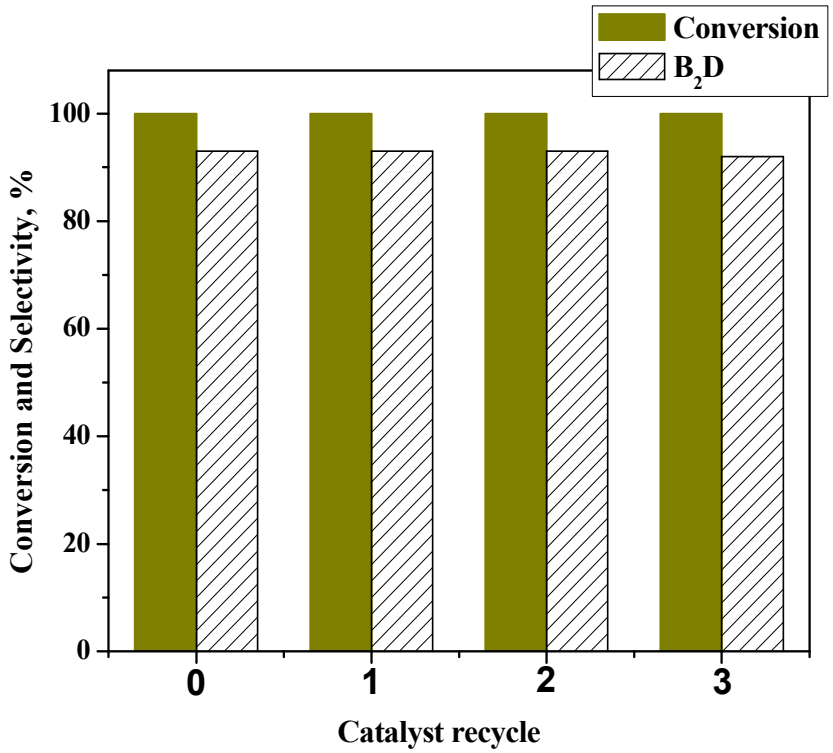

Figure 3.23. Catalysts recycle experiment

Reaction conditions: B_3D, 0.034 mol; temperature, 333 K; hydrogen pressure, 0.69 MPa; water, 87 mL; catalyst weight, 0.005 g; agitation speed, 1000 rpm.

3.9. Conclusion:

Hydrogenation of 2-butyne-1,4-diol (B_3D) was carried out using 1% $Pt/CaCO_3$ catalyst in a fixed-bed reactor. This process represents a consecutive reaction scheme giving 2-butene-1,4- and butane-1,4- diols. In a continuous hydrogenation process, the ratio of butene- and butane diols could be manipulated by tailoring the operating conditions for the same catalyst. The liquid flow rate and pressure of the hydrogenation gas showed a significant effect on the conversion of B_3D and overall rate of hydrogenation. A theoretical model was also developed incorporating the conditions of external and intraparticle mass transfer, partial wetting of the catalyst and reaction kinetics of butyne diol hydrogenation in a batch slurry reactor. The reactor model was validated by carrying

out hydrogenation experiments under various reactor inlet conditions, and model predictions were found to agree well with the observed conversion, selectivity data.

The supported palladium nanoparticles prepared in this work showed a very high catalytic activity with ease of separation for B_3D hydrogenation reactions. The higher activity of palladium nanoparticles than that of bulk Pd catalyst for butynediol hydrogenation was demonstrated by faster hydrogen consumption and lowering (one third) in apparent activation energy of the reaction.

The catalyst activity of Pd/CNTs prepared by thermal decomposition followed by Pd functionalization was compared with that of bulk Pd/C for the hydrogenation of B_3D to B_2D. The intensity ratio of D- to G-band (I_D/I_G) for purified CNTs and –COOH functionalized CNT obtained in Raman spectroscopic characterization were estimated to be 0.7536 and 1.0436 respectively, confirming that the acid treatment created the defects on the nanotube surface and favored the formation of COOH-functionalized nanotubes responsible for Pd deposition. Although Pd/C catalyst had higher surface area of 816 m^2/g than that of Pd/CNTs catalyst (151 m^2/g), both the catalysts gave complete conversion of B_3D. Interestingly, Pd/CNTs showed higher selectivity (93%) to B_2D than that for Pd/C (70% selectivity to B_2D) which could be due to modified electronic environment of Pd on CNTs. The conversion of B_3D increased from 5 to 100% and selectivity to B_2D decreased from 100 to 93% with increase in reaction time from 0.5 to 5 h. The catalyst was found to retain its activity even after the third recycle experiment giving complete conversion of B_3D with 93% selectivity to B_2D.

Appendix I

(1) Dimensionless parameters used in the model

gas-liquid mass transfer	$a_g = k_1 a_B L/U_1$
liquid-solid mass transfer	$a_{1s} = k_s a_p L/U_1$
Gas-solid mass transfer	$a_{gs} = k_{gs} a_p L/U_1$
Nusslet no. in dynamic zone	$N_s = Rk_{sd}/3D_e$
Nusslet no. in stagnant zone	$N_s = Rk_{Ss}/3D_e$
reaction rate constant	$\propto_r = Lwk_1 b_i/U_1$
equilibrium constant	$k_{21} = k_2/k_1;\ k_b = K_B B_1$
Thiele parameter	$\emptyset = \frac{R}{3}\left[\frac{S_p(k_1 B_1 + k_2 C_1}{D_e(1 + K_B B_1 + K_c C_1)^2}\right]^{1/2}$

(2) Correlations used in section 3.6.3 work:

Parameter	Authors	reference
molecular diffusitivity	Wilke and Chang	95
gas-liquid mass transfer coefficient	Goto and Smith	128
liquid-liquid mass transfer coefficient	Satterfield et al.	129
gas-particle mass transfer coefficient (value used)	Zheng Lu et al.	130
volumetric mass exchange coefficient	Hochmann and Effron	131
total liquid hold-up	Sato et al.	132
static liquid hold-up (value used)	Zai-sha Mao et al.	133
saturation solubility	Stephen and Stephen	134
wetting efficiency	Mills and Dudikovic	135

3.10. References:

1. M. Bartók in *Stereochemistry of heterogeneous metal catalysis,* Ch. IV., Wiley & Sons, New York (1985) pp. 457.
2. A. Molnar, A. Sarkany, M. Varga *J. Mol. Catal. A: Chemical* 173 (2001) 185.
3. P. N. Rylander in *Catalytic hydrogenation over platinum metals,* Ch. IV Academic Press, New York, (1967) pp. 59 .
4. C. V. Rode *J. Jpn. Petro. Insti.* 51 (2008) 119 .
5. Hoechst *DE-AS 1015797* (1954) .
6. J. M. Winterbottom, H. Marwan, J. Viladevall, S. Sharma, S. Ramashasay *Stud. Surf. Sci. Catal.* 108 (1997) 59.
7. G. W. Parshall, W. A. Nugent *Chemtech.* (1988) 184.
8. G. W. Parshall, W. A. Nugent *Chemtech.* (1988) 314.
9. G. W. Parshall, W. A. Nugent *Chemtech.* (1988) 376.
10. R. V. Chaudhari in *Proceedings of the Indo-German workshop on high pressure technology-engineering*, R. V. Chaudhari, H. Hofmann (Eds.), Forschungszentrum Julich GmbH, (1993) pp. 197.
11. *Ullmans Encyclopedia of chemical Technology*, Vol. A4, 457.
12. R. A. Frestone, E. E. Harris, W. Reuter *Teterahedron* 23 (1967) 943.
13. Tieckelmann in *Pyridine and its derivatives*, *Sppl. Part III,* R. A. Abromovitch (Ed) John Wiley & Sons, Inc. New York, (1974) pp 670.
14. H. Schwartz *US Pat. 2840598* (1958).
15. K. Weissermel, H. J. Arpe in *Industrial organic chemistry* 4th ed. Wiley-VCH Weinheim, (2003) pp 99.
16. A. M. Brownstein, H. L. List *Hydrocarbon Process* 9 (1977) 159.
17. *Ullmans Encyclopedia of Chemical Technology* Vol. A19 405.
18. C. Wang, X, Hua, Y. Zhang *Shiyou Huagong* 21 (1992) 359.
19. A. M. Kuliev, T. A. Kadyrov, G. G. Gaibor, A. G. Sinaiskii, V. N. Matiyasevch *Fr Pat. 2448551* (1980).
20. S. Liao, Y. Xu, W. Zhang, D. Yu *Yingyoung Huaxue* 14 (1997) 18.

21. S. Lchikawa, Y. Ohgomori, N. Sumitani, H. Hayashi, M. Imanari *Ind. Eng. Chem. Res.* 34 (1995) 971.
22. R. Fischer, R. Pinkos *US Pat. 5905159* (1999).
23. D. P. Minh, M Besson, C. Pinel, P. Fuertes, C. Petitjean *Top. Catal.* 53 (2010) 1270.
24. C. J. S. Appleyard, J. F. C. Cartshore *BIOS Rep.* 367 (1946) 22.
25. R. Stanley, D. T. Waldo *DE Pat. 2145297* (1972).
26. T. Fritz, G. Rainer, O. Burkhard, S. Hogler, W. Lothar, U. Alfred, B. Doris, F. Peter, W. Sigrid *DD Pat. 216184 A1* (1985).
27. F. M. Bautista, J. M. Campelo, A. Garcia, R. Guardeno, D. Luna, J. M. Marinas *Stud. Surf. Sci. Catal.* 59 (1991) 269.
28. W. Reppe, W. Schmidt, A. Schulz, H. Wenderlein *US Pat 2319707* (1943).
29. E. Hort, De Thomas, R. Waldo *GB Pat. 2104794 A* (1983).
30. E. Hort, W. Dethomas *EP Pat. 61042 A1* (1982).
31. H. Lindlar *US Pat* 2681938 (1954).
32. H. Lindlar *Helv. Chem. Acta.* 35 (1952) 446.
33. L. Zhang, S. Guo, S. Su *Huozhayao* 19 (1996) 18.
34. T. Fukuda *Bull. Chem. Soc. Jpn.* 31 (1958) 343.
35. T. Fukuda, T. Kusama *Bull. Chem. Soc. Jpn*. 31 (1958) 339.
36. M. M. Telkar, C. V. Rode, R. V. Chaudhari, S. S. Joshi, A. M. Nalawade *Appl. Catal. A.:General* 273 (2004) 11.
37. M. M. Telkar, C. V. Rode, V. H. Rane, R. Jaganathan, R. V. Chaudhari *Appl. Catal. A: General* 216 (2001) 13.
38. F. Codignola, B. Aries *US Pat. 4438285* (1984).
39. H. Hoffmann, G. Boettger, K. Baer, H. Wache, H. Graefje, W. Koerning *US Pat. 4001344* (1977).
40. J. Y. Johnson, G. W. Johnson *DE Pat. 871804* (1961).
41. E. V. Hort *US Pat. 2953604, 2961471* (1960).
42. C. Fairweather *DE Pat. 832141* (1957).
43. A. Tungler, C. Fogassy *J. Mol. Catal. A:Chemical* 173 (2001) 231.

44. T. Herbert, S. Juergen, G. Heinz, R. Wolfgang, S. Roland, I. Mathias, H. Walter, K. Gerhard *EP Pat. 394842 A1* (1990).
45. K. Baer, W. Reiss, W. Schroeder, D. Voges *US Pat. 4287099* (1981).
46. R. Stanley, D. T. Waldo *DE Pat. 2145297* (1972).
47. M . G. Musolino, C. M. S. Cutrupi, A. Donato, D. Pietropaolo, R. Pietropaolo *J. Mol. Catal. A: Chemical* 195 (2003) 147.
48. E. Drent *EP Pat. 333296 A1* (1989).
49. E. Drent *EP Pat. 337572 A2* (1989).
50. M. M. Telkar, C. V. Rode, V. H. Rane, R. V. Chaudhari *Catal. Commun.* 6 (2005) 725.
51. G. A. Somorjai, L.L. Kesmodel, L. H. Dubois *J. Chem. Phys.* 70 (1979) 2180.
52. F. Zhao, Y. Ikushima, M. Arai *Green Chem.* 5 (2003) 656.
53. F. Zhao, Y. Ikushima, M. Arai *Catal. Today* 93-95 (2004) 439.
54. L. Kiwi-Minisker, E. Joannet, A. Renken *Ind. Eng. Chem. Res.* 44 (2005) 6148.
55. E. Joannet, K. Lioubov, R. Albert *WO Pat. 2006072441 A2* (2006).
56. N. Semagina, E. Joannet, S. Parra, E. Sulman, A. Renken, L. Kiwi-minsker *Appl. Catal. A: General* 280 (2005) 141.
57. S. Natalia, E. Joannet, P. Sandra, S. Esther, R. Albert, K. Lioubov *Appl. Catal. A: General* 208 (2005) 141.
58. J. M. Winterbottom, H. Marwan, E. H. Stitt, R. Natividad *Catal. Today* 79-80 (2003) 391.
59. E. Joannet, C. Horny, L. Misker, A. Renken *Chem. Eng. Sci.* 57 (2002) 3453.
60. C. Shukla, J. Das, M. Sriram *IN Pat. 174519 A* (1994).
61. C. V. Rode, M. M. Telkar, R. V. Chaudhari *JP Pat. 2002191981 A2* (2002).
62. P. J. Dyson, D. J. Ellis, T. Welton *Can. J. Chem.* 79 (2001) 705.
63. H. Marwan, S. Raymhasay, J. M. Winterbottom *BHR Group Conf. Ser. Publ.* 28 (1997) 109.
64. A. Drelinkiewicz, A. Knapik, W. Stanuch, J. Sobczak, A. Bukowska, W. Bukowski *Reac. Func. Poly.* 68 (2008) 1652.
65. F. Zhao, C. Wang, H. Xu *Shiyou Huagong* 22 (1993) 650.

66. R. V. Chaudhari, M. G. Rarande, P. A. Ramchandran, P. H. Brahme, H. G. Vadgaonkar, R. Jaganathan *AIChE J.* 31 (1985) 1891.
67. H. Mueller *DE Pat. 19529721 A1* (1997).
68. J. Wood, L. Bodenes, J. Bennett, K. Beplanche, L. E. Macaskie *Ind. Eng. Chem. Res.* 49 (2010) 980.
69. J. Y. Johnson, G. W. Johnson *DE Pat. 871804* (1961).
70. G. Bollger, R. Boer, W. Wache, H. Gratze, W. Koerning *DE Pat. 2451929* (1976).
71. M. A. Sathe, S. B. Shinde *In Pat. 2008MU02215A* (2009).
72. A. Sintetica *BE Pat. 868597* (1978).
73. J. Bauer, U. Muller, R. Pfannschmidt , W. Guenther *DD 246986* (1987).
74. C. Fairweather *DE Pat. 832141* (1957).
75. M. M. Telkar, C. V. Rode, R. Jaganathan, V. H. Rane, R. V. Chaudhari *J. Mol. Catal. A: Chemical* 187 (2002) 81.
76. E. V. Pyatnitsyna, M. M. Elchaninov, A. P. Savostyanov. *Russ. J. Appl. Chem*. 79 (1) (2006) 89.
77. C. Wang, X. Hua, Y. Zhang *Shiyou Huagong* 21 (1992) 359.
78. G. Bai, F. Huang, H. Xu *CN Pat. 1081174 A1* (1994).
79. H. Mueller, R. Wolfgang, *DD Pat.* 3437429 *A1* (1986).
80. H. Mueller, R. Wolfgang, *EP Pat. 177912 A1* (1986).
81. D. Voges, K. Baer, J. Boudier, S. Winderl, H. Hoffmann *US Pat. 4072714* (1978).
82. K. Baer, W. Reiss, W. Schroeder, D. Voges *US Pat. 4287099* (1981).
83. W. Reppe, W. Schmidt, A. Schulz, H. Wenderlein *US Pat. 2319707* (1943).
84. E. V. Hort *US Pat. 2953605* (1960), *2967893* (1961).
85. R. Stanley, D. T. Waldo *DE Pat. 2145297* (1972).
86. K. Kriaa, J. P. Serin, F. Contamine, P. Cezac, J. Mercadier *J. Supercritical. Fluid*. 49 (2009) 227.
87. F. Zhao, Y. Ikushima, M. Arai *Catal. Today* 93-95 (2004) 439.
88. F. Zhao, Y. Ikushima, M. Arai *Green Chem.* 5 (2003) 656.
89. K. P. De Jong , J. W. Geus *Catal. Rev.-Sci. Eng.* 42 (2000) 481.
90. B. Coq, J. M. Planeix, V. Brotons *Appl. Catal. A: General* 173 (1998) 175.
91. D. W. Marquardt *J. Sco. Ind. Appl. Math.* 11 (1963) 431.

92. C. S. Tan, J. M. Smith *Chem. Eng. Sci.* 35 (1980) 1601.
93. P. A. Ramchandran, R. V. Chaudhari in *Three Phase Catalytic reactors,* Gordan and Breach (Ed), New York, 1983.
94. K. B. Bischoff *AIChE J.* 11 (1965) 351.
95. C. R. Wilke, P. Chang *AIChE J.* 1 (1955) 246.
96. K. B. Bischoff *AIChE J. 11* (1965) 351.
97. M. M. Telkar *PhD Thesis* University of Pune (2003).
98. J. M. Nadgeri, M. M. Telkar, C. V. Rode *Catal. Commun*. 8 (2009) 441.
99. M. L. Toebes, J. A. van Dilen, K. P. de Jong *J. Mol. Catal. A: Chemical* 173 (2001) 75.
100. P. A. Sinonov, A. V. Romanenko, I. P. Prosvisin, E. M. Moroz, A. I. Boronin, A. L. Chuvlin, V. A. Likholobov *Carbon* 35 (1997) 73.
101. T. H. Galow, U. Drechsler, J. A. Hanson, V. M. Rotello *Chem. Commun*. (2002) 1076.
102. R. V. Malayala, C. V. Rode, M. Aria, S. G. Hegde, R. V. Chaudhari *Appl. Catal. A: General* 193 (2000) 71.
103. J. W. Park, Y. M. Chung, Y. W. Suh, H. K. Rhee *Catal. Today* 93-95 (2004) 445; P. B. Wells *J. Catal*. 52 (1978) 498.
104. P. C. Aben *J. Catal*. 10 (1968) 224.
105. M. Boudart, H. S. Hwang *J. Catal.* 39 (1975) 44.
106. Z. Zhang, B. Zao, L. Hu *J. Sol. State Chem.* 121 (1996) 105.
107. R. Schlogl in *Preparation of solid catalysts*, G. Ertl, H. Knozinger, J. Weitkamp (Eds), Wiley-VCH, Weinheim (1999).
108. F. Rodriguez-Reinoso *Carbon* 36 (1998) 159.
109. M. Hillert, N. Lange *Zeitschr. Kristall.* 111 (1958) 24.
110. S. Lijima *Nature* 354 (1991) 56.
111. D. W. Marquardt *J. Sco. Ind. Appl. Math.* 11 (1963) 431.
112. J. P. Issi, J. C. Charlier in *The science and technology of carbon nanotubes*, K. Tanaka, T. Yamabe, K. Fukui (Eds), Elsevier, Amsterdam (1999).
113. H. Li, J. Ding, J. Chen. C. Xu, B. Wei, J. Liang, D. Wu *Mater. Res. Bull*. 37 (2002) 313.

114. J. Tessonnier, L. Pesant, G. Ehret, M. J. Ledoux, C. Pharm-Huu. *Appl Catal. A: General* 288 (2005) 203.
115. N. I. Kovtyukhova, T. E. Malouk, L. Pan, E. C. Dickey *J. Am. Chem. Soc.* 125 (2003) 9761.
116. M. Krishna Kumar, S. Ramaprabhu *J. Phy. Chem. B* 110 (2006) 11291.
117. K. Nakamoto in *Infrared and Raman Spectra of Inorganic and Coordination Compounds*, 4th ed., John Wiley & Sons, Inc., New York (1986).
118. J. Xu, X. Huang, W. Li, L. Wang, X. Huang, K. Chen, J. Xu, I. H. Wilson *Appl. Phys. Lett*. 79 (2001) 141.
119. H. Hiura, T. W. Ebbensen, K. Tanigaki, H. Takahashi *Chem. Phys. Lett.* 202 (1993) 509.
120. C. Eklund, M. Holden, A. Jishi *Carbon* 33 (1995) 959.
121. M. S. Dresselhaus, P. C. Eklund *Adv. Phys.* 49 (2000) 705.
122. S. Tan, P. Zhang, K. Yue, F. Huang, Z. Shi, X. Zhou, Z. Gu. J. in *Raman Spectroscopy* 28 (1997) 369.
123. M. Endo, K. Takeuchi, T. Hiraoka, T. Furuta, T. Kasai, X. Sun C. H. Kiang, M. S. Dresselhaus *J. Phys. Chem. Solids* 58 (1997) 1707.
124. C. Pirot, I. Yoshida, N. Takagi, S. Komai, A. Satsuma, T. Hattori *Appl. Catal. B: Environ.* 19 (1998) 261.
125. Y. Yazawa, H. Yoshida, N. Takagi, S. Komai, A. Satsuma, T. Hattori *Appl. Catal. B: Environ.* 19 (1998) 261.
126. Z. Ferhat-Hamida, J. Barbier, S. Labruquere, D. Duprez *Appl. Catal. B: Environ.* 29 (2001) 195.
127. D. S. Bethune, C. H. Klang, M. S. D. Vries, J. Gorman *Nature* 363 (1993) 605.
128. S. Goto, J. M. Smith *AIChE J.* 21 (1975) 706.
129. C. N. Satterfield, M. W. Vab. Eek, G. S. Bliss *AIChE J.* 24 (1978) 709.
130. L. P. Zheng, J. M. Smith, M. Herkowitz *AIChE J.* 30 (1984) 500.
131. J. M. Hochmann, E. Effron *Ind. Eng. Chem. Fund.* 8 (1969) 63.
132. Y. Sato, T. Hiros, F. Takahashi, M. Toda *J. Chem. Eng. Jap*. 6 (1973) 147.
133. M. Zai-Sha, X. Tian-Ying, J. Chen *Chem. Eng. Sci.* 48 (1993) 2697.

134. H. Stephen, J. Stephen in *Solubilities of inorganic and organic compounds,Part I* Pergamon Press, UK, Vol. 1 (1963) .

135. P. L. Mills, M. P. Dudukovic *AIChE J.* 27 (1981) 893.

Chapter IV

Semi-hydrogenation of phenylacetylene to styrene

4.1. Introduction:

Hydrogenation of phenylacetylene to styrene achieving the complete conversion of phenylacetylene and selectivity towards side chain olefinic intermediate styrene is a highly challenging task for the researcher [1]. In this process, styrene is the intermediate product of the first hydrogenation step which readily undergoes further hydrogenation to give ethylbenzene. Scheme 4.1 shows the reaction pathway for hydrogenation of phenylacetylene.

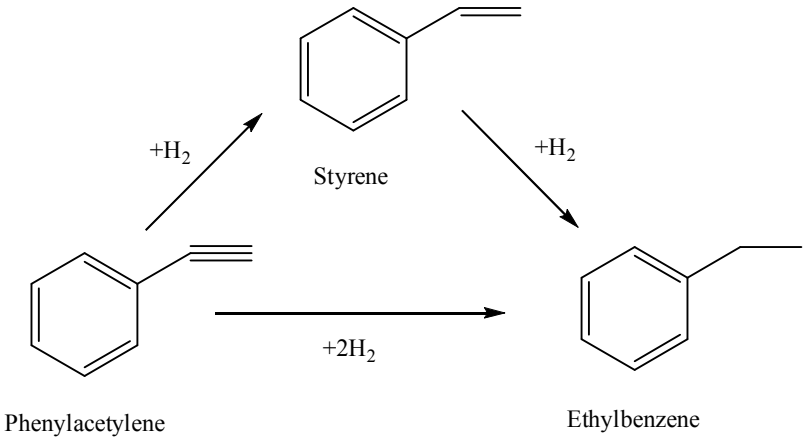

Scheme 4.1. Reaction pathway for hydrogenation of phenylacetylene

For polymerization of styrene, pure styrene feedstock is needed for a longer catalyst life. Even very small amount of phenylacetylene (less than 10 ppm) in the styrene stream can deactivate the catalyst hence, styrene feed with very low concentration of phenylacetylene is mandatory [2].

World wide requirement for styrene monomer was 26 x 10^6 tones per annum in year 2006 with annually growing demand at an average rate of 4.0%. Nearly about 80 companies are producing styrene monomer, and the major producers of styrene are shown in Table 4.1 [3].

Table 4.1. Styrene producing companies

Sr. No	Name of company	Capacities, %
1	Badger	40
2	ABB Lummus Crest	24
3	PO/Styrene	13
4	Dow Chemical	11
5	BASF	7
6	Miscellaneous	5

4.1.1. Importance of styrene:

Styrene is one of the important industrial monomer used in a variety of polymer products such as preparation of polystyrene, latexes, rubber, elastomers, theromoplastics, polyester resins, thermoset plastic, dispersions, resins, copolymer and terpolymer (Figure 4.1) [3]. Majority of styrene, approximately 66% is used for the production of polystyrene having variety of applications, e.g. in preparation of toys, housings for room air conditioners, television cabinets, cassettes, combs, furniture parts, disposable food containers, packing material, electrical and electronic parts, thermal insulation, sports goods etc. Near about 6% styrene is used in the synthesis of styrene-butadiene rubber elastomer (SBR), which gives variety of products for industrial hose, footwear, consumer goods, vehicle parts etc. Approximately 7% of styrene goes into production of styrene butadiene latexes which is used in the paper coatings, paper adhesives, latex paints, carpet backing, cement additives etc. Styrene acrylonitrile copolymer and terpolymers used for sewer pipes, vehicle parts, appliance parts, business machine casings, sports goods, luggage, toys, drinking tumblers, battery cases, automotive components, refrigerator doorliners and shower stalls. Additionally polyester resins are used in fiberglass-reinforced boats, storage tanks, shower units, and simulated marble products.

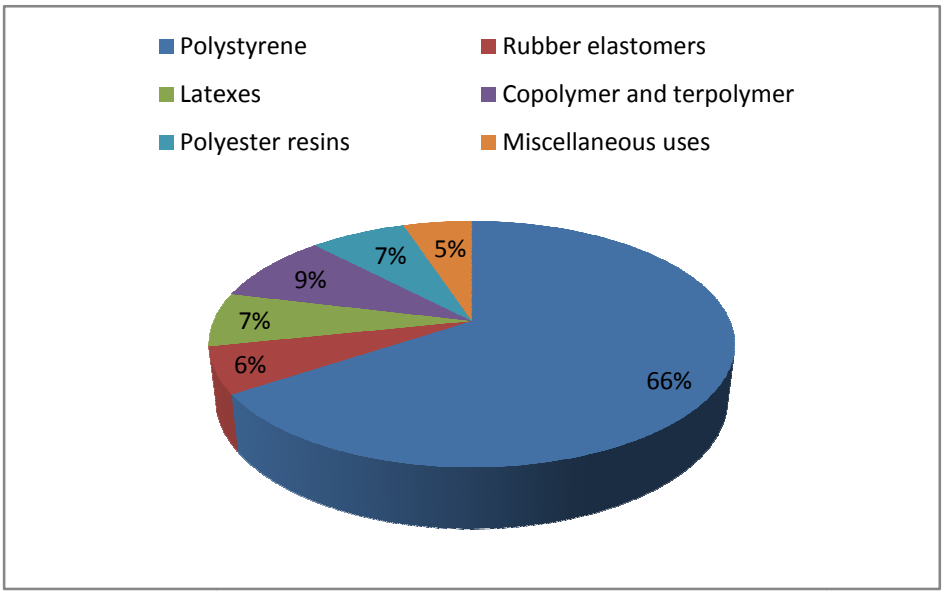

Figure 4.1. Uses of styrene

4.1.2. Traditional routes for synthesis of styrene:

There are several methods for styrene manufacture, the details of which are given below [3].

A. Dehydrogenation of ethylbenzene
B. Propylene oxide process
C. Butadiene process
D. Toluene process
E. Pyrolysis of gasoline

A. Dehydrogenation of ethylbenzene:

Dehydrogenation of ethylbenzene is one of the simple concepts for styrene manufacture (Scheme 4.2). Near about 90% of manufacturing industries are using dehydrogenation process.

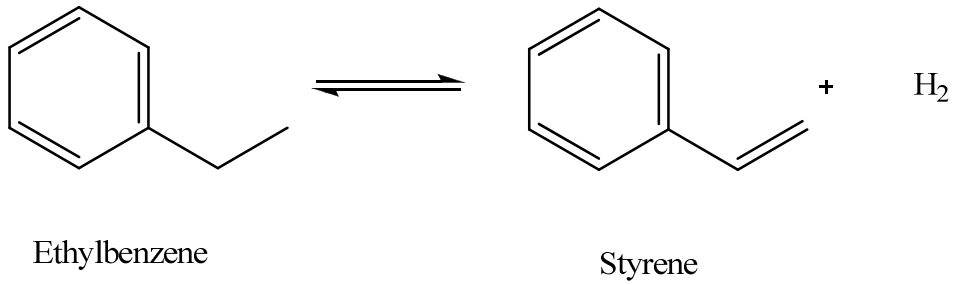

Scheme 4.2. Dehydrogenation of ethylbenzene

Dehydrogenation of ethylbenzene is generally carried out using iron oxide-potassium oxide catalyst at very high temperature i.e. 823-953 K in presence of steam. Major drawback of this reaction system is its high operating temperature which leads to formation of side products such as toluene and benzene. Toluene is generally formed from styrene along with formation of methane and coal (Scheme 4.3). Other byproducts include carbon dioxide, ethylene, phenylacetylene, allylbenzene, vinyltoluene, xylenes, etc. which can affect the cost of purification and the quality of the styrene product.

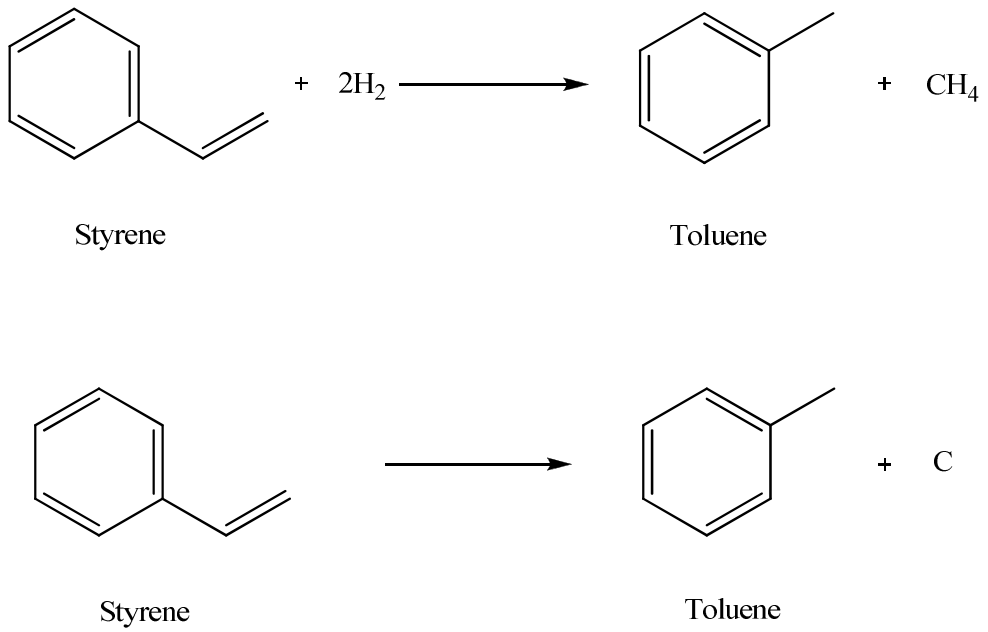

Scheme 4.3. Formation of methane and coal while production of styrene

B. Propylene oxide process (ARCO process):

The most important commercial production route for styrene is the oxidation of ethylbenzene to ethylbenzene hydroperoxide, which is subsequently reacted with propene to give styrene and propylene oxide. As shown in Scheme 4.4, various steps involved in this process are:

1. Oxidation of ethylbenzene to ethylbenzene hydroperoxide
2. Epoxidation of ethylbenzene hydroperoxide with propylene to form α–phenylethanol and propylene oxide
3. Dehydration of α-phenylethanol to styrene

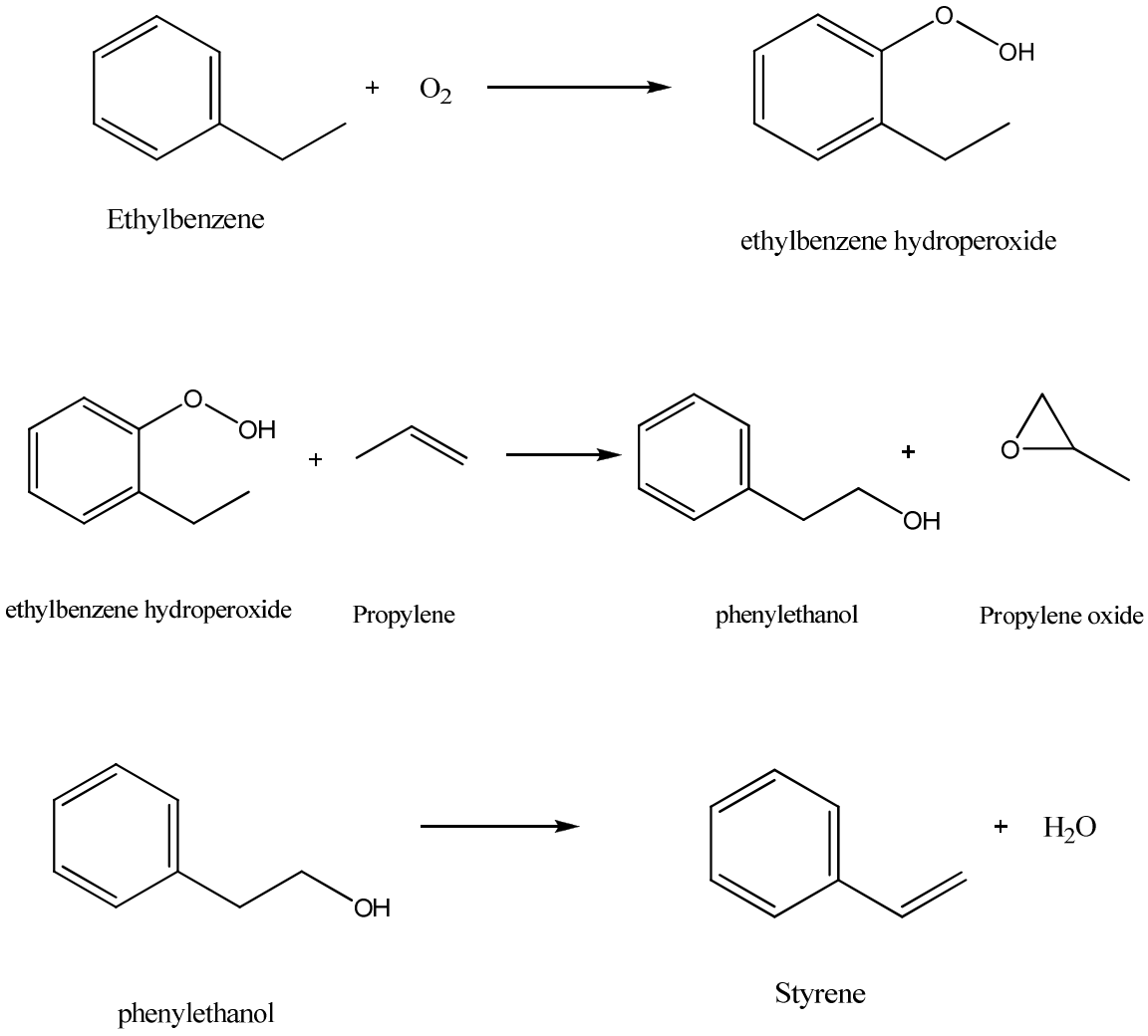

Scheme 4.4. ARCO process

Epoxidation of ethylene hydroperoxide to α-phenylethanol and propylene oxide is the key step of this reaction and is carried out in liquid phase at 373-403 K using molybdenum naphthenate catalyst. Further dehydration step takes place over an acidic catalyst at 498 K.

C. 1,3-Butadiene route:

Another choice to obtain the styrene involves Diels-Alder dimerization of 1,3-butadiene to 4-vinylcyclohexene-1 followed by its dehydrogenation (scheme 4.5). This route is highly exothermic and can be carried out by either thermal or catalytic route. Thermal process requires high temperature of 413 K and 4 MPa pressure [4, 5]. The catalytic route is based on nitrosyl halide-iron complexes [6, 7]. Further 4-vinylcyclohexene-1 is dehydrogenated to get the ethylbenzene and styrene [8-11].

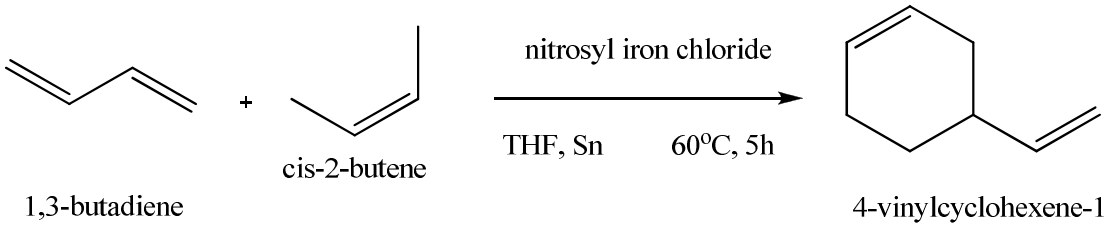

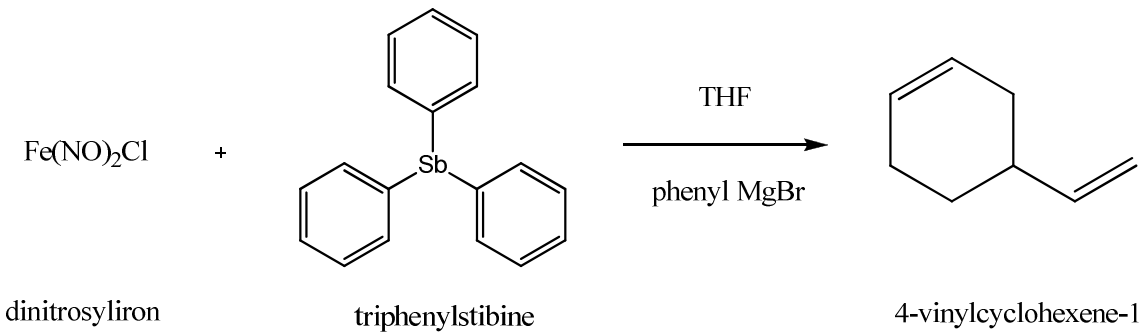

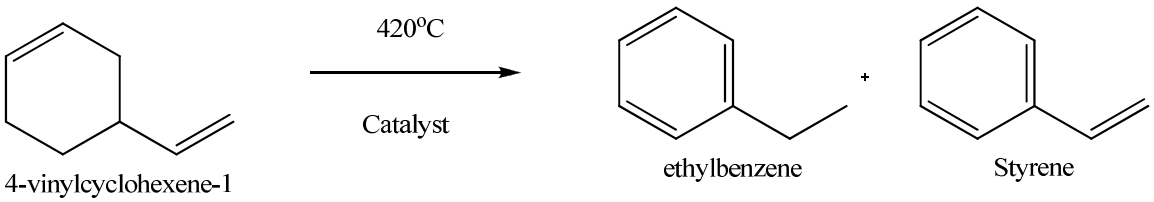

Scheme 4.5. Butadiene route

D. Toluene route:

Preparation of styrene from toluene as a starting material is one of alternative routes due to 15% cheaper price of toluene than the benzene. Unland and Barker developed the oxidative coupling of toluene to stilbene (Scheme 4.6) [9, 10].

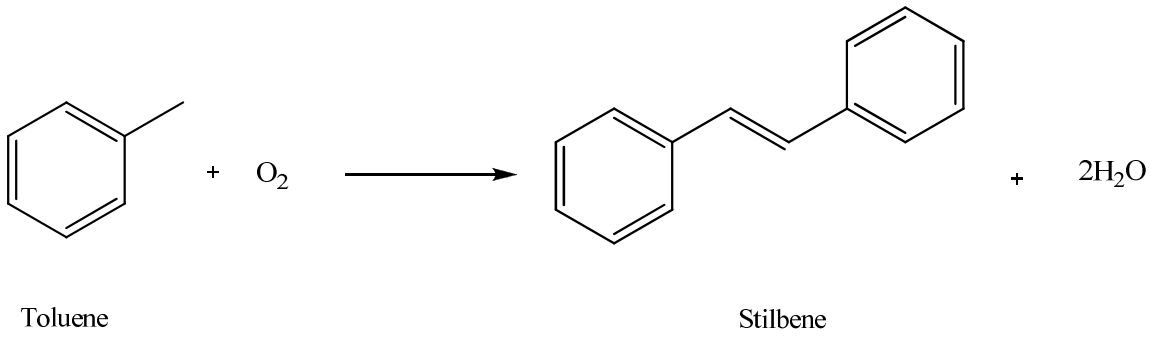

Scheme 4.6. Oxidative coupling with toluene to stilbene

Further stilbene is reacted with ethylene in presence of molybdenum catalyst to form styrene. (Scheme 4.7)

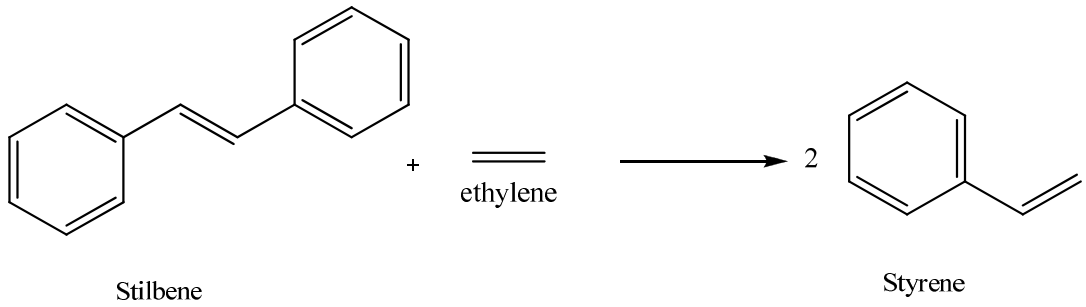

Scheme 4.7. Styrene from stilbene

Another route for the preparation of styrene from toluene is alkylation of toluene with methanol over zeolite catalysts [9, 10].

E. Styrene from pyrolysis of gasoline:

Thermal cracking of naphtha or gas-oil gives styrene as a product along with the mixture of aromatic compounds.

Major drawbacks of these processes are:

1. Majority of the commercial units run adiabatically and under vacuum at high temperature which leads to coke deposition on the catalyst surface and catalyst gets easily deactivated.
2. Due to high temperature, change in catalyst solid-state occurs adversely affecting the rate of reaction, and the catalyst lifetime.
3. Multistep synthesis.

4.1.3. Literature survey:

A summary of the literature on phenylacetylene hydrogenation is presented in Table 4.2. The hydrogenation of phenylacetylene to styrene has been mainly focused on the use of palladium based catalysts because the palladium is most selective catalyst due to its strong affinity towards alkynes [12-14]. For the hydrogenation of C≡C, large stoichiometric amount of hydrogen is necessary, which may lead to further hydrogenation of styrene to ethylbenzene, reducing the selectivity to styrene [15-17]. Mono Pd, Pt and bimetallic Pd-Pt catalysts with different ratios dispersed on amorphous materials such as SiO_2, Al_2O_3 were studied by Carturan et al. [18]. He found that the selectivity was affected by the metal dispersion in monometallic Pd catalyst. The palladium nanoparticles were stabilized by using anionic surfactant (sodium dodecyl sulfate) incorporated in hydrotalcite showed 100% selectivity towards the styrene at 87 % conversion studied by Mastalir et al. [19]. Effect of strong-metal support interaction (SMSI) on catalytic activity and selectivity of Pd catalyst supported on nano-TiO_2 studied by Weerachwanasak et al. for hydrogenation of phenylacetylene to styrene [20]**.** The catalyst with SMSI effect showed high activity [TOF, 1.284 x 10^3 h^{-1}] with 86-90% selectivities to styrene [20].

Effect of catalyst pretreatment on activity and selectivity for hydrogenation of phenylacetylene was studied by Chaudhari et al. [21]. They observed the change in catalyst activity and selectivity behavior due to the change in nature of active species of Pd metal. This change occurs due to the initial catalyst pretreatment given to the catalyst and metal dispersion [21]. Wilhite et al. studied the hydrogenation of phenylacetylene to styrene and ethylbenzene at low temperature (348 K) and atmospheric pressure condition by using Pt/alumina in three phase catalytic packed bed reactors [22].

Catalyst systems involving noble metals with various supports have also been reported for the hydrogenation of phenylacetylene to styrene such as nanoparticles of Rh [23], different compositions of Ni-Pd, Fe-Pd, Mg-Pd, Pd, Pt [24], polymer protected Ni-Pd bimetallic catalyst in colloid or supported form [25]. Role of acid-base and structural properties of Ni catalyst supported on $AlPO_4$, SiO_2, Al_2O_3, natural sepiolite, activated carbon and Ni-Cu alloy catalyst was studied [26]. Mandal et al. obtained very good activity using zeolite-immobilized Pd and Pt nanoparticles, but with low selectivity (35-40%) to styrene [27]. Hydrogenation of phenylacetylene to styrene was influenced by various factors such as solvent, temperature, hydrogen pressure and amines with varying basic strength [28]. Armendia et al. found that adsorption of triple bond was more favored than that of double bond using cylcohexane as a solvent and in presence of quinoline, at low pressure and temperature using Pd catalyst [28].

Table 4.2. Literature summary for hydrogenation of phenylacetylene to styrene

Sr. No.	Catalyst	Conversion, %	Reaction conditions	Selectivity, %		Ref. No.
				Sty	**EB**	
1.	Pt/γ-Al_2O_3	100	T=303-363 K; P_{H_2}=0.13-0.69	65.6		14

			MPa; Solvent= tetradecane			
2.	5% Pt/C	14-48	T=283-313 K; P_{H_2}=0.1-7.1 MPa; Solvent= ethanol	78-54		15
3.	Nanocatalysts of Ni-Pd, Fe-Pd, Mg-Pd, Pd, Pt	100	T=323 K; P_{H_2}= 0.1 MPa; Solvent=MeOH	97.3		24
4.	Pd-Complex	100	T= 303 K; P_{H_2}=0.1 MPa; Solvent= DMF, pyridine	96	3	30
5.	Lindlar catalyst (Pd-$CaCO_3$-PbO), quinoline poisoning agent	100	T= 295 K; Solvent= cyclohexane	100		31
6.	1% Pd/C	100	T=298-323 K; P_{H_2}=0.2 MPa; Solvent,=dodecane	80	20	32
7.	Pd/Pumice supported	100	T=288- 308 K	73	27	33
8.	Polymer supported Pd	100	T=294 K;	95	5	34

	complex		P_{H_2}=0.1 MPa; Solvent= MeOH			
9.	Pd/CNTs, Pd/C	100	T=323 K; P_{H_2}= 0.1 MPa H_2 flow 30 mL/min; Solvent=MeOH	> 95		35
10.	Cu, Ni, Co, Mn, Ag. Cr/Al_2O_3, SiO_2, C	100	T=278-308 K; P_{H_2}= 0.069 MPa; Solvent=dodecane	5	90	2
11.	0.5 % Pt/Al_2O_3	100	T=333-363 K; P_{H_2}= 0.04 MPa; Solvent= tetradecane		60	22
12.	Pd	100	T=295 K; P_{H_2}= 0.04 MPa (atm); Solvent=THF	> 99		36
13.	Pd supported on Sepiolite, SiO_2-$AlPO_4$	86	T= 306-323 K; P_{H_2}= 0.276-0.483 MPa; Solvent= MeOH, cyclohexane, THF, DMF, dioxane, *n*-hexene	> 95		28
14.	Pd, Pt, Pd-Pt supported on	100	T= 298K;	> 91		18

	Xerogel		P_{H_2}= 0.1 MPa; Solvent=THF			
15.	Pd-complexes	20	T= 313 K; P_{H_2}= 0.1 MPa; Solvent= THF, *n*-hexane	100		37
16.	Nano Rh	92	T= 333 K; P_{H_2}= 0.7 MPa;		100	23
17.	Cu-Pd/Pumice	95	T= 298 K; P_{H_2}=0.1 MPa; Solvent=THF	> 90		38
18.	Nano Pd/hydrotalcite, Al_2O_3, C	55-80	T= 298 K; P_{H_2}= 0.1 MPa; Solvent=THF, toluene, ethanol, hexane	100		19
19.	Pd/SiO_2	30-55	T= 303 K; P_{H_2}= 0.1 MPa; Solvent=THF	> 95		39
20.	Pd/C, Na_2O, SiO_2, Al_2O_3	90-100	T= 298K; P_{H_2}= 0.1MPa; Solvent=*n*-heptane	100		40
21.	5% Pt/C	100	T= 283-323 K; P_{H_2}= 1.01- 9.1 MPa Solvent= ethanol	74	25	16

			0.1N H_2SO_4			
22.	Cu promoted Fe catalyst supported on SiO_2, Fe/SiO_2	> 95	T= 333 K; P_{H_2}= 1.0 MPa; Solvent=ethanol	> 99		41
23.	Pt, Pt-Sn supported on Nylon 66 powder	100	T= 283 K; P_{H_2}= atmospheric; Solvent=ethanol	75	24	17
24.	$Au/\alpha\text{-}Al_2O_3$, $Au/\gamma\text{-}Al_2O_3$	100	T=423 K; P_{H_2}= atmospheric;	73	23	42
25.	Pt, Mo -Cluster ligand PEt_3 or PPh_3	> 98	T=333 K; P_{H_2}= 1.38 MPa; Solvent=THF	99	-	43
26.	Pt/TiO_2	100	T=273-333 K; P_{H_2}= 1.38 MPa; Solvent=THF	87	13	44
27.	Ionic liquid 1-Butyl-3-methylimidazolium bis{(trifluoromethyl)sulfonyl} imide *(*[C4mim][NTf2]*)* 5% $Pd/CaCO_3$	100	T=273-333 K; P_{H_2}= 0.1-0.6 MPa; Solvent=heptane; RDR, STR reactor	100	-	45
28.	Rhenium sulfide cluster	3.3	T=523-673 K;	86.7		46

	catalyst				
29.	Pd/γ-Al_2O_3, MCM-41, Al-MCM-41, β-Zeolite	100	T=323 K; P_{H_2}= 0.1 MPa H_2 flow; Solvent=MeOH	96	47
30.	1%Pd/HMS, MCM-41, MSU-X,	80%	T=298 K; P_{H_2}= 0.1 MPa, H_2 flow; Solvent=THF	96	48
31.	Pd/C	100	T=301-353 K; P_{H_2}= 5.5-9.6 MPa; Solvent= toluene	70	21

4.1.4. Objectives:

The main objective of this work was to prepare and characterize the colloidal Pd nano as well as supported Pd nano catalysts for the selective hydrogenation of phenylacetylene to styrene. The activity and selectivity behavior of the Pd nanocatalysts was also compared with the conventional Pd bulk catalyst. The effect of various reaction parameters such as temperature, and hydrogen pressure on the activity and particularly on styrene selectivity was also studied.

4.2. Experimental:

4.2.1. Catalyst preparation:

Details of preparation of colloidal Pd nano, nano Pd/C and bulk Pd/C catalyst are described in chapter II, section 2.2.

4.2.2 Catalyst activity testing:

4.2.1.1. High pressure reaction set up:

The details of high pressure hydrogenation reaction setup and experimental procedure are described in chapter II, section 2.4.2.

4.2.1.2. Atmospheric pressure reaction setup:

The experimental batch setup used for reactions under atmospheric pressure conditions and the experimental procedure are described in chapter II, section 2.4.3

4.2.3. Catalyst characterization:

The details of catalyst characterization are described in chapter II, sections 2.3.

4.2.4. Analytical techniques:

The quantitative analysis of liquid samples was carried out by gas chromatography method using FID detector, HP-5 capillary column and helium as a carrier gas. Other details of temperature programming method (333-463 K) etc. are described in chapter II, section 2.5.

4.3. Results and discussion:

4.3.1. Catalyst characterization:

Since the catalyst sample was in the colloidal form, the preparation of sample for X-ray powder diffraction study was done as per the following procedure. A layer of the prepared colloidal Pd nano solution was made on the glass plate, and sample was dried under IR lamp. This procedure was repeated three to four times to increase to concentration of Pd layer on XRD glass plate for diffraction analysis. The X-ray

diffractogram as shown in Figure 4.2 of the prepared colloidal catalyst displays the strong peak at 45.4^{o} (I = 100%), which is associated with fcc phase. The peak at 45.4^{o} shows the presence Pd-X phase [49]. Particle size of Pd particles was calculated for the peak at 45.4^{o} , using Scherrer equation which showed the particle size of 4 nm.

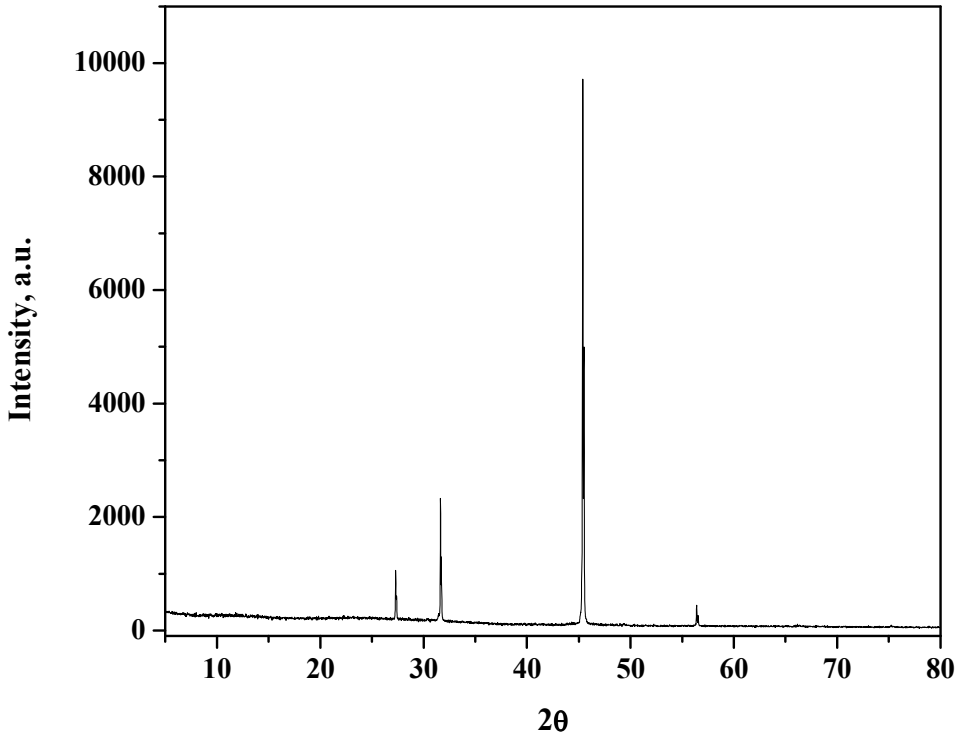

Figure 4.2. X-ray diffraction of colloidal Pd catalyst

The external morphology of prepared colloidal Pd nanoparticle is shown in Figure 4.3. Colloidal Pd catalyst prepared by ethanol reduction, shows particles size in the range of 3-5 nm and its average particle size was found to be 3.9 nm that matched closely with the XRD measurement.

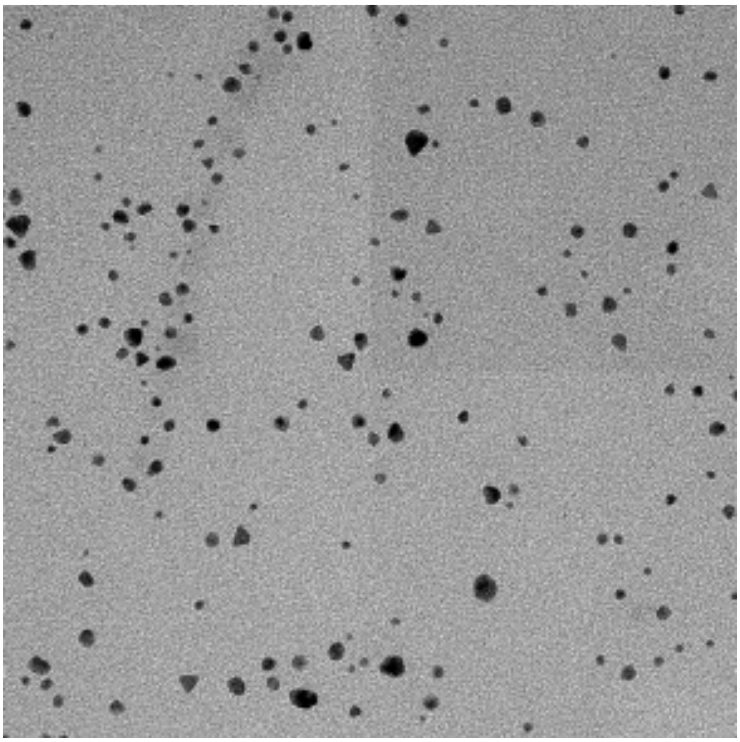

Figure 4.3. TEM image of colloidal Pd nanoparticle

4.3.2. Catalyst activity measurement:

The catalytic performance studies using colloidal, carbon supported nano and bulk Pd catalyst for the phenylacetylene hydrogenation were performed at 313 K temperature , 0.34 MPa hydrogen pressure and using methanol as a solvent. The activity of catalyst is expressed in TOF (Turn over frequency, h^{-1}), and the results are shown in Table 4.3. The colloidal Pd catalyst showed higher activity than that for Pd/C nano and Pd/C bulk catalysts. In terms of turn over frequency (TOF, h^{-1}) colloidal Pd nano catalyst was 3.5 times more active than bulk Pd catalyst as well as 1.5 times more active than supported Pd nano catalyst. This is due to the enhancement in rate of hydrogenation as evident from the hydrogen absorption vs. time plot for phenylacetylene hydrogenation shown in Figure 4.4. Increase in activity of Pd colloidal catalyst was due to more availability catalytic active sites for the hydrogenation.

Table 4.3. Comparision of activity results for hydrogenation reactions using bulk, nano Pd/C and colloidal Pd catalysts

Sr. No.	Catalyst	TOF, h^{-1}
1	bulk catalyst	1.4×10^{-4}
2	Pd /C (nano)	3.4×01^{-4}
3	Pd, nano colloidal	5.0×10^{-4}

Reaction conditions: phenyl acetylene, 0.04908 mol; temperature, 313 K; hydrogen pressure, 0.34 MPa; catalyst weight (bulk and nano Pd/C), 0.075 g; colloidal Pd catalyst, 5 mL; MeOH, 90 mL; agitation speed , 1000 rpm

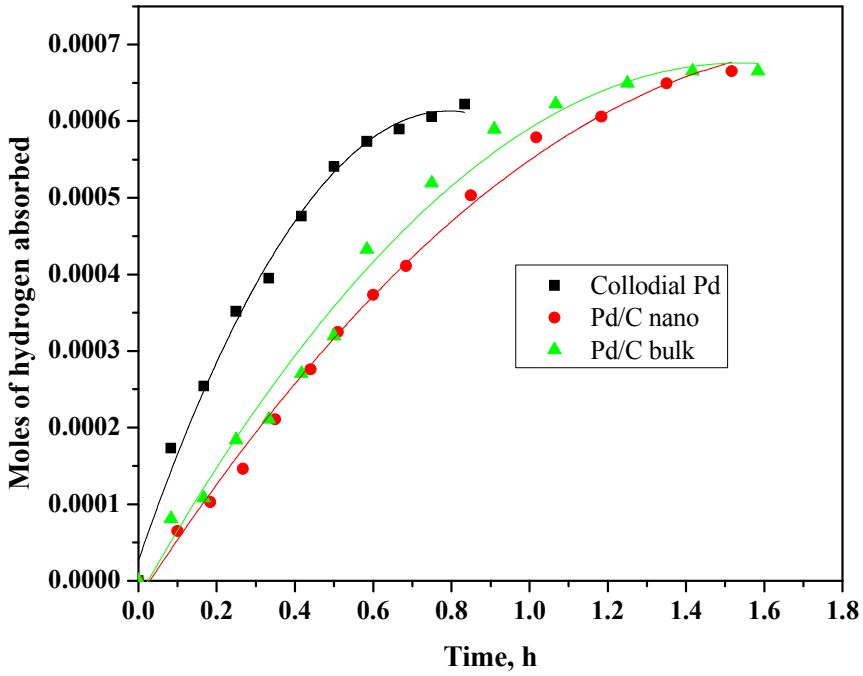

Figure 4.4. Moles of hydrogen absorbed vs. time for colloidal, Pd/C nano and bulk catalysts

Reaction conditions: phenyl acetylene, 0.04908 mol; temperature, 313 K; hydrogen pressure, 0.34 MPa; catalyst weight (bulk and nano Pd/C), 0.075 g; colloidal Pd catalyst, 5 mL; MeOH, 90 mL; agitation speed, 1000 rpm.

4.3.3. Conversion and selectivity profile for colloidal Pd nano catalyst:

Figure 4.5 shows a typical conversion, selectivity Vs time profile for the hydrogenation of phenylacetylene at 313 K temperature and 0.34 MPa pressure. Initial hydrogenation of phenylacetylene at 0.083 h gave 36% conversion with > 97 % selectivity towards styrene. Complete conversion of phenylacetylene was observed at 0.45 h along with 64 % selectivity towards the styrene and 34% ethylbenzene. Further increase in reaction time caused decrease in selectivity to styrene due to excessive hydrogenation of styrene to ethylbenzene.

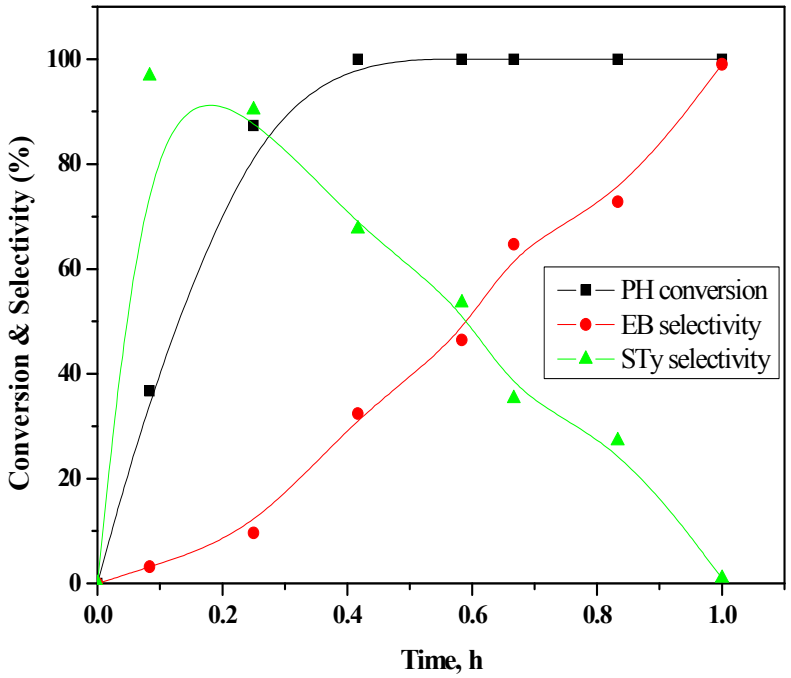

Figure 4.5. Conversion & selectivity vs. time profile for phenylacetylene hydrogenation

Reaction conditions: phenylacetylene, 0.04908 mol; temperature, 313K; hydrogen pressure, 0.34 MPa; colloidal Pd catalyst, 5 mL; MeOH, 90 mL; agitation speed 1000 rpm.

PH: phenylacetylene, EB: ethylbenzene, STy: Styrene

4.3.4. Effect of temperature:

The effect of temperature on conversion of phenylacetylene and selectivity to styrene was studied by varying the temperature from 313 K to 333 K at constant hydrogen pressure, substrate and catalyst loadings. It was observed that as temperature increased from 313 K to 333 K the selectivity towards styrene marginally decreased from 68 to 64% for complete conversion of phenylacetylene as shown in Figure 4.6. 313 K showed the higher selectivity to styrene i.e. 68% along with 32% selectivity to ethylbenzene. It was also observed that initially at 90% conversion the selectivity towards styrene was higher

i.e. 80- 90%, however with further increase in phenylacetylene conversion from 90 to 100% the selectivity to styrene dropped down (Figure 4.7).

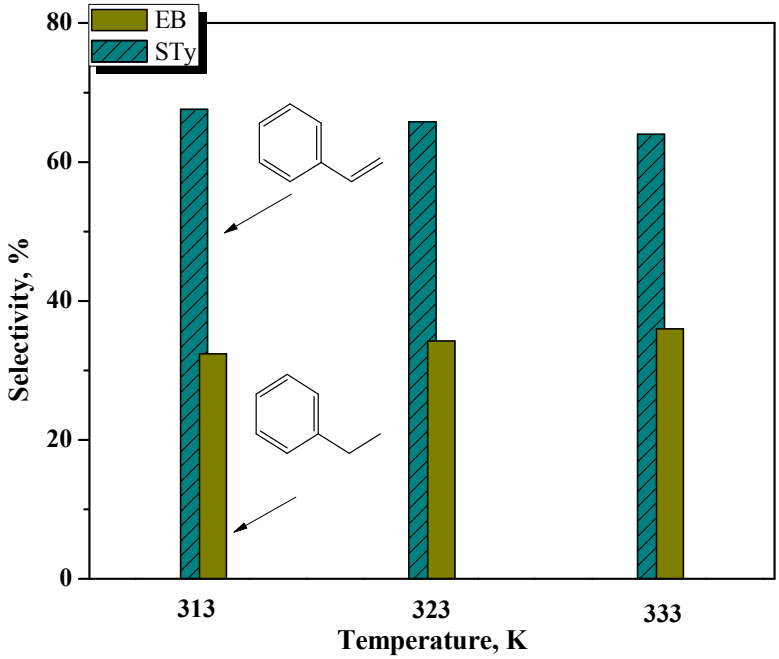

Figure 4.6. Effect of temperature on selectivity pattern at complete conversion of phenylacetylene

Reaction conditions: phenyl acetylene, 0.04908 mol; hydrogen pressure, 0.34 MPa; colloidal Pd catalyst, 5 mL; MeOH, 90 mL; agitation speed, 1000 rpm.

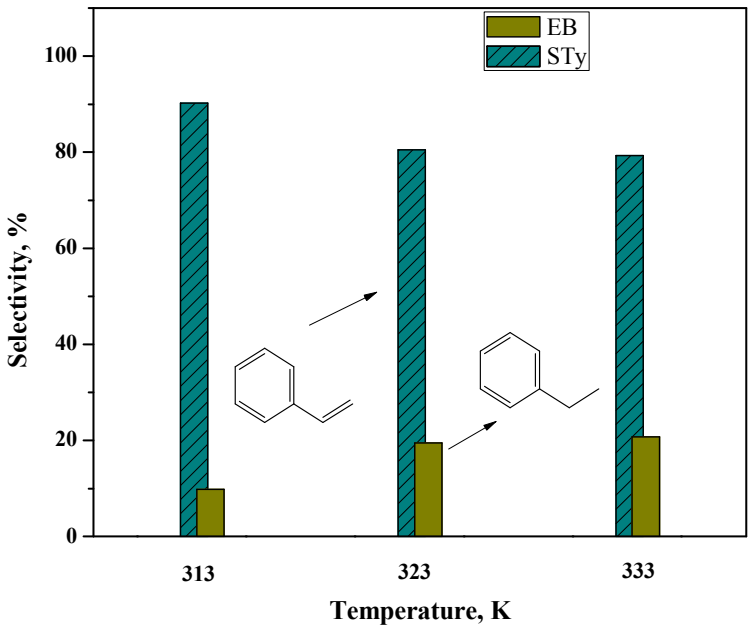

Figure 4.7. Effect of temperature on selectivity at 90% conversion of phenylacetylene

Reaction conditions: phenyl acetylene, 0.04908 mol; hydrogen pressure,0.34 MPa; colloidal Pd catalyst, 5 mL; MeOH, 90 mL; agitation speed, 1000 rpm.

The apparent activation energy of hydrogenation of phenylacetylene over colloidal Pd nanoparticle catalyst evaluated in our work (Figure 4.8) was found to be 32 kJ/mol.

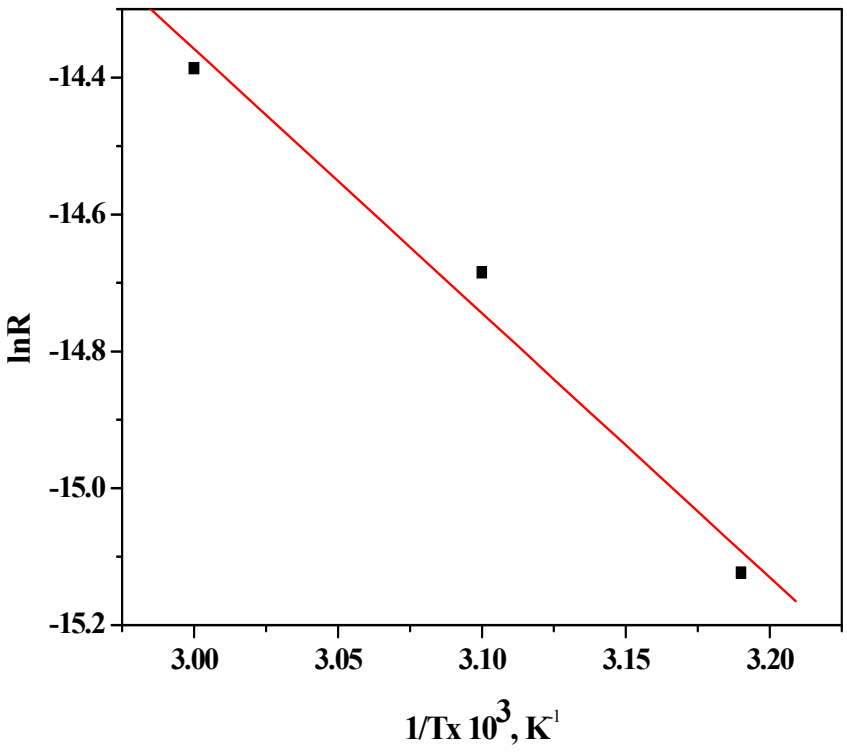

Figure 4.8. Arrhenius plot

Reaction conditions: phenyl acetylene, 0.04908 mol; hydrogen pressure, 0.34 MPa; colloidal Pd catalyst, 5 mL; MeOH, 90 mL; agitation speed, 1000 rpm.

4.3.5. Effect of hydrogen pressure:

Effect of hydrogen pressure on the selectivity of styrene was studied for ambient to 1.72 MPa, at 313 K and the results are shown in Figure 4.9. The highest selectivity of 92 % to styrene was achieved at ambient pressure conditions while it decreased from 92 to 8% with increase in pressure upto 1.72 MPa. At the same time, the selectivity to ethylbenzene increased from 8 to 92% indicating higher concentration of hydrogen leads to further hydrogenation of styrene to ethylbenzene. Catalyst activity in terms of TOF increased from 0.34 to 8.36 x 10^4 h^{-1}

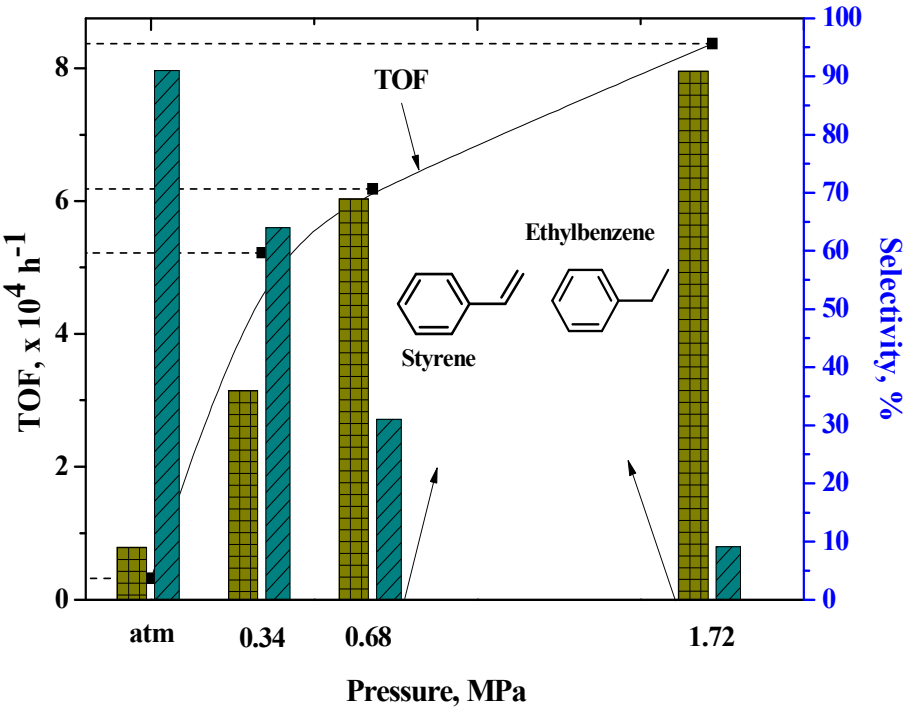

Figure 4.9. Effect of pressure on activity and selectivity

Reaction conditions: phenyl acetylene, 0.04908 mol; temperature, 313K; colloidal Pd catalyst, 5 mL; MeOH, 90 mL, agitation speed, 1000 rpm.

4.3.6. Concentration vs. time profile:

The effect of reaction time on the phenylacetylene and products concentration was also studied at 313 K and at ambient hydrogen pressure (flow rate, 30ml/min) and the results are presented in Figure 4.10. It was clearly observed from the Figure 4.10, upto 40% conversion at 3.5 h reaction time, only formation of styrene was observed. Formation of ethylbenzene was observed with increase in styrene conversion beyond 40%, after 3.5 h. For complete conversion of phenylacetylene, selectivities to styrene and ethylbezene obtained were 92 % and 8% respectively.

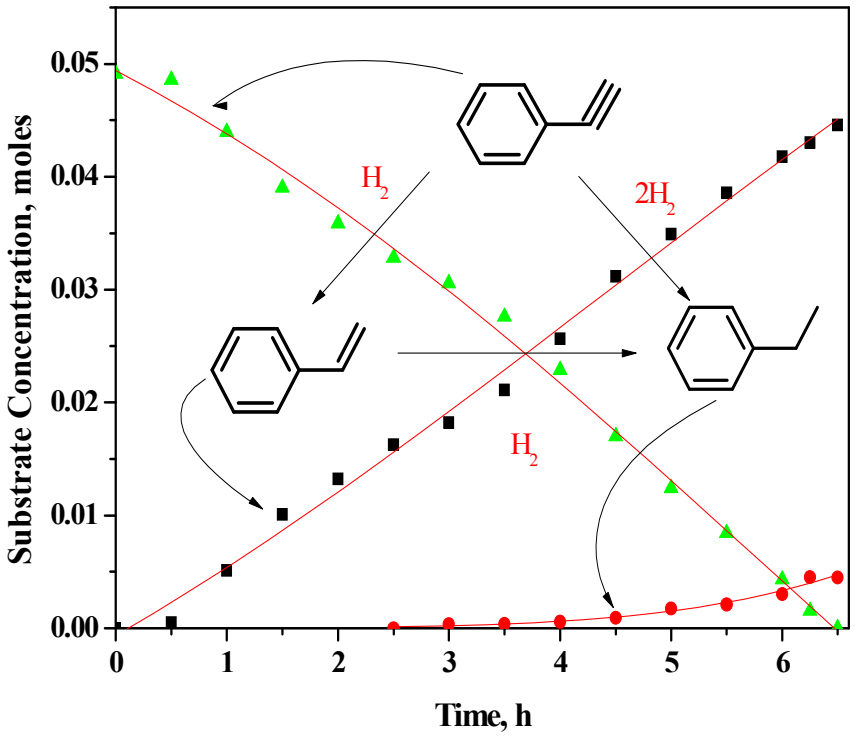

Figure 4.10. Concentration vs. time profile

Reaction conditions: phenyl acetylene, 0.04908 mol; temperature, 313 K; hydrogen flow rate, 30 ml/min; colloidal Pd catalyst, 5 mL; MeOH, 90 mL.

It is believed that α and β-Pd-hydride species are formed during the hydrogenation, where α site is selective for olefin formation and β sites promote the alkane formation [50]. Chaudhari et al. observed that the catalyst pretreated with phenylacetylene leads to formation of stable allyl type complexes of Pd with phenylacetylene and it inhibits the formation of β-Pd-H species, which is responsible for formation of alkane by further hydrogenation of styrene [21]. Due to increase in residence time of the reaction formation of such allyl type complexes of Pd may be possible. Under ambient pressure conditions, higher selectivity towards styrene could be achieved due to inhibition of β-hydride species.

4.4. Conclusion:

Colloidal palladium nanoparticles were prepared using PVP as a stabilizer and evaluated for the hydrogenation of phenylacetylene. Under ambient pressure, the highest 92% selectivity to styrene was achieved while it decreased from 92 to 8% with increase in hydrogen pressure. It was found that the colloidal Pd nanoparticles catalyst showed higher (3.5 times) activity than bulk 0.25% Pd/C catalyst prepared by conventional method for hydrogenation of phenylacetylene reaction. At 90% conversion of phenylacetylene, selectivity to styrene was found to be 90% which decreased to 68% for complete conversion of phenylacetylene. The apparent activation energy of hydrogenation of phenylacetylene over colloidal Pd nanoparticle catalyst evaluated in our work found to be 32 kJ/mol.

4.5. References:

1. A. Molnar, A. Sarkany, M. Varga *J. Mol. Catal. A: Chemical* 173 (2001) 185.
2. B. R. Maurer, M. Galobardes *US Pat 4822936* (1989).
3. D. H. James, W. M. Castor in *Ullmann's Encyclopedia of Chemical Technology* Online edition (2000).
4. T. C. Liebert *US Pat 4117025* (1978).
5. A. H. Gleason *US Pat 2943117* (1960).
6. P. L. Maxfiel *US Pat 3377397* (1968).
7. D. J. Strope *US Pat 4144278* (1979).
8. H. H. Vogel, H. M. Weitz, E. Lorenz, R. Platz *US Pat 3903185* (1975).
9. R. W. Rieve, H. Shalit *US Pat 4029715* (1977).
10. M. L. Unland, G. E. Barker *US Pat* 4115424 (1978) .
11. M. L. Unland, G. E. Barker *US Pat 4140726* (1979).
12. G. C. Bond, P. B. Wells *Adv. Catal.* 15 (1964) 91.
13. M. Bartok in *Stereochemistry of Heterogeneous Metal Catalysis*, Wiley, Chichester, M. A. (1985).
14. B. A. White, M. J. McCready, A. Varma *Ind. Eng. Chem. Res.* 41 (2002) 3345.
15. F. B. Bizhanov, Sh. D. Dinasylova, D. V. Sokolakii *React. Kinet. Catal. Lett.* 12 (1979) 291.
16. Sh. D. Dinasylova, F. B. Bizhanov, D. V. Sokolskii *React. Kinet. Catal. Lett.* 14 (1980) 423.
17. S. Galvagno, Z. Poltarzewski, A. Donato, G. Neri, R. Pietropaolo *J. Mol. Catal.* 35 (1986) 365.
18. G. Carturan, G. Cocco, G. Facchin, G. Nacazio *J. Mol. Catal.* 26 (1984) 315.
19. Á. Mastalir, Z. Király *J. Catal.* 220 (2003) 372.
20. P. Weerachawanasak, O. Mekasuwandumrong, M. Arai, S. Fujita, P. Praserthdam, J. Panpranot *J. Catal.* 262 (2009) 199.
21. R. V. Chaudhari, R. Jaganathan, D. S. Kolhe, G. Emig, H. Hofmann *Ind. Eng. Chem. Prod. Res. Dev.* 25 (1986) 375.
22. B. A. Wilhite, R. Wu, X. Huang, M. J. McCready, A. Varma *AIChE* 47 (2001) 2548.

23. J. Pellegatta, C. Blandy, V. Colliere, R. Choukroun, B. Chaudret, P. Cheng, K. Phillippot *J. Mol. Catal. A: Chemical* 178 (2002) 55.
24. S. Domínguez, Á. Berenguer-Murcia, D. Cazorla-Amorós, Á. Linares-Solano *J. Catal.* 243 (2006) 74.
25. P. Lu, N. Toshima *Bull. Chem. Soc. Jpn*. 73 (2000) 751.
26. F. M. Bautista, J. M. Campelo, A. Garcia, D. Luna, J. M. Marinas, R. A. Quiros, A. A. Romero *Catal. Lett.* 52 (1998) 205.
27. S. Mandal, D. Roy, R. V. Chaudhari, M. Sastry *Chem. Mater.* 16 (2004) 3714.
28. M. A. Aramendia, V. Borau, C. Jimenez, J. M. Marinas M. E. Sempere, F. J. Urbano *Appl. Catal.* 63 (1990) 375.
29. M. M. Telkar, C. V. Rode, R. V. Chaudhari, S. S. Joshi, A. M. Nalawade *Appl. Catal. A: General* 273 (2004) 11.
30. P. Pelagatti, A. Venturini, A. Leporati, M. Carcelli, M. Costa, A. Bacchi, G. Pelizzi, C. Pelizzi *J. Chem. Soc. Dalton Trans.* (1998) 2715.
31. R. Dhamodharan *Chem. Lett.* 25 (1996) 235.
32. S. D. Jackson, L. A. Shaw *Appl. Catal. A: General* 134 (1996) 91.
33. D. Duca, L. F. Liotta, G. Deganello *J. Catal.* 154 (1995) 69.
34. M. M. Dell'Anna, M. Gagliardi, P. Mastrorilli, G. P. Suranna, C. F. Nobile *J. Mol. Catal. A. Chemical* 158 (2000) 515.
35. S. Domínguez-Domíguez, A. Berenguer-Murcia, B. K. Pradhan, A. Linares-Solano, D. Cazorla-Amoro's *J. Phys. Chem. C.* 112 (2008) 3827.
36. M. W. Van Laren, C. J. Elsevier *Angew. Chem. Int. Ed.* 38(1999) 3715.
37. M. Costa, P. Pelagatti, C. Pelizzi, D. Rogolino *J. Mol. Catal A: Chemical* 178 (2002) 21.
38. L. Guczi, Z. Schay, G. Stefler, L. F. Liotta, G. Deganello, A. M. Venezia *J. Catal.* 182 (1999) 456.
39. J. Panpranot, K. Phandinthong, T. Sirikajorn, M. Arai, P. Praserthdam *J. Mol. Catal. A: Chemical* 261 (2007) 29.
40. G. Carturan, G. Facchin, G. Cocco, S. Enzo, G. Navazios *J. Catal.* 76 (1982) 405.
41. Yuriko Nitta, S. Matsugi, T. Imanaka *Catal. Lett.* 5 (1990) 67.

42. S. A. Nikolaev, V. V. Smirnov *Catal. Today* 147S (2009) S336.
43. C. U. Pittman Jr., W. Honnick, M. Absi-Halabi, M. G. Richmond *J. Mol. Catal.* 32 (1985) 177.
44. T. Lopez, R. Gomez, E. Romero, I. Schifter *React. Kinet. Catal. Lett.* 49 (1993) 95.
45. C. Hardacre, E. A. Mullan, D. W. Rooney, J. M. Thompson, G. S. Yablonsky *Chem. Eng. Sci.* 61 (2006) 6995.
46. S. Kamiguchi, S. Nagashima, T. Chihara *Chem. Lett.* 36 (2007) 1340.
47. S. Domínguez-Domíguez, A. Berenguer-Murcia, A. Linares-Solano, D. Cazorla-Amoro *J. Catal.* 257 (2008) 87.
48. M. A. Norman, P. Gina, J. P. Thomas, A. Gabriela, R. Patricio *J. Mol. Catal. A: Chemical* 247 (2006) 145.
49. Z. Ferhat-Hamida, J. Barbier Jr., S. Labruquere, D. Suprez *Appl. Catal. B: Environ.* 29 (2001) 195.
50. A. Borodzinski, R. Dus, R. Frak, A. Janko, W. Palczewska *React. Kinet. Catal. Lett.* 12 (1979) 291.

Part II

Hydrogenation of nitroaromatics

Chapter V

Hydrogenation of nitrobenzene to *p*-aminophenol

5.1. Introduction:

p-Aminophenol is one of the important intermediates used in the manufacture of products having applications in various sectors, such as pharmaceuticals, dye industries and fine chemicals, details of which are shown in Figure 5.1. [1, 2]. More than 80% of *p*-aminophenol is used in the manufacture of antipyretic, paracetamol (Scheme 5.1)

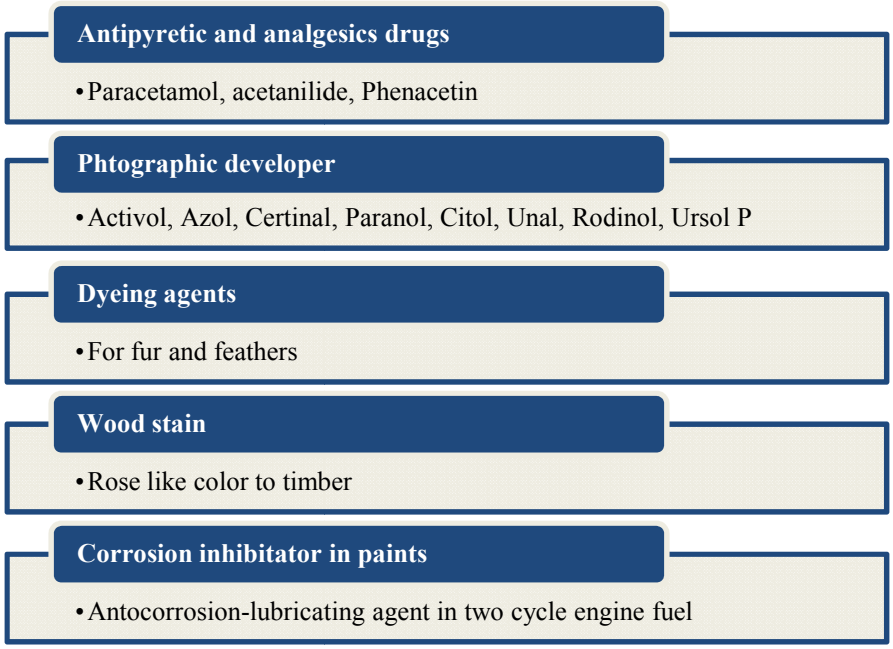

Figure 5.1. Importance of *p*-aminophenol

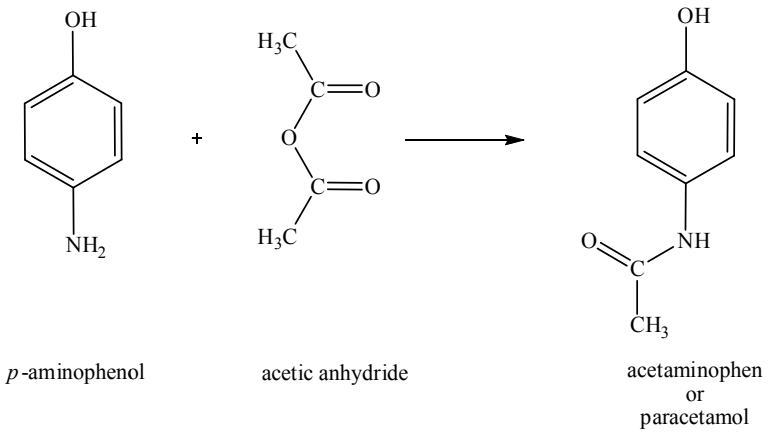

Scheme 5.1. Acetylation of *p*-aminophenol

p-Aminophenol (PAP) is mainly used in the production of paracetamol (acetaminophen, APAP), a mild and safest (declared by WHO) analgesic drug. It is used both alone and in combination with many other drugs including codeine or antihistamines. APAP dominates the global market for bulk analgesics. The APAP segment of the bulk analgesics market is estimated to ~1,10,000 tpa with a global market value of $350 million, out of which Europe and America accounting for nearly 40% of the total market. The world market for APAP is growing @ 5-6% per annum, primarily attributed to the growing third world market.

Major producers of APAP globally are:

- Mallinkrodt, USA
- Hoechst Celanese Corp., USA
- Rhone Polenc/Rhodia, USA
- Sterling Organics, UK
- RTZ Chemicals, UK

Mallinkrodt is the world's largest manufacturer of APAP, with production of about twice that of its nearest competitor. The company's largest APAP facility is a 30,000 tpa APAP production unit in Raleigh. The first process for PAP via catalytic hydrogenation of NB was patented over 60 years ago.

Apart from these manufacturers, China is also one of the producers and exporters of APAP. Asia (including India), Africa, and Europe are the major export destinations of China's APAP. China's production capacity of paracetamol has reached 62,000 tons at the end of 2008. However, out-of date manufacturing process (conventional Bechamp reduction of *p*-nitrophenol), excessive production capacity and low product quality make it difficult for Chinese paracetamol manufacturers to expand into high-end markets outside China.

Production cost has long been a critical factor for APAP, since it is price-intensive commodity type of market. Although the current U.S. list price is over $ 8/kg, the estimated world market price could be lower. Mallinkrodt has undertaken a variety of process improvements to remain competitive [3-5].

p-Aminophenol can be prepared by various methods such as electrolytic reduction [6-8], chlorophenol amination [9], hydroquinone amination [10, 11], iron-acid reduction of *p*-nitrophenol to *p*-aminophenol [1, 2], catalytic hydrogenation of nitrobenzene to *p*-aminophenol [1, 2]. Conventionally reagent based processes have been commercially used for the manufacture of *p*-aminophenol. Some of these processes are summarized below

5.1.1. Reduction of nitrophenol:

Conventionally *p*-aminophenol synthesized from *p*-nitropheol as a starting material. The reduction of *p*-nitrophenol carried out using Fe-HCl (Bechamp reduction) as a reducing agent (Scheme 5.2), which is having several drawbacks as discussed below in section 5.1.1.1.

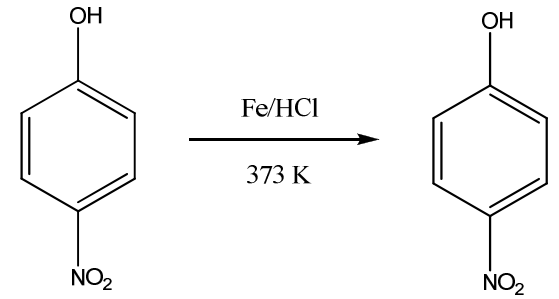

p-nitrophenol PAP

Scheme 5.2. Reduction of *p*-nitrophenol

p-Nitrophenol in turn can be obtained by nitration of phenol (Scheme 5.3) in which nitronium ion, NO_2^+ is condisered to be an active species. Typically, the nitronium ion is generated by reacting a mixture of 20% nitric acid, 60% sulfuric acid, and 20% water. Generally, the nitration reaction is performed under mild reaction conditions at 278- 283 K temperature to give the product *p*-nitrophenol along with formation of *o*-nitrophenol and 2,4-dinitrophenol [9].

$$HNO_3 + 2H_2SO_4 \rightleftharpoons NO_2^+ + H_3O^+ + 2HSO_4^-$$

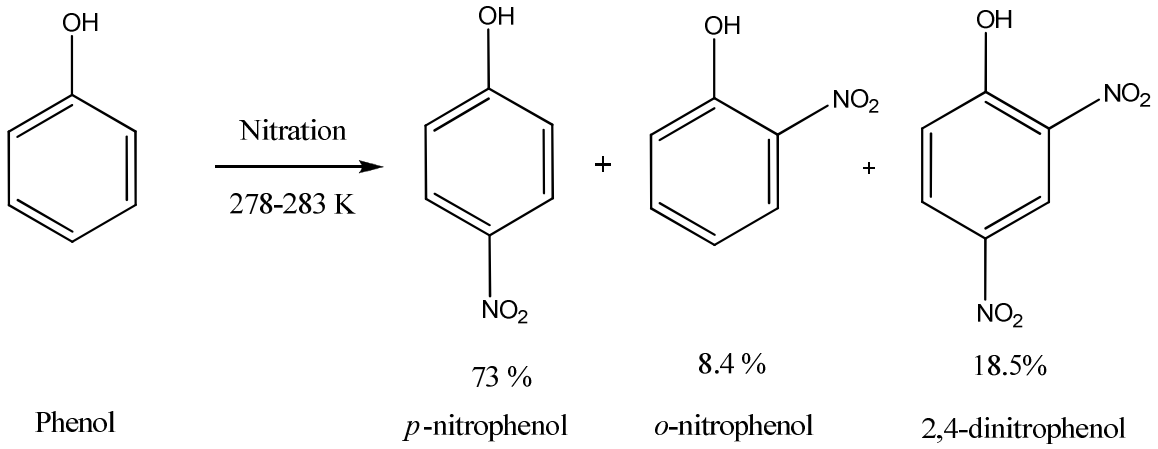

Scheme 5.3. Nitration of phenol [9]

p-Nitrophenol can be also sythesized by hydrolysis of *p*-chlorobenzene, carried out using 8.5 % NaOH solution and heating gradually to 443 K in an autoclave (Scheme 5.4). The resulting solution is cooled and acidified to give the product with 95% of yield.

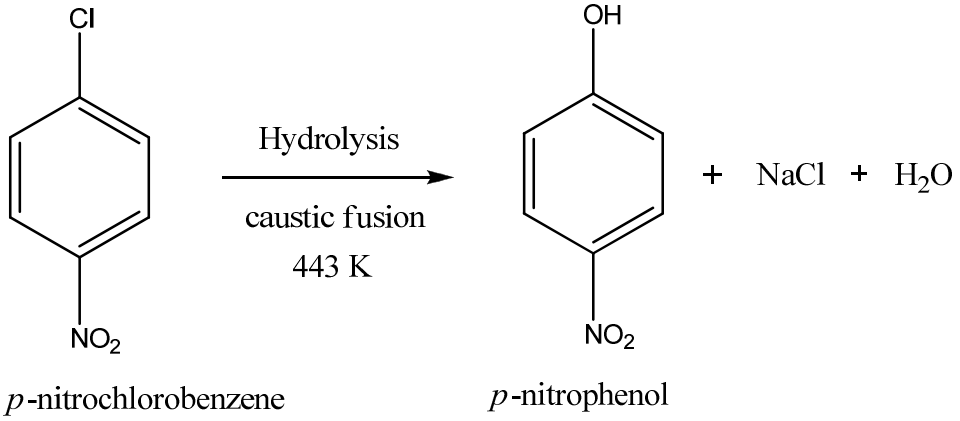

Scheme 5.4. Hydrolysis of *p*-nitrochlorobenzene

Since, reduction of nitro group is a crucial step in PAP synthesis, various methods of reduction are also briefly described here [13].

- Bechamp reduction
- Sulfide reduction
- Catalytic hydrogenation

5.1.1.1.Bechamp reduction:

Bechamp reduction is a simple reduction system used for the large scale production of variety of aromatic amines. This is a very commonly used method for reducing the aromatic nitro compound due to its lower cost. This involves the reaction of Fe with a mineral acid e.g. HCl, commonly used in the industry to produce nascent hydrogen (Scheme 5.5) which then reacts with an aromatic nitro compound to give the corresponding amine (Scheme 5.6) [14]. As can be seen from Scheme 5.5, along with the formation of a hydrogen, several moles of iron salts/ oxides are formed. Salts of iron produced from this reaction, which get converted in to iron hydroxide sludge (Scheme 5.6). Atom economy for producing hydrogen by reagent based iron/acid route can be calculated as follows.

$$Fe + 2HCl \longrightarrow FeCl_2 + 2[H]$$

$$56 + (2 \times 36.2) \rightarrow 127 + \mathbf{2} = \mathbf{0.015}\% \qquad \ldots\ldots\ldots \; 5.1$$

$$\left(\text{atom economy} = \frac{\text{molecular weight of desired product}}{\text{molecular weight of all reactants}} \times 100 = \frac{2}{56+73} \times 100 = 0.015\%\right)$$

$$FeCl_2 + 2HCl \longrightarrow FeCl_4 + 2[H]$$

$$127 + (2 \times 36.2) \rightarrow 198 + \mathbf{2} = \mathbf{0.01}\% \qquad \ldots\ldots \; 5.2$$

$$Fe(OH)_2 + 2Fe(OH)_3 \longrightarrow Fe_3O_4 + 4H_2O$$

Scheme 5.5. Atom economy for formation of hydrogen by Fe/HCl route

Thus, atom economy for producing 1 mol of hydrogen by Bechamp route is 0.01-0.015%, which is 10000 times lower than the catalytic hydrogenation (atom economy = 100%) method.

Overall atom economy for producing the *p*-aminophenol by Fe/HCl reduction method is 13.33%.

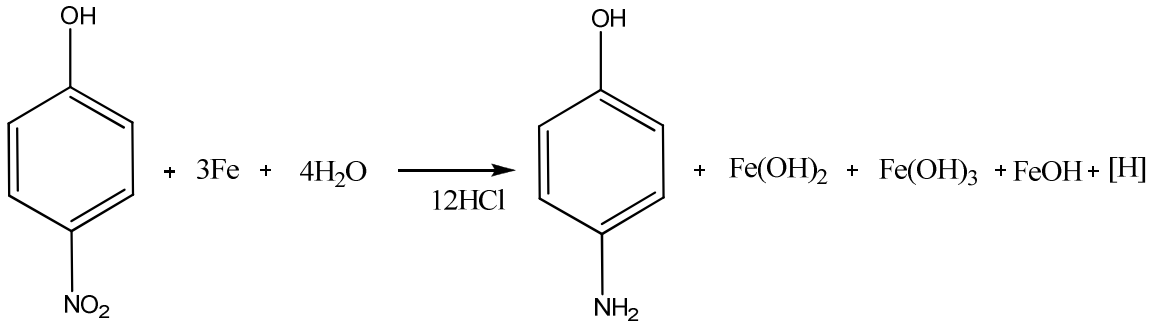

p-nitrophenol *p*-aminophenol

Atom economy

$$139 + (3 \times 56) \; + \; 72 + \; 438 \rightarrow \mathbf{109} + 88 + 107 + 73 = \mathbf{13.33}\% \quad \ldots. 5.3$$

Scheme 5.6. Atom economy for PAP synthesis by metal/acid reduction route

This Bechamp reduction process suffers from several disadvantages:

- Quantity of formation of Fe-FeO sludge is very large (1.2 kg/kg of product) and cannot be recycled, creating a serious effluent disposal problem.
- Fe-FeO sludge always contains the adsorbed reaction product and is difficult to filter and having a serious dumping problem.
- Erosion of reactor takes place due to Fe particles.
- Formation of side products.
- Rate of reaction varies from batch to batch.
- Work up of reaction crude is cumbersome.
- Difficult to separate the final product from the reaction mass.

5.1.1.2. Sulfide Reduction:

Depending on pH, different sulfide reducing agents can be employed such as hydrogen sulfide, NaHS, Na_2S as shown below (Scheme 5.7) [13].

pH ~ 7: $3H_2S + ArNO_2 \rightarrow ArNH_2 + 2H_2O + 3S^0$

pH < 7: $6NaHS + 4ArNO_2 + H_2O \rightarrow 4ArNH_2 + 3Na_2SO_3$

pH > 7: $6Na_2S + ArNO_2 + H_2O \rightarrow 4ArNH_2 + 6NaOH + 3Na_2SO_3$

Scheme 5.7. Sulfide reduction at various pH

This sulfur reduction process also has major drawbacks:

- Use of stoichiometric quantities of reagents generating large amount of inorganic wastes
- Toxicity and odor due to sulfur
- Formation of sulfur-containing organic side-products
- Formation of elemental sulfur

5.1.1.3. Catalytic Hydrogenation method:

Due to the serious problem of effluent disposal of the above reagent based reduction processes, stringent regulatory laws have been implemented in various countries including India to ban such processes. To overcome this problem, catalytic hydrogenation is the best alternative for the preparation of *p*-aminophenol from nitrobenzene. The catalytic route minimizes the effluent disposal problems to a great extent and is also expected to improve overall economics as well as the product quality. The catalytic route involves hydrogenation of nitrobenzene in a single step to *p*-aminophenol using supported noble metal catalysts in the presence of acid like H_2SO_4. Initial reduction of nitrobenzene to give β-phenylhydroxylamine (PHA) as an intermediate (Scheme 5.8) which then rearranges in situ to *p*-aminophenol in the presence of an acid (Bamberger rearrangement). Formation of aniline (AN) is the main competing side reaction in this process [15-20]. Atom economy for synthesizing *p*-aminophenol is 48.5/ 86 %, which is 3.6/6.5 times more than Bechamp reduction method.

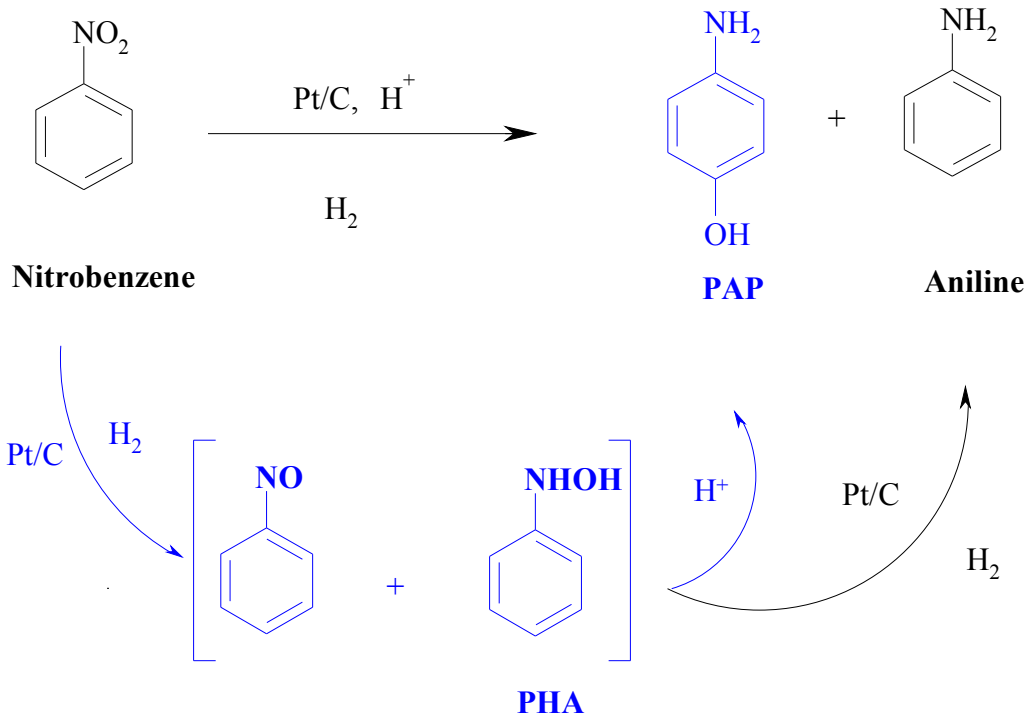

$$NB + (2H_2) + \text{sulfuric acid} \rightarrow PAP + AN$$

Atom economy based on sulfuric acid used for rearrangement of PHA,

$$123 + (2 \times 2) + 98 \rightarrow \mathbf{109} + 93 = \mathbf{48.45}\% \qquad \text{…..5.4}$$

Atom economy based on only H^+ which is the species responsible for rearrangement of PHA.

$$123 + (2 \times 2) \rightarrow \mathbf{109} + 93 = \mathbf{85.83}\% \qquad \text{…..5.5}$$

Scheme 5.8. Catalytic hydrogenation of nitrobenzene to *p*-aminophenol

5.1.1.4. Comparison of Catalytic, Bechamp and Sulfide reduction methods:

Catalytic hydrogenation process for PAP has several unique advantages over the reagent based Bechamp and sulfide reduction methods. A comparison of three processes is shown in Table. 5.1 [13].

Table 5.1. Comparison of Catalytic hydrogenation, Bechamp and Sulfide reduction processes for *p*-aminophenol [13].

	Catalytic hydrogenation	**Bechamp reduction**	**Sulfide reduction**
Selectivity	Broad scope with special catalytic systems e.g. Pt	Restricted scope	Broad scope
Synthetic potential	Broad	Broad	Narrow
Combination with other reactions	Possible	Not possible	Not possible
Starting material	Sensitive to catalyst poisons	Robust	Very Robust
Reaction medium	Organic solvents and aqueous media	Aqueous media	Aqueous media
Reaction conditions	10-100 % v/v 20-150^{o}C	10-25 % v/v 80-100^{o}C	10-40% 30-160^{o}C
Reaction characteristics	Heat removal 560 kJ mol^{-1} catalyst separation	Heat removal ca 280 kJ mol^{-1} Separation of large amounts of solid	Separation of (Soluble) oxidized sulfur compounds
Reactors	High pressure reactors and equipment	Standard stirred tank (acid resistant)	Standard stirred tank
Safety	Handling of hydrogen and pyrophoric catalysts Accumulation of thermally unstable intermediates	Formation of hydrogen possible	Formation of H_2S
Ecology	Environmentally friendly No critical wastes	Disposal of Fe sludge Large amounts of waste water	Large amounts of waste water

As can be seen from the Table 5.1, the catalytic hydrogenation method is the most adaptable, effective, economical and ecological method for the reduction of aromatic

nitro compound for which several types of heterogeneous catalysts involving supported/bulk transition metals are being used.

5.1.2. Literature survey:

Synthesis of PAP was first reported by Bassford involving two steps, (i) initial reduction of nitrobenzene using Zn metal in aqueous ammonium chloride solution under stirring by maintaining < 298 K. After the reaction, zinc oxide was removed by filtration and washed with warm water. Further the filtrate was placed in a saturated mixture of ice-salt mixture and cooled to 273 K. After an hour yellow crystals of phenylhydroxylamine were separated by filtration at inert atmosphere [21-23]. (ii) rearrangement to phenylhydroxylamine to PAP. Thereafter, the first catalytic hydrogenation route for PAP using PtO_2 catalyst in presence of sulfuric acid was reported by Henke and Vaughen in 1940 [24]. Benner has reported Pt/C catalyst for hydrogenation of nitrobenzene to *p*-aminophenol where in interruption of the hydrogenation step before all nitrobenzene was consumed, helps in the suspension of the catalyst in the nitrobenzene layer [25]. However in such case, conversion of nitrobenzene was always less than 75% and purity of recovered PAP was also affected to some extent. Caskey and Chapman has suggested the low temperature hydrogenation in presence of modified catalyst system containing sulfur compound and the rearrangement step in a separate vessel [4]. Greco reported the use of powdered molybdenum sulfide on carbon [26], while, Dunn has reported platinum on γ-alumina catalyst for the hydrogenation of nitrobenzene to PAP [3]. Recently, Rode et al. reported nickel based supported mono or bimetallic Ni-Pt catalysts for hydrogenation of nitrobenzene to *p*-aminophenol in an acidic medium with 55 % selectivity towards the *p*-aminophenol [27]. Majority of the literature on catalytic hydrogenation reaction of nitrobenzene to *p*-aminophenol, report the use of Pt/C catalyst due to its highest activity and selectivity towards the *p*-aminophenol (Table 5.2). Some of the other catalysts reported are MoS [26], Rh [28, 29], WC [30], Ru [29, 31, 32], Ni [33-36] etc.

Acid rearrangement of intermediate phenylhydroxylamine to *p*- aminophenol is a key step, usually facilitated in presence of a mineral acid. Bean observed that sulfuric acid is more effective than other acids to get higher yields of the corresponding aminophenol

[37]. Enhancement in activity and selectivity of *p*-aminophenol was studied by Lee et al. He observed that addition of the sulfuric acid with other organic acids for the acid rearrangement step helps to increase the selectivity to *p*-aminophenol [25]. Among various organic acid such as acetic , formic, trichloroacetic and methanesulfonic, he found that formic acid along with sulfuric acid gives the highest selectivity (83.3%) towards the *p*-aminophenol. Rylander et al. disclosed a process of hydrogenation of nitrobenzene to *p*-aminophenol in an acidic medium and platinum oxide catalyst in presence of dimethyl sulfoxide [38]. A solid acid catalyst like ion exchange resin is also reported for hydrogenation of nitrobenzene to PAP by Rode et al. wherein, maximum selectivity to PAP obtained was 17% [39].

Surfactants such as quaternary ammonium salts (dodecyltrimethyl ammonium chloride, octadecyl trimethyl ammonium chloride) and non quaternary ammonium compounds (triethylamine sulfate, tributylamine sulfate etc.) also play an important role in the hydrogenation of nitrobenzene to *p*-aminophenol, and to improve the yield of *p*-aminophenol [40, 41]. Spiegler observed that the quaternary ammonium salts are better than non-quaternary compounds [40,41] . Brown et al. used non-ionic surfactants such as polyethers, polyols [42]. Sathe reported the maximum yield (98%) of *p*-aminophenol using dimethyldodecylamine as a surfactant [5].

Though, several variations in catalysts and processes for hydrogenation of nitrobenzene to PAP have been reported so far, there is still scope for an improved process for PAP with respect to enhanced selectivity and recovery of PAP.

Table 5.2. Literature summary on nitrobenzene to *p*-aminophenol

Sr. No.	Catalyst	Reaction conditions	Conversion, %	Selectivity, %	Ref.
1.	Zn-NH_4Cl	T=323 K; P_{H_2}=0.1MPa; water, Rearrangement in separate vessel using H_2SO_4	50	64	21
2.	Al flakes	T=353 K; P_{H_2}=0.1 MPa; water: H_2SO_4	100	75	37

3.	PtO_2	T=373 K; P_{H_2}= 3.44 MPa; water: H_2SO_4	90	57	30
	PtO_2	T=373 K; P_{H_2}= 3.44 MPa; water:HCl	90	67	
	MoS	T=423 K; P_{H_2}= 3.44 MPa; water: H_2SO_4	70	53	
4.	0.3%Pt/C	T=388 K; P_{H_2}= 3.44 MPa; water: H_2SO_4 Octadecyl trimethyl ammonium chloride (surfactant)	100	83	40
5.	1% Pt/C,	T=358 K; P_{H_2}= 0.1 MPa; water: H_2SO_4	100	79	41
6.	MosS,	T=428 K; P_{H_2}= 2.06 MPa; water:H_2SO_4.	100	78	26
	Pt-S/C,	T=408 K; PH2= 1.41 MPa; water H_2SO_4			
7.	Pt/γ-Al_2O_3,	T=360 K; P_{H_2}= 0.1 MPa; water: H_2SO_4; Dodecyl trimethyl ammonium chloride (surfactant)	80	85	3
8.	1%Pt/C	T=353 K; water: H_2SO_4; RSo_3H, R=alkyl, alkylphenyl acids added	41	82	43
9.	1% Pt/C,	T=353 K; P_{H_2}=0.1 MPa; water :H_2SO_4 Dimethylalkylamine sulfate	80	73	5
10.	3%Pt/C,	T=358 K; P_{H_2}= 0.1 MPa; water:H_2SO_4 ; dimethylalkylamine oxide (surfactant)	57.1	80	44
11.	PtO_2/	T=298 K; P_{H_2}=0.1 MPa; water:H_2SO_4; DMSO added	100	56	38
12.	5%Rh/C +$RhCl_3$,	T=363 K; P_{H_2}=2.04 MPa; water:H_2SO_4	88	85	45
13.	3%Pt/C,	T=358K; P_{H_2}=0.1 MPa;	88	73	25

		water:H_2SO_4			
14.	3%Pt/C,	T=358 K; P_{H_2}=0.1 MPa; methanol: H_2SO_4 ;diethyl sulphide added	75	79	4
15.	1%Pd/Pt/C , γ-alumina	T=333 K; P_{H_2}=0.344 MPa; water :different acids are used like formic acid, acetic acid etc.	99	83	46
16.	2%Pt-Ru/C (Pt/Ru=5),	T=368 K; P_{H_2}=0.202 MPa; water:H_2SO_4 ; dodecyltrimethyl ammonium bromide	100	86	32
17.	Pt.Pd.Rh and Ru	T=353 K; P_{H_2}=0.303-0.709 MPa; water	100	Pt=70 Pd=20,	47
18.	WC (Tungstate carbide)	P_{H_2}=0.202 MPa; Ethanol	99	80, without EtOH sel: 58.5	30
19.	5% Pt/C,	T=373 K; P_{H_2}=0.1 MPa; water:H_2SO_4	80	83	48
20.	Pt/CMK-1	T= 353 K; P_{H2}= 0.1 MPa	67	84 in 4 hrs	49
21.	1 to 5% Pt/CMK-1	T= 353 K; P_{H_2}= 0.1 MPa; H_2SO_4; DMSO (N,N-dimethyl-n-dodecylamine)	53	88	50
22.	Solid acid catalyst	T= 353 K	(PHA) = 100	PHA to PAP, 100	51
23.	Pt-PSZ	T= 423 K; P_{H_2}= 0.405 MPa	(PHA)= 100	PHA to PAP, 43.4	52
24.	Pt/C, PTA	T= 363 K; P_{H_2}=0.1 MPa	70-75	88	53
25.	Pt/C	T= 353 K; P_{H_2}= 2.73 MPa	100	75	54
26.	Pt/C	T= 353 K; P_{H_2}=2.73 MPa	100	88	55
27.	1%Pt-S/C,	T= 353 K; P_{H_2}= 3.74 MPa	97	14	56

		ion exchange resin			
28.	10% Ni/C	T= 393 K; P_{H_2}= 2.73 MPa	14	14	27
	10% Ni/SiO_2	T= 393 K; P_{H_2}= 2.7 MPa	30	11	
	10%Ni/ZSM-5	T= 393 K; P_{H_2}= 2.7 MPa	45	45	
	10%Ni-1%Pt/ZSM-5	T= 393 K; P_{H_2}= 2.7 MPa	93	63	
29.	Polymer supported Pd mono and Pd- Fe, Co, Ni, Cu, Ru, Zr-HCl, Ti, Yb, La, V, Sn	T= 357 K; P_{H_2}= 0.1MPa; H_2SO_4;DMSO Thiomaleic acid Ethyl sulfide 2-Mercaptopyrimidine	32.9 33.6 40.6 90.7	66.8 36.9 49.1 64.6	57
30.	Acid ionic liquid (N,N,N-trimethyl-N-sulfobutyl ammonium hydrogen sulfate		100	92	58
31.	Pt/HZSM-5	T = 523 K	40	45	59
32.	Pt/C	T= 353 K; P_{H_2}= 0.069 MPa; H_2SO_4; Ethomeen TM C/12 & docecyldimethyl	78	75	34

5.1.3. Objectives:

The process of *p*-aminophenol from nitrobenzene involves two-step reaction carried out in a single reactor. Initial reduction of nitrobenzene gives phenylhydroxylamine (PHA) as an intermediate, which undergoes a Bamberger rearrangement in presence of an aqueous acid to give PAP. (Scheme 5.8). Formation of aniline via further hydrogenation to PHA is a major competing reaction affecting the selectivity to PAP. In order to achieve the highest selectivity to PAP, the suppression of the competing hydrogenation of PHA to aniline is highly desirable. The main objectives of the present work was to study these two reaction steps separately viz. (i) partial hydrogenation of NB to PHA, and (ii) rearrangement of PHA to PAP. For this purpose, hydrogenation of NB to PHA was carried out under very mild temperature (303 K) and pressure (pH_2, 0.68-4.1 MPa) conditions and its acid rearrangement to PAP was observed at elevated temperature (353 K), both in presence of hydrogen and in an inert atmosphere (argon) under atmospheric pressure conditions. Another aim of this work was also to improve the process for a single step preparation of *p*-aminophenol from nitrobenzene and device a strategy for workup of the reaction crude in order to recover practically all the *p*-aminophenol from the reaction crude.

5.2. Experimental details:

5.2.1. Catalyst preparation:

Details of preparation of Pt/C catalyst are described in chapter II section 2.2.2.

5.2.2. Catalyst activity testing:

The experimental batch setup used for the hydrogenation reaction and the experimental procedure is described in section 2.4.2.

5.2.3. Catalyst Characterization:

The details of catalyst characterization are described in section 2.3.

5.2.4. Analytical technique:

The quantitative analysis of liquid samples was carried out by HPLC method, the details of which are described in section 2.5. A typical HPLC chromatogram showing the separation of reactants and products in the hydrogenation of nitrobenzene to PAP is shown in Figure 5.2.

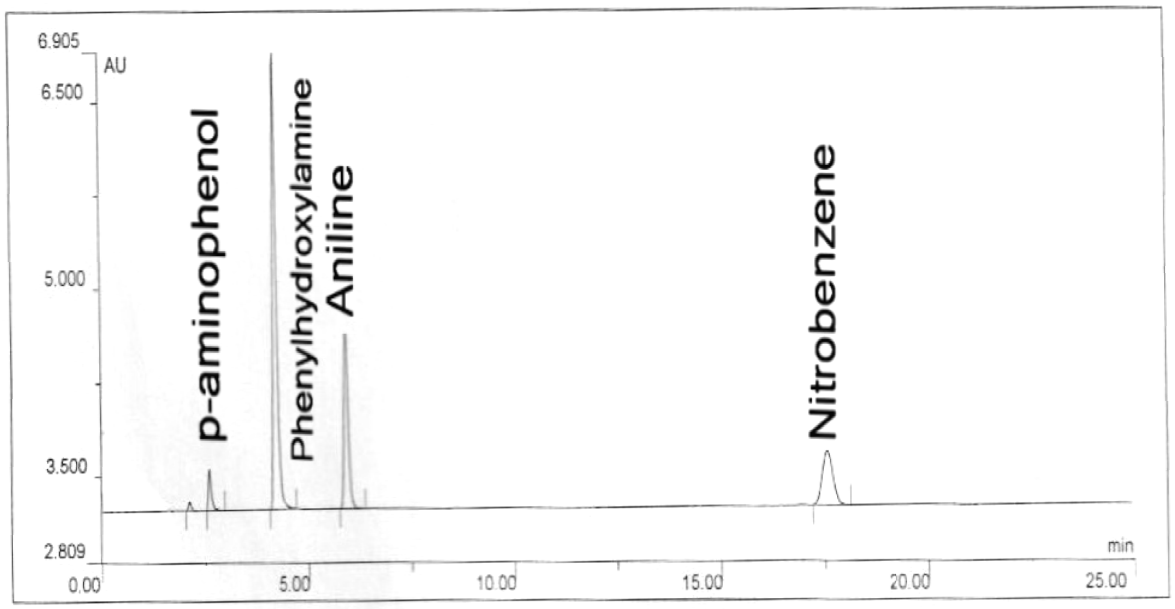

Figure 5.2. HPLC chromatograph for reactant and product

The results of the work done on nitrobenzene hydrogenation to PAP process consists of two parts: (i) studies on role of process parameters on enhancement of selectivity to PHA, which is an intermediate of first step hydrogenation of NB. (ii) studies on role of process parameters on conversion of NB and PAP selectivity in a single step hydrogenation process for PAP. First, the catalyst characterization results are discussed, since these are common for both NB to PHA and direct PAP synthesis form NB.

5.3. Results and discussion:

Various samples of Pt/C catalysts were prepared by varying Pt loading from 1 to 5 %. The characterization details are discussed below.

5.3.1. Catalyst Characterization:

5.3.1.1. BET surface area:

The BET surface area of activated carbon and Pt/C with Pt loading varying from 1 to 5% was evaluated from nitrogen adsorption isotherm recorded at 77K. As can be seen from Table 5.3, the surface area of carbon was found to be 1100 m^2/g, which decreased consistently from 1100 to 482 m^2/g with increase in Pt loading from 1 to 5% Pt metal loading on the surface of the carbon. The decrease in S_{BET} values suggests that Pt species were dispersed on the support [60].

Table.5.3. BET surface area of 1 to 5% Pt/C catalysts

Pt Metal Loading, %	Surface area, m^2/g
0	1100
1	703
2	656
3	620
5	482

5.3.1.2. XRD study:

The Powder XRD patterns of Pt/C with 1-5% metal loadings are shown in Figure 5.3. The reflection peaks 2θ at 39°, 46° and 68° are based on 111, 200, 220 reflection peaks for metallic platinum, represent the typical character of crystalline Pt Face centered cubic (fcc) lattice structure [61]**.** The X-ray diffraction (Figure 5.3) study clearly showed that as metal loading increased, the crystallanity of platinum metal also increased [62]**.** The diffraction peaks for 1 and 2% Pt/C catalysts are much broader than those for the 3 and 5% Pt/C catalysts, which indicates that the 1% and 2% Pt/C catalyst samples have smaller particle sizes. The peak broadening increases as the particle size decreases,

which is predicted by Scherrer's equation [63]. Based on Scherrer formula, the particle sizes of the catalysts having Pt loading from 1 to 5% Pt were found to be 8.6, 8.9, 10.5 and 13.06 nm respectively. The diffraction peaks at 2θ of 43° is observed in XRD patterns for the Pt/C catalyst because the graphitic carbon is the supporting material.

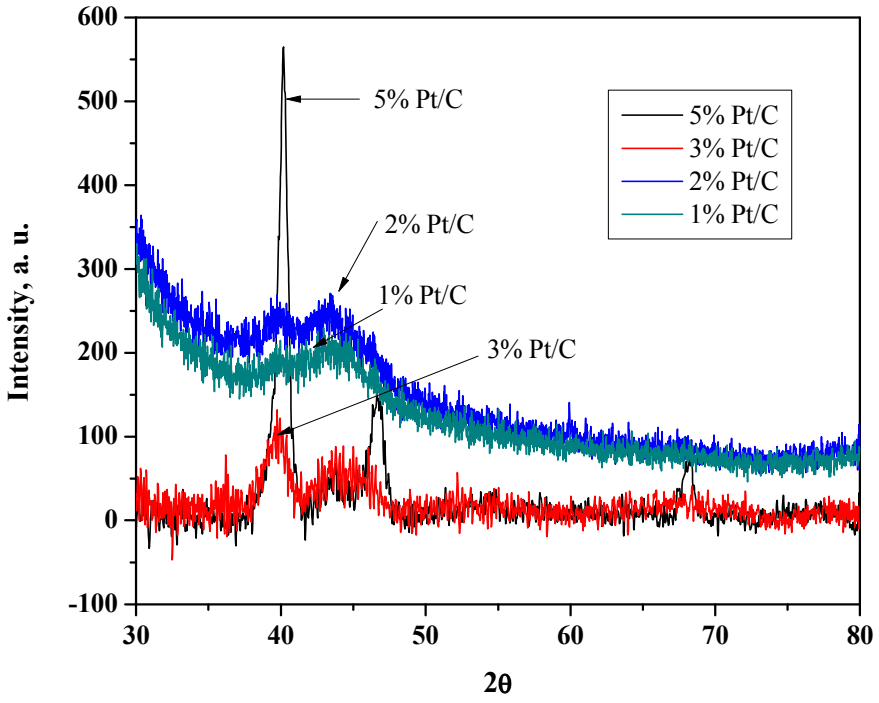

Figure 5.3. XRD pattern of 1 to 5% Pt/C catalysts

5.3.1.3. TPR studies:

Extent of reducibility of different Pt/C catalyst was obtained by temperature programmed reduction method, which also gives the information about unreduced Pt species present in the catalyst. TPR profiles of Pt/C catalyst with Pt loading varying from 1 to 5 % , obtained in a range of 303 K to 773 K are shown in Figure 5.4. The TPR profiles of Pt/C catalysts showed a broad reduction profile extending from 363 K to 673 K. Except 1% Pt/C sample, the TPR profiles of all other samples showed two major peaks, (i) at 363 K and (ii) a broad peak at 513-523 K. The broadening suggests the presence of several Pt species. The TPR peak appeared at 363 K was due to the reduction of a surface species

PtO [64-65]. The peak appeared at 523 K was attributed to the reduction of Pt^{+4} species [66]. For 5% Pt/C sample two additional peaks were observed near 403 and 445 K indicating presence of some other superficial platinum species. Among all these samples, only 3% Pt/C showed maximum reduction (14.5 % of Pt^{+2} and 85.5 % of Pt^{+4}) which was also in accordance with its activity results (70% selectivity to PHA). Hence, further characterization of only 3% Pt/C sample was carried out.

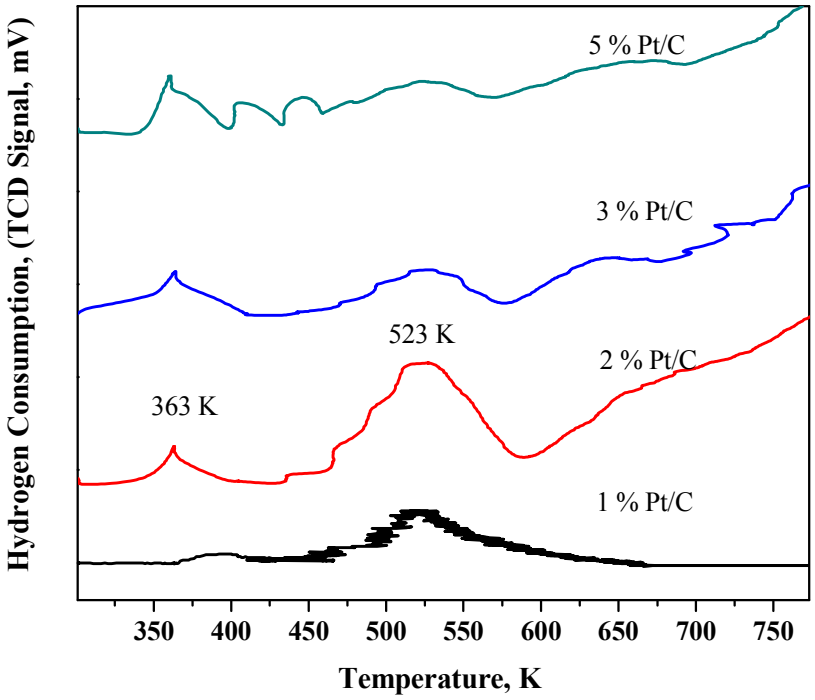

Figure 5.4. TPR profile of 1 to 5% Pt/C catalysts

5.3.1.4. SEM and EDX study for 3% Pt/C catalyst:

Figure 5.5 shows the SEM of 3% Pt/C catalyst in which Pt metal particles being uniformly dispersed onto the carbon surface. The external morphology of the Pt metal particles was found to irregular. Figure 5.6 shows the EDX spectrum of a 3% Pt/C catalyst confirming the presence of Pt, oxygen and carbon without any impurity.

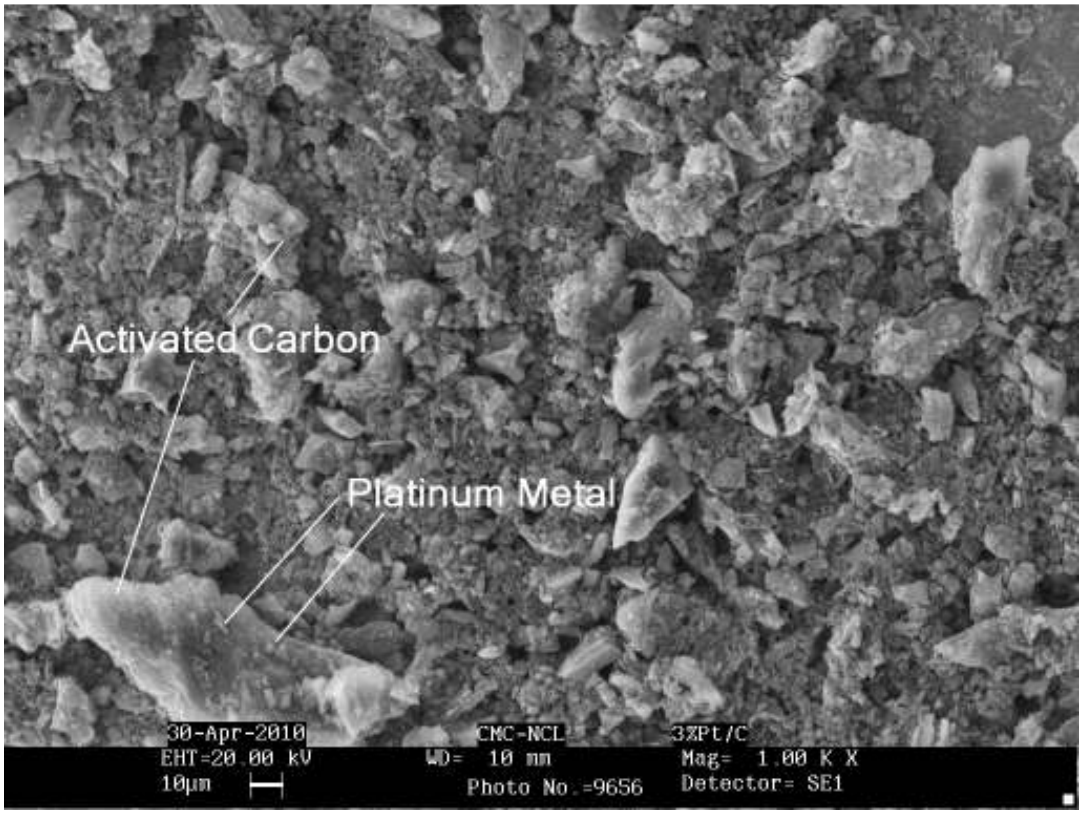

Figure 5.5. SEM image for the 3% Pt/C catalyst

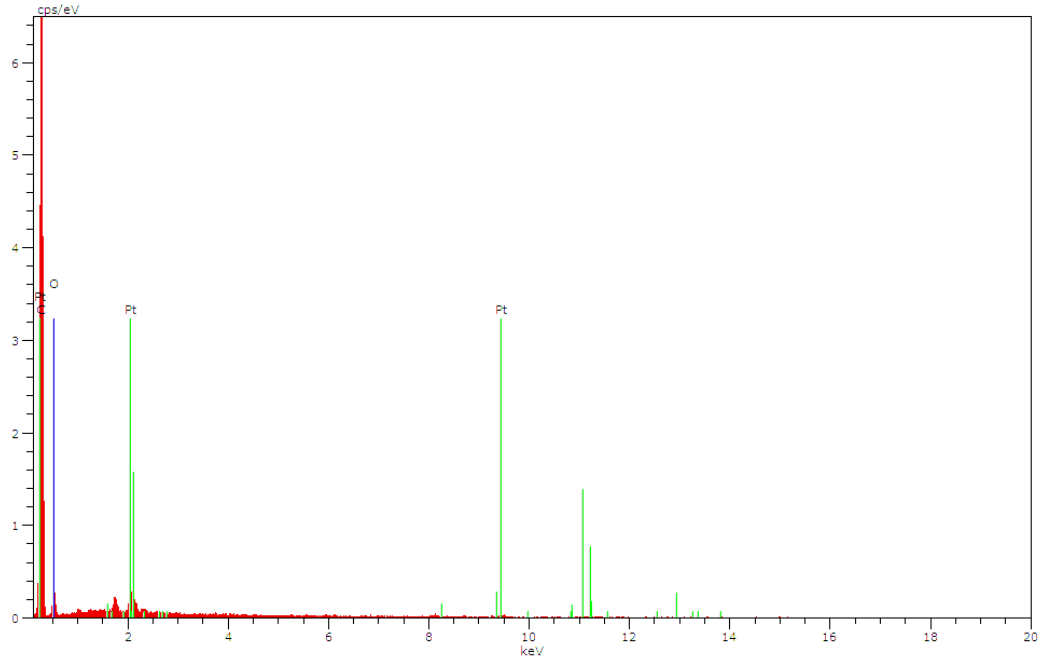

Figure 5.6. EDX of 3% Pt/C catalyst

5.3.1.5. XPS study for 3% Pt/C catalyst:

Figure 5.7 presents the XPS of 3% Pt/C catalyst in which Pt*4f* spectrum of the catalyst shows Pt is in different states. The most intense doublet for $Pt4f_{7/2}$ and $Pt4f_{5/2}$ (71.4 and 74.7 eV) is due to metallic Pt. The second set of doublets for $Pt4f_{7/2}$ and $Pt4f_{5/2}$ (73.4 and 76.7 eV) could be assigned to the Pt (II) chemical state as PtO or $Pt(OH)_2$ [67-68]. Third doublet of Pt is the weakest in intensity, and occurred due to binding energies of $Pt4f_{7/2}$ and $Pt4f_{5/2}$ (75.5 and 78.8 eV) which could be assigned to the Pt (IV). The Pt4*f* spectrum of the Pt/C catalyst is fitted with two pairs of overlapping Gaussian curves. The percentage of the Pt metal species are calculated from the relative areas of these peaks and XPS data suggest that 49.7% of the Pt $4f_{7/2}$ is present as Pt metal, and 31.5% is present as divalent Pt-oxide (PtO) and remaining 18.8% of the Pt is also present in a higher oxidation state, expected as platinum-dioxide (PtO_2) [69]. XPS of our 3% Pt/C catalyst did not show the presence of Cl^- peak, which ensured the complete conversion of chloroplatinic acid during the catalyst preparation.

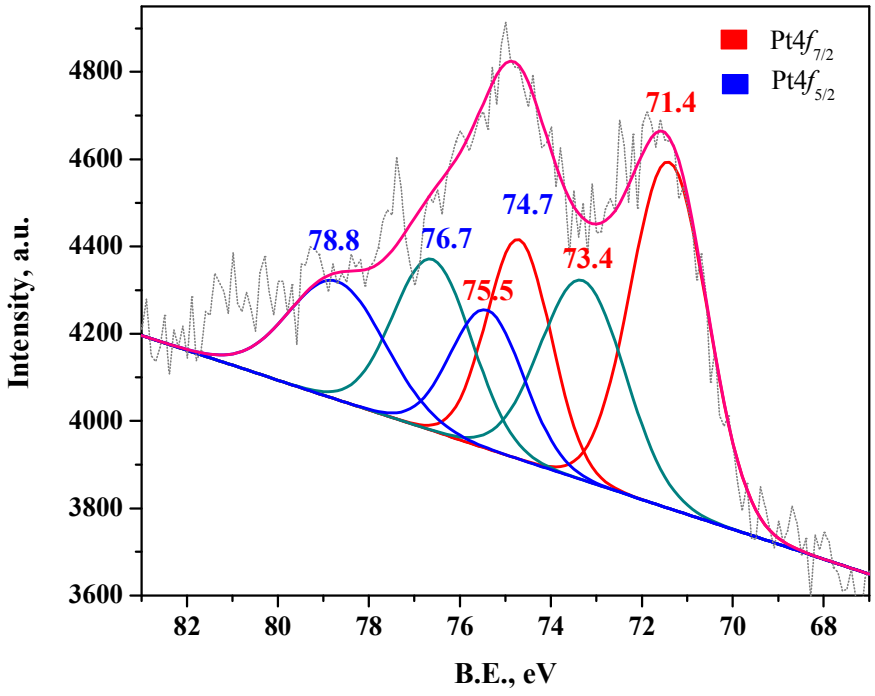

Figure 5.7. XPS spectra for 3% Pt/C catalyst

5.3.2. Nitrobenzene hydrogenation to PHA followed by its rearrangement to PAP:

Since, PHA is an intermediate, which undergoes an acid catalyzed rearrangement to give PAP, systematic study of effect of various reaction parameters on the first step of hydrogenation of nitrobenzene to PHA, was carried out. For this purpose, % conversion of nitrobenzene, selectivity to various products vs. time data was obtained. A summery of these results is discussed below.

Catalytic hydrogenation of NB to PAP involves a four phase system: an organic phase of nitrobenzene, an aqueous phase of dilute sulfuric acid, a solid catalyst and hydrogen as a gas phase as shown in Figure 5.10. It was observed that the Pt/C catalyst remained within the nitrobenzene (organic layer) interface in the form of droplets. When reaction proceeds, the phenylhydroxylamine migrates out into the aqueous sulfuric acid phase and Bamberger rearrangement takesplace to get the *p*-aminophenol. As nitrobenzene

conversion increases, the size of the nitrobenzene layer which is in the form of globule decreases; however catalyst concentration remains same in the organic layer. The catalyst rich environment was observed after increase in nitrobenzene conversion. PHA formed in this catalyst rich environment immediately undergoes further hydrogenation to gives aniline. This may be one of the reasons for decrease in the PAP selectivity with increase in the conversion of nitrobenzene.

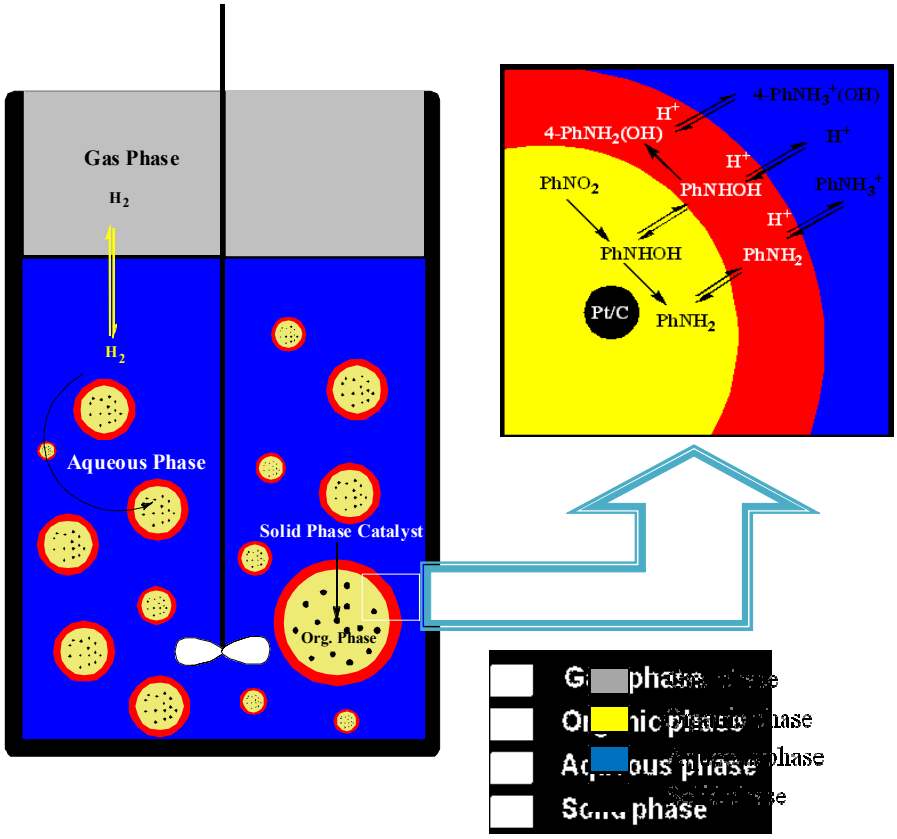

Figure 5.8. PAP four phase system

5.3.2.1. Effect of temperature:

Figure 5.9 shows a typical conversion, selectivity vs. time profile for the partial hydrogenation of nitrobenzene to PHA at 303 K and 0.68 MPa H_2 pressure in a biphasic mixture consisting of nitrobenzene and aqueous sulfuric acid. The analysis of samples taken from time to time, showed that only PAP, PHA, and aniline were formed during the course of hydrogenation reaction. As can be seen from this Figure, at the end of first

hour of the reaction, PHA selectivity as high as 95% was obtained with nitrobenzene conversion of >35% after first hour reaction. As the reaction proceeded, almost complete conversion of nitrobenzene was obtained after ~3 h however, appreciable amount of aniline started forming while PAP formation was < 1%. As nitrobenzene conversion was > 97% after 6 h, for acid rearrangement reaction temperature was increased to 353 K. Before increasing the temperature hydrogen pressure was released in order to prevent aniline formation and to promote the higher PAP selectivity. As soon as reaction temperature increased, PHA selectivity dropped down abruptly to give PAP indicating that the Bamberger rearrangement is facilitated at higher temperature.

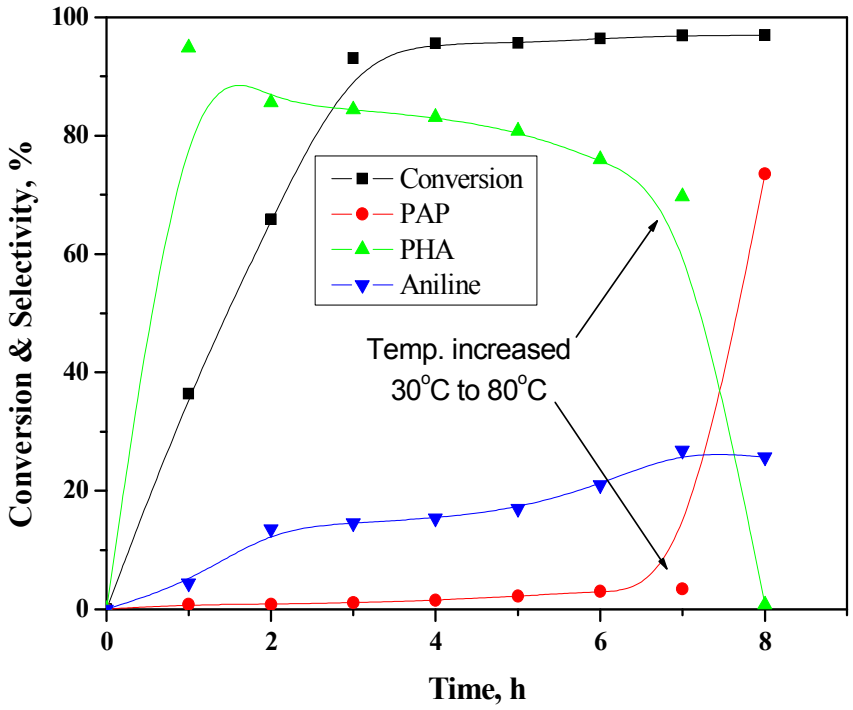

Figure 5.9. Conversion, selectivity vs. time profile

Reaction conditions: nitrobenzene,0.0813 mol; temperature, 303K; hydrogen pressure, 0.69MPa; acid,10 g; water,84 g; 3%Pt/C, 0.035g; agitation speed, 1000 rpm

Figure 5.10 shows the nitrobenzene conversion and PHA/Aniline ratio vs. time profile at 303 K. During first hour of the reaction and up to 40% conversion of nitrobenzene, PHA/AN ratio was as high as 22 however, as nitrobenzene conversion was > 95% after 2 h. PHA/AN ratio dropped down to ~3 and remained almost constant at this value. Thus, over the period of time, further hydrogenation of PHA to aniline was much more dominant reaction than the rearrangement of PHA to PAP.

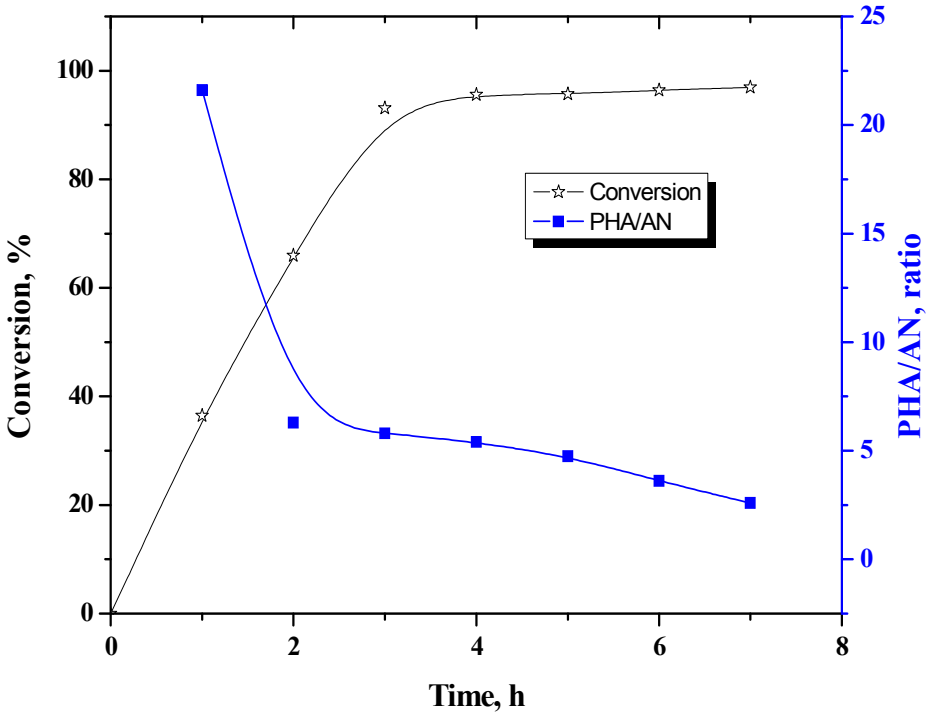

Figure 5.10. Effect on PHA/AN ratio

Reaction conditions: nitrobenzene,0.0813 mol; temperature, 303 K; hydrogen pressure, 0.69MPa; 3%Pt/C, 0.035g; acid,10 g; water,84 g; agitation speed, 1000 rpm.

5.3.2.2. Effect of hydrogen pressure:

Since, the first step involves hydrogenation of nitrobenzene to PHA, the effect of hydrogenation pressure on catalyst activity and selectivity to both PHA and aniline was also studied at 303 K and the results are shown in Figure 5.11. As H_2 pressure increased from 0.69 to 4.1 MPa (six fold), TOF also increased linearly from 2.4 x 10^3 to 12.25 x 10^3 h^{-1}, while the selectivity to PHA decreased marginally from 70 to 63%. Due to increase in hydrogen pressure, higher concentration of surface hydrogen becomes available on the platinum surface leading to higher TOF as well as accelerating PHA hydrogenation to aniline hence, selectivity to aniline increased from 27 to 29%.

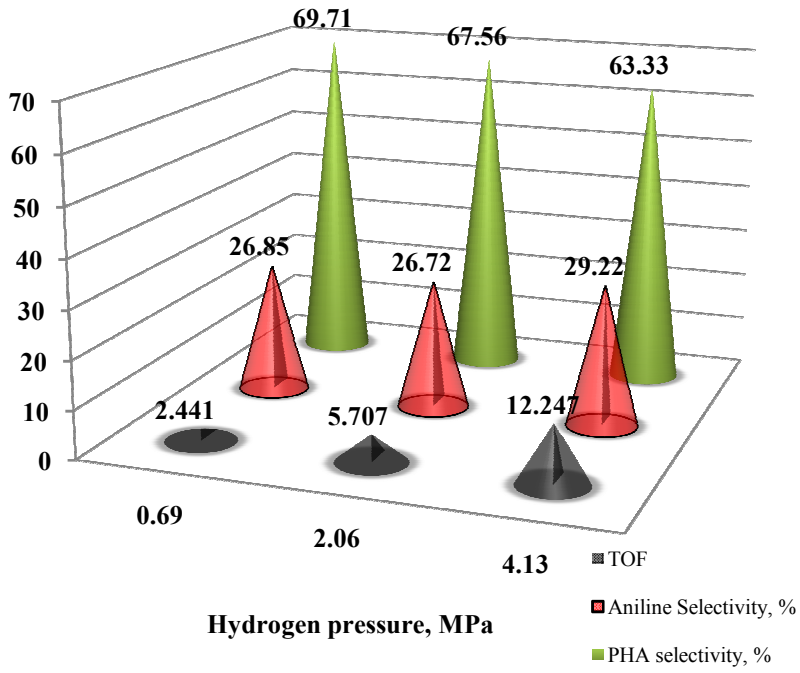

Figure 5.11. Effect of pressure on PHA selectivity

Reaction conditions: nitrobenzene,0.0813 mol; temperature, 303 K; acid,10 g; 3%Pt/C, 0.035g; water,84 g; agitation speed, 1000 rpm; TOF, 10^3 hr^{-1}

5.3.2.3. Effect of acid concentration:

Although, the first step involves hydrogenation of nitrobenzene to PHA, this hydrogenation has to be carried out in presence of an aqueous acid otherwise, only aniline formation was observed in absence of acid even at 303 K. Hence, it was necessary to study the effect of acid concentration on the selectivity to PHA. This study was carried out by varying the acid concentration in a range of 5-15% w/w, keeping other reaction conditions constant, and the results are shown in Figure 5.12. The conversion of nitrobenzene remained almost constant (> 99%) while the selectivity to PHA increased from 30 to 70% with increase in acid concentration from 5-10%. At higher acid concentration of 15%, rearrangement of PHA to PAP was initiated even at lower temperature of 303 K hence lowering the PHA selectivity from 72 to 66%. Thus, acid concentration of 10% w/w was found to be the optimum for the highest selectivity of PHA.

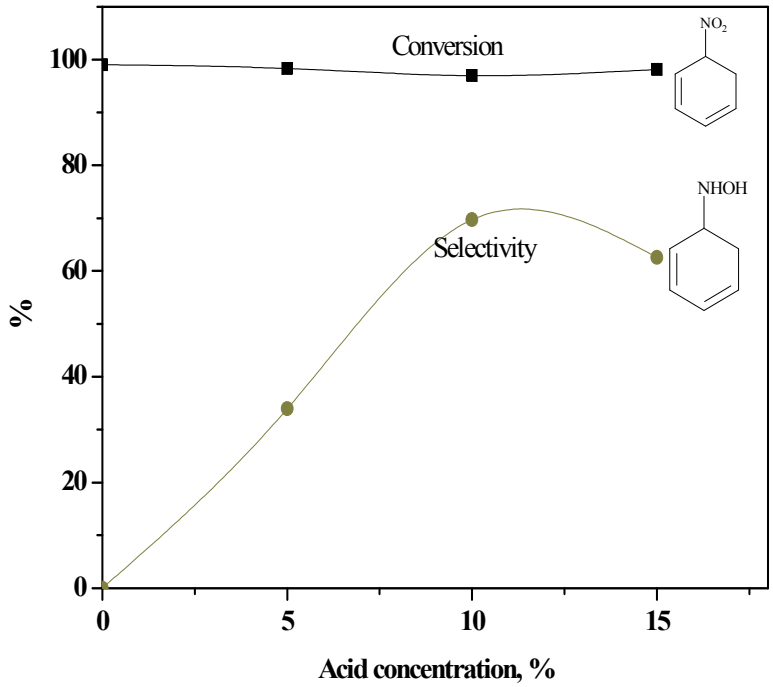

Figure 5.12. Effect of acid concentration on PHA selectivity

Reaction conditions: nitrobenzene,0.0813 mol; temperature, 303 K; hydrogen pressure, 0.69 MPa; 3% Pt/C, 0.035 g; water,84 g; agitation speed, 1000 rpm

5.3.2.4. Effect of nitrobenzene concentration:

Typical results of the effect of initial concentration of nitrobenzene in the range of 0.04 to 0.12 mol on conversion and selectivity pattern are shown in Figure 5.13. Marginal lowering in nitrobenzene conversion from (99 to 97%) was observed with increased in nitrobenzene concentration 0.04 to 0.12 mol. Selectivity to PHA remained almost constant at ~ 72% up to nitrobenzene concentration of 0.08 moles while it decreased to 50% with further increase in nitrobenzene concentration to 0.12 mol.

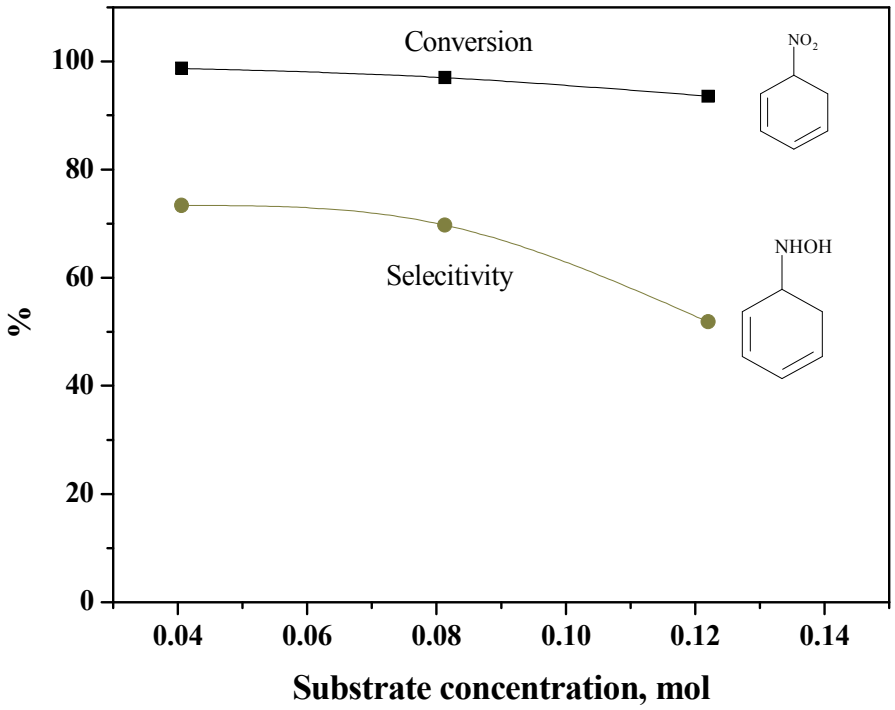

Figure 5.13. Effect of substrate concentration

Reaction conditions: temperature, 303 K; hydrogen pressure, 0.69 MPa; 3% Pt/C, 0.035 g; acid, 10 g;water,84 g; agitation speed, 1000 rpm

Once PHA is formed as a result of first step hydrogenation of nitrobenzene, its further rearrangement to give PAP doesn't require hydrogen hence, it was thought appropriate to compare the PAP selectivity under an inert atmosphere with that under H_2 atmosphere.

5.3.2.5. PHA to PAP rearrangement under inert atmosphere:

It was found that under inert atmosphere, PAP selectivity achieved was 77% (Figure 5.14) along with formation of 23% aniline while under H_2 atmosphere, selectivity to PAP lowered to 74% (Figure 5.15) due to higher amount of aniline formed. Since, the first step essentially involves hydrogenation of nitrobenzene to PHA, further

hydrogenation of PHA to aniline also gets initiated which could only be controlled by keeping the lower temperature of 303 K.

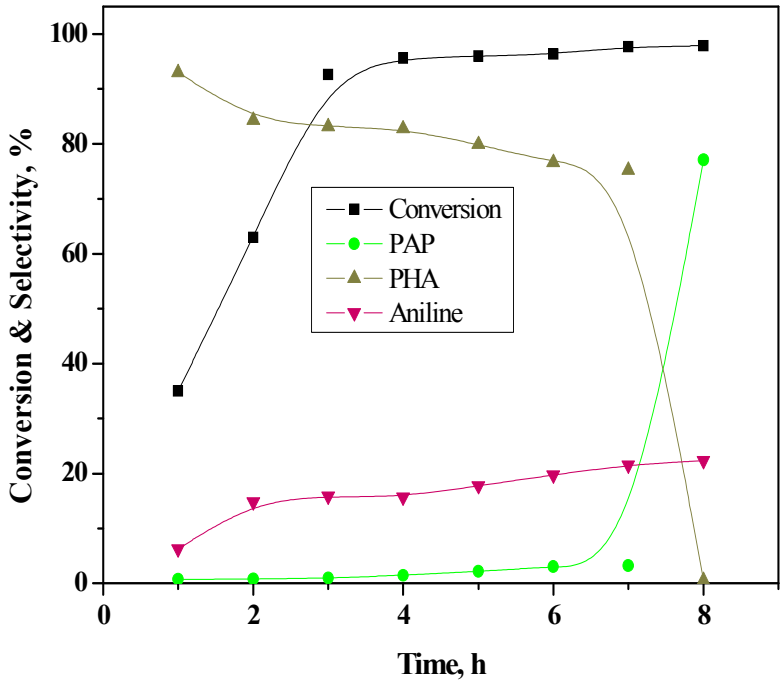

Figure 5.14. Bamberger rearrangement facilitated under inert atmosphere

Reaction conditions: nitrobenzene,0.0813 mol; acid,10 g;water,84 g; 3% Pt/C, 0.035 g; temperature, 303K; hydrogen pressure, 0.69MPa; agitation speed, 1000 rpm.

5.3.2.6. Effect of hydrogen pressure on PAP selectivity:

Figure 5.15 shows the effect of H_2 pressure on the PAP selectivity during the rearrangement of PHA at 353 K. PAP selectivity decreased from 74 to 57% with increase in H_2 pressure from 0.69 to 4.1 MPa, due to a competitive hydrogenation of PHA to aniline reaction at 353 K. This clearly shows that the selectivity to PAP as high as 74% can be achieved if the reactor is depressurized after the first hydrogenation step carried out at 303 k and the next step Bamberger rearrangement is continued under H_2 atmosphere by enhancing the temperature to 353 K.

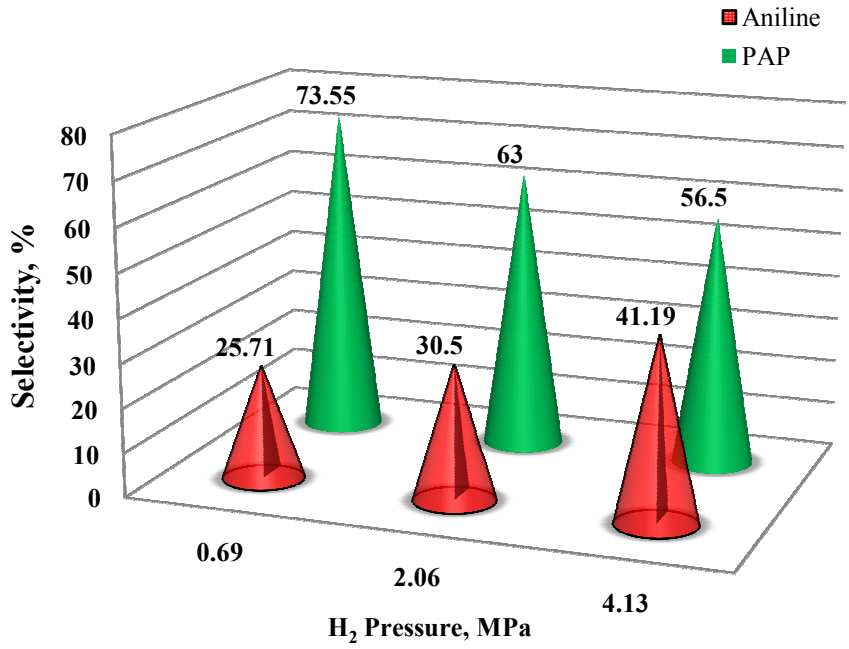

Figure 5.15. Effect of hydrogen pressure on PAP selectivity

Reaction conditions**:** nitrobenzene,0.0813 mol; temperature, 353 K; 3%Pt/C, 0.035 g; acid, 10 g; water, 84 g; agitation speed, 1000 rpm.

5.3.2.7. Effect of metal loading:

Effect of platinum loading on activity and selectivity pattern was studied by varying the Pt metal loading on carbon support in a range of 1 to 5% and the results are shown in Figure 5.16. For all the metal loadings, conversion of nitrobenzene remained constant i.e. > 99% while the selectivity to PHA increased from 55 to 70% with increase in metal loading from 1 to 3%, with further increase in metal loading upto 5%, selectivity to PHA dropped down to 65% . On other hand, it was found that as metal loading increased, TOF also increased from 0.27 to 5.8 x 10^3 h^{-1}. Here 3% Pt/C showed the optimum results i.e. 70% selectivity to PHA.

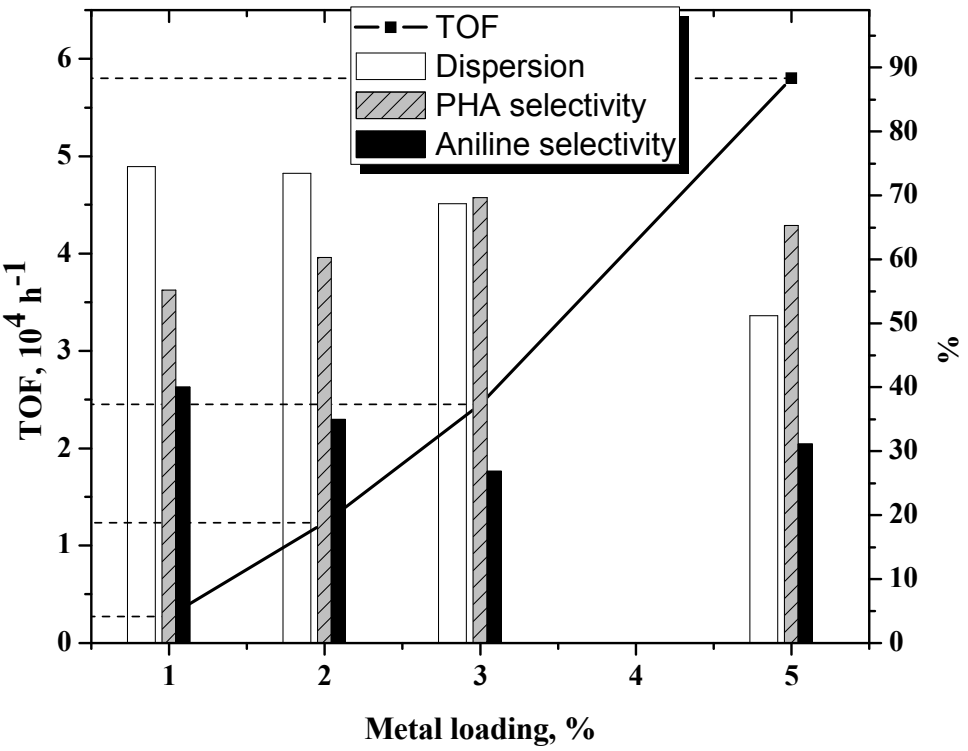

Figure 5.16. Effect of metal loading on PHA selectivity, dispersion and TOF

Reaction conditions**:** nitrobenzene,0.0813 mol; temperature, 303 K; hydrogen pressure, 0.69 MPa; Pt/C, 0.035 g; acid,10 g; water, 84 g; agitation speed, 1000 rpm.

Metal loading influences the metal dispersion on the support (carbon in this case), hence the catalysts with varying Pt loading in this work, were characterized by pulse titration method. This method involves the adsorption of the H_2 gas (used as titrate gas) on the surface of metal atom. As can be seen from Figure 5.16, the highest (74%) metal dispersion was obtained for 1% Pt loading which started decreasing gradually to 69% with increase in metal loading from 1 to 3%, further metal dispersion substantially decreased to 51% for the higher Pt loading, 5%. X-ray diffraction study for 1 to 5% Pt/C catalyst showed particle size increases from 8.6 to 13 nm with increasing metal loading.

The reason for decrease in dispersion is due to increase in particle size of Pt with increase in metal loading.

5.3.2.8. Effect of catalyst loading:

Effect of catalyst loading on selectivity to PHA was studied in the rage of 0.02 g to 0.105 g by keeping other reaction parameters constant for 3% Pt/C catalyst and the results are shown in Figure 5.17. It was found that at lower catalyst loading (0.02 g) the selectivity towards the PHA was 72% and as catalyst loading increased from 0.035 to 0.105 the selectivity towards PHA decreased from 70 to 60%.

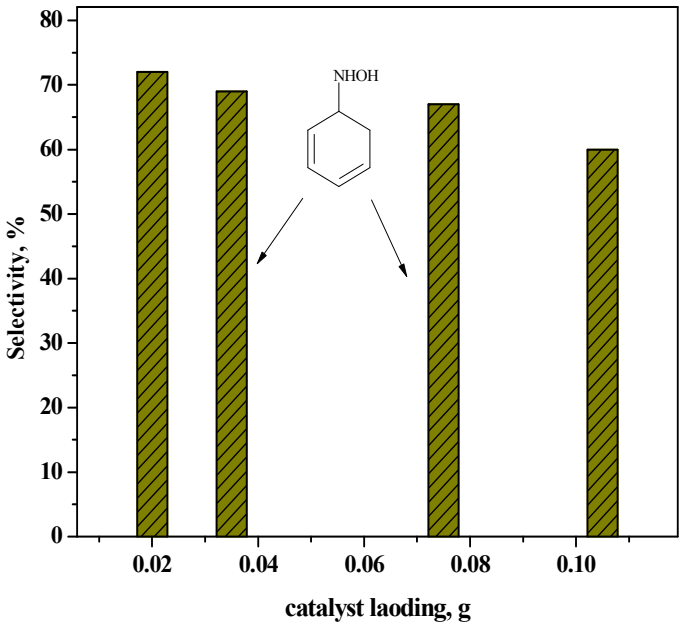

Figure 5.17. Effect of catalyst loading on PHA selectivity

Reaction conditions: nitrobenzene,0.0813 mol; temperature, 303 K; catalyst.3% Pt/C; hydrogen pressure, 0.69 MPa; acid,10 g;water,84 g; agitation speed, 1000 rpm;

5.3.3. Single step synthesis of *p*-aminophenol from nitrobenzene:

This is a commercially practiced process for PAP, in which insitu rearrangement of PHA takesplace since the hydrogenation is carried out in presence of a mineral acid at an uniform temperature of 358 K.

Some initial experiments on single step preparation of *p*-aminophenol via hydrogenation of nitrobenzene showed that the material balance of reactants (H_2 and nitrobenzene) consumed and product (PAP *[2 mol of H_2]* + aniline *[3 mol of H_2]*) formed agreed to the extent of 97-98% as per the stoichiometry shown in Scheme 5.8. It was also observed that the reaction in absence of acid gives only aniline as a major product. Further work on the effect of various process parameters were studied over 3% Pt/C catalyst in the presence of aqueous sulfuric acid at 353 K and 2.41 MPa hydrogen pressure. In each experiment, almost complete conversion of nitrobenzene was observed. After completion of reaction, the product was recovered by the following work procedure.

- The resultant reaction crude product was removed from the autoclave and the solid catalyst was separated by filtration in hot condition
- The pH of the filtrate was adjusted to 4 by addition of aqueous ammonia to remove the aniline from the reaction crude.
- After attaining the pH 4, the filtrate was extracted with toluene (30mL) two to three times to remove the byproduct aniline and traces of any unconverted nitrobenzene.
- The pH of the aqueous layer after extraction was adjusted to 8 by the addition of aqueous ammonia leading to the complete precipitation of solid PAP.
- The solid PAP was filtered under vacuum and washed with toluene and distilled water twice, vacuum-dried and weighed.

This process was developed at NCL and the effect of some of the process parameters as well as kinetics was well studied in our group previously. These results have been already published [26, 54-56]. However, in continuation of our efforts to improve this

process further, the study of some parameters, critical from scale up point of view was under taken and these results are summarized below.

5.3.3.1. Effect of metal loading:

Effect of metal loading on TOF and isolated yields of PAP and aniline was carried out by varying the metal loading in a range of 1 to 5% and by keeping other conditions constant : nitrobenzene concentration of 0.1951 mol; acid 13 g; hydrogen pressure of 2.41 MPa, and temperature of 353 K and the results are shown in Figure 5.18. For all metal loadings almost complete conversion of nitrobenzene was observed. While isolated yield of PAP increased from 37 to 56% with increase in metal loading from 1 to 3%, at higher metal loading of 5%, isolated yield of PAP showed a marginal increase to 57%. It was also observed that as metal loading was increased from 1 to 5%, the catalyst activity (TOF) also increased linearly from 0.4141 to 13.93 x 10^4 h^{-1} upto 3% metal loading beyond which it remained almost constant.

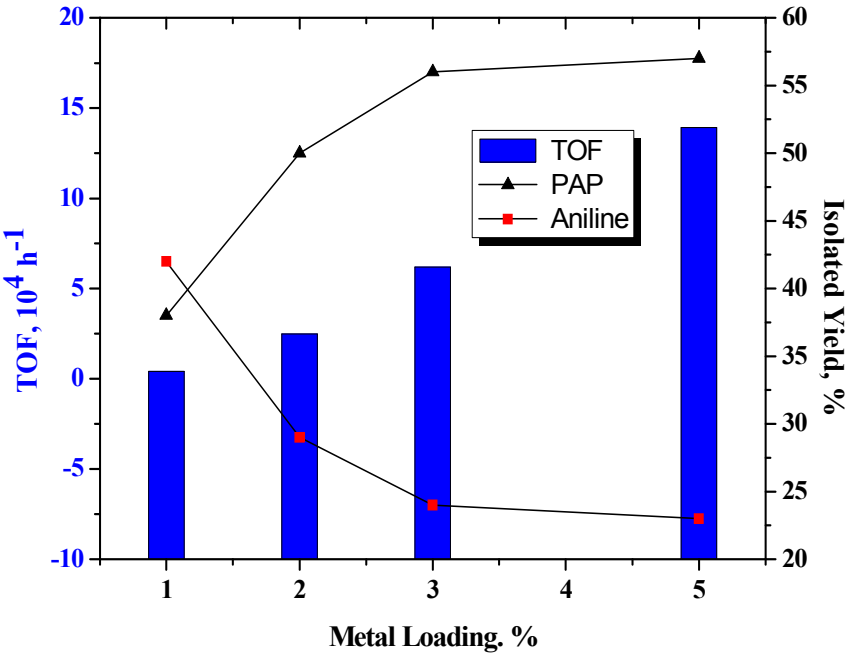

Figure 5.18. Effect of metal loading on PAP selectivity

Reaction conditions: nitrobenzene,0.1950 mol; temperature, 353 K; hydrogen pressure; 2.41 MPa; acid,13 g; water,71 g; agitation speed, 1000 rpm.

5.3.3.2. Effect of acid concentration:

Effect of acid concentration on isolated yield of PAP and aniline was carried out by varying the acid concentration from 12 to 22 g while keeping the other reaction conditions constant and the results are shown in Figure 5.19. Increase in acid concentration from 12 to 22 g leads to substantial increase in PAP isolated yield from 51 to 63%, with simultaneous decrease in aniline yield.

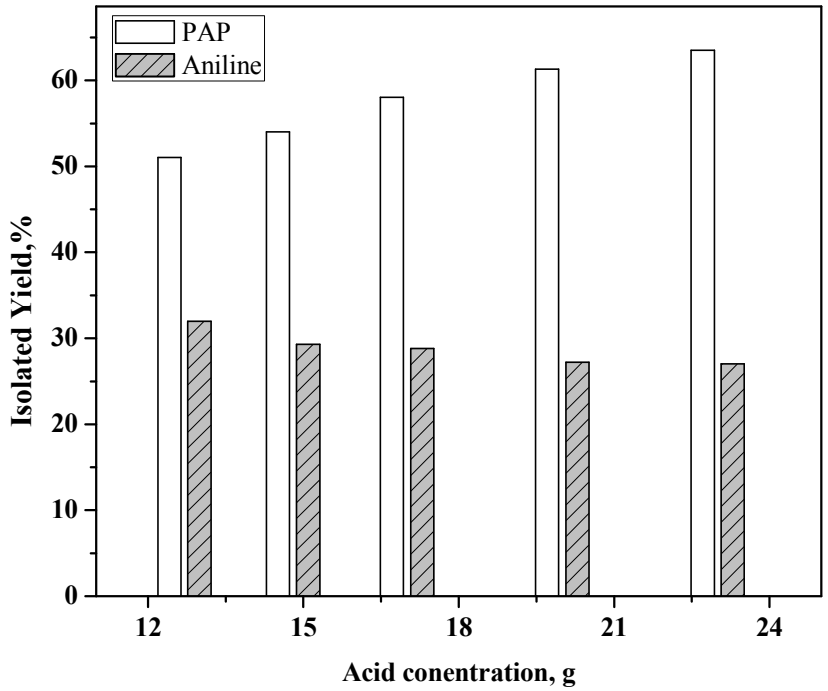

Figure 5.19. Effect of acid concentration

Reaction conditions: nitrobenzene, 0.1950 mol; temperature, 353 K; hydrogen pressure; 2.41 MPa water, 71 g; 3% Pt/C: 0.035 g; agitation speed, 1000 rpm.

5.3.3.3. Improved modified procedure for recovery of PAP:

In order to improve the recovery of PAP in hand, the work up procedure was modified which involved a single step neutralization procedure. The modified work up procedure is given below (Figure 5.20).

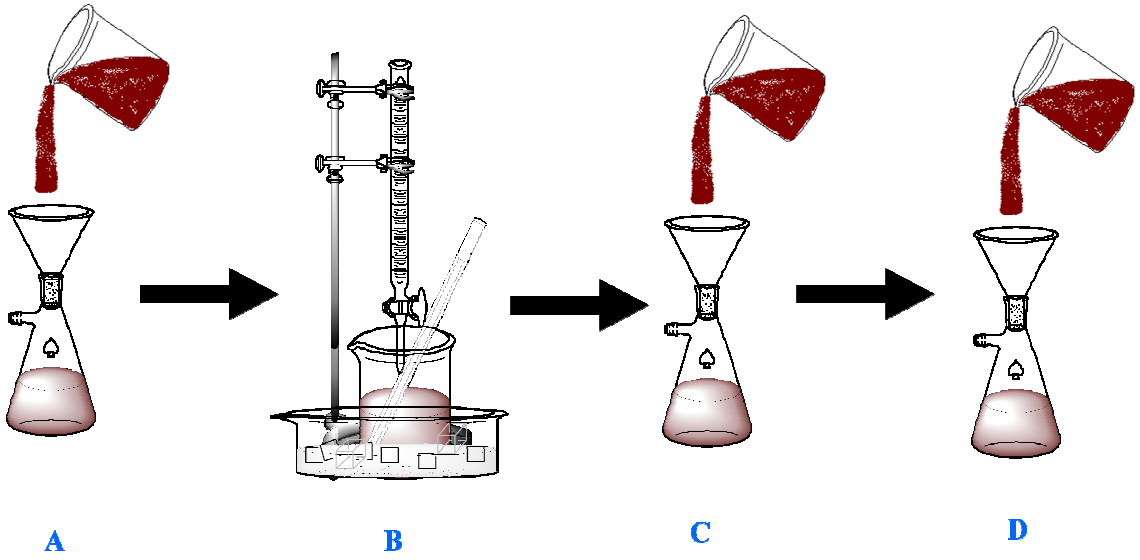

Figure 5.20. Imporved process for PAP

- After separation of the solid catalyst by filtration under vacuum, the resultant filtrate **(A)** was kept in an ice bath and allowed to cool to 5-8 ^{o}C, which was then neutralized by slow addition of ammonia up to pH 8 by maintaining the temperature of 5-8^{o}C **(B)**. Formation of the solid PAP was observed during the neutralization.

- The solid cake of crude PAP was filtered **(C)** under vacuum and washed with cold toluene (3 x 30 mL) to remove aniline adhering to the solid PAP **(D)**, further the solid PAP was vacuum dried and weighed.

The lower temperature and single step neutralizing procedure favors the formation of precipitation and decrease the solubility of PAP in the aqueous layer, which leads to increase the isolated yield.

In all the experiments carried out to study the effect of process parameters, the modified single step neutralization work up procedure was followed and the results are discussed below.

5.3.3.4. Effect of catalyst loading:

The effect of catalyst loading of 3% Pt/C on nitrobenzene conversion and PAP isolated yield is shown in Figure 5.21 by keeping other conditions constant: acid concentration, substrate concentration, temperature and hydrogen pressure. It was observed that with increase in catalyst loading from 0.035 g to 0.048 g, the isolated yield of PAP also increased from 68.5 to 73.5%. However with further increase in catalyst loading to 0.052 g, the isolated yield of PAP decreased to 72.5%. This was because an increase in metal concentration led to further hydrogenation of PHA to aniline.

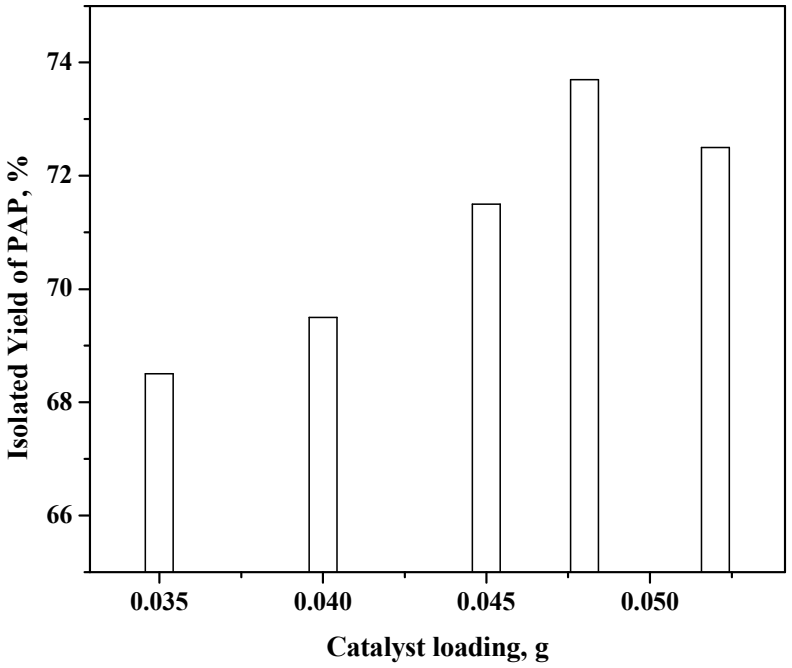

Figure 5.21. Effect of catalyst loading

Reaction conditions: nitrobenzene, 0.1950 mol; temperature, 353 K; hydrogen pressure; 2.41 MPa; acid, 22 g; water,60 g; catalyst, 3% Pt/C; agitation speed, 1000 rpm;

5.3.3.5. Effect of acid concentration:

The effect of acid concentration on isolated yield of PAP was studied using 3% Pt/C catalyst at constant catalyst loading, substrate concentration, temperature and pressure conditions and the results are shown in Figure 5.22. The increase in acid concentration from 13 % to 22% leads to increase in isolated yield of PAP from 68.5 to 73.5%. The results on the effect of acid concentration on PAP yield using the two step neutralization procedure (section 5.3.3.2, Figure 5.19) is also shown in Figure 5.22. This comparison showed that new modified procedure gave 5-10% enhancement in the isolated yield of PAP.

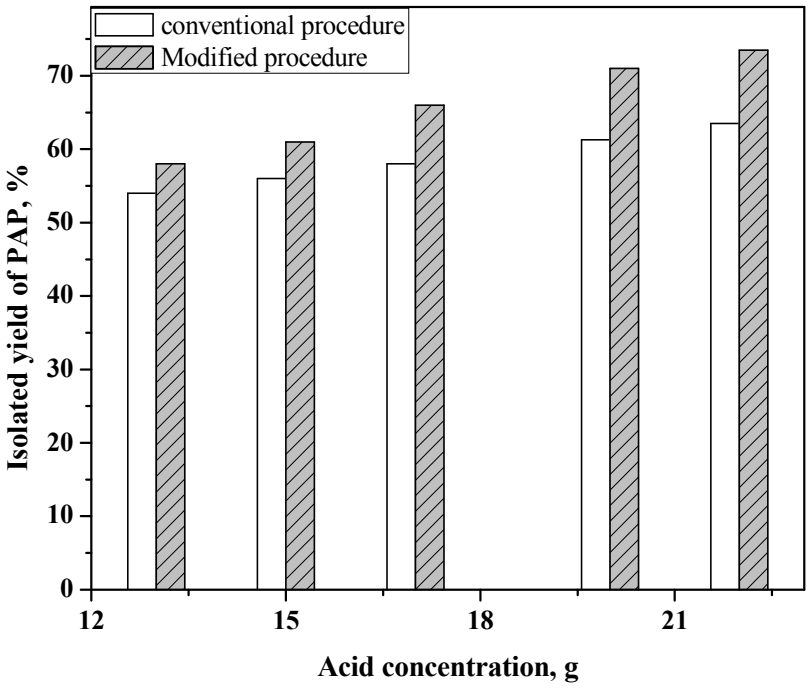

Figure 5.22. Effect of acid concentration

Reaction conditions: nitrobenzene, 0.1950 mol; temperature, 353 K; hydrogen pressure, 2.41 MPa; water, 60 g; 3% Pt/C: 0.048 g; agitation speed, 1000 rpm.

5.3.3.6. Aqueous layer recycle:

In another attempt to increase the recovery of PAP in hand, several runs were conducted where the aqueous layer obtained after the work up of reaction crude was recycled back to the hydrogenation reactor and fresh make up acid was added to maintain the initial pH = 2. These results are presented in Table 5.4. This strategy was found to enhance the PAP recovery from 73 to 77% (Table 5.4), since PAP remaining in the dissolved form in aqueous reaction crude gets recovered in the subsequent recycle of the aqueous layer.

Table 5.4. Effect of aqueous layer recycle

Sr. No.	Charge in gm		Conversion, %	Isolated yield, %	
	Acid	**water**		**PAP**	**Aniline**
1	22	60	100	73.5	25.5
2	22	60 [aq.1]	100	76.2	23
3	22	60 [aq.2]	100	77.2	22.7
Reaction conditions: nitrobenzene, 0.1950 mol; temperature, 353 k; hydrogen pressure, 2.41 MPa; 3% Pt/C- 0.048 g; agitation speed, 1000 rpm.					

5.3.3.7. Purification of p-aminophenol :

The crude PAP obtained after precipitation was almost black in color hence, the purification of PAP was carried out by using activated charcoal treatment. For this purpose, 5 g solid PAP was heated at 358-363 K in 50 ml of distilled water until it dissolved completely . Then 0.250 g activated charcoal was added slowly under stirring kept it for 10 min and this hot solution was immediately filtered under vacuum. The faint brown colored PAP crystallized out from the clear filtrate kept at room temperature. The changes in color of crude and crystallize PAP are shown in Figure 5.23.

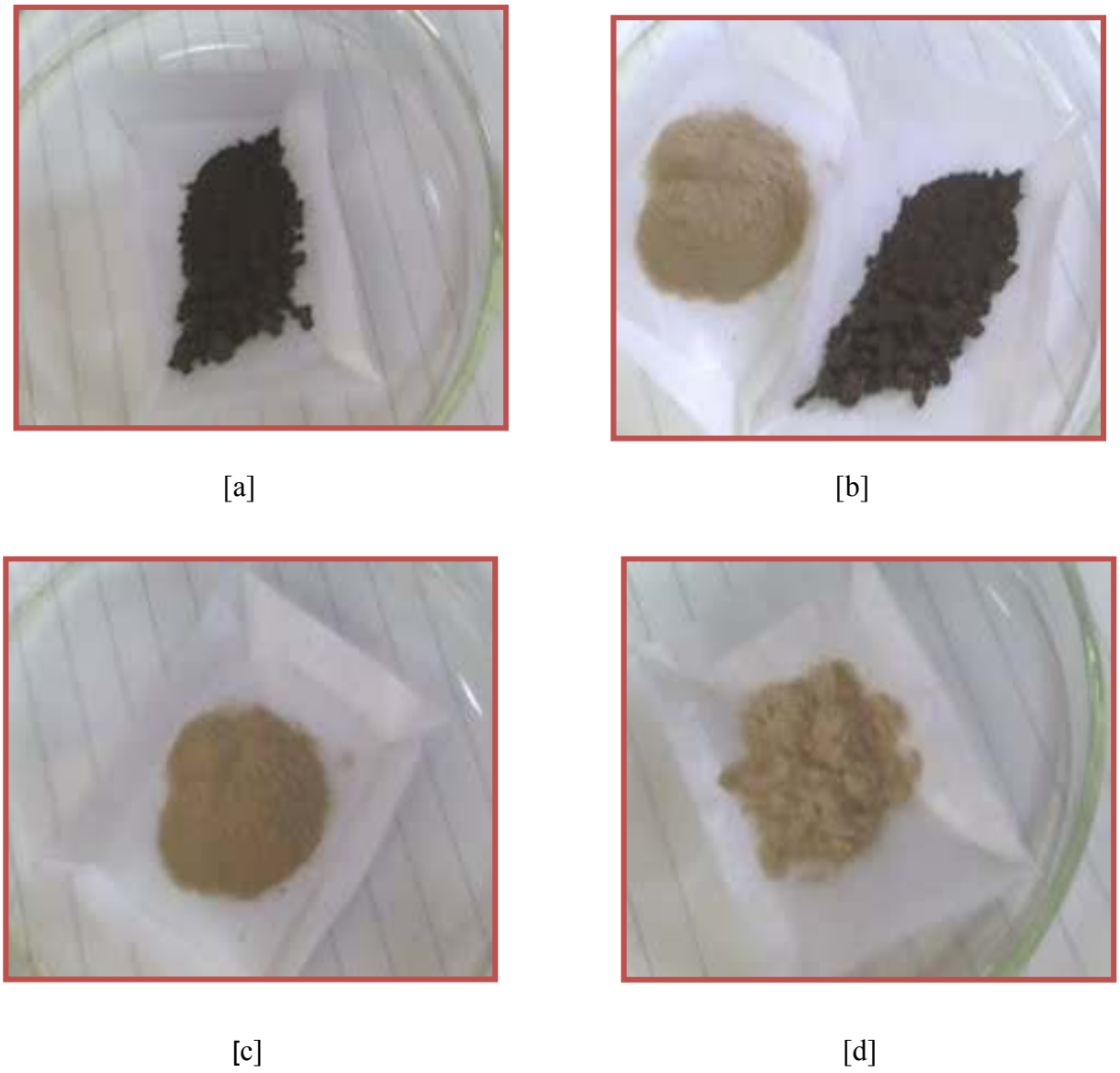

[a] [b]

[c] [d]

Figure 5.23. (a) solid crude PAP; (b) crude PAP and charcoal treated PAP; (c) & (d) purified PAP.

5.3.3.8: Path forward:

The laboratory scale demonstration runs were given to the client by utilizing new improved modified process, based on which the pilot plant (approximately 100 kg of PAP per day) has been commissioned at the clients site. These demonstration runs reconfirmed the performance of our bench scale process and the material balance of reactants consumed and the products formed. The photographs of the PAP pilot plant are

shown below. Based on pilot plant trials, a commercial plant of 30,000 tpa PAP is being planned by the client.

PAP pilot plant photo:

PAP pilot plant

Continuous high pressure hastalloy lined reactor

5.4. Conclusion:

p-Aminophenol via catalytic hydrogenation of nitrobenzene was studied involving first the hydrogenation of nitrobenzene to an intermediate PHA at 303 K followed by its rearrangement at elevated temperature of 353 K. Aqueous acid medium is essential for the first hydrogenation step however; increase in temperature from 303 K to 353 K initiates the rearrangement of PHA to PAP. Initially, selectivity to PHA was as high as 95% at 36% conversion of nitrobenzene, which then decreased to 75% for complete conversion of nitrobenzene due to aniline formation. Increase in H_2 pressure also had a dramatic effect in lowering the PHA selectivity due to availability of higher concentration of surface hydrogen causing the further hydrogenation of PHA to aniline. Rearrangement of PHA in an inert atmosphere (argon) gave a higher selectivity (77%) to PAP as compared to the rearrangement carried out under hydrogen atmosphere. TOF was increase from 0.27 to 5.8 x 10^3 h^{-1} and dispersion of Pt decreased from 74 to 51% with increase in metal loading 1 to 5%. The selectivity to PHA decreased from 72 to 60% with increase in catalyst loading from 0.02 to 0.105 g.

In case of direct hydrogenation of nitrobenzene to PAP, with new improved work up procedure, we found that the following process variations have considerably increased the selectivity and yield of PAP. i) increase in catalyst loading gives higher hydrogenation rate and higher selectivity to *p*-aminophenol. ii) the appropriate concentration of acid (~ 10%) has increased the selectivity to PAP. iii) One step neutralization process at lower temperature and iv) recycle of the aqueous layer enhances the PAP recovery in hand. The new strategy developed for workup of the reaction crude showed > 90% recovery of all the reaction products from the reaction crude. Based on NCL process, commercialization of the PAP process (30,000 tpa) in envisaged by end 2012.

5.5. References:

1. *Kirk-Othmer* e*ncyclopedia of chemical technology* 4th edition, Wiley Interscience Vol. 2 (1995).
2. S. Mitchell, R. Waring in *Ullamann's encyclopedia of industrial chemistry*, 5th edition VCH, Weinheim, A2 (1985).
3. T. J. Dunn *US Pat. 4264529* (1981).
4. D. Caskey, D. Chapmann *US Pat. 4571437* (1986).
5. S. S. Sathe *US Pat. 4176138* (1979).
6. N. Noel, P. N. Anatharama, H. V. K. Udupa *J. Appl. Electrochem*. 12 (1982) 291.
7. K. S. Upuda, G. S. Subramanian, H. V. K. Udupa *Trans. Soc. Adv. Electrochem. Sci. Technol.* 7 (1972) 49.
8. Q. Gao, S. Chen *Huaxue Shijie* 35 (1994) 432.
9. T. Komiyama, T. Kazuhiro *JP Pat 54036200* (1979).
10. K. Watabe, Y. Naganuma, S. Tokumoto, E. Sugyama *JP Pat 3127761* (1991)
11. F. Bean, S. Thomas *US Pat. 2376112* (1945).
12. K. Hideki, C. Hiroyuki, O. Yurie *US Pat 5847231* (1998).
13. R. A. Sheldon (Ed) in *Fine chemicals though heterogeneous catalysis*, Weinheim, Wiley-VCH (2001).
14. A. A. Vogel in *Textbook of practical organic chemistry*, 4th edition, ELBS, Longmann, London, (1978) pp. 657.
15. E. Bamberger *Ber.* 27 (1894) 1347.
16. E. Bamberger *Ber.* 27 (1894) 1548.
17. E. Bamberger *Ber*. 33 (1900) 3600.
18. H. Shine in *Aromatic rearrangements,* Elsevier, Amsterdam (1967) pp 129.
19. J. March in *Advanced Organic chemistry: Reaction mechanisms and structures*, Wiley Publications, 4th edition (1991) pp 674.
20. T. Sone, K. Hamamoto, Y. Seiji, S. Shinkai, O Manabe *J. Chem. Soc. Perkin II* (1981) 1596.
21. F. Bassford *US Pat. 2132454* (1938).
22. O. Kamm, C. S. Marvel *Org. Synth. Coll. Vol. 1* (1941) 445.
23. S. Li, Z. Ximin, S. Baoqui *CN Pat. 1087623.*

24. C. O. Henke, J. V. Vaughen *US Pat. 2198249* (1940).
25. R. G. Benner *US Pat. 3383416* (1968).
26. N. Greco *US Pat. 3953509* (1976).
27. C. V. Rode, M. J. Vaidya, R. V. Chaudhari *US Pat. 6403833* (2002)
28. E. Medcalf *US Pat. 4051187* (1977).
29. T. Juang, J. Hwang, H. Ho, C. Chen, J. Chin *Chem. Soc*. 35 (1988) 135.
30. R. Jocquot, C. Mercier *EP Pat. 536070* (1993).
31. Y. Gao, F. Wang, S. Liao, D. Yu *React. Kinet. Catal. Lett*. 64 (1998) 351.
32. X. Chen, Y. Liu *CN Pat. 85103667* (1986).
33. T. Komatsu, T. Hirose *Appl. Catal. A: General* 276 (2004) 95.
34. D. C. Miller *US Pat 5312991* (1994).
35. Y. Gao, F. Wang, S. Liao, D. Yu *React. Kinet. Catal. Lett*. 64 (1998) 351.
36. Y. Wang, Y. Cui, X. Zhao *CN Pat. 101391227* (2009).
37. F. Bean *US Pat. 2446519* (1948).
38. P. Rylander, I. Karpenko G. Pond *US Pat. 3715397* (1973).
39. R. V. Chaudhari, S. S. Divekar, M. J. Vaidya, C. V. Rode *US Pat. 6028227* (2000).
40. L. Spigler, N. Woodbury *US Pat. 2765342* (1956).
41. L. Spigler, N. Woodbury *GB Pat. 713622* (1954).
42. B. Brown, A. Fredrick *US Pat 3535382* (1970).
43. A. Tamaoki, K, Yamamoto, K. Kuroda *JP Pat. 54066632* (1979).
44. E. Derrenbacker *US Pat. 4307249* (1981).
45. E. Medcalf *US Pat. 4051187* (1977).
46. L. Lee, M. Chen, C. Yao *US Pat. 4885389* (1989).
47. T. Juang, J. Hwang, H. Ho, C. Chen, J. Chin *Chem. Soc*. 35 (1988) 135.
48. S. Li, Z. Ximin, S. Baoqui *CN Pat. 1087623.*
49. W. Ahn, K. Min, Y. Chung, H. Rhee, S. Joo, R. Ryoo *Stud. Surf. Sci. Catal.* 135 (2001) 4710.
50. K. Min, J. Choi, Y. Chung, W. Ahn, R. Ryoo, P. Lim *Appl. Catal. A: General* 337 (2008) 97.
51. K. JeevaRatnam, R. SudarshanReddy, N. S. Sekhar, M. LakshmiKantam, A. Deshpande, F. Figueras *Appl. Catal. A :General* 348 (2008) 26.

52. S. Wang, Y. Ma, Y. Wang, W. Xue, X. Zhao *J. Chem. Technol. Biotechnol.* 83 (2008) 1466.
53. S. K. Tanielyan, J. J. Nair, N. Marin, G. Alvez, R. J. McNair, D. Wang, R. L. Augustine *Org. Proc. Res. Dev.* 11 (2007) 681.
54. C. V. Rode, M. J. Vaidya, R. V. Chaudhari *Org. Proc. Res. Dev.* 3 (1999) 465.
55. C. V. Rode, M. J. Vaidya, R. Jaganathan, R. V. Chaudhari *Chem. Eng. Sci.* 56 (2001) 1299.
56. R. V. Chaudhari, S. S. Divekar, M. J. Vaidya, C. V. Rode *US Pat. 6028227* (2000).
57. Y. Gao, F. Wang, S. Liao, D. Yu *React. Kinet. Catal. Lett*. 64 (1998) 351.
58. Y. Wang, Y. Cui, X. Zhao *CN Pat. 101391227* (2009).
59. T. Komatsu, T. Hirose *Appl. Catal. A: General* 276 (2004) 95.
60. P. Ubilla, R. García, J.L.G. Fierro, N. Escalona. *J. Chil. Chem. Soc.* 55 (2010) 35.
61. X, Xue.; C, Liu.; T, Lu.; W, Xing *J. Fuel Cells* 06 (2006) 347.
62. T. Yogo, H. Suzuki, H. Iwahara, S. Naka, S. Hirano *J. Mater. Sci*. 26 (1991) 1363.
63. E. Antolini, F. Cardellini, E. Giacometti, G. Squadrito *J. Mater. Sci*. 37 (2002) 133.
64. H. Lieske, G. Lietz, H. Spindler, J. Volter *J. Catal*. 81 (1983) 8.
65. P. K. Cheekatamarla, A. M. Lane *Prepr. Pap. Am. Chem. Soc. Div. Fuel Chem*. 49 (2004) 139.
66. J. Kim, H. Ahn *Appl. Catal. B: Environ*. 91 (2009) 308.
67. K. S. Kim, N, Winograd, R. E. Davis *J. Am. Chem. Soc.* 93 (1971) 6296.
68. P. J. M. Dijkraaf, H. A. M. Duisters, B. F. M. Kuster, K. van der Wiele *J. Catal.* 112 (1988) 337.
69. J. Wang, G. Yin, Y. Shao, S. Zhang, Z. Wang, Y. Gao. *J. Power Sources.* 171 (2007) 331.

Chapter VI

Hydrogenation of

m-chloronitrobenzene to *m*-chloroaniline

6.1. Introduction:

Selective hydrogenation of chloronitroaromatics give the corresponding haloanilines having wide range applications in dye industries, for the manufacture of substituted phenyl carbamates [1], drugs, herbicides, pesticides, polyanilines [2, 3], and other specialty chemicals [4-6]. Traditionally, haloanilines were synthesized by the reduction of corresponding chlronitroaromatics using Fe/HCl (Bechamp Process) or sulfide reduction method. These processes are no longer feasible due to formation of large amounts of toxic wastes, posing serious disposal problems [7]. Details of Bechamp process is discussed in chapter V, under section 5.3. Haloamines are now synthesized by liquid phase catalytic hydrogenation of corresponding chlronitroaromatics [8-19]. Major drawback of this process is formation of acid due to the dehalogenation reaction. Hence, selective hydrogenation of nitro- to amine without dehalogenation is a challenging task in the hydrogenation of halonitroaromatics. Since, this is a seminal process from both fundamental as well as industrial point of view, we have studied the liquid phase catalytic hydrogenation of *m*-chloronitrobenzene in detail.

Hydrogenation of *m*-chloronitrobenzene (*m*-CNB) to *m*-chloroaniline (*m*-CAN) involves two main reaction path ways giving rise to formation of several by products as shown in Scheme 6.1. According to the pathway A (Scheme 6.1), the hydrogenation of *m*-CNB proceeds via intermediates, *m*-nitrosochlorobenzene and *m*-(chlorophenyl)-hydroxylamine to give the desired product *m*-CAN. However, nitroso, and hydroxylamine being very reactive intermediates, can give rise to the formation of side products such as 3,3'-dichloroazobenzene (DAB) and 3,3'-dichlorohydrazobenzene (DHAB), which also subsequently undergo hydrogenation to give *m*-CAN, normally formed in basic medium. The competing pathway B, involves first the dehalogenation step to give nitrobenzene (NB) and then aniline via a nitrosobenzene intermediates. The formation of acid during dehalogenation steps either via pathway A or B, is detrimental since it deactivates the catalysts as well as produces undesired side product to a substantial extent. Further hydrogenation of *m*-CAN leads to formation of aniline and chlorobenzene along with formation of acids, (shown in red in Scheme 6.1), causing lowering yields of the desired product (*m*-CAN).

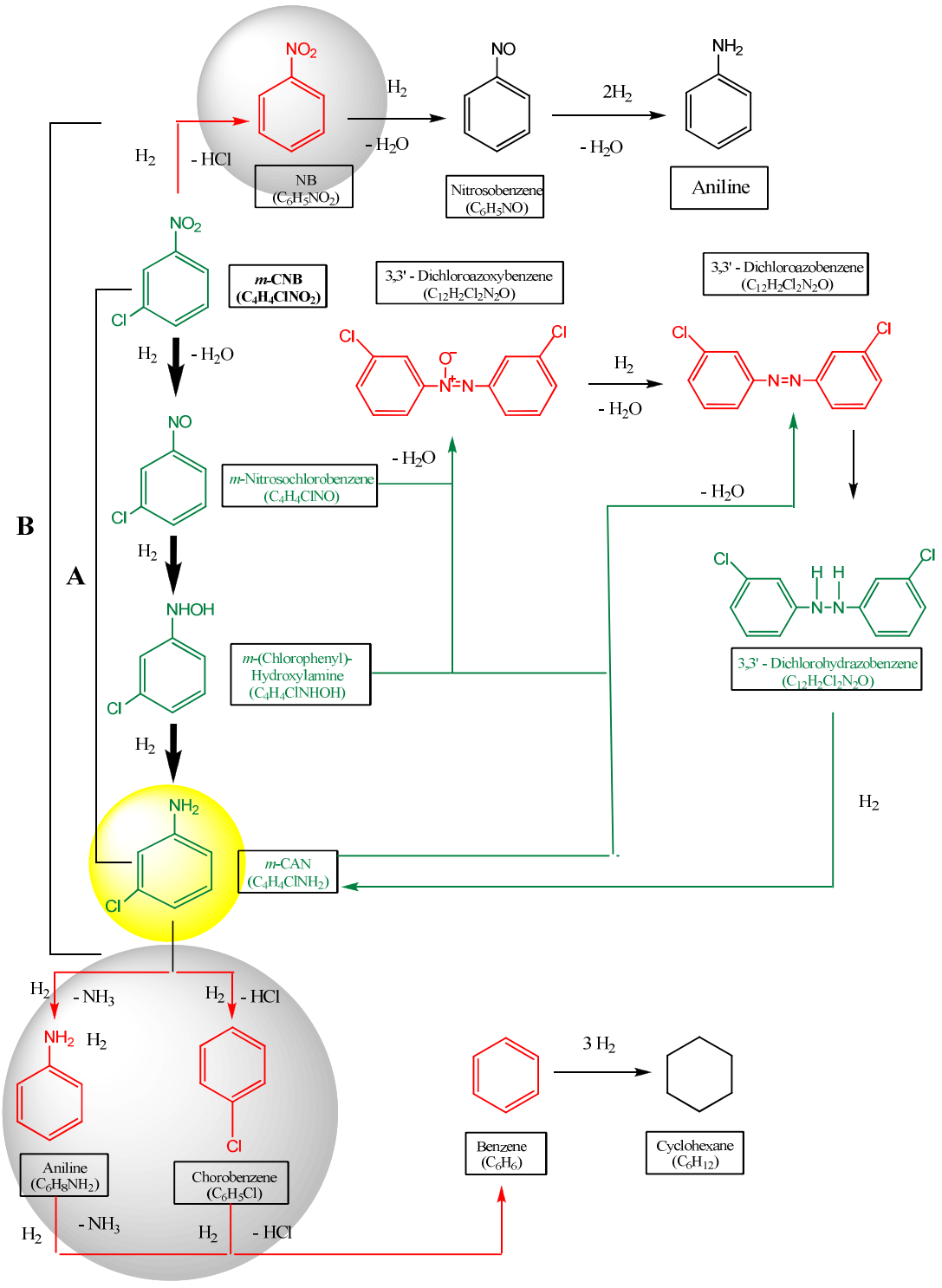

Scheme 6.1. Reaction pathway for hydrogenation of *m*-CNB to *m*-CAN [20-22]

Azoxy- and azo- benzene are highly toxic, hence their formation must be avoided or at least minimized by a suitable choice of catalyst and reaction conditions. The desired pathway is shown in green, which contributes to the highest productivity of *m*-CAN.

6.1.1. Literature survey:

A summary of literature on hydrogenation of *m*-CNB to *m*-CAN is shown in Table 6.1. Several catalyst systems involving monometallic Ni catalyst [8, 23-27], Pd [27-29], Pt and modified Pt [12-14, 19, 27, 30, 31], and bimetallic catalysts have been reported for the hydrogenation of *m*-CNB to *m*-CAN [8, 14, 32-35]. Polymer (PVP) protected $PdCl_2$, $FeCl_3$, $Co(Ac)_2$, $NiCl_2$, $RhCl_3$ and $RuCl_3$ and their bimetallic catalyst systems were reported by Yu et al. in which the formation of aniline was also observed due to the competing dechlorination reaction[32]. It was found that the bimetallic PVP-$PdCl_2$-$2RuCl_3$ catalyst showed 97% conversion with 95% selectivity to CAN [32]. Interestingly, the addition of sodium acetate to this system increased the catalytic activity by 40 times [32]. Palladium metal supported on anionic polymer (D) and carbon has been studied by Kratky et al. He found that the Pd/D catalyst showed more activity and selectivity (93%) towards *m*-CAN then Pd/C catalyst[36].

During the course of reaction, the support might be attacked by hydrochloric acid formed in the reaction, causing surface modification and/or structural deformation of the catalyst. Among these metals, Pt is the first choice for hydrogenation of C-Cl due to its better activity, selectivity and stability than other metals [37]. To minimize the deactivation of catalyst, various types of supports also have been investigated for hydrogenation of *m*-CNB. Ma et al. prepared the novel supports for this hydrogenation reaction i.e. platinum supported on HCl-acidified attapulgite catalyst which showed very high activity and selectivity (> 99%) [38]. Han et al. studied Pt supported on series of oxides (Al_2O_3, TiO_2, ZrO_2), in which Pt/TiO_2 showed the higher activity and selectivity towards CAN due to strong metal/support interactions [31]. A comparative study of various supports such as TiO_2, SiO_2 and carbon showed that Pt/C gave the highest conversion (99%) and selectivity (96%) to CAN [30]. Nomura reported the selective catalytic reduction of nitro compounds using ruthenuim-carbonyl complexes under supercritical CO_2/H_2O conditions. He achieved high activity and > 99 % yield towards the haloanilines as a product [39]. Greenfield and Dovell prepared a series of selectively sulfur poisoned carbon supported catalyst systems such as Pt, Pd, Co, Rh and Ru for minimizing the

reductive dehalogenation. In this work, complete selectivity to the haloamines was achieved using Pt-S/C catalyst [40]. The kinetic studies of the selective hydrogenation of CNB to CAN in a stirred reactor over temperature range of 313-363 K, using sulfided 1% Pt/C catalyst has been studied by Rode et al. [19].

Kosak studied the effect of various inhibitors as listed in Table 1.1 for the selective hydrogenation of halonitrobenzene to haloamines [27]. It can be seen from this Table that Pt-morpholine catalyst system showed the best results because morpholine acts as an inorganic acid acceptor to control the amount of carbon-halogen cleavage [27]. In this hydrogenation reaction morpholine acts (i) as a true suppressor to inhibit the dehalogenation reaction and (ii) as an acid acceptor when some dehalogenation occurs. He also studied various metal oxide systems, among which magnesium oxide acts only as acid acceptor, neutralizing the hydrohalide after dehydrohalogenation [27].

It is clear from the literature that obtaining the highest selectivity to chloroaniline is difficult mainly due to (i) the competing dehydrohalogenation reaction and (ii) catalyst deactivation due to carboneous deposition on the catalyst.\

Table 6.1. Summary literature on hydrogenation of *m*-chloronitrobenzene to *m*-chloroaniline

Sr. No.	Catalyst	Conversion, %	Reaction conditions	Selectivity, %		Ref. No.
				***m*-CAN**	**AN**	
1.	NanoPd/MCM-41	100	T=300 K; P_{H_2}=3 MPa	91	9	41
2.	Pt/CNT, PtM/CNT M=La, Ce, Pr, Nd and Sm	99.7	T=303 K; P_{H_2}=0.1 MPa	98	0.3	42
3	Pt/C, PtM/C M=La, Ce, Pr, Nd and Sm	99.4	T=303K; P_{H_2}=0.1 MPa	95.8	2.2	43
4	Ni/CNFs-EG-160	99	T=413 K; P_{H_2}=2MPa	98	-	36
5	Pt/HCl-acidified attapulgite-	100	T=323 K; P_{H_2}=2 MPa	100	-	38
6.	Pd (II) chelates	100	T=318 K; P_{H_2}=0.1 MPa	90		45
7.	PVP-M- Pt catalyst M=La, Ce, Pr, Nd and Sm	100	T=303 k; P_{H_2}=0.1 MPa; NaOH	97.2	2.1	46
8.	Ionic liquid Trans PtCl2; [BMIM] [BF4]	100	T=383 K; P_{H_2}=2 MPa		0.5	8
9.	Ni/Al_2O_3	100	T=393 K; P_{H_2}=0.1 MPa (gas phase hydrogenation)	100		47
10	Pd/D, Pd/C	100	T=298 K; P_{H_2}=0.5 MPa	100		36
11.	Pt/C	100	T=363K; P_{H_2}=3.45 MPa; Morpholine and	95		35

			other inhibitor		
	Pd/C	100		30	
	Ni/Kieselguhr	100		25	
13.	PVP-Pt	99	T=303; P_{H_2}=0.1 MPa	99	48
14.	Pt/ZrO_2, PtM/ZrO_2, (Sm, Pr, Ce, Nd, and La)	100	T=303; P_{H_2}=0.1 MPa	95	49
15	Ni-M-P (M = Cu, Ca, Zn, Sn, Co)	99		99	50
16.	PtM/TiO_2 M=La, Ce, Pr, Nd and Sm	99	T=303K; P_{H_2}=	96	51
18.	1 % Pt-S/C	100	T=363 K; P_{H_2}=0.1 MPa	99	19
19.	Co/C	97	T=413 K; P_{H_2}=2.0MPa	99	52

Table 6.2. Inhibitors for selective hydrogenation of CNB to CAN [32].

Inhibitors, catalyst	Dechlorination, %
Morpholine, Pt/C	0.5
5% Morpholine Pd/C	~30
25% Morpholine, Pd/C	~30
1% Morpholine Ni/Kieselguhr	>25
N-Methylmorpholine Pt/C	1
N-Ethylmorpholine Pt/C	1.5
3,5-Dimethylmorpholine Pt/C	2.5
Piperazine Pt/C	1
Dimethylformamide, Pt/C	>5.0
Piperidine Pt/C	2
Pt-S_2/C	0.1
Triphenyl phosphite Pt/C	<0.01
Pd-S/C	96
Morpholine Pt/C+Ni(II) + Cr (III)	0.19
$Ca(OH)_2$, Rh/Al_2O_3	?
$Ca(OH)_2$, Raney Ni	?
MgO, Pt/C	0.3

6.1.2. Objectives:

The main objectives of this work were (i) to develop supported mono and bimetallic catalyst systems for selective hydrogenation for *m*-chloronitrobenzene (ii) study of effect of reaction parameters such as effect of substrate concentration, temperature, hydrogen pressure, catalyst loading on conversion of *m*-chloronitrobenzene and selectivity to *m*-chloroaniline. The stability of the catalyst was also studied by catalyst recycle experiments.

6.2. Experimental:

6.2.1. Catalyst preparation:

Details of preparation of 1% Pt/C, 10% Ni supported on carbon and Al_2O_3, and 10% Ni-1% Pt/C catalyst are described in chapter II, section 2.2.

6.2.2.Catalyst Characterization:

The details of catalyst characterization are described in chapter II, section 2.3.

6.2.3. Catalyst activity testing:

The experimental batch setup used for the hydrogenation reaction and experimental procedure is described in chapter II, section 2.4.2.

6.2.4. Analytical methods:

The quantitative analysis of liquid samples was performed by Hewlett-Packard GC model 6890 gas chromatograph equipped with FID. Other details of temperature programming method $(80^oC \rightarrow 5\ \text{min} \xrightarrow{20^oC/\text{min}} 300^oC \rightarrow 5\ \text{min})$ etc. are described in chapter II, section 2.5. Product identification was carried out by using GC and GCMS spectra as shown in Figures 6.1 and 6.2 respectively.

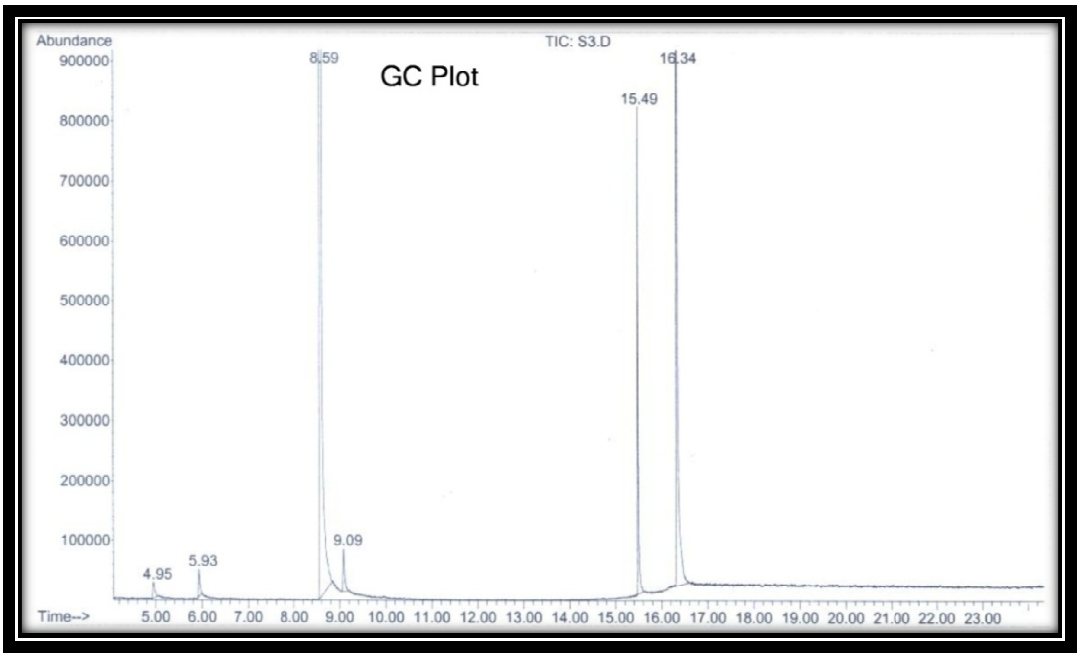

Figure 6.1. Standard gas chromatograph of the reaction crude of hydrogenation of *m*-CNB

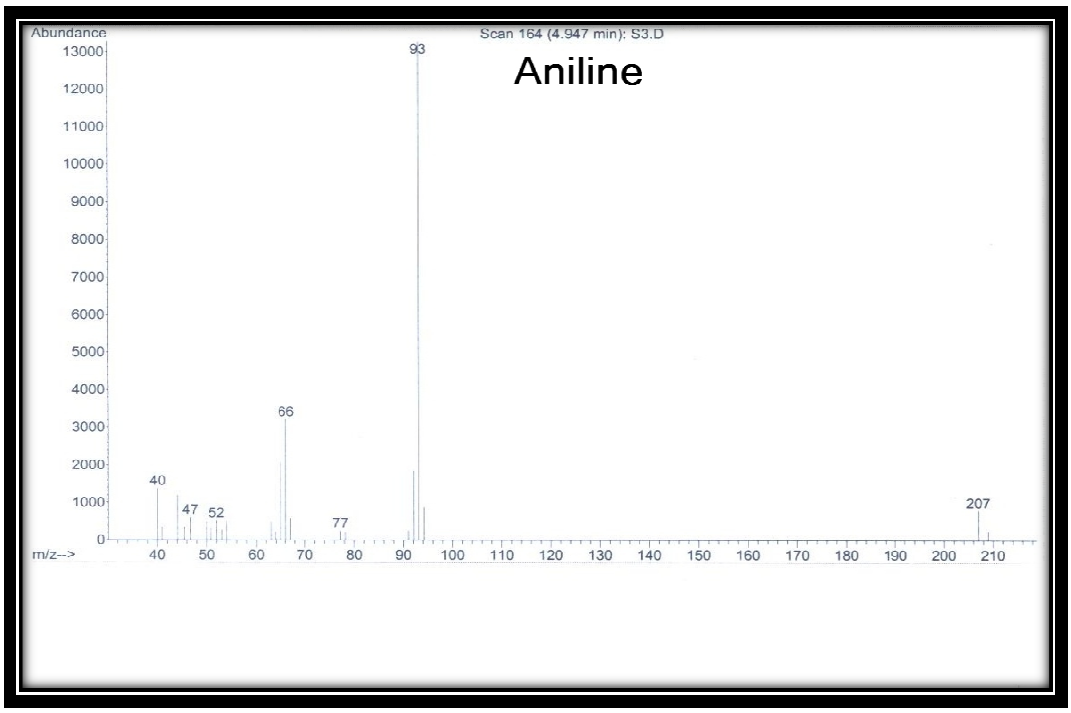

Figure 6.2. (a) GCMS spectra of Aniline

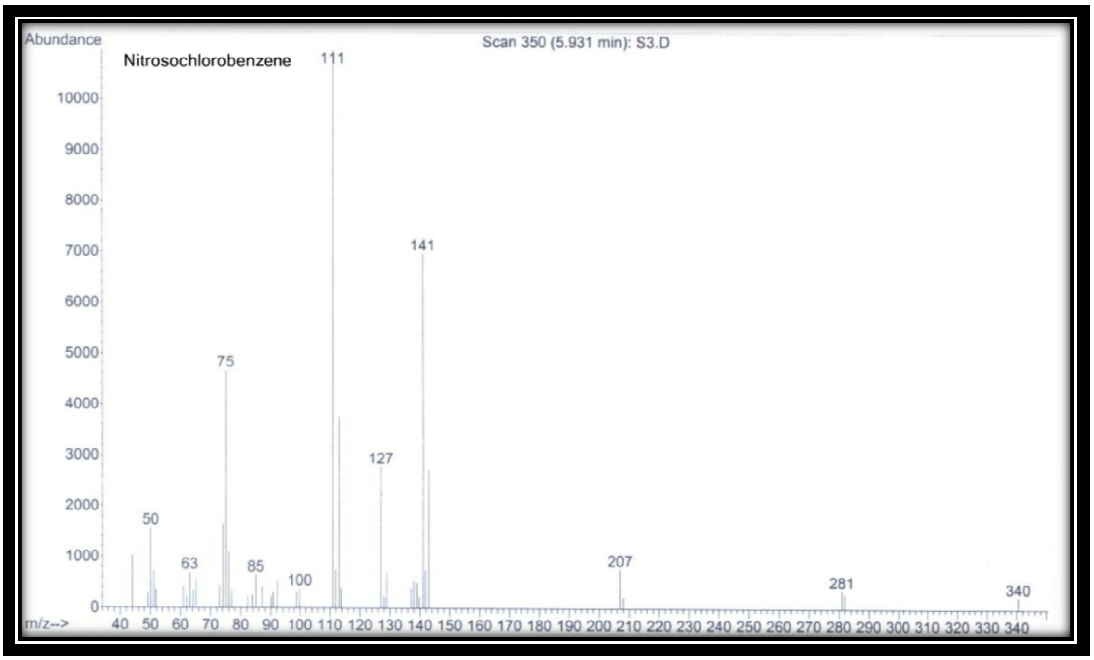

Figure 6.2. (b) GCMS spectra for nitrosochlrobenzene

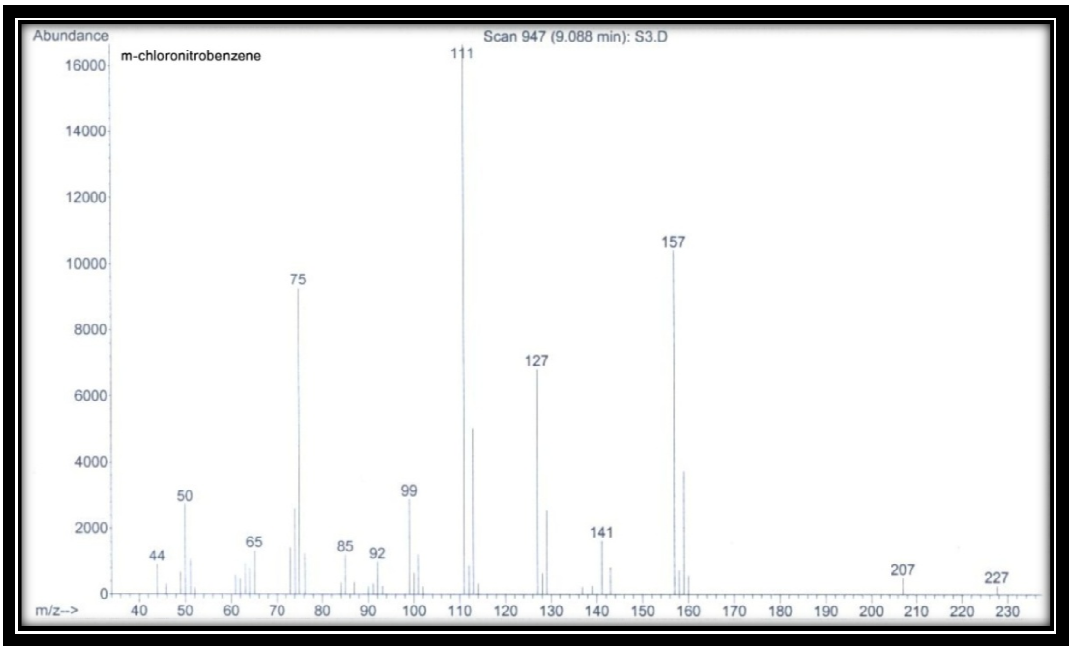

Figure 6.2. (c) GCMS spectra for *m*-chloronitrobenzene

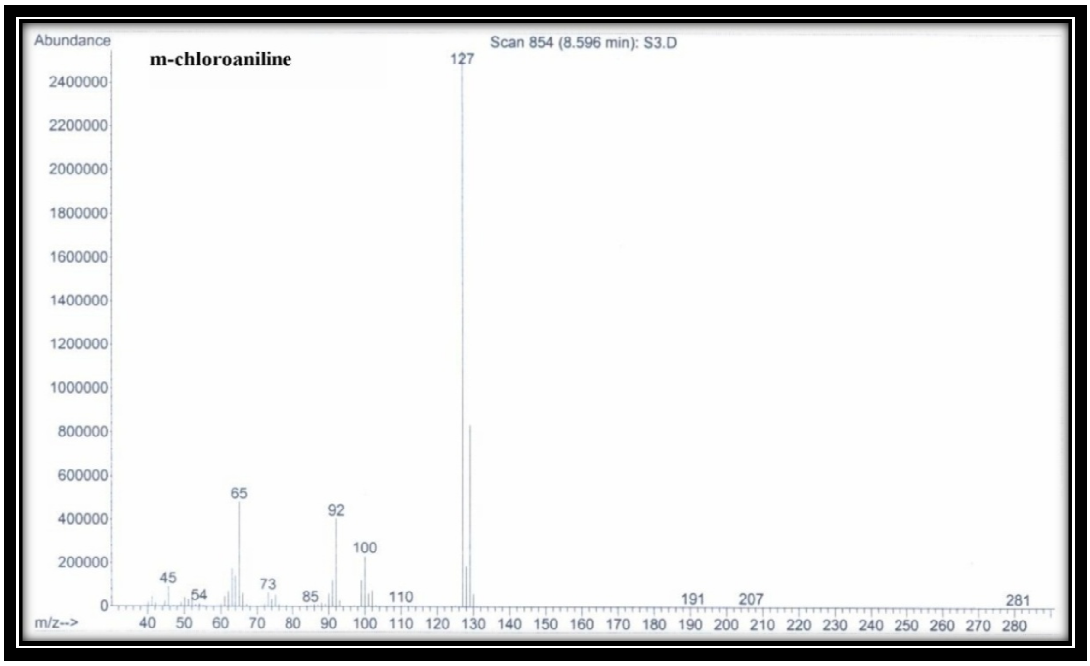

Figure 6.2. (d) GCMS spectra of *m*-chloroaniline

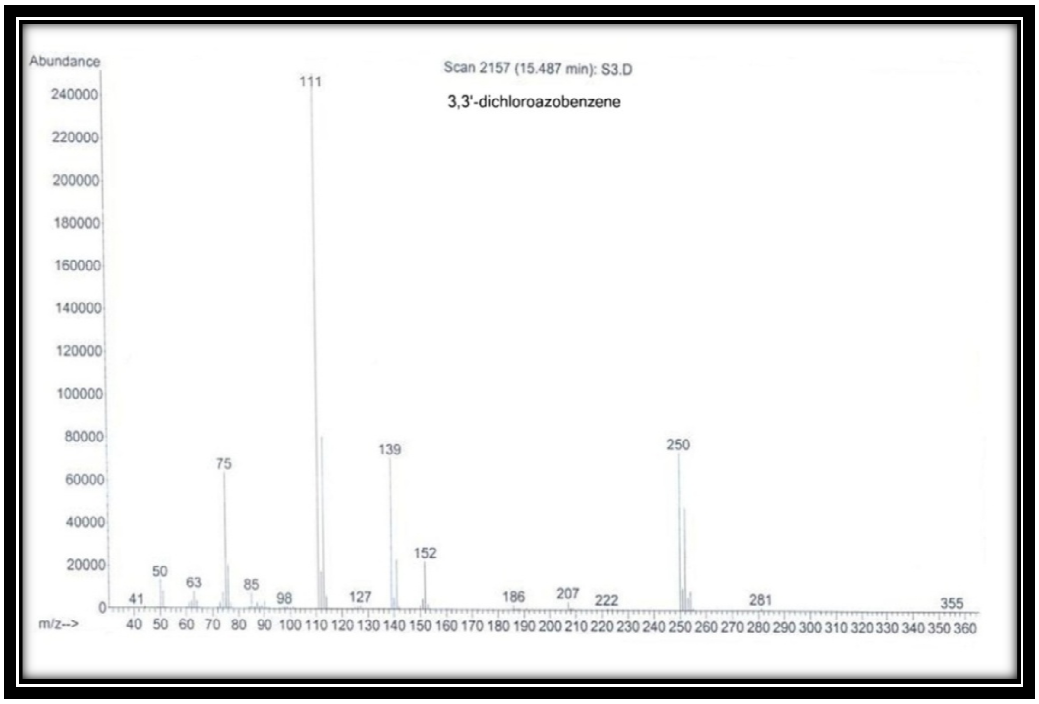

Figure 6.2. (e) GCMS spectra of 3,3'-dichloroazobenzene

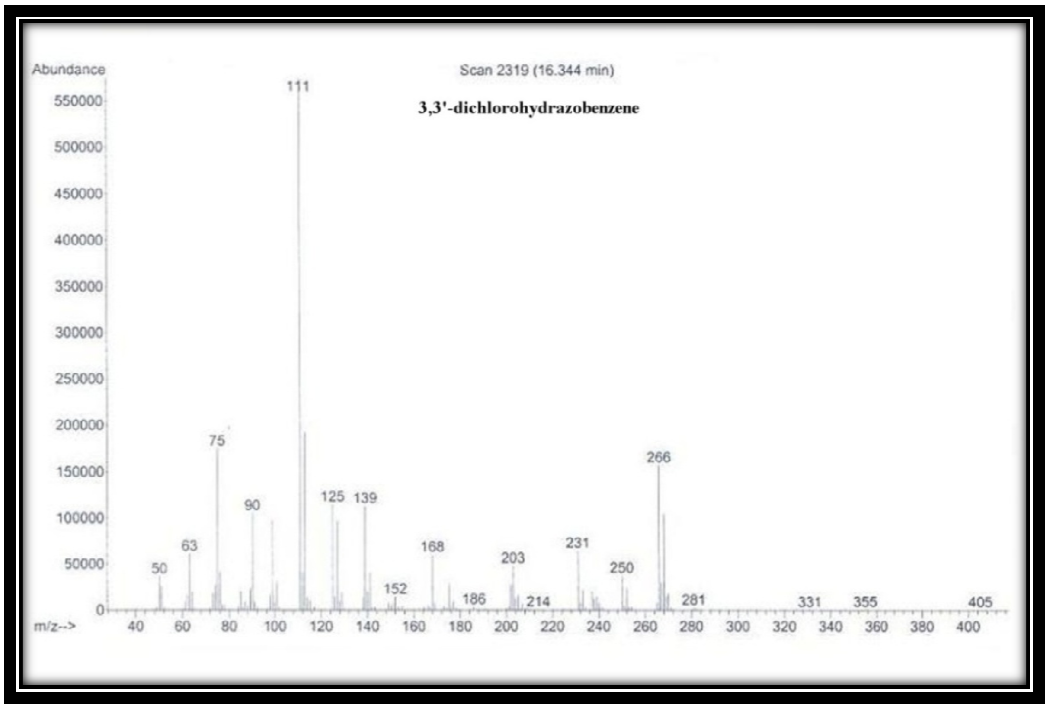

Figure 6.2. (f) GCMS spectra of 3,3'-dichlrohydrazobenzene

Figure 6.2. GCMS of reactant and products formed during hydrogenation of *m*-CNB

6.3. Results and discussion:

6.3.1. Catalyst characterization:

6.3.1.1. XPS study:

Surface composition of 1% Pt/C fresh (PtF), 1% Pt/C used (PtU) and 1% Pt/C catalyst used in presence of sodium carbonate (PtUS) were characterized by XPS. The composition of various species was calculated using the intensity of an appropriate line and atomic sensitivity factor (as given by Sconfiled) **[**53**].** Table 6.3 shows the comparision of fresh and used catalysts samples. It was observed that chlorine and nitrogen were absent in case of a fresh 1% Pt/C catalyst while, PtU and PtUS catalysts showed the presence of chlorine and nitrogen along with oxide species formation higher than that observed for fresh catalyst indicating oxidation of Pt species to some extent due to nitro compound. The used catalyst (PtU) also showed 1.65 and 3.5 times higher composition of chlorine and nitrogen respectively, than the fresh catalyst. The higher

surface concentration of chlorine species in PtU could be due to HCl formed during hydrodechlorination reaction. For the PtUS catalyst, surface concentration of chlorine has reduced substantially as compared to the PtU catalyst since the extent of dehydrohalogenation was reduced due to sodium carbonate addition.

Table 6.3. Surface compositions of catalyst (atom%) estimated by XPS for PtF , PtU used and PtUS catalysts

	Platinum	Oxygen	Chlorine	Carbon	Nitrogen
PtF	0.40	7.70	0.180	91.72	-
PtU	0.38	12.94	2.07	78.28	5.95
PtUS	0. 39	10.31	1.247	86.36	1.68

PtF : 1% Pt/C fresh catalyst

PtU: 1% Pt/C used catalyst

PtUS: 1% Pt/C catalyst used in presence of sodium carbonate

Figure 6.3 presents XPS spectra of PtF, PtU and PtUS catalysts in which Pt4*f* spectrum shows Pt in different oxidation states. For PtF and PtUS catalysts (Figure 6.3 (a) and (b)) the most intense doublet for Pt $4f_{7/2}$ and Pt $4f_{5/2}$ (71.8 and 75.1 eV) is due to metallic Pt. The second set of doublets for Pt $4f_{7/2}$ and Pt $4f_{5/2}$ (73.6 and 76.9 eV) could be assigned to the Pt (II) due to PtO or Pt(OH). The third doublet of Pt is the weakest in intensity, and was observed due to the binding energies for Pt $4f_{7/2}$ and Pt $4f_{5/2}$ (75.8 and 79.1 eV) assigned to Pt (IV) due to PtO_2[54-56]. The XPS spectra of PtU catalyst (Figure 6.3 (c)) showed binding energies of 72.5 and 75.8 eV for Pt $4f_{7/2}$ and Pt $4f_{5/2}$ assigned to Pt (II) species in $(NH_4)_2$ Pt(II) Cl_4 [57]. This was consistent with the activity studies in which the deactivation of the catalyst was observed hence, the formation of $(NH_4)_2$ Pt(II) Cl_4 species could be due to interaction of the catalyst with the amine formed in the reaction. The second set of doublets for Pt $4f_{7/2}$ and Pt $4f_{5/2}$ (73.6 and 76.9 eV) corresponds to PtO, which could be due to mild oxidation of Pt in presence of nitro compound [55]. It was interesting to note that the peak corresponding to metallic Pt was

not observed for PtU catalyst (Table 6.4), which was also consistent with the fact that this catalyst deactivated during the 1st use.

Table 6.4. Percentage of the Pt metal species.

	Binding energy, eV			
	71.8, Pt^0	**72.5, Pt (II)**	**73.6, Pt (II)**	**75.8, Pt (IV)**
PtF, %	**40.5**	**-**	**27**	**32.5**
PtUS, %	**37.21**	**-**	**32.3**	**30.47**
PtU, %	**-**	**74.3**	**25.7**	**-**

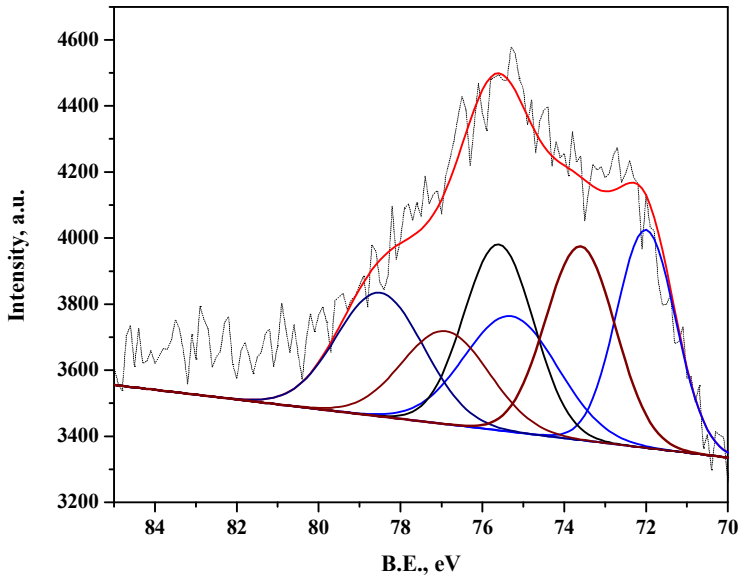

Figure 6.3. (a) XPS of PtF catalyst

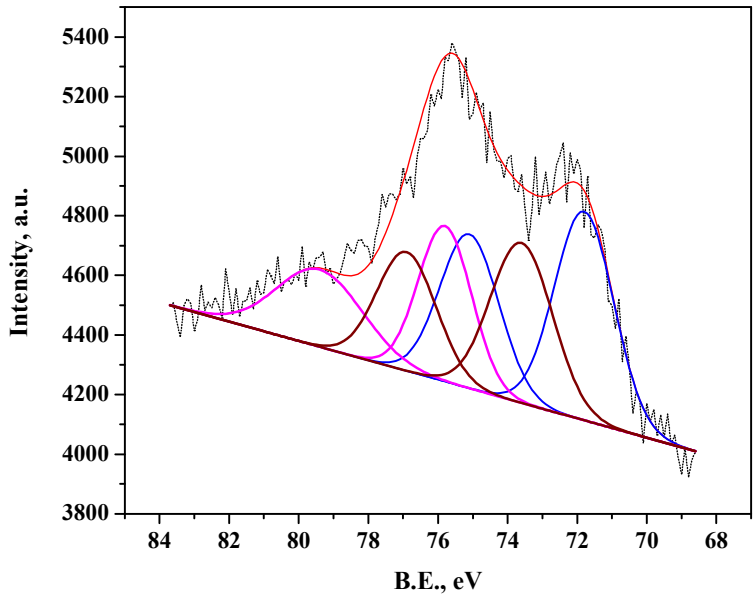

Figure 6.3. (b) XPS of PtUS catalyst

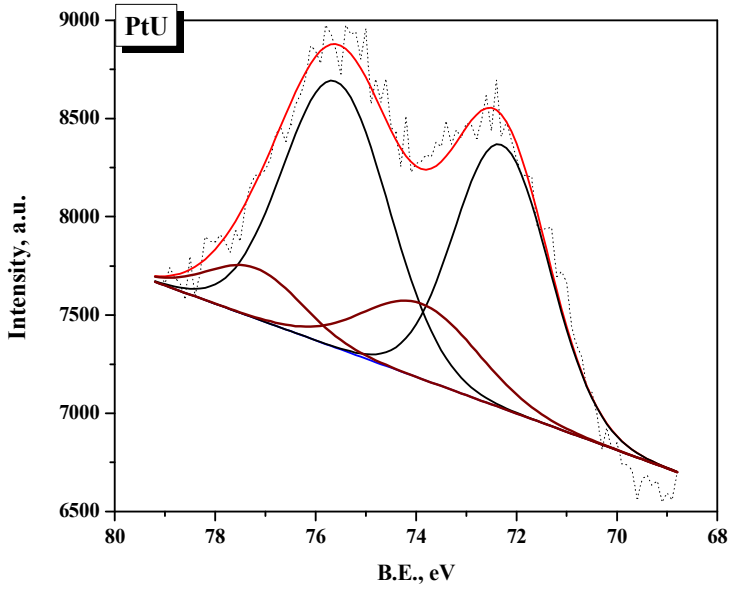

Figure 6.3. (c) XPS of PtU catalyst

Figure 6.3. XPS spectra of PtF, PtU and PtUS catalysts

The XPS spectrum of N 1s was also studied for PtU and PtUS catalysts. In both PtU and PtUS catalysts, peak at 400.5 eV corresponding to nitrogen of amine was observed. In addition to this, in case of PtU (Figure 6.4) catalyst, a peak at 404 eV was also observed which could be due to the N-O species [58].

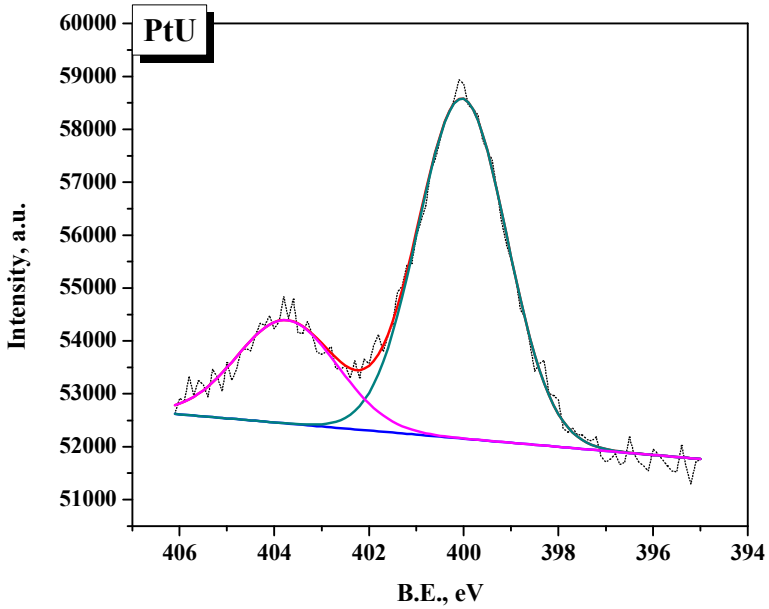

Figure 6.4. XPS of nitrogen spectra for PtU catalyst.

The deposition of carbonaceous material on the catalyst surface was studied by comparing the intensity area ratio of carbon peaks of the PtF, PtU, and PtUS samples. The XPS study of carbon spectra for PtF, PtU, and PtUS catalysts showed marginal deposition of carbonaceous material in PtU catalyst as compared with the PtUS catalyst. The intensity area ratio of I_{PtU}/I_{PtF} and I_{PtUS}/I_{PtF} was found 1.07 and 1.01 respectively.

6.3.1.2. X-ray diffraction study:

X-ray diffraction patterns for the monometallic 10% Ni/C and bimetallic 10%Ni-1%Pt/C catalysts are presented in Figure 6.5. It could be seen that Ni/C and Ni-Pt/C catalysts exhibited the comparable diffraction patterns. For the Ni/C catalyst, typical diffraction peaks centered at 2θ = 43.5 (NiO), 44.5^{o}(Ni^{0}) were observed, which agrees well with the

face-centered cubic nickel phase [59] however, no diffraction peaks corresponding to platinum were observed due to its low concentration in the bimetallic system. By addition of Pt as a co-metal in monometallic Ni/C catalyst, the peak at 43.5^{o} corresponding to NiO disappeared and a peak at 40^{o} appeared indicating the stabilization of completely reduced Ni^{o} as was observed by Telkar et al. [63]. It also indicated that the catalyst Ni-Pt/C combined the crystals features of Ni and Pt, indicating the co-existence of both of them [61, 62].

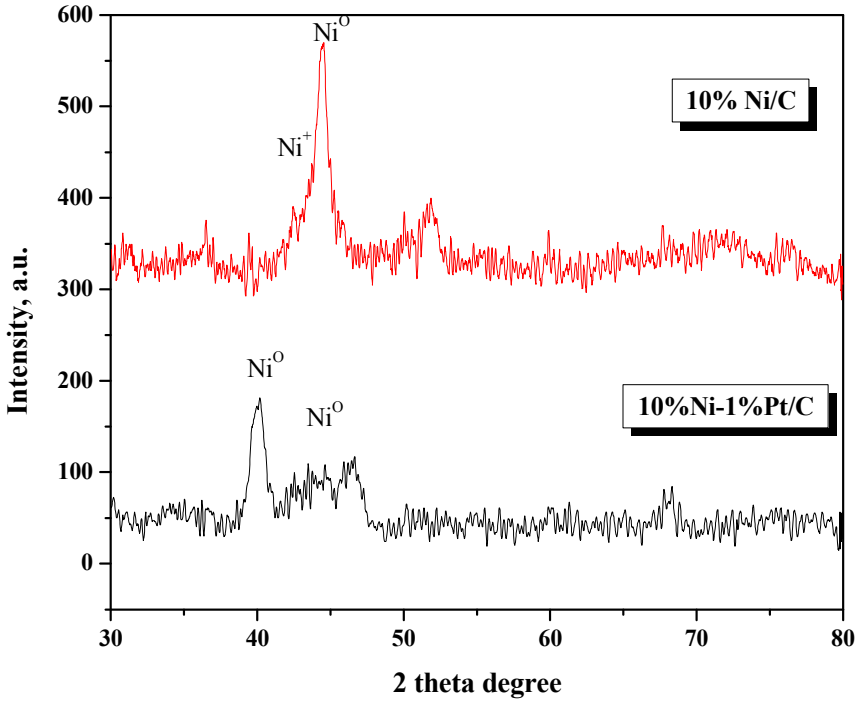

Figure 6.5. X-ray spectra of 10% Ni/C and 10%Ni-1%Pt/C catalysts

6.3.1.3. BET surface area measurement:

The specific surface areas of the PtF, PtU and PtUS (after recycling tests) catalysts were determined by BET method and the results are shown in Table 6.5. A decrease in surface area of PtU and PtUS catalysts was observed as compared with PtF catalyst. A substantial decrease in surface area of the used catalyst samples could be attributed to the agglomeration and/or deposition of carbonecious species on the catalyst surface.

Table 6.5. BET surface area of PtF, PtU and PtUS catalyst

Catalyst	PtF	PtU	PtUS
Surface area, m^2/g	1087	513.11	802.13

6.3.2. Preliminary hydrogenation experiments:

Some initial experiments on hydrogenation of *m*-CNB without any additives gave several by products along with the desired product *m*-CAN, as per the Scheme 6.1. In these experiments, the hydrogenation reaction was monitored by hydrogen absorption as well as liquid-phase analysis as a function of time, and the various intermediates and products formed were identified as I. 3,3'-dichloroazoxybenzene, II. 3,3'-dichlorobenzene, III. 3,3'-dichlorohydrazobenzene IV. aniline and, V. *m*-chloroaniline**.** In each experiment, the final sample was analyzed by GC to calculate the conversion of *m*-CNB and selectivity to *m*-CAN. In order to achieve the highest selectivity to *m*-CAN, role of an additive, sodium carbonate was studied and the results are discussed below.

6.3.2.1. Catalyst performance study:

Initially the catalyst activity and stability was studied by repeated use of 1% Pt/C catalyst without using any additive, at 358 K temperature and 1.03 MPa hydrogen pressure and results are presented in Figure 6.6. As it can be seen from Figure 6.6, initially at 0.25 h of the reaction, *m*-CAN selectivity was found to be 42% and DAB was the major competiting side product (35%), along with formation of DHAB and aniline with 45% conversion of *m*-CNB. As reaction proceeded, DAB undergoes further hydrogenation and selectivity to *m*-CAN increased 74%. Almost complete conversion of *m*-CNB was obtained after 0.9 h with 74% selectivity towards *m*-CAN. After complete conversion of *m*-CNB the reaction was kept for 5-10 min for complete conversion of the intermediates DAB and DHAB which showed 84% selectivity towards the *m*-CAN. During the recycle study, loss of catalyst activity was observed. XPS study (section 6.2.2.1) clearly showed the presence of amine, N-O and chloride species on the surface of the PtU catalyst. N-O species have higher affinity towards the metal surface [47] and it may remain on the active sites of Pt metal surface due to which catalyst activity was retarded. Another

possibility of catalyst deactivation is change in Pt^0 active species (71.8 eV) to Pt (II) (72.5 eV) for PtU, which may be due to the formation of $(NH_4)Pt(II)Cl_4$ species during the reaction.

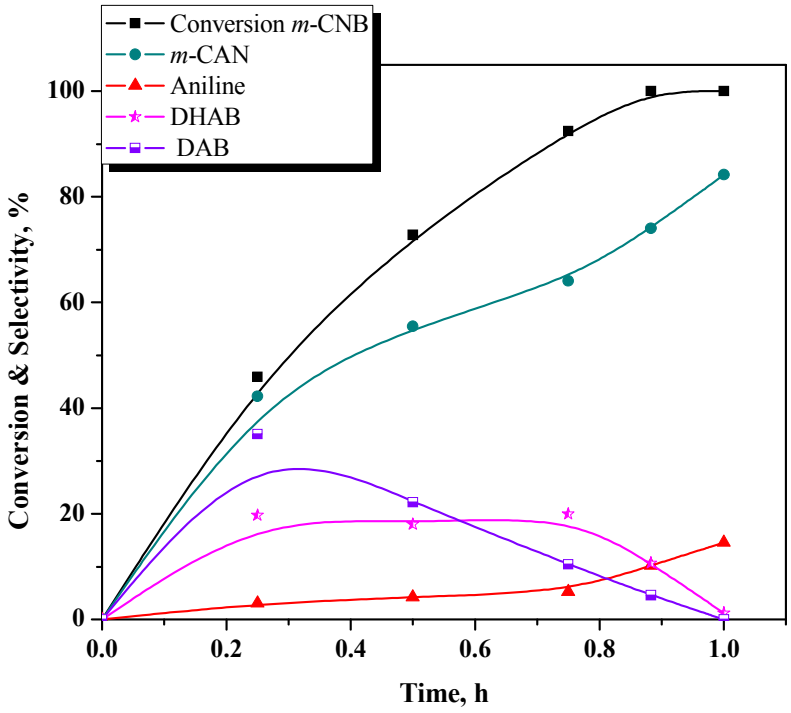

Figure. 6.6. Hydrogenation of *m*-CNB to *m*-CAN

Reaction conditions: *m*-CNB, 0.0317 mol; temperature, 358 K; hydrogen pressure, 1.03 MPa; 1% Pt/C catalyst, 0.050 g; MeOH, 95 mL; agitation speed, 1000 rpm.

The liquid phase hydrogenation of *m*-CNB was then carried out using Pt/C catalyst in presence of sodium carbonate as an additive by keeping the reaction conditions same as in case of Pt/C without additive. Figure 6.7 clearly shows the increase in selectivity from 84 to 93% as compared to the hydrogenation carried out in absence of an additive. The catalyst activity and stability was studied by repeated use of 1% Pt/C catalyst at 358 K and 1.03 MPa hydrogen pressure and the results are presented in Figure 6.8. After

completion of the reaction, reactor was cooled down to room temperature and stirring was stopped for 10 min to settle down the catalyst. Reaction crude from upper layer was taken out from liquid sampling valve by ensuring the catalyst remained in the reactor and then fresh charge was added to continue to the next reaction. The catalyst activity was found to be consistent even after third recycle.

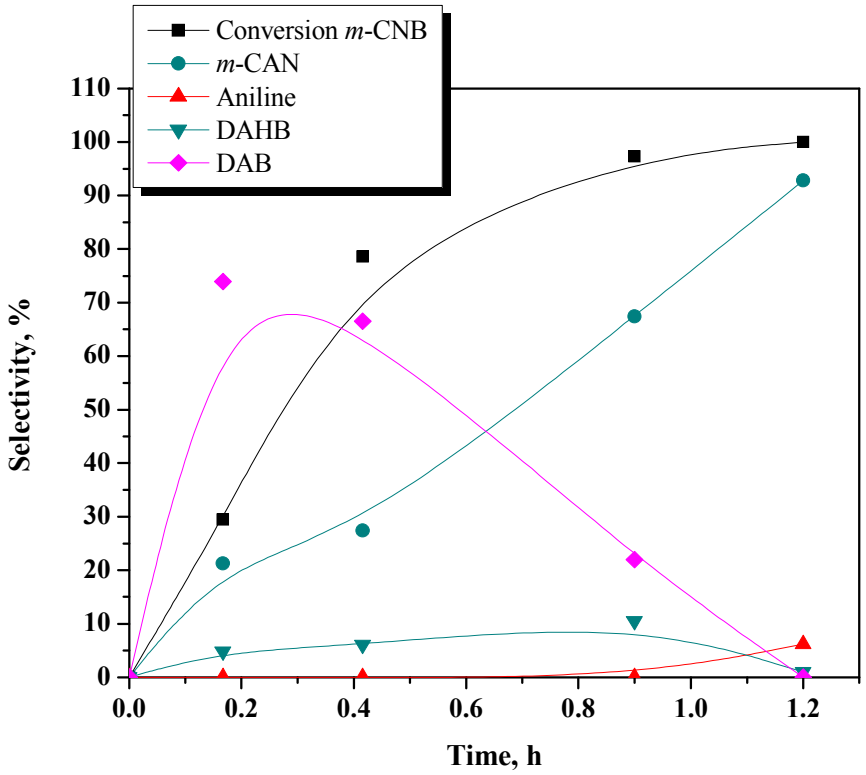

Figure 6.7. Hydrogenation of *m*-CNB to *m*-CAN in presence of sodium carbonate

Reaction conditions: *m*-CNB, 0.0317 mol; temperature,358 K; hydrogen pressure, 1.03 MPa; 1%Pt/C catalyst, 0.050 g; water, 0.5 mL; sodium carbonate, 0.02%; MeOH, 95mL; agitation speed- 1000 rpm.

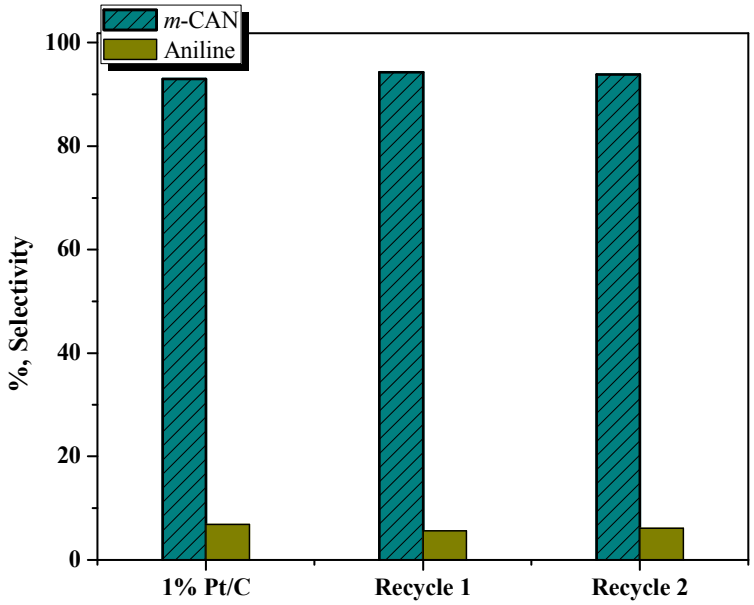

Figure. 6.8. Catalyst recycle study in hydrogenation of *m*-CNB to *m*-CAN

Reaction conditions: *m*-CNB, 0.0317 mol; temperature, 358 K; hydrogen pressure, 1.03 MPa; 1%Pt/C catalyst, 0.050 g; MeOH, 95 mL; sodium carbonate, 0.02%; water, 0.5 mL; agitation speed- 1000 rpm.

6.3.3. Effect of reaction parameters:

Further work on effects of various reaction parameters on conversion of *m*-CNB and selectivity to *m*-CAN was studied over 1% Pt/C catalyst. Table 6.6 shows the range of various process parameters studied in the present work.

Table 6.6. Range of operating conditions

1	Partial pressure of hydrogen	1.03-2.06 MPa
2	Temperature effect	338 – 378 K
3.	Substrate concentration	0.317- 0.952 mol
4.	Catalyst loading	0.025-0.100 g
5.	sodium carbonate concentration	0.02 -0.08 %
6.	Total reaction volume	1.0×10^{-4} m^3
7.	Agitation speed	1000 rpm

6.3.3.1. Effect of substrate concentration:

Effect of concentration of *m*-CNB was studied in the range of 0.317 to 0.952 mol by keeping constant hydrogen pressure, temperature and catalyst loading and the results are shown in Figure 6.9. With increase in concentration of *m*-CNB from 0.317 to 0.952 mol, the catalytic activity expressed in TOF, decreased from 1.4 to 1.1 x 10^6 h^{-1}, while selectivity to *m*-CAN remained almost the same at 94-93% with 6% formation of aniline. The linear decrease in TOF with increase in substrate concentration indicates a negative order dependence with respect to the substrate.

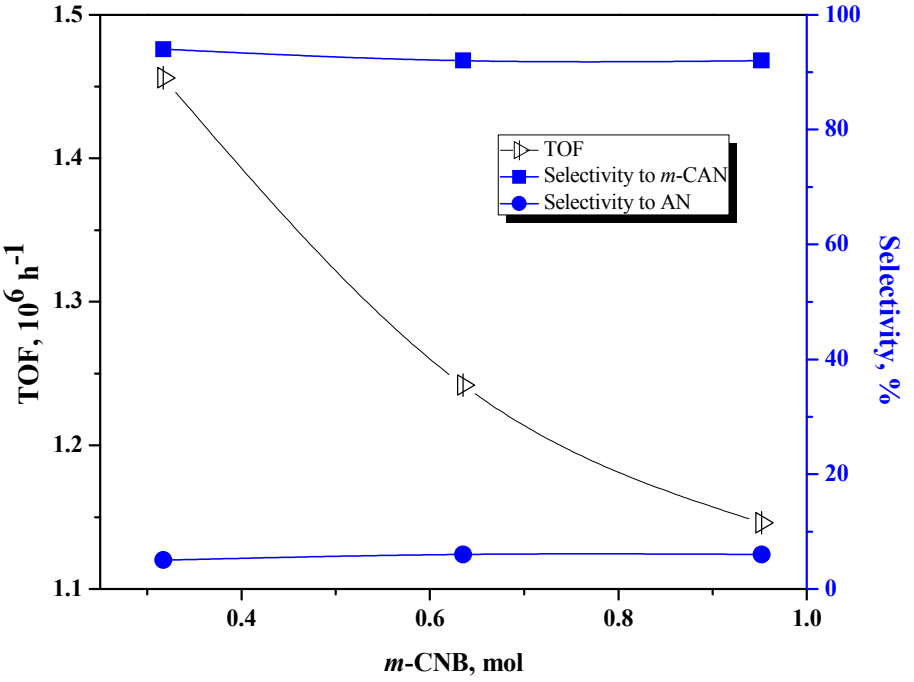

Figure 6.9. Effect of substrate concentration

Reaction conditions: temperature, 358 K; hydrogen pressure, 1.03 MPa; 1%Pt/C catalyst, 0.050 g; MeOH, 85 mL; sodium carbonate, 0.02 %; water, 0.5 mL; agitation speed, 1000 rpm.

6.3.3.2. Effect of temperature:

Effect of temperature on the selectivity to *m*-CAN was studied by varying the temperature from 338 to 378 K by keeping constant hydrogen pressure and catalyst loading and the results are shown in Figure 6.10. It was observed that increase in temperature from 338 K to 378 K led to the increase in formation of aniline from 6 to 8 % along with decrease in selectivity to *m*-CAN from 94 to 90 %. It was also observed that as temperature increased, catalytic activity also increased from 0.573 to 1.77 x 10^6 h^{-1}.

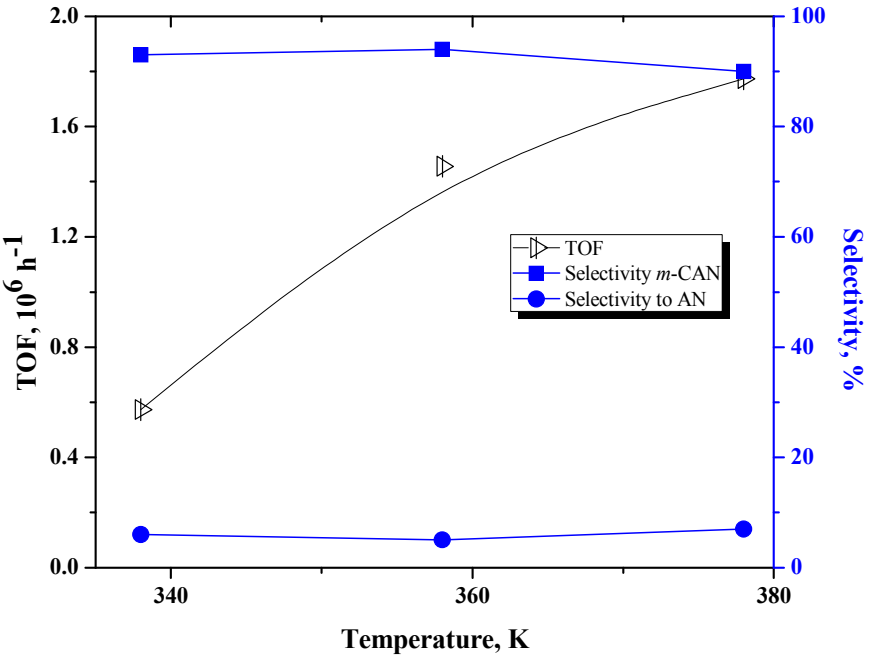

Figure 6.10. Effect of temperature

Reaction conditions: *m*-CNB, 0.0317 mol; hydrogen pressure, 1.03 MPa; 1%Pt/C catalyst, 0.050 g; MeOH, 95mL, sodium carbonate, 0.02 %; water, 0.5 mL; agitation speed, 1000 rpm.

6.3.3.3. Effect of pressure:

The effect of hydrogen pressure on activity and selectivity in hydrogenation of *m*-CNB was studied by varying the hydrogen pressure from 1.03 to 2.03 MPa, keeping constant temperature, substrate, catalyst loading and the results are presented in Figure 6.11. It was observed that *m*-CAN selectivity decreased from 94 to 90 % with increase in hydrogen pressure from 1.03 to 2.06 MPa, with simultaneous increase in the formation of aniline from 5 to 8%. It was also found that as pressure increased from 1.03 to 2.06 MPa, the catalytic activity also increased by almost two folds i.e. from 1.4 to 2.66 x 10^6 h^{-1}.

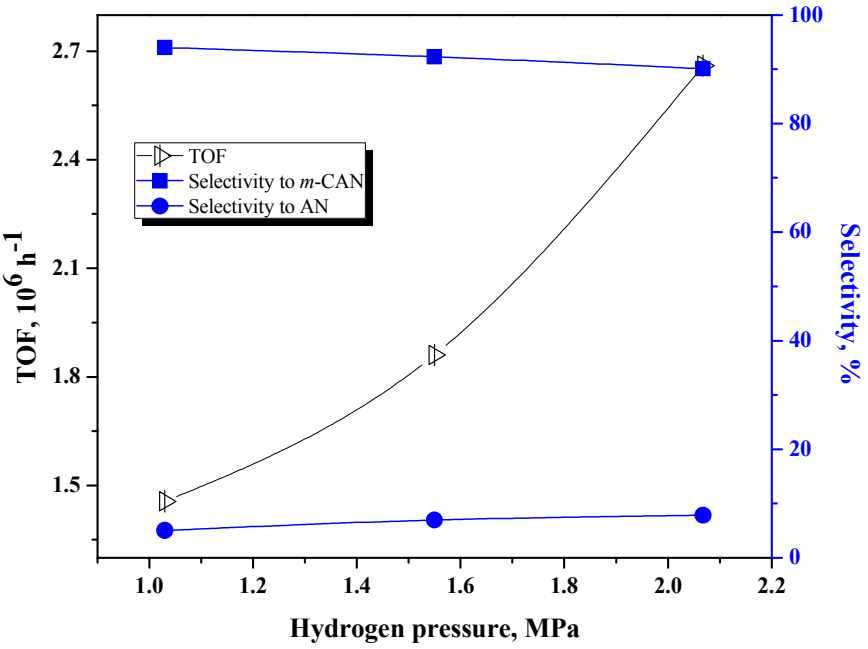

Figure 6.11. Effect of pressure

Reaction conditions: *m*-CNB, 0.0317 mol; temperature, 358 K; 1%Pt/C catalyst, 0.050 g; water, 0.5 mL; MeOH, 95mL; sodium carbonate, 0.02 %; agitation speed, 1000 rpm.

6.3.3.4. Effect of catalyst loading:

Effect of catalyst loading on selectivity to *m*-CAN was studied by varying the catalyst loading in a range of 0.025 g to 0.1 g at 358 K and 1.03 MPa hydrogen pressure and the results are shown in Figure 6.12. It was found that at lower catalyst loading (0.025 g) the selectivity towards the *m*-CAN was 96 % and as the catalyst loading increased from 0.050 to 0.100 g, the selectivity towards *m*-CAN decreased from 94 to 88% with increase in AN selectivity. TOF also increased from 0.38 to 7.5 x 10^6 h^{-1} with increase in catalyst loading.

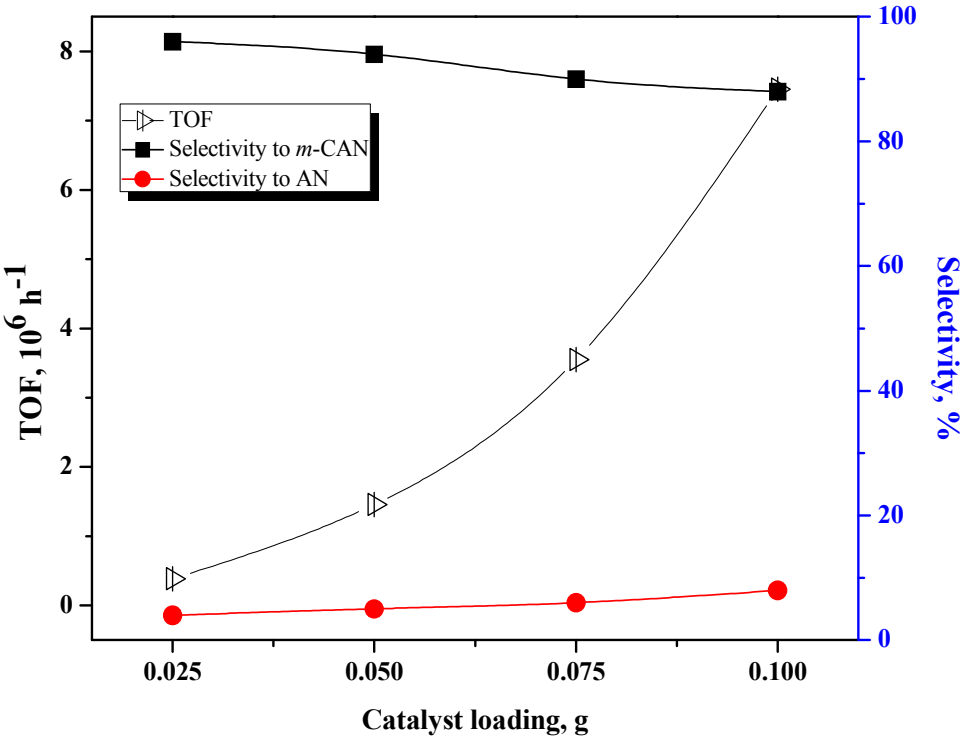

Figure 6.12. Effect of catalyst loading

Reaction conditions: *m*-CNB, 0.0317 mol; temperature, 358 K; hydrogen pressure, 1.03 MPa, water, 0.5 mL; sodium carbonate, 0.02 %; MeOH, 95 mL; agitation speed, 1000 rpm.

6.3.3.5. Effect of concentration of sodium carbonate:

To minimize the dehalogenation and to increase the selectivity towards the *m*-CAN the effect of concentration of sodium carbonate in hydrogenation of *m*-CNB was studied by varying the concentration of sodium carbonate in a range of 0.02 to 0.08% (w/w) while keeping other reaction parameters constant. As can be seen from Figure 6.13, with increase in concentration of sodium carbonate from 0.02 to 0.06%, selectivity to *m*-CAN also increased from 93 to ~96% while it remained same with further increase in sodium carbonate concentration upto 0.08% .

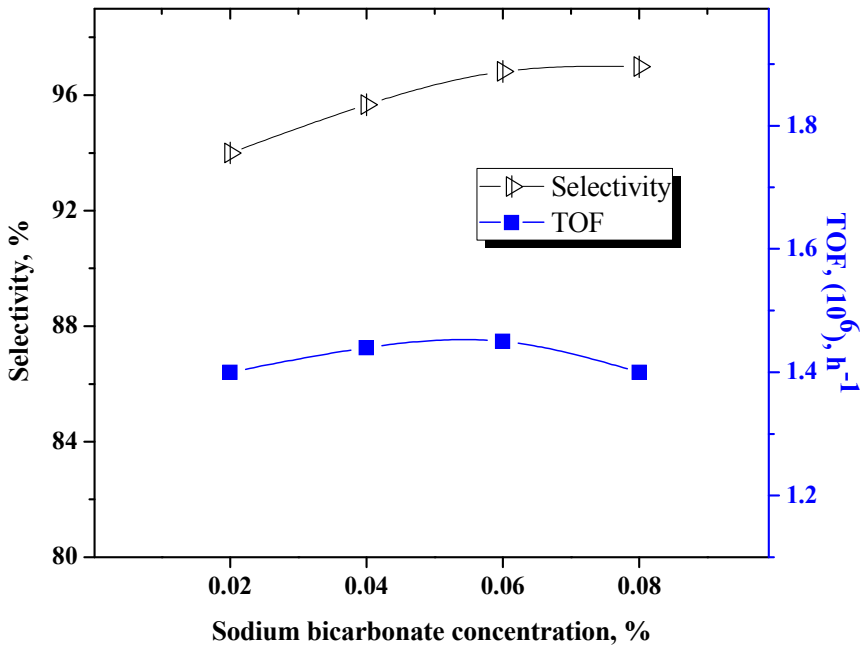

Figure 6.13. Effect of concentration of sodium carbonate

Reaction conditions: *m*-CNB, 0.0317 mol; temperature, 358 K; hydrogen pressure, 1.03 MPa; 1% Pt/C catalyst, 0.050 g; water, 0.5 mL; MeOH, 95 mL; agitation speed, 1000 rpm.

Role addition of a co-metal (Pt) to monometallic Ni/C catalyst in increasing the selectivity by minimizing the dechlorination was also studied and the results are discussed below.

6.3.4. Supported nickel mono and bimetallic catalysts:

Effect of supported mono- and bimetallic nickel catalysts on the selectivity to *m*-CAN was studied at 358 K temperature and 1.03 MPa hydrogen pressure and the results are presented in Figure 6.14. A dramatically different activity and selectivity trends were observed for mono- and bimetallic supported nickel based catalysts for the hydrogenation of *m*-CNB. Monometallic Ni supported on alumina and carbon catalysts showed 50 and 70% conversion with 78 to 82% selectivity respectively towards the *m*-CAN. While, for a bimetallic 10% Ni-1% Pt/C catalyst more than 99% selectivity to *m*-CAN was achieved

with complete conversion of *m*-CNB. Based on XRD results (section 6.2.2.2) it was concluded that the catalytic activity was affected by the change in electronic structure of the nickel metal by addition of co-metal i.e. Pt. The addition of Pt to Ni/C catalyst caused the stabilization of completely reduced Ni^{o} which is mainly responsible for the hydrogenation reaction. It is important to note that nitro compounds are known to be good oxidants hence, stabilization of Ni^{o} phase is critical in the catalytic hydrogenation nitro compounds.

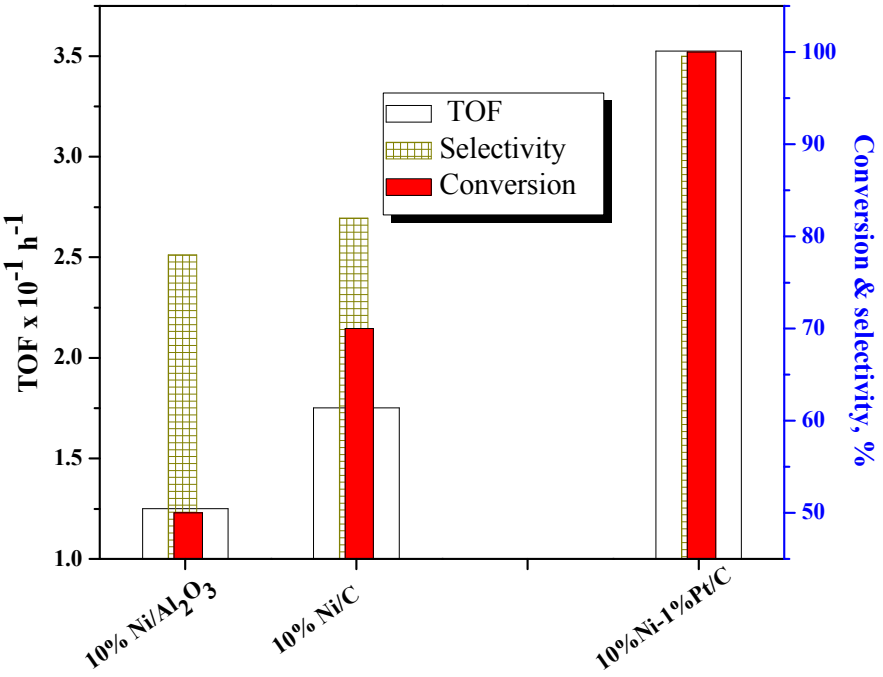

Figure 6.14. Activity, selectivity performance of nickel based mono and bimetallic catalysts

Reaction conditions: *m*-CNB, 0.0317 mol; hydrogen pressure, 1.03 MPa; temperature, 358 K; catalyst loading, 0.050 g; MeOH, 95 mL; agitation speed, 1000 rpm; water, 0.5 mL.

.

6.3.5. Hydrogenation of substituted chloronitrobenzene:

Hydrogenation of substituted chloronitrobenzene like *o*-, *p*-, *m*-CNB were also studied using 10%Ni-1%Pt/C catalyst at 358 K and 1.03 MPa hydrogen pressure and the results are shown in Figure 6.15. It can be seen from Figure 6.15 that the selectivity to CAN of

all substrates was found to be >99% but as the substrate varied from *o*-, *p*-, *m*-CNB the catalytic activity also varied i.e. from 7.5 to 3.5 x 10^{-1} h^{-1} due to the induction effect of –Cl at various positions of nitrobenzene.

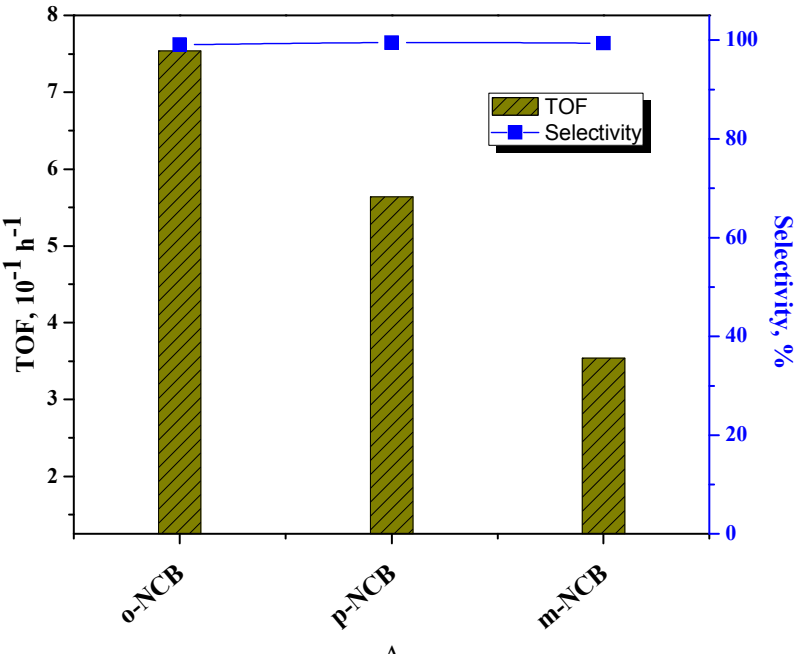

Figure 6.15. Effect of substituted chloronitrobenzene

Reaction conditions: CNB, 0.0317 mol; temperature, 358 K; hydrogen pressure, 1.03 MPa;10%Ni-1%Pt/C catalyst, 0.050 g; MeOH, 95 mL; water, 0.5 mL; agitation speed, 1000 rpm;

6.4. Conclusion:

The liquid phase hydrogenation of *m*-CNB to *m*-CAN carried at 358K and 1.03 MPa pressure using 1% Pt/C catalyst without any additive gave 84% selectivity to *m*-CAN due to the dehydrohalogenation reaction. During the catalyst recycle study, activity was lost due to the formation of $(NH_4)Pt(II)Cl_4$, amine and N-O species on the surface of catalyst which was observed by XPS study. The improvement in selectivity *m*-CAN from 84 to 94% was observed by addition of sodium carbonate in Pt/C catalyst. Bimetallic 10%Ni-1% Pt/C catalyst also showed the two fold enhancement in the activity and gave 99%

selectivity to *m*-CAN. This was due to the stabilization of Ni^{o} state by incorporation of co-metal, platinum. The order of hydrogenation rate of substituted CNB is *m*- < *p*- < *o*- with >99% selectivity towards the CAN.

6.5. References:

1. R. A. Surrey, H. F. Hammer *J. Am. Chem. Soc.* 68 (1946) 111.
2. S. Pilaniappan *Polym. Int.* 49 (2000) 659.
3. Y. Ding, A. b. Padias, H. K. Hall *J. Polym. Sci. A Polym. Chem.* 37 (1999) 2569.
4. F. Notheisz, M. Bartok in *Fine chemical through heterogeneous catalysis,* R. A. Sheldon, H. van Bekkum (Ed) Wiley, New York, (2001) pp. 415.
5. H. U. Blaser, U. Siegrist, H. Steiner, M. Studer in *Fine chemical through heterogeneous catalysis*, R. A. Sheldon, H. van Bekkum (Ed) Wiley, New York, (2001) pp. 389.
6. H. Arnold, F. Dobert, J. Gaube in *Handbook of heterogeneous catalysis,* Vol. 5, Wiley, New York, (1997) pp. 2165.
7. Y. D. Smirnov, L. A. Fedorova, A. P. Tomilov *Russ. J. Electrochem.* 33 (1997) 1168.
8. Y. Z. Chen, Y. C. Chen *Appl. Catal. A: General* 115 (1994) 45.
9. Y. An, D. Yuan, M. Y. Huang, Y. Y. Jiang *Micromol. Symp.* 80 (1994) 257.
10. M. H. Liu, W.Y. Yu, H.F. Liu *J. Mol. Catal. A: Chemical* 138 (1999) 295.
11. A. Tijani, B. Coq, F. Figueras *Appl. Catal.* 76 (1991) 255.
12. X. L. Yang, H.F. Liu, H. Zhong *J. Mol. Catal. A: Chemical* 147 (1999) 55.
13. Z. K. Yu, S.J. Liao, Y. Xu, B. Yang, D.R. Yu *J. Mol. Catal. A: Chemical* 120 (1997) 247.
14. B. Coq, A. Tijani, F. Figueras *J. Mol. Catal.* 71 (1992) 317.
15. Y. Gao, F. Wang, S. Liao, D. Yu *React. Kinet. Catal. Lett.* 64 (1998) 351.
16. L. Kurc, L. Cerveny *Chem. Prum.* 4 (1992) 85.
17. M. Studer, S. Neto, H.U. Blaser *Top. Catal*. 13 (2000) 205.
18. S. L. Karwa, R.A. Rajadhyaksha *Ind. Eng. Chem. Res.* 26 (1987) 1746.
19. C. V. Rode, R. V. Chaudhari *Ind. Eng. Chem. Res.* 33 (1994) 1645.
20. F. Visentin, G. Puxty, O. M. Kut, K. Hungerbuehler *Ind. Eng. Chem. Res.* 45 (2006) 4566.
21. M. Studer, S. Neto, H. U. Blaser *Top. Catal.* 13 (2000) 205.
22. P. Baumeister. H. U. Blaser, M. Studer *Catal. Lett.* 49 (1998) 219.
23. N. P. Sokolova, A. A. Balandin, N. P. Maksimova, Z. M. Skul'skaya *Russ. J. Inorg. Chem*. 15 (1966) 1824.

24. Y. Z. Chen, Y. C. Chen *Appl. Catal A: General* 115 (1994) 45.
25. Y. C. Liu, C. Y. Huang, Y. W. Chen *Ind. Eng. Chem. Res.* 45 (2006) 2973.
26. Y. C. Liu, Y. W. Chen *Ind. Eng. Chem. Res* 45 (2006) 62.
27. J. R. Kosak *Ann. of N. Y. Acad. Sci.* 172 (1970) 175.
28. H. Amold, F. Dobert, J. Gaube in *Handbook of heterogeneous catalysis, Hydrogenation reactions*, G. Ertl, H. Knozinger, J. Weitkamp (Eds), Vol. 5, Wiley, New York, (1997) pp 2165.
29. P. N. Rylander in *Catalysis-science and technology,* J. R. Anderson, M. Boudart (Eds), Vol 4, Akademie-Verlag, Berlin, (1993) pp 1.
30. V. L. Khilnani, S. B. Chandalia *Org. Proc. Res. Dev.* 5 (2001) 257.
31. X. X. Han, R. X. Zhou, G. H. Lai, X. M. Zheng *Catal. Today* 93-95 (2004) 433.
32. Z. Yu, S. Liao, Y. Xu, B. Yang, D. Yu *J. Chem. Soc. Chem. Commun.* 11 (1995) 1155.
33. N. P. Sokolova, A. A. Balandin, N. P. Maksimova, Z. M. Skul'skaya *Russ. Chem. Bull*. 15 (1966) 1824.
34. X. X. Han, R. X. Zhou, G. H. Lai, X. M. Zheng *React. Kinet. Catal. Lett.* 83 (2004) 55.
35. X. X. Han, R. X. Zhou, G. H. Lai, B. H. Yue, X. M. Zheng *J. Mol. Catal. A: Chemical* 209 (2004) 83.
36. V. Kratky, M. Kralik, M. Mecarova, M. Stolcova, L. Zalibera, M. Hronec *Appl. Catal. A: General* 235 (2002) 225.
37. H. Blaser, H. Steiner, M. Studer *Chem. Cat. Chem.* 1 (2009) 210.
38. H. Ma, K. Sun, Y. Li, X. Xu *Catal. Commun.* 10 (2009) 1363.
39. K. Nomura *Catal. Lett.* (1991) 1679.
40. H. Geenfield, F. S. Dovell *J. Org. Chem.* 32 (1967) 3670.
41. N. Maity, P. R. Rajamohanan, S. Ganapathy, C. S. Gopinath, S. Bhaduri, G. K. Lahiri *J. Phys. Chem. C* 112 (2008) 9428.
42. J. Yang, C. Xiong, X. Han, L. Zhou *Ind. J. Chem.* 48A (2009) 1358.
43. X. Han *Ind. J. Chem.* 48A (2009) 168.
44. C. Wang, J. Qiu, C. Liang, L. Xing, X. Yang *Catal. Commun.* 9 (2008) 1749.

45. F. Cárdenas-Lizana, S. Gómez-Quero, M. A. Keane *Appl. Catal. A: General* 334 (2008) 199.
46. X. Han, R. Zhou, G. Lai, B. Yue X. Zheng *React. Kinet. Catal. Lett.* 81 (2004) 41.
47. C. Fernando, G. Santoago, K. A. Mark *Appl. Catal. A:General* 334 (2008) 199.
48. X. Han, R. Zhou, G. Lai, B. Yue, X. Zheng *Catal. Lett.* 89 (2003) 255.
49. X. C. Meng, Y. J. Cheng, S. X. Cai, F. Y. Zhao in *2nd international IUPAC conference on green chemistry*, Russia, 14-19 September (2008).
50. G. H. Lai, X. X. Han, R. X. Zhou, J. X. Zhang, X. M. Zheng, R. R. China *Phy. Theor. Analy. Chem.* 43A (2004) 2545.
51. X. Yan, J. Sun, Y. Wang, J. Yang *J. Mol. Catal. A: Chemical* 252 (2006) 17.
52. L. Xing, J. Qiu, C. Liang, C. Wang, L. Mao *J. Catal.* 250 (2007) 369.
53. J. H. Sconfield *J. Elect. Spectro. Rel. Pheno.* 8 (1976) 129.
54. K. S. Kim, N, Winograd, R. E. Davis *J. Am. Chem. Soc.* 93 (1971) 6296.
55. P. J. M. Dijkraaf, H. A. M. Duisters, B. F. M. Kuster, K. van der Wiele *J. Catal.* 112 (1988) 337.
56. J. Wang, G. Yin, Y. Shao, S. Zhang, Z. Wang, Y. Gao *J. Power Sources.* 171 (2007) 331.
57. A. Katrib, M. S. EL-Ezaby *Inorg. Chim. Acta.* 26 (1979) L405.
58. P. Nowicki, R. Pietrzak, H. Wachowska *Energy Fuels* 24 (2010) 1197-1206.
59. B. Coq, A. Tijani, F. Figuéras *J. Mol. Catal.* 68 (1991) 331.
60. H. Stephane, B. Michel and E. Barbara *Surf. Coat. Technol.* 201 (2006) 2166
61. P. K. Shen, Z. Tian *Electrochimica Acta* 49 (20040 3107
62. X. Geng, H. Zhang, W. Ye, Y. Ma. H. Zhong *J. Power Sources* 185 (2008) 627
63. M. M. Telkar, J. M. Nadgeri, C. V. Rode, R. V. Chaudhari *Appl. Catal. A: General* 295 (2005) 23.

Chapter VII

Conclusion

In this thesis, a detailed study on preparation and characterization of mono, bi-metallic and nano catalysts of nickel, palladium and platinum metals has been carried out. These catalysts were evaluated for the industrially important hydrogenation reactions viz. (i) selective hydrogenation of 2-butyne-1,4-diol to 2-butene-1,4-diol and butane-1,4-diol, (ii) phenylacetylene to styrene, (iii) nitrobenzene to p-aminophenol via phenylhydroxylamine and (iv) *m*-chlronitrobenzene to *m*-chloronitroaniline. The main conclusions of this work are summarized below.

1. Continuous catalytic hydrogenation of 2-butyne-1,4-diol (B_3D) was carried out in a fixed-bed reactor over 1% $Pt/CaCO_3$ catalyst to give 2-butene-1,4-diol (B_2D) and 1,4-butanediol (B_1D) without formation of any other side products. In case of continuous hydrogenation, higher selectivity to B_2D (66%) could be obtained and the selectivity pattern was completely different from that found in case of batch slurry operation in which B_1D selectivity was very much higher (83%) than the B_2D selectivity (17%). Another interesting feature was that by varying the contact time, selectivity to both B_2D as well as B_1D could be varied over a wide range which is an attractive option to obtain the desired products mixture of B_2D and B_1D. Further, a mathematical model for a continuous reactor performance was also developed on the basis of the kinetic data obtained previously in a batch slurry reactor. The predicted values of conversion, selectivity, and rate of hydrogenation were found to agree well with the experimental data over a wide range of conditions.
2. Pd nanoparticles supported on carbon and calcium carbonate were also evaluated for the hydrogenation of B_3D. Pd/C catalyst prepared in the presence of polyvinyl pyrrolidone (PVP) as a stabilizer gave Pd particle size in a narrow range of 3-5 nm. This catalysts showed the higher activity (9-21 times) and selectivity > 99% to B_2D as compared to the bulk Pd catalysts. A proper choice of stabilizer (PVP) gave the smallest particle size responsible for such a dramatic enhancement in activity.
3. Multiwalled carbon nanotubes were prepared by thermal decomposition method followed by acid treatment and Pd-functionalized carbon nanotubes with $PdCl_2$ by wet impregnation method. The Pd-functionalized carbon nanotubes catalyst was characterized by BET, FTIR, Raman, XRD, EDX, ICP-OES, SEM and TEM and

was evaluated for its activity for hydrogenation of 2-butyen-1,4-diol. It showed higher selectivity (93%) to 2-butene-1,4-diol than Pd supported on commercial carbon (70% selectivity to 2-butene-1,4-diol) for complete conversion of 2-butyne-1,4-diol. The catalyst also exhibited excellent stability as evidenced by the three catalyst recycle experiments.

4. Colloidal Pd nanoparticles prepared in presence of polyvinyl pyrrolidone (PVP) as a stabilizer gave Pd particle size of 4 nm. This catalyst showed 3.5 times higher reaction rate than the bulk catalyst for hydrogenation of phenylacetylene under mild reaction conditions. At 90% conversion of phenylacetylene, selectivity to styrene was found to be 90% which decreased to 68 % for complete conversion of phenylacetylene. This was due to formation of ethylbenzene by further hydrogenation of styrene.
5. Catalytic liquid phase hydrogenation of nitrobenzene in acid medium to phenyl hydroxylamine (PHA) and its rearrangement to give *p*-aminophenol (PAP) were studied separately in a batch reactor. First step of hydrogenation of nitrobenzene to PHA was carried out over Pt/C catalyst at 303K and 0.69 MPa hydrogen pressure with complete conversion of nitrobenzene while, selectivity to PHA achieved was >90% with some formation aniline even at lower temperature. PHA rearrangement could be achieved under hydrogen atmosphere at elevated temperature of 353K to give maximum 74% selectivity to PAP. Prepared Pt/C catalyst was characterized by BET, TPR, SEM, EDX, and XPS.
6. Direct synthesis of p-aminophenol involving insitu rearrangement of PHA was also studied. In this study, the modified workup strategy for reaction crude involving single step neutralization at low temperature (5-8^{o}C) showed 5 to 10% enhancement in the isolated yield of PAP. The other parameters such as acid concentration, catalyst loading, and recycle of aqueous layer also played an important role to increase the isolated yield to PAP.
7. Supported mono (Ni, Pt) and bi-metallic (Ni-Pt) catalysts were prepared for the selective liquid phase hydrogenation of *m*-nitrochlrobenzene to *m*-chloroaniline. It was found that the use of sodium carbonate as an additive, substantially reduced the

extent of dehydrohalogenation to give the highest selectivity of 94% to *m*-CAN. Ni-Pt bimetallic catalyst showed high activity and almost complete selectivity (>99%) to m-chloroaniline compared with Ni monometallic catalyst. The increase in activity and selectivity was found to be due to the stabilization of Ni^{o} state by incorporation of the co-metal, platinum.

List of Publications

Research papers published/ communicated in peer reviewed international journals

1. Evaluation of Pd-funtionalized carbon nanotubes for hydrogenation of 1,4-butynediol.
   J. M. Nadgeri, A. C. Garade, R. A. Tambe, S. P. Gokhale, C. V. Rode *Adv. Sci. Lett.* 3 (2010) 313.
2. Hydrogenation activity and selectivity behavior of supported palladium nanoparticles
   J. M. Nadgeri, M. M. Telkar, C. V. Rode *Catal. Comm*. 9 (2008) 441.
3. Reaction kinetics of liquid phase air oxidation of *p*-cresol to *p*-hydroxybenzaldehyde
   V. S. Kshirsagar, **J. M. Nadgeri**, P. R. Tayade, C. V. Rode *Appl. Catal. A: General 339* (2008) 28.
4. Cobalt-salen intercalated montmorillonite catalyst for air oxidation of *p*-cresol under mild conditions
   C. V. Rode, V. S. Kshirsagar, **J. M. Nadgeri**, K. R. Patil *Ind. Eng. Chem. Res.* 46 (2007) 8412.
5. Continuous hydrogenation of 2-butyne-1,4-diol to 2-butene-and butane-1,4-diols
   C. V. Rode, P. R. Tayade**, J. M. Nadgeri**, R. Jaganathan, R. V. Chaudhari *Org. Proc. Res. Dev*. 10 (2006) 278.
6. Role of co-metal in bimetallic Ni-Pt catalyst for hydrogenation of *m*-dinitrobenzene to *m*-phenylenediamine
   M. M. Telkar**, J. M. Nadgeri**, C. V. Rode, R. V. Chaudhari *Appl. Catal. A: General* 295 (2005) 23.
7. Selective synthesis of *p*-hydroxybenzaldehyde by liquid-phase catalytic oxidation of *p*-cresol
   C. V. Rode, M. V. Sonar, **J. M. Nadgeri**, R. V. Chaudhari *Org. Proc. Res. Dev.* 8 (2004) 873.
8. Synthesis of *p*-aminophenol via catalytic hydrogenation of nitrobenzene
   J. M. Nadgeri, N. S. Biradar, S. T. Jadkar, A. C. Garade, C. V. Rode, "*p*-aminophenol via hydrogenation of nitrobenzene" communicated.

Posters/oral presentation for national /international symposium

1. *p*-Aminophenol via hydrogenation of nitrobenzene

   C. V. Rode, **J. M. Nadgeri** (oral presentation) in *2nd international conference on Green process Engineering (GPE-2009),* Vanice, Italy (June 14-17, 2009) .

2. Hydrogenation of nitrobenzene to phenylhydroxylamine followed by its rearrangement to *p*-aminophenol

   J. M. Nadgeri, N. S. Biradar, C. V. Rode (Poster presentation) on *Science day*, National Chemical Laboratory, Pune, India (Feb 25-27, 2009).

3. Hydrogen adsorption studies on Pd-MWNTs at low temperatures

   J. M. Nadgeri, C. V. Rode, S. P. Gokhale (Poster presention) in *International Conference on Hydrogen & Hydrogen Storage, Methods and Materials (H-3)*, Indian Institute of Science, Bangalore, India (Jan 03-06, 2009).

4. Hydrogen uptake capacity of Pd-functionalized multi-walled carbon nanotubes

   J. M. Nadgeri, S. D. Patil, C. V. Rode, S. P. Gokhale (Poster presentation) in *International Conference of Advanced material (ICAM-2008)*, (Feb 18-21, 2008)

5. Evaluation cf Pd-functionalized carbon nanotubes for hydrogenation of 1,4-butynediol V. S. Kshirsagar, **J. M. Nadgeri**, S. D. Patil, S. P. Gokhale, C. V. Rode (Poster presention) in *CATWORKSHOP 2008,* Bhuwaneshwar, India (Feb 18, 2008).

6. Pd-functionalization of carbon nanotubes for hydrogen storage

   J. M. Nadgeri, C. V. Rode, S. P. Gokhale (Oral Presentaion) in *5th National symposium and conference on solid state chemistry and allied areas (ISCAS 2007)*, Nagpur, INDIA.

7. Characterization and catalytic activity of supported Pd nanoparticles for selective hydrogenation reactions

   J. M. Nadgeri, M. M. Telkar, C. V. Rode (Poster presentation) in *6th International Symposium on Catalysis in Multiphase Reactors (CAMUR E-6) and 5th International Symposium on Multifunctional Reactors (ISMR-5),* NCL, Pune, India.

8. Montmorillonite intercalated cobalt complexes for liquid phase oxidation of *p* -cresol to *p*-hydroxybenzaldehyde

C. V. Rode, V. S. Kshirsagar **J. M. Nadgeri**, Masayuki Shirai in *Fifth Tokyo Conference on Advanced Catalytic Science and Technology* Tokyo, Japan (July 23-28 , 2006).

9. Cobalt-salen intercalated montmorillonite catalyst for air oxidation of *p* -cresol under mild conditions

   C. V. Rode, V. S. Kshirsagar, **J. M. Nadgeri** (oral presentation) in *The sixth International Symposium on Catalysis in Multiphase Reactors (CAMURE-6) and the fifth International Symposium on Multifunctional Reactors (ISMR-5),* NCL, Pune, India (Jan 14-16, 2007).

10. Solid acid catalyzed intermolecular rearrangement of benzyl phenyl ethers

    J. M. Nadgeri, M. H. Bhure, C. V. Rode (Poster Presentaion) in *Science Day,* NCL, Pune, India (Feb, 2006).

11. Activity and selectivity behavior of colloidal Pt and Ru catalysts in hydrogenation of cinnamaldehyde

    J. M. Nadgeri, P. Shinde, S. S. Hegade, C. V. Rode (Oral Presentation) in *ChemCon 2005*, NewDelhi, India (2005) .

12. Characterization and catalytic activity of supported Pd nanoparticles for selective hydrogenation reactions

    C. V. Rode, **J. M. Nadgeri**, R.V. Chaudhari (oral presentation) in *ChemCon2004,* Deharadun, India (2004) .